# DEVELOPMENT OF NOVEL HEAT-TREATABLE MAGNESIUM ALLOYS FOR LOW-PRESSURE TWIN-ROLL CASTING

A thesis submitted for the degree of Doctor of

Philosophy by

Umar Amin

Brunel Centre for Advanced Solidification Technology, Brunel University London

June 2021

# Abstract

Magnesium alloys are ideal for light weighting, especially given the continued pressure on the automotive industry to reduce $CO_2$ emissions while increasing the fuel efficiencies. Major contribution to weight savings in automotive applications can be made using sheet product. However, due to hexagonal crystal structure magnesium is inherently difficult to deform and a strong basal texture forms during large scale deformation such as rolling or extrusion. Twin-roll casting (TRC) process provides a pathway to producing sheet material by casting directly into thickness close to final thickness, opening a path to produce sheet magnesium. The conventional sheet production routes, such as rolling, requires many homogenisation steps and small rolling passes which is energy-intensive, time consuming and ultimately not economical. Currently, majority of TRC research is based on magnesium alloy AZ31 (Mg-3Al-1Zn (wt%)) which can only be strengthened by grain size control. The new alloy development for conventional twin-roll casting considers alloys with very dilute concentrations that relies on grain size strengthening as the main strengthening mechanism.

However, the low-pressure TRC developed within BCAST, relies on solidification to control the microstructure. This process minimises the severe segregation issues associated with conventional TRC and produce a thin strip that may be directly stamped. This requires a different approach to alloy design as the constraints associated with the conventional TRC process no longer controls the microstructure evolution. The approach used in the design of alloy compositions considers both the availability of the additions as well as individual and combined effect of these additions on both mechanical properties' enhancement and texture modification of the TRC strip. Alloying elements and compositions that lends to precipitation hardening following final forming are chosen to provide enhanced strengthening.

The thesis reports the development of novel thermo-mechanically processed low-pressure TRC magnesium alloys based on Mg-1Al-1Zn-0.3Mn, Mg-1Al-4Zn-0.3Mn and Mg-4Al-1Zn-0.3Mn, with and without Ca additions. Alloys show enhancement of age hardening response following small scale deformation at room temperature which allows enhancement of the mechanical properties of the low-pressure TRC alloys. The addition of calcium to Mg-1Al-1Zn-0.3Mn led to rapid peak ageing

response within 1 hour and significant grain refinement of 48%, this resulted in grain size reduction from 238±9μm to 114±7μm. The greatest increment in age-hardening was observed through increasing concentration of zinc to 4%wt with calcium containing alloy. At 48hrs, a hardness value of 71HV was achieved, an increment of 25HV from as-quenched condition. TEM micrographs of peak-aged Mg-1Al-4Zn-0.3Mn and Mg-1Al-4Zn-0.3Mn-0.3Ca showed precipitates are mainly rod like precipitates that form parallel to the <0001> direction. In low-pressure TRC Mg-1Al-1Zn-0.3Mn-0.3Ca, the columnar grains measured to approximately 153±13μm with minimal sign of centreline segregation. T6 treatment of low-pressure TRC Mg-1Al-1Zn-0.3Mn-0.3Ca drastically improved yield strength from 93.5MPa to 140.3MPa. As for low-pressure TRC Mg-1Al-4Zn-0.3Mn-0.3Ca it was greater as the yield strength increased from 85.1MPa to 171.4MPa.

# Acknowledgements


In the name of Allah, the Entirely Merciful, the Especially Merciful.

I would like to begin by thanking Almighty God for giving me good health and the fortitude to complete my PhD research.

During the experimental work and writing of this dissertation, I have received a great deal of support and assistance. I would first like to thank my supervisor, Dr Chamini Mendis, whose expertise was invaluable. From first to the last day, her support and guidance was immeasurable. I would like to make a special mention of Professor Zhongyun Fan for giving me the opportunity to study at BCAST.

I wish to show my gratitude to Professor Hari-Babu Nadendla, Dr Yan Huang and Professor Isaac Chang for their continuous guidance and constructive criticism of my research work. I greatly appreciate the help given in my experimental work by Dr Xinliang Yang, Dr Jayesh Patel, Mr Graham Mitchell, Mr Jon Gadd, Mr Warren Lee, Ms Samantha Melvin and Ms Loredana Saccone.

Finally, I would like to make an honourable mention of my family for their invaluable love and support of which I could not have done without. My wife, Sidra Jabeen became my soulmate and biggest motivation to keep going at the end. My mother, Kausar Amin, was a true inspiration whose comfort and warmth cannot be repaid in this lifetime. My father, Mohammed Amin, was my rock in the most difficult of times. And finally, my baby sister, Khadijah Amin, was a bundle of joy who distracted me for my own sanity.

# List of Engagements/Reports

1. **Amin, U.**, Mendis, C. L., Fan, Z., Poster Presentation 2017. National Student Conference in Metallic Materials 2017, University of Sheffield. Development of novel heat treatable magnesium alloys for twin-roll casting.

2. Mendis, C. L., **Amin, U.**, Yang, X. L., Fan, Z., Annual Report 2018. Progress in the development of new magnesium alloys for the low-force TRC process, London: Liquid Metal Engineering Hub, BCAST.

3. **Amin, U.**, Mendis, C. L., Yang, X. L., Fan, Z., Poster Presentation 2018. 11$^{th}$ International Conference on Mg Alloys and Their Applications, Beaumont Estate, Old Windsor. Development of novel heat-treatable magnesium alloys for twin-roll casting.

4. **Amin, U.**, Mendis, C. L., Yang, X. L., Fan, Z., Poster Presentation 2019. Industrial Steering Panel Meeting, Brunel University London. Development of novel heat treatable magnesium alloys for twin-roll casting.

5. **Amin, U.**, Mendis, C. L., Yang, X. L., Fan, Z., Poster Presentation 2019. UK Solidification Workshop, Brunel University London. Development of novel heat treatable magnesium alloys for twin-roll casting.

6. Mendis, C. L., Patel, J., Yang, X., Das, S., **Amin, U.**, Qiu, Y., Assadi, H., Huang, Y., Fan, Z., Annual Report 2021. Low-force MC-TRC processing of magnesium alloys, London: Liquid Metal Engineering Hub, BCAST.

# Contents

# List of Symbols and Abbreviations

| | |
|---|---|
| g/cm$^3$ - | grams per centimetre cubed |
| % - | percent |
| ℃ - | degrees celsius |
| MPa - | megapascals |
| HCP - | hexagonal closed packed |
| TRC - | twin-roll casting |
| mm - | millimetre |
| K/s - | kelvin per second |
| $\sigma_y$ - | yield strength |
| $\sigma_i$ - | dislocation stress |
| $k_y$ - | hall-petch coefficient |
| *d* - | average grain size |
| m$^{-0.5}$ - | metre to the power minus zero point five |
| μm - | microns metre |
| BCAST - | brunel centre for advanced solidification centre |
| at% - | atomic percent |
| wt% - | weight percent |
| S.S - | solid solution |
| $\Delta\tau$ - | shear stress |
| G - | shear modulus |
| *C* - | atom concentration |
| m - | screw dislocation |
| FCC - | face-centred cubic |

| | |
|---|---|
| b - | burgers vector |
| $\varepsilon$'G - | modulus mismatch |
| $\alpha$ - | alpha phase |
| $\beta$ - | beta phase |
| L - | liquid phase |
| $T_a$ - | ageing temperature |
| $T_m$ - | melting temperature |
| $T_s$ - | solid solution temperature |
| $C_0$ - | alloy composition |
| G.P. - | guinier-preston zones |
| $L_p$ - | mean planar centre-to-centre distance |
| F - | resistance to dislocation shearing |
| $\Gamma$ - | dislocation line tension |
| M - | taylor factor |
| $\nu$ - | poisson's ratio |
| $\lambda$ - | mean spacing of particles |
| $d_A$ - | mean diameter of particles |
| $r_0$ - | inner cut-off radius |
| BCC - | body centred cubic |
| nm - | nanometre |
| hrs - | hours |
| T4 - | homogenisation heat treatment |
| T6 - | homogenisation + peak aged heat treatment |
| YS - | yield strength |
| UTS - | ultimate tensile strength |

| | |
|---|---|
| K - | kelvin |
| LDH - | erichsen value |
| SEM - | scanning electron microscope |
| TEM - | transmission electron microscope |
| RD - | rolling direction |
| TD - | transverse direction |
| r-value - | plastic strain ratio |
| n-value - | strain hardening exponent |
| Ø - | diameter |
| $SF_6$ - | sulphur hexafluoride |
| m/min - | metre per minute |
| kW - | kilowatts |
| OPS - | oxide polishing suspension |
| ml - | millilitre |
| EDX - | energy dispersive spectrometry |
| kV - | kilovolts |
| SAED - | select area electron diffraction |
| HV1 - | hardness vickers with 9.8N force |
| $T_L$ - | experimental liquidus temperature |
| $T_H$ - | homogenisation temperature |
| J - | joules |
| ± - | plus or minus |
| BSD - | backscattered electron detector |
| h - | hour |
| VHN - | vickers hardness number |

| | |
|---|---|
| L/min - | litre per minute |
| EBSD - | electron backscatter diffraction |

# Chapter 1- Introduction

Research and development on magnesium reached a peak in between the years 1930-1950 (Kainer, 2003), a time when magnesium use increased for non-commercial applications such as the military, afterwards the interest decreased due to relatively low property profile of magnesium. Since 2000, magnesium alloy development has become an area of great interest, especially for commercial use due to its advantageous strength to weight ratio making it the lightest structural metal. The density of magnesium is 1.74 g/cm$^3$ which is one-fourth of steel and two-third of aluminium. As for aluminium and magnesium, the common denominator for the two is that they are structural metals that have relatively low density allowing them to be in competition amongst themselves in lightweight applications.

Due to higher specific strength, successful research and development into magnesium alloys should eventually lead to their use becoming greater in scale, especially where light weighting is of priority. Light weighting in industries like the automotive, aerospace and electronics has developed to become one of the most important driving forces for present and future manufacturing. This is primarily due to increased global demands for energy conservation i.e., fuel efficiency and environmental protection i.e., lower carbon footprint. A separate reason that has increased importance of light weighting in industries is the need to improve product performance.

Application of magnesium-based alloys is mainly used in interior of products manufactured by the automotive industry in the form of cast parts. The last decade has seen the use of magnesium alloy upscale in passenger cars for gear box housings and crank cases (Aghion, et al., 2003). Magnesium alloys in military applications have increased with the use of rare earth alloying elements. The US military has used various magnesium alloys in the Expeditionary Fighting Vehicle including ZE41 alloy for the transmission housing (Jeal, 2005). This military vehicle was only recently discontinued due to high cost in procurement and maintenance (DoD, 2011). Table 1.1 Lists number of magnesium alloy that have been developed including the details of their properties and applications.

To tackle potential drawbacks, it is incumbent to use and develop low density metals that also satisfy the requirement of having suitable mechanical properties such as applicable strength and formability. Magnesium alloy is the optimal choice but concerningly, use of the lightest structural metal in sheet form in automotive industry is limited to 1% of the average automobile by weight (Kim, 2014). The scope for using magnesium alloy sheets is particularly wide but their application is severely limited for justifiable reasons. Considering steel and aluminium, magnesium alloys come with significantly higher cost coupled with the fact that the corrosion resistance, strength and formability are not ideal.

In general, application of wrought magnesium alloys is hampered as the hexagonal closed packed (hcp) crystal structure of magnesium restricts the ability to form economically i.e., at room temperature. hcp crystalline structure of magnesium has limited number of active slip systems, namely 3 independent slip systems on the basal plane. The low number of active slip systems cause a strong basal texture of a processed magnesium alloy and so to accommodate further deformation, twinning is readily observed. Magnesium has a shortcoming in its ability to resist corrosion, another reason why the industries are further hesitant to adopt it in places where there is requirement for the metal to interact with atmospheric conditions. What has been established is that addition of rare earth elements has shown overall improvement in mechanical properties which are comparable to aluminium alloy 5xxx series but economically it is not feasible to turn to this critical resource group. (Hoppe, et al., 2016).

**Table 1.1- Commercially developed Mg alloys and their applications (Kulekci, 2008)**

| Alloy designation | Alloying additions | Applications | Property Profile |
|---|---|---|---|
| AZ91 | 9% Al, 0.7% Zn, 0.13% Mn | General casting alloy | Good castability, good mechanical properties at T<150℃ |
| AM60 | 6% Al, 0.15% Mn | High pressure die-casting alloy | Greater toughness and ductility than AZ91, slightly lower strength. Often preferred for automotive structural applications |
| AM50 | 5% Al, 0.15% Mn | General casting alloy | Good strength, ductility, energy absorption |

| | | | |
|---|---|---|---|
| | | | properties and castability |
| AE44 | 4% Al and 4% rare earth elements | General casting alloy | Better creep behaviour and castability than AE42 |
| AE42 | 4% Al and 2% rare earth elements | General casting alloy | Low castability, good creep behaviour |
| AS41 | 4.2% Al and 1% Si | General casting alloy | Better creep resistance than AZ91 at elevated temperatures but lower strength |
| ZE41 | 4.2% Zn, 1.2% RE and 0.7% Zr | Specialist casting alloy | Rare earth addition improves creep strength at elevated temperatures |
| AZ31 | 3% Al, 1% Zn and 0.2% Mn | Wrought alloy | Good extrusion alloy |
| AM20 | 2% Al and 0.15% Mn | Casting alloy | High ductility, toughness and poor die-castability |
| MRI 153M | Mg-Al-Ca-Sr system | Casting alloy | For high temperature applications up to 150℃ |
| MRI 230D | Mg-Al-Ca-Sr system | Casting alloy | For high temperature applications up to 190℃ |
| AS21 | 2% Al and 1% Si | Casting alloy | For use in temperatures in excess of 120℃ |
| AJ62 | 6% Al and 2% Sr | High pressure die-casting | Good thermal and mechanical strength, superior castability, corrosion resistance and creep resistance |

As it has been established, use of wrought magnesium alloy sheets on an industrial scale is limited. Even though magnesium alloys have the highest specific strength, one of the main factors that has contributed to its limitation in use is the considerably poor mechanical properties. This judgement of undesirable mechanical properties is handed down in the context of comparative analysis i.e., in relation to other low-density metals such as aluminium alloys. Effort has been exerted to address long lasting issues with the applicability of magnesium alloy sheets by analysing established alloying systems with differing compositions to understand their suitability with demands of industries. Focus has been put on finding a solution that

would randomise basal texture for formability improvement. There is a consensus on the traditional method of producing wrought sheets that it is costly and has ill-effect on formability. Magnesium alloy sheets have previously been produced through hot rolling with a yield strength around 250MPa. Unfortunately, along the way this causes strong basal texture by the increased rolling directions which results in strong yield anisotropy (Mendis, et al., 2010).

Numerous studies of TRC magnesium alloy sheet AZ31 have been conducted and there is significant pessimism regarding it due to insufficient strength, casting defects and poor formability. With increased zeal to match current and future trend of light weighting for performance and environmental reasons, there is a considerable need to develop high-strength magnesium alloys that also show appreciable formability. To date, majority of TRC processing is based on Mg alloy AZ31 (Mg-3Al-1Zn (wt%)) alloy. For many applications, alloys with higher strengths but with appreciable formability are required. The alloy design rational illustrated in Figure 1.1 is different to the standard processing path which includes hot rolling. There are four stages to the process, the first is to twin roll cast an alloy which is then heat treated to homogenize the microstructure. The next stage is to deform the sheet to the required shape which is then age hardened to obtain higher strength.

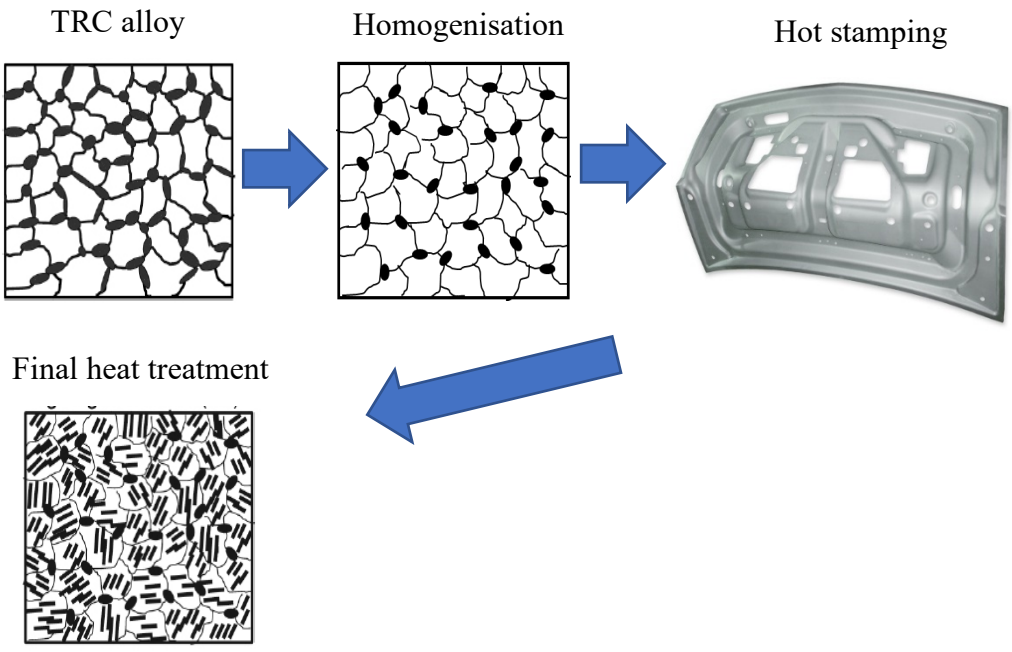


**Figure 1.1- Schematic illustration of the alloy design rational and pathway to producing high strength alloys**

Kim states that overall cost of using magnesium alloy sheets was one of the most important factors preventing earlier adoption in the automotive industry. The high cost is associated with several reasons such as high raw materials cost, unpredictable supply of material, the repetitive nature of many rolling steps and use of rare-earth elements in specific cases (Kim, 2014). Stated above are several reasons why it is costly to produce magnesium alloy sheets including use of rolling steps to reduce thickness of sheet to match final product thickness and use of rare-earth elements. Kim states that the repetitive nature of rolling can be eliminated completely by adopting twin roll casting which has previously shown to produce sheets thin as 2mm. Commercial application of wrought magnesium alloy sheets has for a long time lacked and one of the reasons for this is that the production involves several energy intensive manufacturing steps by the traditional route. The traditional route to produce magnesium alloy sheets entails hot rolling ingots which are produced by direct chill casting. As the as-cast structure of magnesium alloy ingots is very much coarse, a hot rolling process is carried out to produce thin sheets. This process means controlling the high temperature precisely, reheating the metal for each rolling step (Bian, et al., 2008). The typical process of producing a magnesium alloy sheet consists of many rolling and homogenisation steps. Therefore, what is being proposed is a unique alloy design that evidently considers some of the issues mentioned above by excluding processes that are energy intensive which mount up production cost.

Twin roll casting is an economically viable alternative manufacturing method which was initially developed by Sir Henry Bessemer in 1846 (Barekar & Dhindaw, 2014) for steel industry and it has only recently gained a lot of attention for magnesium production as there has been significant development in the technology and need to adopt wrought magnesium alloys. The technology makes a compelling case as it leads to labour and energy savings by the reduction of rolling steps. This reduction leads to lower energy consumption which inevitably points to decrease in investment cost. The TRC concept developed by Sir Henry Bessemer was for steel production and therefore did not take into account the inherent characteristics of magnesium.

Twin roll casting is a manufacturing process which combines casting and rolling to produce cast metal sheets by fast solidification of liquid metal at a rate of around $10^2$

K/s to $10^3$ K/s as opposed to approximately 50 K/s in conventional ingot casting (Tripathi 2016). There are differing designs and orientations of TRC that have been developed over the years including vertical TRC and melt drag TRC but horizontal TRC design shown in Figure 1.2 has been the focal point for research and development. In the case for the horizontal twin roll caster, the methodology of casting is as follows, molten metal is poured continuously into a tundish. The tundish allows smooth flow of molten metal towards two counter-rotating water-cooled rollers. As soon as there is contact between metal and rollers with continuous flow of liquid metal, fast solidification occurs to produce a metal strip. Parameters such as molten metal temperature, roll speed and strip dimension are variables depending on the metal and the specific application.

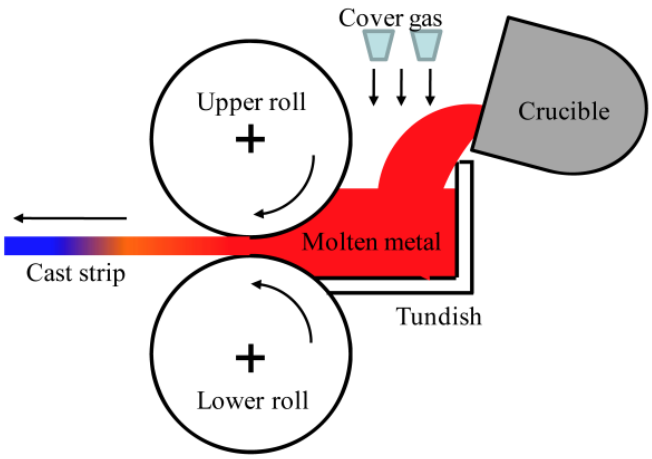


**Figure 1.2- Horizontal TRC setup (Noda, et al., 2014)**

So, there is a strong case to be made for further alloy development considering the potential and obstacles that have been highlighted. Suh et al mentions that novel alloy designs must be developed that seek to randomize texture by using cheaper alloying elements. He also puts forth a case for developing high-strength magnesium alloys that do not have a sluggish response to age-hardening which is a common theme to be found (Suh, et al., 2014). The report will therefore review ways in which enhancement of strength and weakening of basal texture can be achieved in conjunction with knowing the fact that twin roll casting is an economically viable manufacturing method that can be deployed. A greater understanding will be sought about the stage at which current development of magnesium alloys is at and seek a

solution for large scale industrial production of magnesium alloys that exhibit appropriate properties which can be compared with aluminium alloys.

## 1.1 Aims & Objectives

### 1.1.1 Aims

*'Develop thermally processed magnesium alloys for low-pressure twin roll casting with improved strength by low-cost alloying addition of Al, Zn, Ca and Mn and thus experimentally investigating the effect on microstructure, deformation behaviour and mechanical properties.'*

### 1.1.2 Objectives

Develop magnesium alloy(s) through a chosen alloy & TRC design process:

- To minimise cost, use non-rare earth elements as alloying additions.
- Develop Al, Ca, Mn, and Zn containing Mg alloys that are designed for TRC producing which will be followed by heat treatment to enhance the mechanical properties.
- Understand the role of alloying elements on solidification behaviour.
- Microstructural characterisation of novel alloy(s).
- Understand the age-hardening response and precipitation behaviour.
- Develop low-cost age-hardenable TRC magnesium alloy(s) with sufficient formability.

# Chapter 2- Literature Review

# Contents

## 2.1 Introduction

This chapter will review existing theories of strengthening mechanisms that are generally applicable to metals but more specifically to magnesium-based alloys. Alongside this, an evaluation of magnesium alloys that have recently been developed for general wrought applications. As part of the chapter, conventional horizontal twin-roll casting process will be assessed in accordance with magnesium alloy production suitability, this will involve alloy development constraints associated with this technology. A new twin-roll casting process called low-pressure TRC will be discussed in relevance to development of magnesium alloys.

## 2.2 Strengthening Mechanisms

There are number of mechanisms available to metallic materials for strengthening the base metal through alloying additions. These include work hardening, grain size strengthening (Hall-Petch strengthening), solute strengthening and precipitation hardening. From these, grain size strengthening has been used in magnesium alloys extensively in comparison to the remaining three mechanisms. Solute strengthening has been readily observed by adding common elements such as aluminium and zinc. Recent developments of precipitation hardening of magnesium alloys has been positive with clear instance of rapid ageing through alloying of Zn and Ca (Bian, et al., 2017). Work hardening may not be a viable mechanism in most magnesium alloys due to the limited number of deformation mechanisms available. In the following sections strengthening using grain size, solute and precipitation strengthening will be discussed with mechanisms that may be used to enhance each of the strengthening pathways.

### 2.2.1 Grain Boundary Strengthening

Grain boundary strengthening encompasses the Hall-Petch relationship, $\sigma_y = \sigma_i + \frac{k_y}{\sqrt{d}}$ which focuses on grain size and the observed phenomenon of grain boundaries impeding dislocations. $\sigma_y$ represents the yield strength of material, $\sigma_i$ is a material's constant that states the stress at which dislocations begin to occur, $k_y$ is the Hall-Petch coefficient and *d* is the average grain size. The Hall-Petch coefficient has contrasting values which are dependent on the grain size due to deformation

mechanisms. Small grain sized magnesium alloys are dominantly deformed through dislocation slip which have a reduced $k_y$ value, whereas the larger grain sized magnesium alloys deform by twinning (Jain, et al., 2008) which have a higher $k_y$ value. $k_y$ value is approximately 0.7 MPa $m^{-0.5}$ for coarse grains in the region of 30-87μm and 0.13 MPa $m^{-0.5}$ for grains in the region of 17-30μm (Koike, 2005). Study on the compressive deformation of AZ31 alloy with grain size smaller than 17μm showed two Hall-Petch coefficient values, one observed at 10μm at 150°C and 15μm at 200°C. This was due to change in deformation mechanism from twinning to dislocation slip with reduction in grain size (Barnett, et al., 2004). The $k_y$ values are considerably greater than aluminium alloys, which means grain refinement is a sensible approach to adopt. The Hall-Petch relationship states that when there is a decrease in grain size, there is increase in strength.

Grain size strengthening of a metal can be adversely affected if grains grow too large, this results fewer grain boundaries for dislocations to impede. Grain growth occurs when heat treatment is applied at an elevated temperature for a prolonged period. Grain growth begins when there is observation of grain boundary straightening, this phenomenon paves way for fine grains to shrink and coarse grains to grow at their expense. Grain boundary energy is reduced when grains grow, in which reduction in total boundary area occurs, resulting in decrease in total energy. As is the reality of binary and other multicomponent systems, there is inevitability of intermetallic phases being present. So, grain boundary strengthening also takes into consideration their impact on the microstructure in terms of strengthening. Mendis et al explains in their work on the development of high-strength magnesium alloys that intermetallic phases at grain boundaries can halt grain growth and at elevated temperatures, it is possible to prevent deformation that is to do with grain boundary motion (Mendis, et al., 2015). To decrease this susceptibility, grain refinement or decreasing grain size contributes to making it more difficult for cracks to propagate through the easier path so to speak and hence this leads to strengthening. As for magnesium alloy grain refinement, this can occur in several ways such as by controlling solidification rate, adding alloying elements, and wrought processing. High rate of solidification gives arise to finer grains as observed in twin-roll casting in comparison to ingot casting. The study of Sun et al on trace addition of Zr for alloy Mg–10Gd–3Y has shown to produce finer grains (Sun, et al., 2009). Interestingly, it

is debatable as to whether there is a need to specifically add an element for grain refinement because it has been seen that magnesium has the potential to self-grain refine. The high shearing technology developed at BCAST has been shown to promote a refined and equiaxed magnesium microstructure (Bian, et al., 2008). In one study, melt shearing reduced the size of grains in AZ91D from 550μm to 170μm, this has been attributed to magnesium oxide films being dispersed effectively which results in them acting as heterogenous nucleation sites for magnesium grains (Patel, et al., 2017).

### 2.2.2 Solute Strengthening

Solute strengthening which is also termed as solid solution strengthening is another mechanism of strengthening and it explains the relationship between the interaction of solvent and solute atoms. This mechanism relies on an alloying element (solute atoms) to dissolve into the matrix (Magnesium in this case). When a solute atom embeds into the matrix, it causes lattice strain in the surrounding atoms. There are two types, namely interstitial solid solution, and substitutional solid solution. Interstitial solid solution strengthening describes the solute atoms that are much smaller in size to their counterparts i.e. solvent atoms and this difference in size allows them to occupy space found in between solvent atoms. This phenomenon means there is impeding of dislocations as space is occupied therefore leading to strengthening. This form of solid solution is not common due to restriction in availability of interstice size in most known crystal lattices, therefore only atoms with small atomic radii can form interstitial solid solution (Smallman, 1985). As for substitutional solid solution strengthening, this requires solute atoms to be of the same or similar size of solvent atoms.

For a homogeneous solid solution to be formed, the crystal structure of host material must remain the same. There are other important factors that determine the suitability of solute atoms forming homogeneous solid solution, these include atomic size factor, electronegativity, and valences. It is understood that if the difference in atomic radii of solvent and solute atoms is less than ±15%, then considerable quantity of solute can be added to obtain solid solution. As an example, copper and nickel are completely soluble in one another as they have the same crystal structure, little difference in atomic radii and electronegativities of 1.9 and 1.8 (Callister, 2007).

On the other end of the spectrum is the case of adding an alloying element that does not interact with host material, such as the complete insolubility of sodium and potassium with magnesium.

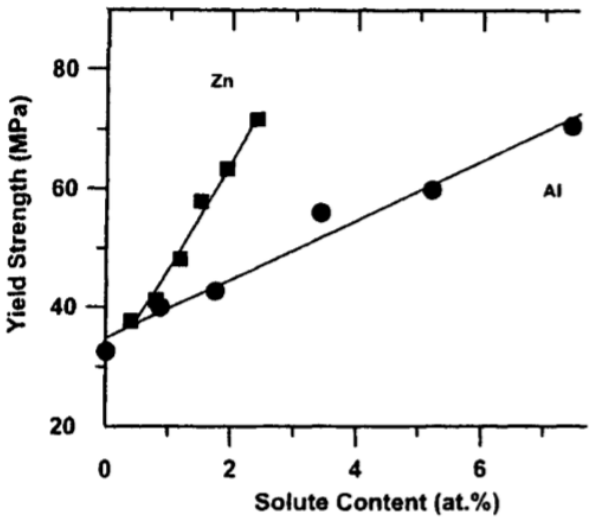


**Figure 2.1- Yield strength increase in respect of solute content of Al and Zn in Mg (Polmear, 1994)**

Most magnesium alloys are comprised of aluminium and zinc as the main alloying elements because of observed strengthening as shown in Figure 2.1. Aluminium and zinc as alloying additions are soluble with magnesium, their maximum solubility limit is defined by a eutectic point on a phase diagram. The maximum solid solubility limit of aluminium is 11.6 at% and for zinc it is 2.4 at% as shown in Table 2.1. Formation of primary solid solution is not possible beyond the limit and instead intermetallic compounds form. As an example, solid solution strengthening has readily been observed in Mg-Zn binary alloy (Caceres & Blake, 2002).

**Table 2.1- Solubility data for binary magnesium alloys (Polmear, 2005)**

| Element | At. % | Wt. % | System |
|---|---|---|---|
| Lithium | 17 | 5.5 | Eutectic |
| Aluminium | 11.8 | 12.7 | Eutectic |
| Silver | 3.8 | 15 | Eutectic |
| Yttrium | 3.75 | 12.5 | Eutectic |
| Zinc | 2.4 | 6.2 | Eutectic |
| Neodymium | 1 | 3 | Eutectic |
| Zirconium | 1 | 3.8 | Peritectic |
| Manganese | 1 | 2.2 | Peritectic |
| Thorium | 0.52 | 4.75 | Eutectic |
| Cerium | 0.1 | 0.5 | Eutectic |
| Cadmium | 100 | 100 | Complete S.S |
| Indium | 19.4 | 53.2 | Eutectic |
| Thallium | 15.4 | 60.5 | Eutectic |
| Scandium | 15 | 24.5 | Peritectic |
| Lead | 7.75 | 41.9 | Eutectic |
| Thulium | 6.3 | 31.8 | Eutectic |
| Terbium | 4.6 | 24 | Eutectic |
| Tin | 3.35 | 14.5 | Eutectic |
| Gallium | 3.1 | 8.4 | Eutectic |
| Ytterbium | 1.2 | 8 | Eutectic |
| Bismuth | 1.1 | 8.9 | Eutectic |
| Calcium | 0.82 | 1.35 | Eutectic |
| Samarium | 1 | 6.4 | Eutectic |
| Gold | 0.1 | 0.8 | Eutectic |
| Titanium | 0.1 | 0.2 | Peritectic |

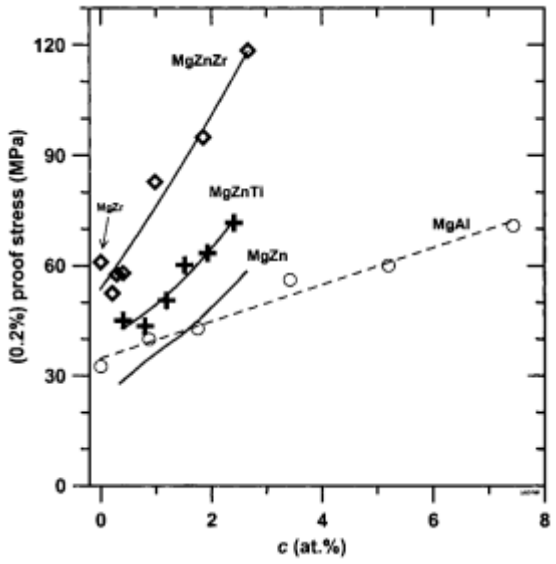


**Figure 2.2- (0.2%) proof stress of the Mg-Zn alloys compared with that of Mg-Al and Mg-Zr alloys as a function of the atom concentration of solute (Caceres & Blake, 2002)**

Outlined above in Figure 2.2 is solute strengthening heat treatment and subsequent mechanical testing performed by Caceres et al for Mg-Zn binary alloy. As can be observed, 0.2% proof stress shows significant improvement in strength with increase of solute content. In the case of Mg-Al binary alloy, solute strengthening has readily been observed and documented. To highlight this, Caceres et al plotted proof stress against at% of Mg-Al binary alloy. It can be said with certainty that increment of proof stress coincided with increase in at% of aluminium. Magnesium alloys therefore react positively to this form of strengthening. Solid solution strengthening can be theoretically predicated through two models that seek to understand the interaction between dislocation and solute atoms, the name of these two models is Fleischer's model and Labusch's model. The fundamental difference between the two models is that Fleischer's model considers solute atoms as isolated pinning sites and whereas Labusch's model considers the collective action of the solute atoms lying on the gliding plane, therefore the latter model is more applicable to highly concentrated solid-solutions whereas Fleischer's model is used for dilute concentration of solute of less than 1at% (Kadambi, et al., 2017).

$$\Delta\tau = \frac{G|\varepsilon'_G - m\varepsilon_b|^{\frac{3}{2}} c^{\frac{1}{2}}}{\alpha}$$

**Equation 2.1**

(Fleischer, 1963)

$$\Delta\tau = \frac{G\left[\varepsilon'^{2}_{G} + (15\varepsilon_b)^2\right]^{\frac{2}{3}} c^{\frac{2}{3}}}{\varphi}$$

**Equation 2.2**

(Labusch, 1972)

In the above equations, $\Delta\tau$ stands for shear stress that is required for dislocation movement while G is the shear modulus. *C* represents the concentration of atoms while m is for screw dislocations. $\alpha$ and $\varphi$ represent 700 and 550 respectively for FCC alloys. $\varepsilon b = (db/dc)/b$ is the atomic size mismatch (b: Burgers vector) and $\varepsilon'G$ is the modulus mismatch parameter given as:

$$\varepsilon_G^{'} = \frac{\varepsilon_G}{1 + 0.5\varepsilon_G}$$

**Equation 2.3**

The symbol εG = (dG/dc)/G which is the modulus mismatch.

### 2.2.3 Precipitation Strengthening

Precipitation strengthening which is also commonly referred to as age hardening requires thermal processing to produce second phase nanoscale particles that are ideally uniformly dispersed within matrix of first phase. These nanoscale particles are known as precipitates and their presence impedes dislocations to enhance strength.

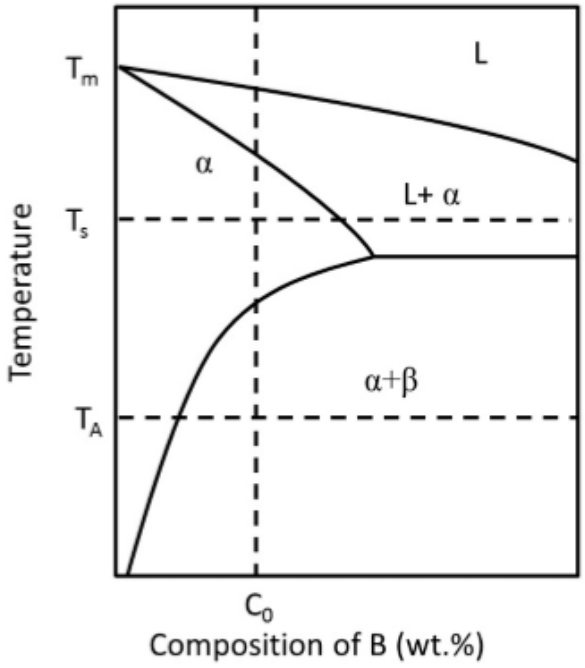


**Figure 2.3- Precipitation activity shown on a diagram (Bhattacharjee, 2014)**

Above is Figure 2.3 to schematically illustrate how generally precipitation strengthening works in relation to a phase diagram. $T_A$ represents ageing temperature while $T_s$ and $T_m$ represent solid solution temperature and melting temperature respectively and finally $C_0$ represents the composition of the alloy being examined. The first step is to homogenise the alloy by doing solid solution heat treatment $T_s$, noting that the temperature and composition meet at the single phase α region. As mentioned previously, the idea is to dissolve solute atoms into the α-

phase to produce a uniform solid solution structure. As for magnesium alloys, homogenization step is completed when quenching in water is done immediately but there are other methods too to cool down an alloy such as oil quenching. This process of rapid cooling preserves the supersaturated solid solution structure below the homogenization temperature by not allowing the solute atoms to diffuse out of phase if the temperature is slowly lowered. At this stage, the alloy is ready to be age hardened, so the alloy is heat treated to a temperature below $T_s$ in the two-phase region for a period until peak hardness is achieved (ageing).

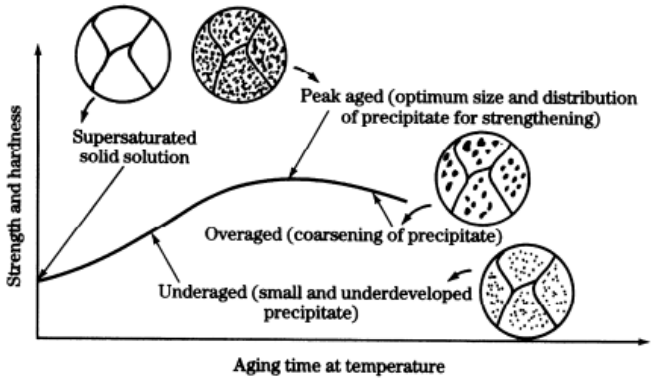


**Figure 2.4- Stages in precipitation hardening (Smith, 1993)**

There are three stages in an age hardening process as illustrated in Figure 2.4, the initial stage i.e. under aged stage involves clustering of solute atoms in a coherent fashion with the matrix meaning it can be observed that the clustering matches the crystal lattice of solvent atoms, this occurrence is termed as Guinier-Preston zones. For most instances, G.P. zones are not common in magnesium alloys but for an example, G.P. zones have been observed in Mg-Zn-Al alloy when aged at 70°C, these zones are enriched with Zn atoms and act as heterogeneous nucleation sites for metastable phases which lead to finer distribution of precipitates (Nie, 2012). The second stage is when peak ageing occurs whereby hardening has reached pinnacle, this is due to equilibrium distribution of fine precipitates. The final stage is when over ageing occurs which is also known as Ostwald ripening, this is when precipitates coarsen i.e. particle enlargement leading to eventual decrease in strength.

The precipitation strengthening activity is categorised by the behaviour of dislocations towards precipitates, whether dislocations shear i.e. cut through precipitates, known as the Friedel effect or loop around the precipitates which is called Orowan looping. When the Friedel effect occurs, the particles upper part is displaced in relation to the dislocation slip plane. As a result of this displacement, the phase boundary area is increased causing increase in critical shear stress. Dislocation shearing occurs in the case of coherent precipitates while Orowan looping occurs in the case of non-coherent precipitates as the dislocation bypasses the precipitate due difference in lattice structure (Barrilao, 2017).

The contribution of shearable precipitates can be ascertained through the following equation,

$$\Delta\tau_p = \frac{2}{L_p b\sqrt{\Gamma}}\left(\frac{F}{2}\right)^{\frac{3}{2}}$$

**Equation 2.4**

$L_p$ is the mean planar centre-to-centre distance between particles, b is the Burgers vector, F is a measure of the resistance of the precipitates to dislocation shearing and T is the dislocation line tension in the magnesium matrix (Nie, 2012).

Looping or bowing stress can be theoretically established through the Orowan equation which considers M, Taylor factor, G, shear modulus, b, Burgers vector of dislocation, *v,* Poisson's ratio, λ, mean spacing of particles in the slip plane, $d_A$, mean diameter of particles in the slip plane $r_o$ is the inner cut-off radius of the dislocation taken equal to b (Kelly & Nicholson, 1971).

$$\sigma_{orowan} = \left(\frac{MGb}{2\pi\sqrt{1-\nu}}\right)\frac{1}{\lambda}\ln\left(\frac{d_A}{r_0}\right)$$

**Equation 2.5**

(Gradwell, 1972) sought to understand precipitation hardening of QE22 alloy and observed that peak hardness occurred after transition between dislocations cutting/shearing precipitates to eventually looping precipitates with the presence of two types of precipitates. Whereas (Bae, et al., 2009) characterized $Al_2Ca$ precipitate particles that couldn't be sheared in AZ31-0.7Ca, the same has also been observed for the β-phase $Mg_{17}Al_{12}$ in the Mg-Al binary alloy. It can be understood that

precipitates regardless of where they originate from have their specific capacity to resist dislocation shearing and looping.

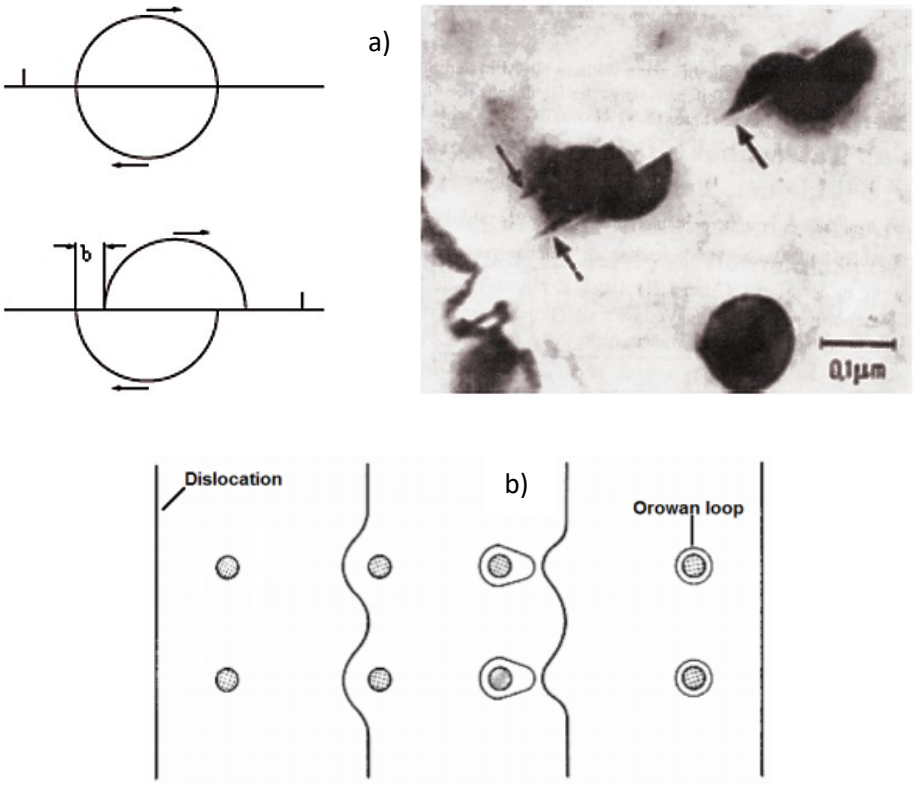


**Figure 2.5- Dislocation behaving in two ways; a) shearing of precipitate particles (Riehle & Simmchen, 2000) and b) looping of precipitate particles (Gottstein, 2007)**

## 2.3 Precipitation Hardening in Magnesium Alloys

The precipitate morphology is dependent on the concerned alloy system but generally the following morphologies are to be commonly observed:

- Plate like formation on the basal plane
- Plate like formation on the prismatic plane
- Rod like formation parallel to [0001] direction
- Lath like particles
- Spherical like particles

The strengthening contribution depends on the orientation and the morphology of the particles. Precipitate phases can be either metastable or in equilibrium and (Nie, 2012) explains that these phases are formed parallel or normal to the basal plane of the magnesium matrix phase.

As for Mg-Al binary alloy with phase diagram shown in Figure 2.7, the eutectic temperature is 437°C and therefore the maximum solid solubility at this point is 12.9% wt. Below the eutectic temperature, phases such as $Mg_{17}Al_{12}$, $Mg_2Al_3$ and R have been presented. The R-phase has a composition of 42 at% magnesium with a rhombohedral crystal structure and forms due to a peritectoid reaction of β-phase and $\gamma$-phase at $370 \pm 5$°C (Murray, 1982). Precipitates in Mg-Al system are categorised into two; 1) continuous precipitates and 2) discontinuous precipitates, continuous precipitates occur within grains whereas discontinuous precipitates initiate at grain boundaries but have the potential to expand all the way to the centre of a grain. The precipitate that has been characterized in the Mg-Al binary alloy is the β-phase $Mg_{17}Al_{12}$ which is shown in Figure 2.8. The Mg-Al system has reportedly shown lath like particles forming on [0001] planes of magnesium and there has not been any reports of intermediate or metastable phases reported to form prior to the formation of equilibrium of $Mg_{17}Al_{12}$ phase. The precipitate phase sequence is illustrated in Figure 2.6 below,

Mg-Al SSSS→ β ($Mg_{17}Al_{12}$)

BCC (143m, $a$ = 1.06nm); $(0001)_a$ plate/lath

**Figure 2.6- Precipitate sequence in Mg-Al binary alloy (Nie, 2012)**

Both, continuous and discontinuous precipitates have been established as following the Burgers orientation relationship, $(011)_\beta // (0001)_\alpha$, $[1\bar{1}1]_\beta // [2\bar{1}\bar{1}0]_\alpha$ (Crawley & Miliken, 1974).

The age hardening response of highly concentrated AZ91 at temperatures 150°C is relatively slow with peak hardness achieved approximately after 100 hours (Celotto, 2000). (Nie, 2012) mentions that this phase can resist dislocation shearing but its slow ageing response is attributable to coarse distribution throughout. There are two possible causes for this behaviour and one of them is that aluminium atoms have high diffusion rate so they diffuse relatively well into the α-magnesium matrix, the other reason being is the possibility of high concentration of vacancies in the α-magnesium matrix. (Bettles, et al., 1997) did research into microalloying of several elements to AZ91 to understand and more importantly try to enhance the age hardening response of Mg-Al systems, they found that there wasn't significant enhancement in response. Though more recently, work on Mg-Al system with dilute alloying additions has significantly enhanced response, as it will be demonstrated later in (Bian, et al., 2017) study on novel composition Mg-1.1Al-0.3Ca-0.2Mn-0.3Zn (at%).

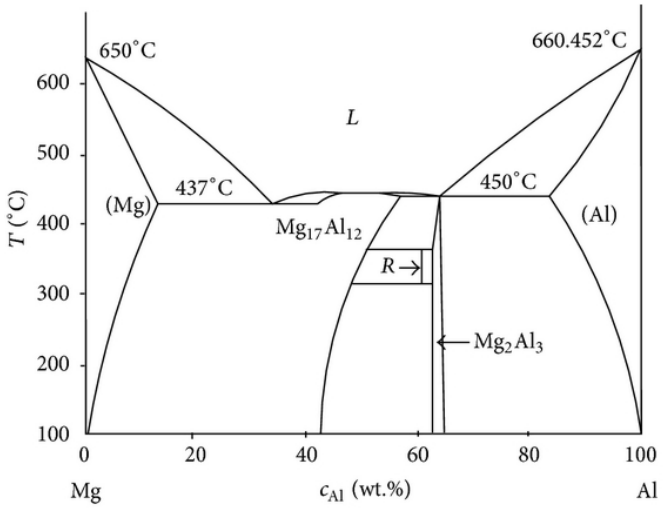


**Figure 2.7- Mg-Al binary alloy phase diagram (Okamoto, 1998)**

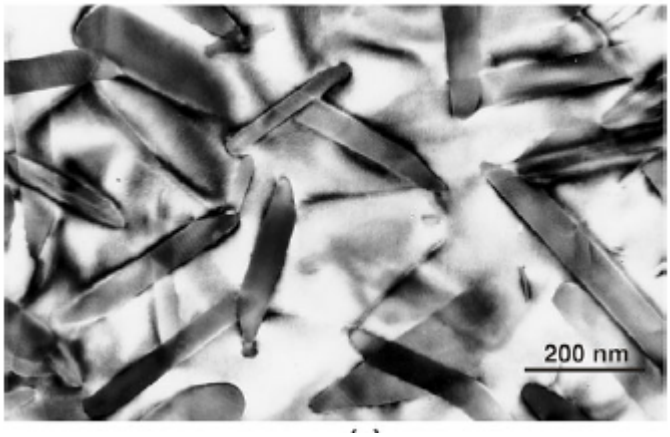


**Figure 2.8- β-phase precipitates in AZ91 sample aged for 8 hours at 200°C (Nie, 2002)**

The Mg-Zn binary alloy with phase diagram shown in Figure 2.9 has a eutectic temperature of 340°C and the maximum solid solubility of zinc is 6.2% wt or 2.4% at.

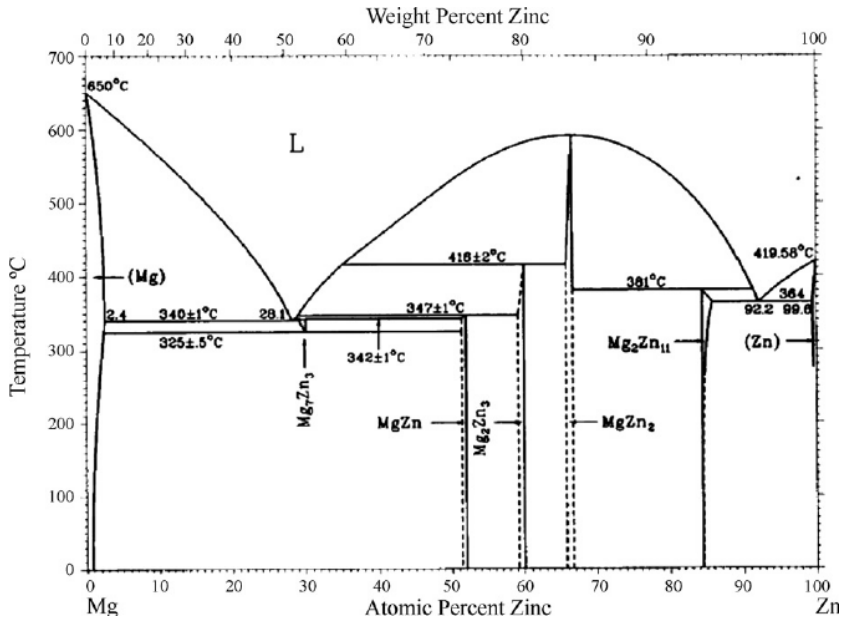


**Figure 2.9- Mg-Zn binary alloy phase diagram (Okamoto, 1994)**

The Mg-Zn binary alloy phase diagram is much more complex in comparison to the Mg-Al binary alloy phase diagram as shown in Figure 2.9. The Mg-Zn binary alloy phase diagram shows that after reduction of temperature from the eutectic point, a $Mg_7Zn_3$ intermetallic phase is formed and it remains stable above 325°C coinciding with α-magnesium phase. Below the mentioned temperature, a eutectoid reaction occurs which leaves MgZn intermetallic phase alongside α-magnesium phase. The maximum solid solubility of Zn decreases substantially with decrease in temperature from the eutectic temperature and the MgZn phase remains stable just above 50% at

of the Mg-Zn binary alloy as shown in the phase diagram. As for precipitates, it is known that after the decomposition of the supersaturated solid solution, three phases are formed in stages which are classified into three distinct morphological phases. Nie illustrates this sequentially in Figure 2.10,

| Mg-Zn | SSSS→ G.P. Zones→ | $\beta'_1$ ($Mg_4Zn_7$) | → | $\beta'_2$ ($MgZn_2$) | → $\beta'_2$ (MgZn) |
|---|---|---|---|---|---|
| | | Monoclinic, B/2m | | HCP, $P6_3/mmc$ | Monoclinic |
| | | *a* = 2.60nm | | *a* = 0.52nm | *a* = 1.61nm |
| | | *b* = 1.43nm | | *c* = 0.86nm | *b* = 2.58nm |
| | | *c* = 0.52nm | | $(0001)_\alpha$ plate | *c* = 0.88nm |
| | | *γ* = 102.5° | | | *β* = 112.4° |
| | | $[0001]_\alpha$ rod | | | |

**Figure 2.10- Precipitate sequence in Mg-Zn binary alloys (Nie, 2012)**

The precipitate sequence consists of formation of G.P. zones, $Mg_4Zn_7$, $MgZn_2$ and MgZn. The phase $Mg_4Zn_7$ isn't shown on the phase diagram as it is metastable, eventually after heat treatment it transitions to become the equilibrium phase MgZn. Nie et al alludes to the fact that $Mg_4Zn_7$ could possibly be identical to $Mg_2Zn_3$ (Nie, 2012). The metastable $Mg_4Zn_7$ has a Burgers orientation relationship of, $[001]_{Mg4Zn7}$ ~ // $[0001]_\alpha$ and $(630)_{Mg4Zn7}$ ~ // $(01\bar{1}0)_\alpha$ (Gao & Nie, 2007). The other metastable phase $MgZn_2$ has a Burgers orientation relationship of $(0001)_{\beta'2}$ // $(0001)_\alpha$ and $[11\bar{2}0]_{\beta'2}$ // $[10\bar{1}0]_\alpha$ (Wei, et al., 1995).

The age-hardening response of Mg-Zn binary alloys is somewhat limited and so efforts have been made to enhance response through alloying additions. Recently, microalloying of Ca and Ag as has shown to substantially increase peak hardness as illustrated in the following graph shown as Figure 2.11.

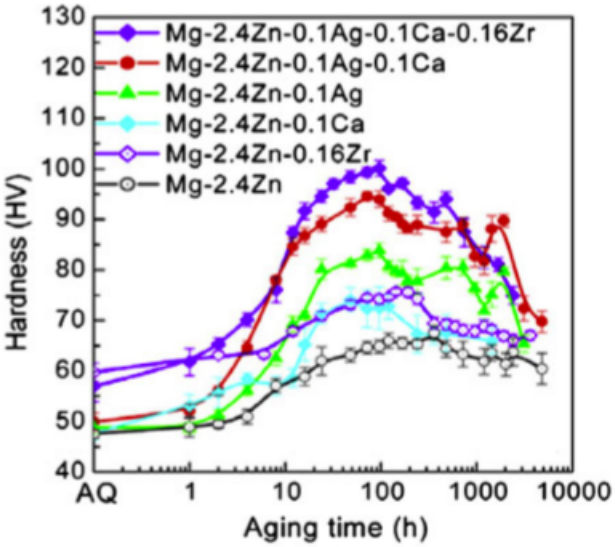


**Figure 2.11- Age hardening response of Mg-Zn system at 160°C with and without the role of microalloying (Mendis, et al., 2009)**

The increased age-hardening response by adding Ca and Ag is attributed to refined distribution of rod-shaped precipitates, Mendis et al reported these precipitates to be of $MgZn_2$ phase. In an age-hardened binary alloy of this alloy system, $MgZn_2$ are readily observed to be distributed coarsely but by adding alloying elements, number density increase has been achieved. Elsewhere, the addition of Zn to Mg-Ca alloy has shown an enhancement to ageing response through formation of large number density of single layer ordered G.P. zones (Oh, et al., 2005). Current understanding indicates that the formation of G.P. zones is due to large negative enthalpy of mixing between Ca and Zn atoms due to difference in size. It can be ascertained that increasing number density of precipitates is essential for improving yield strength and through microalloying, heterogenous nucleation sites become readily available. Heterogenous nucleation has also been explored through double ageing and deformation i.e. cold working. To illustrate that there are several methods, previously in the Mg-Al system, heterogenous nucleation has occurred of $Mg_{17}Al_{12}$ phase on lattice defects due to cold working. Cold working caused the density of dislocations to increase alongside twinning before the ageing treatment. Park et al produced Mg-Zn alloy containing 6wt% zinc, 3wt% aluminium and 1wt% manganese through twin roll casting and hot rolling. Double ageing treatment was applied with an initial pre-ageing treatment of 70°C for 24hrs and subsequent ageing treatment at 150°C for 24hrs. The tensile yield strength came to a high value of 319MPa even though

elasticity was compromised at 6% (Park, et al., 2007). The same alloy was worked on by Oh-ishi et al but analysed with a longer pre-ageing treatment of 48hrs. The analysis showed an increase in age hardening due to pre-ageing with microstructure showing finer precipitates in the double aged condition (Oh-ishi, et al., 2008).

Nie stated that majority of magnesium alloys that are respondent to age-hardening, are strengthened by precipitate plates that are located on the basal plane i.e. $(0001)_\alpha$. As alloy strength is dependent on these precipitates, their characterization has led to the understanding that their inherent morphology is less than desirable. They are extremely thin, no more than 1nm and they have a remarkably high aspect ratio and interparticle spacing. A viable solution to increase their contribution to strength is by significant increase in number through heterogeneous nucleation. Therefore (Nie, 2012) acknowledges the limitation and presents a solution which is to introduce prismatic plates of large aspect ratio that would either replace or coexist with the $(0001)_\alpha$ precipitate plates.

Previously prismatic plates have been observed in the Mg-Y-Nd and Mg-Gd-Nd alloys having large diameter and high number density after plastic deformation, as is shown in Figure 2.12 b).

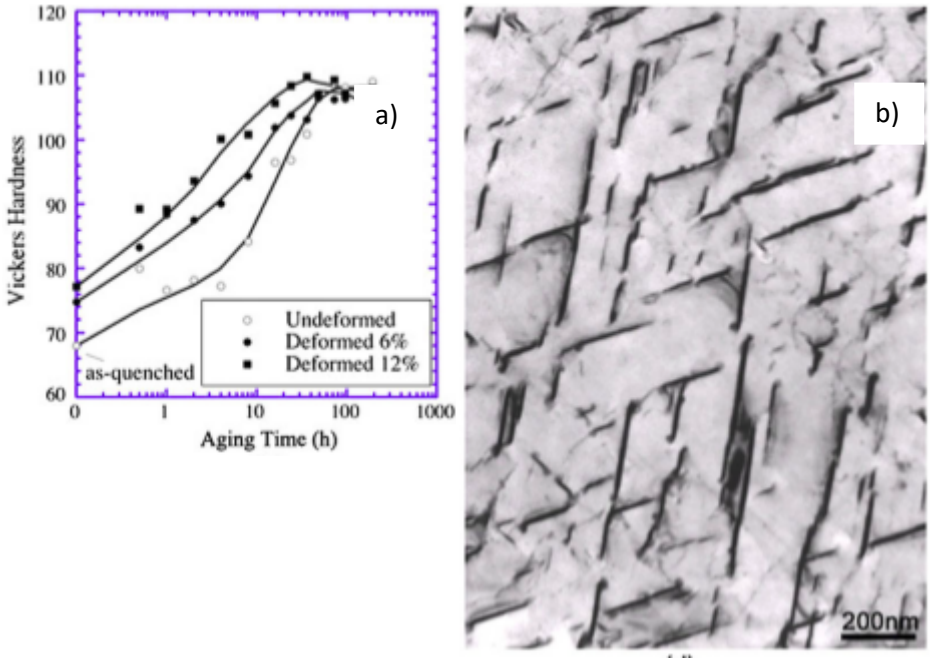


**Figure 2.12- a) Ageing response of WE54 at 200°C and b) TEM image of prismatic plates of samples cold-worked 6% after water quench and then aged to peak hardness at 250°C (Hilditch, et al., 1998)**

As can be seen from the hardness response in Figure 2.12 a), the influence of these precipitates on the age-hardening response is a positive one. Deforming increased number density of these precipitates and as in the non-deformed condition, these precipitates showed coarse distribution. So, it can be stated that the known presence of prismatic plates in this system has successfully decreased interparticle spacing which leads to increase in strength. This reduction in interparticle spacing is due to prismatic plates having large diameter and high number density. Below is Figure 2.13 showing positioning of prismatic plates.

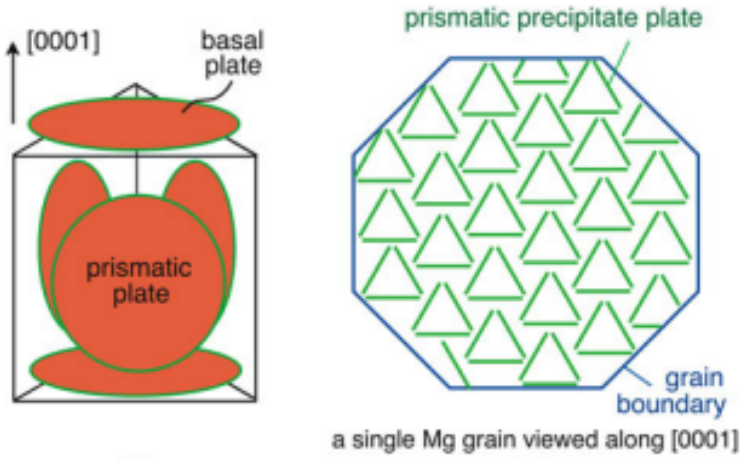


**Figure 2.13- Positioning of prismatic plates viewed along basal plane (Nie, 2012)**

Prismatic plates have also been observed in the Mg-In-Ca system with highly dense distribution on the $\{10\bar{1}0\}_\alpha$ plane. They have been described as fully coherent with the matrix phase and being 20nm in diameter and having a thickness which ranges between three planes of atoms. Mendis et al as shown in Figure 2.14 reported that by adding 0.3 at% of calcium to Mg-In alloy system containing an amount of indium ranging between 0.6 to 1 at% led to significant increase in ageing response, attributed to prismatic plates as mentioned previously.

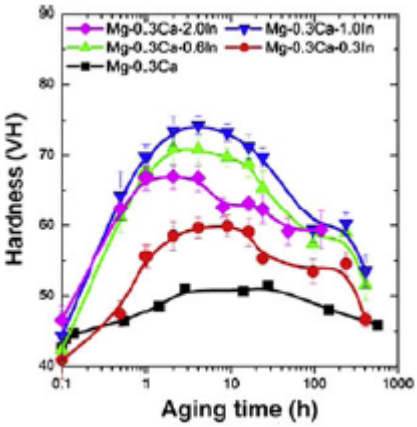


**Figure 2.14- Ageing response of Mg-In alloy with addition of Ca (Mendis, et al., 2011)**

Nie mentions that prismatic precipitate plates give the most resistance against basal dislocations and twins that operate in the plastic deformation process paving way for increase in strength. The effective interparticle spacing of prismatic plates and basal plates is shown in relation to aspect ratio.

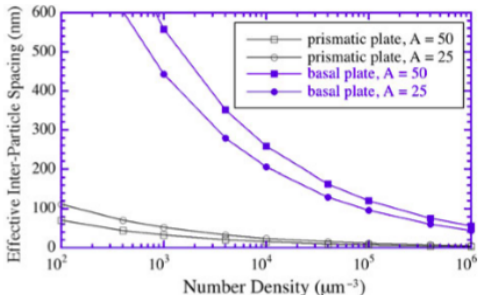


**Figure 2.15- Number density for prismatic and basal precipitate plates calculated assuming Orowan strengthening of shear-resistant particles with a volume fraction of 0.03. (Nie, 2012)**

The graph shown in Figure 2.15 demonstrates that prismatic plates have a considerably small effective interparticle spacing which means these particles are closely spaced regardless of number density and plate diameter. A commonality between the two is that as the number density increases, the interparticle spacing reduces. The contrast in interparticle spacing throughout a range of number density is far more inconsistent for basal plates. Having unearthed the potential that prismatic plates have for the development of high strength magnesium alloys; it is a long way before a systematic understanding is achieved.

Over the years, collative work to understand precipitation activity in magnesium alloys has contributed significantly to sourcing and combining work in this area and summarised in the review paper, *'Precipitation and Hardening of Magnesium Alloys'*, where Nie outlines gaps in knowledge that are yet to be understood. After presenting all the relevant work on ways to strengthen magnesium alloys, he puts forth microalloying amongst others as one plausible path to take. He highlights four areas that need attention if there is going to be a concerted effort to produce high strength magnesium alloys, firstly understanding the structure and composition of early-stage precipitates and their sequential behaviour i.e. how one precipitate phase leads to the nucleation of a completely independent precipitate phase in terms of morphology. Secondly, why basal plates are the dominant precipitate phase to form in majority of magnesium alloys and how to increase their thickness beyond the first unit cell height. Thirdly, how to promote prismatic precipitate plates heterogeneously alongside basal plates with large aspect ratio. Lastly, how the interaction of morphologically different precipitate phases with twinning and dislocation effects the strength.

## 2.4 Wrought Magnesium Alloys

ZK system is considered the strongest wrought magnesium alloy system that is adopted for commercial use. Yet, it responds slowly to age-hardening due to course distribution of $MgZn_2$ precipitates and it has shown to have poor elevated temperature mechanical properties. Aside from strength improvement being an important factor for future development of wrought magnesium alloys, developing alloys that can be appropriately deformed into desired component shapes is another challenge. The most common wrought magnesium alloy is AZ31, this alloy displays considerable anisotropic mechanical properties and strong basal texture which makes deforming at room temperature a problem that translates into brittle failure. Magnesium's crystal structure is a hindrance to formability as only basal slip is in operation at room temperature but by alloying, weakening of basal texture has readily been observed with the addition of rare-earth elements which is beneficial for triaxial deformation. Rare-earth elements also have high solid solubility limit which means they can be useful for strengthening through solid solution treatment and precipitation hardening. Zhou et al studied the mechanical properties of as-extruded binary Mg-3Y at room temperature and found that the elongation to failure was at a high 33%. The reason for this was attributed to several slip modes but one stood out as it is not typically active during ambient temperatures. It was found that non-basal slip was active in amongst basal slip, extension twinning, contraction twinning and slip-twin interaction. Before thorough investigations began on rare-earth containing magnesium alloys, it was commonly understood that non-basal slip such as pyramidal slip can only be activated during elevated temperatures. This is so because the critical resolved shear stress of non-basal slips is reduced at elevated temperatures. Researchers have previously reported yield strength and ultimate tensile strength of novel magnesium alloys exceeding 400MPa respectively. As an example, (Xu, et al., 2012) produced rare-earth containing magnesium alloy by large-strain hot rolling and ageing. There are similar instances observed by other researchers around strengthening by use of rare-earth elements.

There are two major contentions with using rare-earth containing magnesium alloys and the first one is that they increase cost exponentially as rare-earth elements are categorized as a critical resource group. There is also the problem of decreasing

specific strength with high concentrations of rare-earth elements which defeats the purpose of magnesium being a much lighter option to aluminium. As an example, the novel rare-earth containing magnesium alloy produced by (Xu, et al., 2012) contains above 8% of gadolinium and 3.8% of yttrium in weight percentage. Gadolinium's density is reported to be 7.90 g/cm$^3$ and yttrium's density is reported to be 4.47 g/cm$^3$. The adoption of magnesium alloys in light weighting industries wouldn't garner much support due to mentioned grounds. There are clear constraints that should be considered when looking to develop magnesium alloys for the purpose of wanting to increase strength to match requirements of industries.

Focus must be put on rare-earth free magnesium alloy systems as the future if there is serious intention behind alloy development. This inevitably means exploring promising options as stated by (Pan, et al., 2016) such as magnesium-aluminium, magnesium-calcium, and magnesium-zinc systems. Strengthening mechanisms are an essential part to strength enhancement and so characterizing and gaining an in-depth knowledge of their microstructural impact is vital. There are several mechanisms by which are inter-connected in some way or the other, they are grain boundary engineering, solute strengthening and precipitation strengthening.

Recently, it has been observed that microalloying is an effective approach to enhancing mechanical properties of some magnesium-based alloys, whether it is to increase specific strength or improve room temperature formability and ductility. There is significant shortage of wrought magnesium alloys specifically sheet products, so it is crucial to address this issue at hand. In terms of strength, magnesium alloys are known to have limited response to precipitation hardening but studies such as Jayaraj et al on Mg-Ca system with addition of aluminium has shown there is potential for rapid age hardening response within a few hours (Jayaraj, et al., 2010). Having stated this, Mg-Ca system containing high concentration of Ca has previously shown to have poor ductility and formability but of late microalloying has indicated improvement to formability and even enhancement to age hardening. Further study of microalloying by Bian et al of aluminium and zinc to Mg-Ca binary alloys shows enhancement to the age hardening response (Bian, et al., 2016). To illustrate the complexity at hand, dilute content of Ca has shown not to aid in precipitation hardening so a certain amount of concentration is required, between 0.15% wt to 0.3% wt. Recent studies have shown that addition of Ca to Mg-Zn

system can drastically improve formability through the promotion co-segregation and subsequent grain boundary cohesion by Zn and Ca atoms. Studies have shown that adding a trace of Ca to Mg-Zn system weakens basal texture leading to improvement in formability. Zhang et al found that the addition of calcium not only weakens texture that leads to 40% increase in ductility but also refines grain size of the hot extruded Mg-Zn-Ca alloys (Zhang, et al., 2012).

To better characterise the behaviour of improved age-hardening response seen from microalloying, analysis of nano-scale precipitates must be understood. The shape and orientation of precipitates dictates the enhancement in strength. Unfortunately, commonly used commercial magnesium alloys for wrought applications do not have desirable response to precipitation hardening. This has been attributed to precipitates having a preferential habit plane that coincides with the basal plane. K. Hono et al mentions that for effective precipitation hardening of magnesium alloys, finely dispersed precipitates with various habit planes are required (Hono, et al., 2010). Magnesium-zinc system exhibits an equilibrium phase $MgZn_2$ precipitate that is found to be located on basal planes with relatively coarse dispersion, the strength of this system is approximately 240MPa which is moderate. This is down to coarse dispersion of precipitates and so to promote finely dispersed precipitates, work needs to be carried to increase precipitation density and one way is through heterogeneous nucleation.

### 2.4.1 Mg-Al system

Work by (Yim, et al., 2004) on the effect of hot rolling on AZ31 was performed by adding relatively high content of Ca, between 1-1.5 wt%. The sheets underwent significant side cracking and this brittle behaviour according to Yim et al was caused by increase in $Al_2Ca$ precipitates that were formed at the grain boundaries. The side cracking could mean that the particles didn't disperse uniformly throughout the sheet and so gathered into a select region. The author acknowledged presence of $Mg_{17}Al_{12}$ precipitates at grain boundaries but this phase was swiftly eliminated as a potential cause for brittleness due to its observed strengthening characteristic. Apart from this microstructural defect that could be observed physically, high content of Ca also negatively impacted ductility and so Yim et al mentions elongation decreased

dramatically with content of calcium above 1% wt. Even though a formability test wasn't performed, it is obvious that it wouldn't show the desired result. This doesn't mean that alloying Ca with Al spells disaster but rather this finding further strengthens the case for microalloying Ca below a certain amount to avoid brittleness and therefore microstructural defects.

For magnesium alloys to overcome issues surrounding the mechanical properties that have been discussed, it is vital to develop a heat-treatable magnesium alloy that exhibits good room temperature formability and that can be age hardened. So, what has been discussed in terms of microalloying is that in isolation there are cases of alloys displaying good stretch formability and the capacity to be age hardened. But it remains to be seen whether an alloy can sufficiently display these two desired qualities in conjunction with each other.

(Bian, et al., 2017) study on a novel composition Mg-1.1Al-0.3Ca-0.2Mn-0.3Zn (at%) has produced a significant finding in the quest to develop an alloy that has decent formability and response to age hardening. His work entails the study of Zn as a microalloying addition to Mg-1.1Al-0.3Ca-0.2Mn (at%). Ingots are prepared with compositions of Mg-1.1Al-0.3Ca-0.2Mn (at%) and Mg-1.1Al-0.3Ca-0.2Mn-0.3Zn (at%), subsequently 10mm thick sheets are machined, homogenized and rolled to a desired thickness of approximately 5mm. Samples undergo tensile, formability, hardness testing and microstructural analysis comprising of EBSD, TEM and XRD.

Age hardening response of Mg-1.1Al-0.3Ca-0.2Mn (at%) at 200°C, the peak hardness is achieved with a rapid ageing response of 2 hours, whereas with the Zn containing alloy it is evidenced to be at 1 hour minimal difference in HV values between the two alloys. A rapid response of 1 hour is significant especially as magnesium alloys are not known typically as an age-hardenable metal due to their slow and inadequate response. The peak hardness response quickens with the addition of Zn, this rapid response to age hardening is attributable to some sort of interaction between Ca and Zn atoms that is yet to be completely characterized and understood. What we have come to know about Zn and Ca atom behaviour in the Mg-Ca system is that Zn atoms interaction with Ca atoms reduces grain boundary embrittlement and promotes cohesion.

It is to be noted that formability test is conducted at the T4 condition stage which is in line with the design rational of my project. The reasoning for this is straightforward in that biaxial plastic deformation can be better achieved without the presence of precipitates as they reduce ductility. (Bian, et al., 2017) work shows Zn containing alloy significantly weakens basal texture from Erichsen value of 5.9mm to 7.7mm. It is well documented that when the basal texture is weakened, there is a shift of basal poles which means splitting in transverse directions. In this instance, there is a unique observation regarding distribution of basal poles which Bian et al terms as quadruple basal texture. At this point it is clear to see that this alloy satisfies two areas of historical concern regarding magnesium alloys which are not being age-hardenable and limited formability. Bian et al next analysed the tensile properties in the T4 and T6 condition to compare to see at what extent ageing has improved strength and ductility. The results show that there isn't a contrasting difference between Mg-1.1Al-0.3Ca-0.2Mn (at%) and Mg-1.1Al-0.3Ca-0.2Mn-0.3Zn (at%) values in their respective conditions but what is significant is the increase of 0.2% proof strength due to ageing from the T4 condition to T6 condition. An increase from 144 MPa to 204 MPa for the Zn containing alloy is a further encouragement that precipitation activity has a positive impact on this alloy. Observation of 3D atom maps of all elements shows that Al and Ca atoms coexist on the basal plane, an indication of clustering of atoms leading to Guinier-Preston zones. This shows that microalloying Ca to Mg-Al system enhances strength through age hardening but further characterisation is required to understand the exact phase which is responsible for this encouraging find.

Alloying aluminium to pure magnesium is an attractive option due to empirically observed improvement in strength and ductility. This is largely due to aluminium having a considerably high solid solubility limit of 12.7% (wt%) and favourable atomic size. Dargusch et al studied the impact that aluminium content has on the room temperature mechanical properties and microstructure when alloyed with magnesium. Five binary alloys were produced through high pressure die casting, with aluminium content 2%, 5%, 9%, 14% and 18%.

**Table 2.2- Five binary Mg-Al alloys (Dargusch, et al., 2006)**

| Alloy (wt%) | 0.2% YS (MPa) | UTS (MPa) | Elongation (%) |
|---|---|---|---|
| Mg-2Al | 86.6 ± 1.6 | 199.6 ± 2.1 | 19 ± 2.7 |
| Mg-5Al | 112.2 ± 2.4 | 236.5 ± 10 | 16.2 ± 3.6 |
| Mg-9Al | 147.6 ± 3.0 | 244.5 ± 8.1 | 6.3 ± 0.8 |
| Mg-14Al | 191.2 ± 3.8 | 255.6 ± 9.7 | 1.8 ± 0.4 |
| Mg-18Al | 243.9 ± 2.9 | 253.9 ± 5.5 | 0.7 ± 0.1 |

The yield strength saw a dramatic increase with increasing content of aluminium, indicating significant strengthening. Alongside this observation of strengthening, the average grain size reduced from 50-100μm to 10-50μm, this was in accordance to the Hall-Petch theory. Zheng et al did a similar study on binary Mg-Al alloys and found a positive correlation in strengthening and grain size reduction (Zheng, et al., 2006). The yield strength of Mg-18Al (wt%) is triple in magnitude in comparison to Mg-2Al (wt%). Strengthening coincides with increased volume fraction of the eutectic intermetallic phase $Mg_{17}Al_{12}$ (β phase) which nucleates at grain boundaries as shown in Figure 2.16. The morphology of phase $Mg_{17}Al_{12}$ changes from divorced to fibrotic appearance with increasing content of aluminium. The elongation (%) value went from 19% when the alloy was most dilute to 0.7% when most concentrated with aluminium alloying addition. As it is well established, yield strength and ductility are adversely correlated. The eutectic phase $Mg_{17}Al_{12}$ plays a substantial role with the decreasing of ductility, this behaviour is affirmed by Pettersen et al in his study which showed a much higher volume fraction in AZ91 and AM60 in comparison to AM20 (Pettersen, et al., 2002).

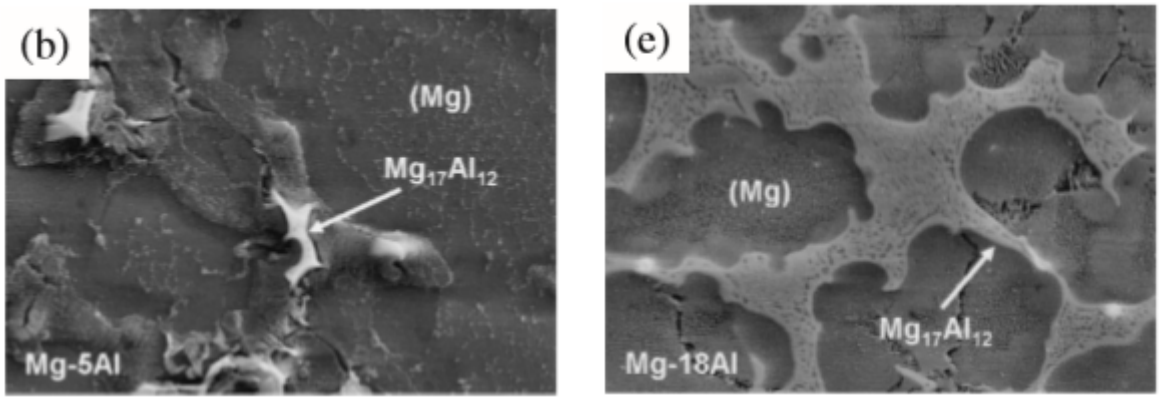


**Figure 2.16- Intermetallic phase concentration in Mg-5Al and Mg-18Al (Dargusch, et al., 2006)**

However, Kabirian et al studied the creep resistance of AZ91 by microalloying Zr to improve creep properties, he showed that $Mg_{17}Al_{12}$ is liable to softening at elevated temperatures due to a low melting temperature of 700K. This softening effect causes the grain boundaries to slide which results in weakened mechanical properties (Kabirian & Mahmudi, 2010).

Apart from reduced ductility and weakened mechanical properties at elevated temperatures, binary Mg-Al alloy have a large freezing range which makes them prone to casting defects such as segregation, shrinkage cavity and hot cracking (Dahle 2001). One way to minimise these defects is to thoroughly control casting parameters to ensure fluidity isn't adversely affected at solidification stage. Another area of concern regarding binary Mg-Al alloy is the rate of corrosion which is detrimental especially in wet or moist conditions. But by alloying manganese to Mg-Al alloy, corrosion resistance improves significantly. This has been attributed to manganese interacting with impurities such as iron by forming intermetallic compounds that don't have the same effect on corrosion. Considering the propensity of binary Mg-Al alloy to have poor creep resistance, limited corrosion resistance, low ductility and casting defects, further alloying is performed to improve these issues and there are noteworthy series such as Mg-Al-Zn, Mg-Al-Mn and Mg-Al-Si. The main casting and wrought alloys originate from binary Mg-Al system, these alloys being AZ91D, AM60B, AM50B, AE42, AS21 and AZ31.

## 2.4.2 Mg-Ca system

Moving onto a different alloy system, a comprehensive study by (Bian, et al., 2016) was performed on Mg-Ca-Zr alloy sheet with and without the addition of Zn in comparison with AZ31 alloy sheet. Focus was put on developing a sheet that would exhibit appreciable formability and strength.

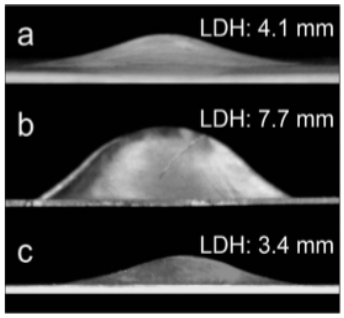


**Figure 2.17- Erichsen cupping test on (a) Mg–0.5Ca–0.1Zr, (b) Mg–0.5Ca–0.1Zr–0.1Zn, and (c) AZ31 sheets (Bian, et al., 2016)**

Bian et al found that the Erichsen cupping test conducted after appropriate ageing treatment shown in Figure 2.17 demonstrated that Mg-0.5Ca-0.1Zr-0.1Zn (at%) exhibited a much higher Erichsen value of 7.7mm in comparison to Mg-0.5Ca-0.1Zr (at%) and double the amount shown by AZ31 (wt%). As for the strength displayed, it was considerably lower than AZ31 alloy from the rolling direction, 45° direction and transverse direction. On average, the ultimate tensile strength of AZ31 (wt%) had shown to be 251 MPa, whereas for Mg-0.5Ca-0.1Zr-0.1Zn (at%) it was 201MPa and for Mg-0.5Ca-0.1Zr (at%) it was 192MPa. A lower value of over 50MPa is clearly not desirable for commercial applications as high strength is what the industries are wanting alongside improved formability. The ductility of Zn free alloy was negligible in all directions tested but Zn containing alloy showed significant elongation to the extent of doubling and tripling elongation values of Zn free alloy in all directions. The reason for the contrasting values was found in the SEM micrographs of fractured surfaces. Micrographs of Mg-0.5Ca-0.1Zr (at%) illustrated brittleness as grain boundary cracking was observed, whereas the improved ductility of Mg-0.5Ca-0.1Zr-0.1Zn (at%) was confirmed after observation of dimples. Grain boundary embrittlement has been observed in Mg-Ca systems lending to poor formability and ductility at room temperature due to segregation of Ca atoms to the boundaries, it is for this particular reason that Bian et al believes poor ductility was observed for Mg-

0.5Ca-0.1Zr (at%). It can be established that microalloying Zn to Mg-0.5Ca-0.1Zr (at%) allowed Zn atoms to interact with Ca and Zr atoms at grain boundaries which led to improvement in ductility in which Bian et al termed it as grain boundary cohesion. At this point, a pattern has developed in that a combination of Zn and Ca shows significant improvement in formability and ductility. Elsewhere, co-segregation of Zn and Ca solute atoms has been observed in cold rolled Mg-0.3Zn-0.1Ca (at%) after annealing by Zeng at al. But he admits that dilute Mg-Zn-Ca alloys have insufficient strengths for practical applications (Zheng, et al., 2015). It can also be concluded with the work of Bian et al on microalloying of Zn to Mg-Ca alloy that the low strength has remained therefore meaning an alternative alloying combination has to be sought to address the issue of strength. AZ31 has a characteristically higher strength in comparison to the observed alloys, the difference being that there is presence of aluminium. So, the obvious question is can alloying Ca to AZ31 solve the problem of low strength and poor formability? Thankfully Yim et al has shed some light on this question.

### 2.4.3 Mg-Zn system

The Mg-Zn binary system can be considerably strengthened in the solid solution and quenched condition on an atomic percentage basis, in fact three times more effectively than Mg-Al binary system as research suggests.

It is for this reasoning that Mg-Zn based alloys are regarded as the strongest current option for wrought applications when only considering non-rare earth elements. But unfortunately, their response to age-hardening is limited due to coarse distribution of $MgZn_2$ precipitates along the basal direction. Microalloying of additional elements has shown to increase nucleation sites for precipitates to grow. Also, improvement in formability of Mg-Zn alloys is required for them to be adopted more widely for wrought applications. Mg-Zn system has responded positively to microalloying in terms of improvement to formability, but it remains to be seen whether strength and formability can both be enhanced to a point of balance.

An example is Ca micro-alloyed (0.066Ca (wt%)) with Mg–1.5Zn (wt%) that was experimented on by (Chino, et al., 2010). Chino et al experimented on an extruded 5mm thick sheet that was heated to a temperature of 390°C for 20 minutes and then rolled at a reduction rate of 20% until 1mm thickness was achieved. It was then

annealed at a temperature of 350°C for 90 minutes. The sample has shown to exhibit superior stretch formability at room temperature with an Erichsen value of 8.2mm as shown in Figure 2.18 which has been likened to 6000 series aluminium alloys (approx. 8-9mm). His study entailed comparison of Mg-1.5Zn (wt%) with and without trace addition of Ca. It was found that an Erichsen value of 3.4 was achieved for Mg-1.5Zn (wt%), which signifies a difference of 4.8mm in Erichsen value, so a compelling improvement in room temperature formability with a minute addition of Ca. The study also revealed that there wasn't significant precipitation activity in the microstructure and that Ca solute atoms dissolved in the magnesium matrix, Chino et al attributes this behaviour to the presence of non-basal texture. Now this improvement in formability is very much comparable to rare-earth containing magnesium alloys, as Chino et al in previous work showed an Erichsen value of 9.0mm by the addition of Ce to the exact same Mg-Zn composition. From his work, we can state with confidence that the beneficial effect of rare-earth elements on formability can be matched there or thereabouts by microalloying through Ca, this inevitably is a breakthrough for low cost commercialisation of non-rare earth containing magnesium alloys for wrought applications.

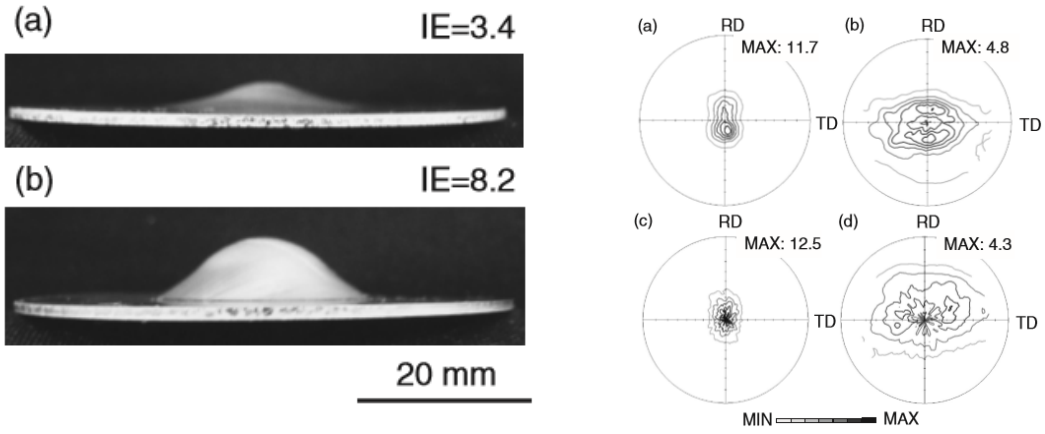


**Figure 2.18- Erichsen cupping test and pole figures in (0002) (Chino, et al., 2010)**

Tensile testing at different angles to the rolling direction was performed and there were two obvious showings as shown in Table 2.3. First it could be observed that the trend of ductility and strength being inversely correlated becoming apparent which is a given. There was also clear indication of plastic anisotropy in that there was contrasting difference between plastic strain ratio known as r-value at different

angles for Mg-1.5Zn with slight improvement after addition of Ca. An ultimate achievement for better formability is to have relatively isotropic properties. Chino's et al work has clearly shown that formability of wrought magnesium alloys through non-rare earth elements can be improved but the question remains as to whether both the strength and formability can be elevated to a point of balance where it can be at a competitive point with aluminium alloys.

**Table 2.3- Mechanical properties of tested alloys (Chino, et al., 2010)**

| Alloys | Angle | UTS (MPa) | TYS (MPa) | FE (%) | *n* | *r* | $r_{avg}$ |
|---|---|---|---|---|---|---|---|
| | 0 | 222 | 84 | 17 | 0.32 | 1.45 | |
| Mg-1.5Zn | 45 | 227 | 117 | 18 | 0.29 | 1.65 | 1.65 |
| | 90 | 229 | 131 | 15 | 0.25 | 1.86 | |
| | 0 | 220 | 120 | 23 | 0.30 | 0.84 | |
| Mg-1.5Zn-0.1Ca | 45 | 211 | 86 | 29 | 0.44 | 0.80 | 0.81 |
| | 90 | 209 | 73 | 30 | 0.50 | 0.79 | |

To briefly highlight the positive impact of microalloying, (Mendis, et al., 2010) work on TRC and hot rolled Mg-Zn system with microalloying of Ag, Ca, Zr has shown far superior mechanical properties than those observed for commercialised wrought magnesium alloys, in terms of strength and formability. TEM imaging and analysis showed that finely distributed rod-like $MgZn_2$ precipitates were responsible for increase in yield strength (above 300MPa), this is a significant find to put it bluntly. As for the influence of adding the costly silver, it is unclear to what extent it had an effect on the microstructure but earlier study on precipitates by Nie suggests Ag solute atoms disperse uniformly into the magnesium matrix before segregating to precipitates at the peak ageing stage. There is a high concentration of Zn, reaching its maximum solid solubility (above 6% in wt) in magnesium. This can be problematic as TRC alloys suffer from centreline segregation but there is ongoing work to bring about a solution and this alloy would be from amongst the first to be available for TRC industrial production.

Zhang's et al quest to minimize cost led him to experimenting on the addition of Mn to Mg-Zn system. His work indicates that zirconium can be replaced by the less costly manganese and that enhancement in strength is obtained through precipitation of G.P. zones and fine distribution of $MgZn_2$ particles. A high ultimate tensile strength of 366MPa is obtained by the Mg-6Zn-1Mn (wt%) alloy (Zhang, et al., 2011). Adding manganese has previously shown to refine grains, leading to

overall strengthening. In another work of Zhang's et al, adding Mn to Mg-Zn showed that Mn dispersed into the α-magnesium matrix, hindering grain growth (Zhang, et al., 2010).

## 2.5 Twin-roll Casting

Twin roll casting is a direct strip casting method which produces sheet metal straight from the molten metal stage, in doing so seeking to reduce subsequent secondary processing. This process was initiated originally in 1846 by Henry Bessemer for lead and tin strips but the process has progressed since then to now produce metals such as steel, aluminium alloys, and magnesium alloys of varied strip thickness (Ferry, 2006). TRC is a path that allows economical production of magnesium alloys in contrast to energy intensive traditional route of slab production and subsequent rolling and intermediary heat treatments to produce sheet products. Over the years, the TRC equipment has been adapted and developed, with numerous variations in design such as vertical and horizontal configurations. The vertically designed TRC equipment has commonly been used for producing steel sheets. Whereas for aluminium and specifically magnesium TRC production, the horizontal TRC setup is preferred (Yang, 2016).

Therefore, in this section, the technology will be assessed, including the BCAST developed low-pressure twin roll caster and the status of magnesium alloy development through conventional TRC will be looked at through this route.

### 2.5.1 Conventional TRC

The traditional route to producing magnesium alloy sheets consists of hot rolling and heat-treating slabs of sizes up to 0.3m x 1m x 2m. Slabs are firstly homogenised typically at around 480°C for several hours and then continuously hot rolled on a reversing hot mill until 5-6mm thickness is achieved. After achieving a sheet metal, the sheet is then annealed at around 340°C before each pass of 5-20% reduction in a final finishing rolling mill (Liang & Cowley, 2004). Figure 2.19 illustrates the detrimental effect of continuous rolling on the texture of AM60 alloys. After 80% reduction, a strong basal texture is developed as shown in the pole figures. A strong basal texture reduces yielding characteristics and enhances anisotropic properties.

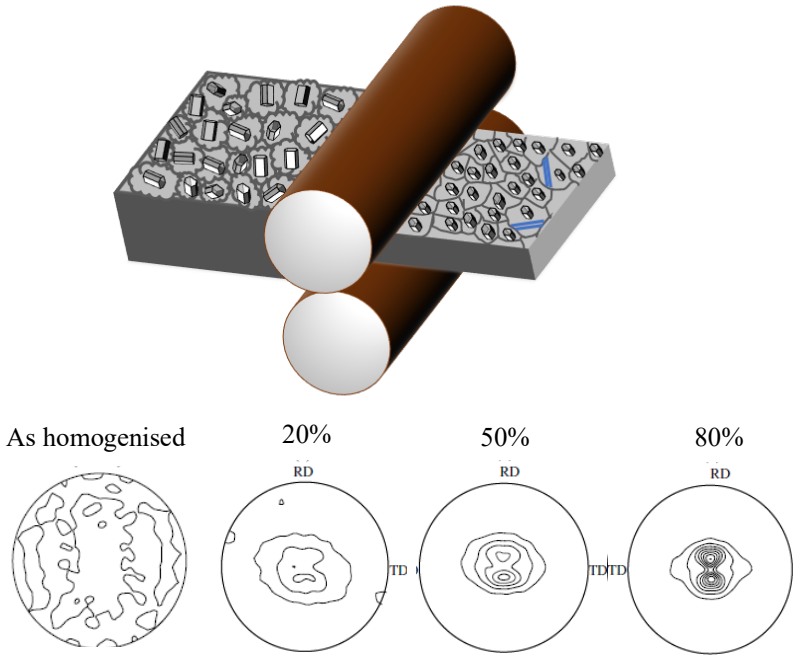


**Figure 2.19- Texture evolution of AM60 alloy after continuous rolling reductions (Pérez-Prado, et al., 2004)**

The conventional setup of TRC adopted from aluminium alloy production consisting of large rolls relies heavily upon the roll force acting on the semi-solid liquid at the roll bite point to weld the eventual solid, as illustrated in Figure 2.20. To enforce this plastic deformation, roll diameter above 500mm have been adopted. The main purpose of using large rolls has been to exercise control of strip thickness and surface finish. This mechanism has shown to aid severe centreline segregation due to squeezing of solute rich liquid to the solidification front. The conventional method

of TRC produces a sheet with a thickness of up to 10mm which is then subsequently hot rolled. Previously, AZ31 was produced through TRC and hot rolling i.e. the conventional method, the investigation found severe segregation of aluminium and zinc atoms at dendrite cell boundaries (Allen, et al., 2001). A different study was performed on 3mm thick AZ61 sheet through the aforementioned casting procedure with a casting speed of 10m/min, the study showed low elongation to failure values and strong basal texture (Mino, et al., 2006). By further increasing concentration of aluminium in the AZ series alloys, the conventional TRC method of producing AZ91 has shown to aid severe centreline segregation of solute additions (Uchida, et al., 2007). The production of ZK60 alloy led to severe anisotropy observed with elongation along rolling direction being 8.3% and 2.2% along transverse direction (Chen, et al., 2009).

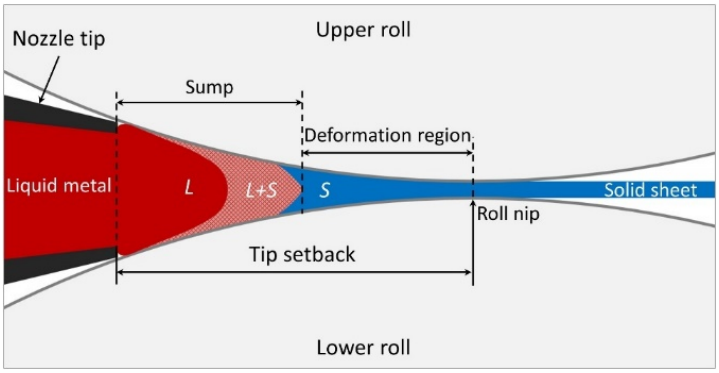


**Figure 2.20- Schematic diagram of conventional twin roll casting process, showing regions of liquid, semi-solid and solid phases and the location of tip setback including sump and deformation region (Yang, et al., 2019).**

Using conventional TRC processing instead of the traditional route does improve mechanical properties but it does not entirely give a solution to the strong basal texture that reduces the formability of magnesium alloys. The path that can be used to reduce this problem is through the development of new magnesium alloys with relatively random distribution of texture, as TRC alloy development is shown in Table 2.4. Addition of calcium to AZ31 (Bae, et al., 2009) and AM60 (Ding, et al., 2015) has led to softening of basal texture which is a promising development. Having said this, there are other challenges that conventional TRC is unable to satisfactorily answer regarding magnesium alloy sheet production, these include oxidation, solidification rate, freezing range, cost and performance (Ferry, 2006).

Some of the challenges associated with magnesium alloy sheet production include oxidation potential, solidification range, freezing range and cost and performance. Molten magnesium oxidises readily and ignites without good protective atmosphere systems and control. This can be solved by developing protection that would enable high quality strip production and prevention of fire ignition. Also, molten magnesium freezes faster than wrought aluminium alloys due to a lower specific heat and latent heat of fusion. This makes it more difficult to achieve uniform solidification across the strip. A way to achieve a uniform solidification would be to control the interfacial heat transfer during casting. Magnesium-base alloys have a larger freezing range than aluminium. This may lead to formation of cracking and segregation defects in the as-cast strip. This problem can be alleviated by careful alloy design and the development of new alloy compositions. There is also a continuous requirement from industry to reduce the operational cost of manufacturing processes, therefore magnesium alloy sheet must compete with other materials on the basis of both cost and performance. Like aluminium, TRC of magnesium is most cost effective for small tonnages (<50,000 tonnes p.a.) (Liang & Cowley, 2004).

**Table 2.4- A list of TRC/Hot rolled magnesium alloys and their subsequent response**

| Alloy(s) | Group/Year/Author | Process/Conditions | Strengthening Mechanism/Texture |
|---|---|---|---|
| AZ31<br><br>*Microstructure and Mechanical Properties of AZ31 Magnesium Alloy Strip Produced by Twin Roll Casting* | CSIRO/2001/Allen et al | TRC and hot rolled | Severe segregation of Al and Zn atoms at dendrite cell boundaries. Much improvement in ductility compared to DC ingot casting. |
| AZ31-Ca<br><br>*Effect of Ca Addition on Microstructure of Twin-Roll Cast AZ31 Mg Alloy* | Postech/2008/Bae et al | TRC and warm rolled<br><br>- Roll speed- 4.5m/min<br>- Strip thickness- 2mm | $Al_2Ca$ particles (200nm to 500nm) precipitate at grain boundaries and observed weakening of texture (0002) |
| ZM61 and ZM61-Al<br><br>*Microstructure and tensile properties of twin roll cast Mg-Zn-Mn-Al alloys* | EMSC/2007/S.S. Park et al | TRC and hot rolled<br><br>- Roll speed- 4m/min<br>- Strip thickness- 2mm | Overall a finer microstructure with addition of Al. Coarse distribution of $MgZn_2$ particles (50-500nm) in ZM61, whilst a finer distribution of $Al_8Mn_5$ particles (10nm) are responsible for strengthening in alloys with Al. |
| ZM21<br><br>*Effect of rolling temperature and reduction in thickness on microstructure and mechanical properties of ZM21 magnesium alloy and its subsequent annealing treatment* | NIT/2011/M. Thirumurugan et al | Hot rolled | Elongation below 10%. Significant increase in UTS with increased reduction (up to 75%) at elevated temperatures. A combination of cleavage and dimple fractures observed on fractographs. |
| AZ61<br><br>*Twin-roll strip casting of AZ61 magnesium alloy and improvement of formability by structure-control rolling* | Waseda University/2006/T. Mino et al | TRC and structure controlled rolled (RT to approx. 573K)<br><br>- Roll speed- 10 m/min<br>- Strip thickness- 1.5mm and 3mm | The 1.5mm cast strip showed improved microstructure in comparison to 3mm cast strip. Reduction of mean grain size and increase in hardness via RT rolling. |

| | | | |
|---|---|---|---|
| AM31<br><br>*Microstructure and mechanical properties of twin roll cast AM31 magnesium alloy sheet processed by differential speed rolling* | KIMS/2011/L.L. Chang et al | TRC and warm rolled<br><br>- Roll speed- 3m/min<br>- Strip thickness- 4mm | Improved strength and ductility due to grain refinement. A preferred basal texture of AM31 in as-cast, rolled and annealed conditions. |
| AZ91<br><br>*Mechanical Properties of Twin Roll Cast AZ91 Magnesium Alloy at Room Temperature* | Osaka University/2007/S. Uchida et al | TRC and hot rolled | High concentration of Al in the magnesium matrix which points to severe centre line segregation. A yield strength that exceeds 200MPa. |
| WE43<br><br>*Twin-Roll-Casting and hot rolling of magnesium alloy WE43* | IBF/2014/K. Neh et al | TRC and hot rolled<br><br>- Roll speed- 1.4m/min<br>- Strip thicknes- 5mm | Yield strength exceeds 300MPa. Elongation values are deemed to be average, ranging between 15-20%. Which indicates work has to be carried out to address this issue. |
| ZK60<br><br>*Effect of heat treatment on microstructure and mechanical properties of twin roll cast and sequential warm rolled ZK60 alloy sheets* | Shadong University/2008/H. Chen et al | TRC and warm rolled<br><br>- Strip thickness- 3.2mm | Optimum T6 treatment; 375°C for 3hrs and 175°C for 10hrs. Fine equiaxed structure with average grain size of 6.8μm. high strength and low elongation. Severe anisotropy observed. Elongation along rolling direction was 8.3% and 2.2% along transverse direction. |
| AM60-Ca<br><br>*Effect of calcium addition on microstructure and texture modification of Mg rolled sheets* | Anhui University of Technology/2014/H.L. Ding et al | Hot rolled | Addition of Ca tilts c-axis from ND to TD, a sign of texture weakening. Proving Ca can potentially replace RE elements with similar benefits. |
| ZKQX | NIMS/2010/Mendis et al | TRC and hot rolled | Finely distributed rod-like MgZn2 |

| | | | |
|---|---|---|---|
| *Microstructures and tensile properties of a twin roll cast and heat-treated Mg-2.4Zn-0.1Ag-0.1Ca-0.1Zr alloy* | | - Roll speed- 4m/min<br>- Strip thickness- 2mm | precipitates were responsible for increase in yield strength (above 300MPa). An improved stretch formability from other Mg alloys. |

Apart from formability problems, the main challenges to overcome with twin roll casting of magnesium alloys is the issue with coarse columnar dendritic grains, segregation of solute elements, both have an adverse effect on strength, ductility and overall strip quality (Das, et al., 2013). Centreline segregation is a casting defect that has been attributed to the wide freezing range between the liquidus and solidus temperatures and to the thermal gradient across the TRC strip where roll surface is colder and giving rise to nucleation on contact with the rolls. It is safe to ascertain that implementation of strengthening mechanisms is a foreseeable requirement for development of magnesium alloy sheets. These mechanisms being grain refinement, solid solution strengthening and precipitation hardening which ultimately all alter the microstructure to enhance mechanical properties.

#### ***2.4.1.1 Segregation***

Segregation of alloying elements is a casting defect that is commonly observed in direct strip cast alloys. Such defects cause brittle failure through crack formation and weakening of corrosion resistance. There are namely two types of segregation that occur at varying scales, macro-segregation and micro-segregation. Macro-segregation is a term associated with alloy compositional change over a significant distance in a cast alloy. This form of segregation occurs in the transient phase when there is movement of liquid or solid during casting. The physical displacement of these segregated phases causes macro-segregation, this occurrence has been attributed to thermal contractions, solidification shrinkage and density difference in interdendritic liquid. As for micro-segregation, this occurs at a localised scale due to inhomogeneous distribution of solute between dendrite arms. Dendrite formation has been attributed to solidification of an alloy occurring over a range of temperatures.

When an alloy is cooled rapidly in the transient phase, atomic diffusion becomes difficult, resulting in poor distribution of solute atoms (Ferry, 2006).

Solute segregation has been readily observed in TRC AZ31 as shown in Figure 2.21, the cause is attributed to the entrapment of highly alloyed liquid phase in the central region of the strip and that the effect of this occurrence means difficulty in rolling due to formation of cracks and resistance to corrosion is also compromised (Wells & Hadadzadeh, 2014). Crack formation is the first step towards premature failure of a material and signifies weakening of mechanical properties. (Krbetschek, et al., 2016) also, strongly correlates in their study that solute segregation acts as a crack initiator. The solute elements gather into the central region of the strip and as solidification progresses, solute elements are rejected from the solidification front towards the liquid phase which is in the centre of a strip (Hadadzadeh & Wells, 2015). This form of segregation has commonly been referred to as centreline segregation and macro-segregation in certain instances. (Yang, et al., 2018)

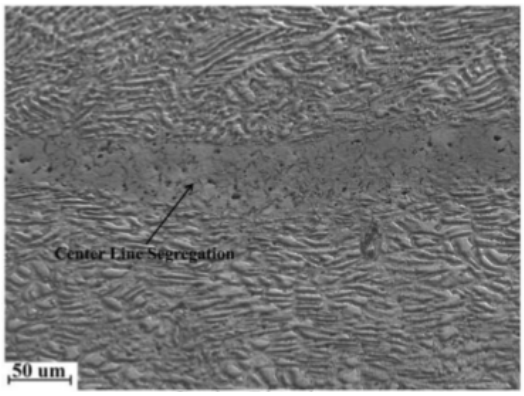


**Figure 2.21- Centreline segregation in AZ31 (Hadadzadeh & Wells, 2015)**

The overwhelming understanding is that the issue of solute segregation is enhanced by a wide freezing range that alloys such as AZ31 tend to exhibit. The mushy zone is first produced when molten metal contacts TRC rolls. Mushy zone or also referred to as the freezing range is the transient phase region between absolute solid and absolute liquid regions in binary and more complex alloys. There is also a consensus that segregation is a serious casting defect that is readily observed with twin roll

casting, the consequence leading to weakening of mechanical properties. The available literature illustrates that there are competing ways to reduce or eliminate segregation. J.H. Bae et al takes the hands-on approach of metallurgy by suggesting that by thoroughly understanding the role of alloying elements, it is possible that they can be either replaced or manipulated to reduce or even eliminate the issue of solute segregation. In his quest, he sets out a premise which is to decrease the freezing range and his pure metallurgical approach leads him to make a like for like replacement of zinc with tin (AZ31 to AT31). Whereas C. Krbetschek et al believes that prevention of segregation is possible by improving the nozzle design and positioning of the nozzle in the roll gap. There is also novel research initiated by BCAST that suggests that by shearing molten AZ31 through twin screws before TRC leads to little to no centreline segregation. The methodology that is utilised by this research to minimise solute segregation is called low-pressure twin roll casting. The technology puts focus on adopting smaller diameter rolls that evidently do not exert as much pressure as larger sized rolls which proliferates issue of segregation.

### 2.5.2 Low-pressure TRC

The need to develop TRC technology is centred around producing thin gauge strip with fine and uniform microstructure, elimination of solute segregation, good surface finish and limited basal texture to give isotropic mechanical properties which will allow for direct component production with little to no need for any rolling reductions (Yang, et al., 2018).

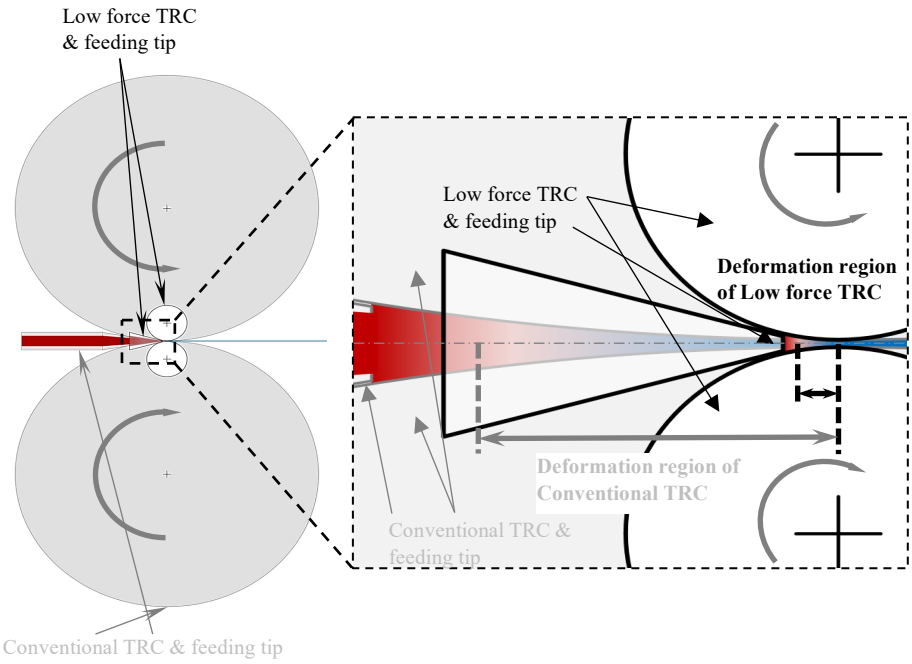


**Figure 2.22- Schematic diagram of low-pressure TRC process comparing to conventional TRC process (Yang, et al., 2018)**

To address this, Brunel Centre for Advanced Solidification Technology (BCAST) has developed a low-pressure TRC equipment that is used to directly cast to the desired thickness, this eliminates the need to do further rolling which proliferates deformation. In effect, the process has gone from being a rolling process with conventional TRC to a casting process through low-pressure TRC. The low-pressure TRC produces thin strips by using smaller diameter rolls. In conjunction with melt-conditioning, a 1.7mm thin strip was produced. The use of smaller diameter rolls means the melt is at a closer proximity to the roll bite, which allows for solidification to occur at the roll gap, leading to faster and efficient production of thinner strips. As illustrated in Figure 2.22, the use of these rolls results in the deformation load being significantly lower in comparison to a conventional TRC. With reduction in deformation load, this goes a long way to address the major concern of strong basal

texture and solute segregation, especially an issue for highly concentrated alloys. AZ31 TRC strip produced by low-pressure TRC had fine and uniform equiaxed grains with no sign of centreline segregation. Alongside this, randomised grain orientation was achieved with texture intensity of 3.81, this is in stark contrast to a strong basal texture continuously observed of AZ31 produced through the conventional TRC method (Yang, et al., 2018).

As the presented research has sought to inform, there is a requirement to develop magnesium alloy(s) through a chosen alloy and TRC design process, as part of this, it is essential to minimise cost by using non-rare earth elements as alloying additions. In order to achieve this, to develop Al, Ca, Mn, and Zn containing magnesium alloy(s) that are designed for TRC producing which will be followed by heat treatment to enhance the mechanical properties. It is important to therefore understand the role of alloying elements on solidification behaviour. Then next stage is to characterise the microstructure of the novel alloy(s) and to understand the age-hardening response and precipitation behaviour.

# Chapter 3- Experimental Procedure

# Contents

## 3.1 Alloy Preparation

The alloy compositions were initially selected based on equilibrium phase diagram calculations using thermodynamic software Pandat 2016 and the PanMg2016 database. Later, thermodynamic software Pandat 2018 and the PanMg2018 were used to re-calculate to establish phase diagram accuracy. The 6 compositions were chosen so that the total solute concentrations are below the maximum solid solubility of Zn, Al and Ca. Two solute concentrations for each of Al and Zn were chosen to investigate the effect of high and low solute content of Al and Zn on the microstructure and property development of the alloys investigated. The nominal compositions selected are shown in Table 4.1 and the compositions are also illustrated on the Iso-compositional phase diagrams where of Al is 0.8 and Zn is 1 where Zn and Al concentrations were varied, Figure 4.1 and Figure 4.2, respectively. Similar iso-compositional phase diagrams are shown for the 0.3 wt% Ca containing alloys in Figure 4.3 and Figure 4.4.

High purity Mg (99.9% purity), Ca (99.9% purity) and Al (99.99% purity) were used for the preparation of alloys used in this investigation while Mn was added as Al20wt.%Mn master alloy. Pure Al was used to make up the difference between Al added as part of the Al20wt.%Mn master alloy and amount of Al required for the alloy.

## 3.1.1 Casting Methodology

### *3.1.1.1 Mould Casting*

For initial investigations detailed in Section 4.3 Microstructure Characterisation, cylindrical ingots of Ø 30mm and 120mm in length were cast. 2kg of each of the alloys were permanent mould cast using elements Mg, Ca, Al and Zn while Al-20wt.%Mn. Magnesium is put into an in-house built tilting furnace steel crucible which is heated to 670°C. A cover gas comprised of 0.05% of $SF_6$ and nitrogen is used to prevent oxidation of Mg. All the alloy additions are pre-heated in an oven at a temperature of 200°C. Once magnesium is molten, melt is stirred, and any dross is removed. Next, alloying elements are added to the melt which are then stirred and held at 670$^o$C for 20 minutes to allow for complete incorporation into the melt. Then the melt is again stirred to ensure uniform distribution of solute in the melt. A RS 51/RS 52 digital thermometer that has a tolerance of ± 2.2°C is used to measure the temperature using a K-type thermocouple. Once the temperature is stable the molten alloy is cast into a permanent mould by controlled pouring and allowed to solidify. Large quantities of selected alloys, up to 10 kg, for twin roll casting experiment were prepared using the same procedure as described above.

### *3.1.1.2 Twin Roll Casting (TRC)*

An in-house built low-pressure twin roll caster is used to produce 2m length TRC strips. The diameter of rolls is 110mm with a width of 150mm and the roller speed is in the range of 0-10 m/min. The counter rotating rolls are driven by two 15 kW motors. The rollers are water cooled using an external chiller unit where the chiller is set at 30°C, inlet water temperature being 30°C. The roll gap is set at 1mm and the setback distance between the nozzle tip and roll biting point is 20mm. The tundish and nozzle are heated to 680°C, once the tundish and nozzle temperatures have stabilised, the molten metal is poured from the tilting furnace into the tundish. Once the melt enters the tundish, it then flows into the nozzle and out through the rollers. The strip is carefully guided using a meshed stainless-steel guide strip which allows the flow to continue producing a long magnesium alloy strip. The temperatures of the nozzle and tundish is recorded to ensure uniform temperature range during the casting of TRC strip.

### 3.1.2 Compositional Analysis

Two ingots of each alloy are selected randomly, and slices of each ingot are then prepared for analysis. The preparation consists of cutting 15mm thick slices and grinding using silicon carbide paper (120P, 320P, 800P and 1200P) through the automatic Saphir 520. The automatic Saphir 520 is set at a base speed of 150 rpm and grinding is performed for 60 seconds for each silicon carbide paper.

A spark optical emission spectrometer (foundry-master pro spectrometer) is used with argon protection gas to analyse the chemical composition of the as-cast alloys. The specimen stage and the spark gun were cleaned prior to the use of the spectrometer. In order to prevent false readings a pure magnesium sample is always used as a reference and a minimum of 10 sparks are done to ensure the composition of the pure Mg sample. 10 spark tests are conducted for each sample with the results collected on proprietary software WasLab3 and resulted are saved.

### 3.1.3 Cooling Curve Measurement

To measure the cooling curve, an in-house built furnace containing extra k-wool for insulation is used as shown in Figure 3.1. A steel crucible containing a 300g ingot is placed inside the furnace and heated to 700°C. Protective gas comprising of 0.05% of $SF_6$ in nitrogen is supplied into the steel crucible. Two K-type thermocouples are inserted to measure the temperature, one is placed to measure temperature at ¾ of the crucible and the second one is placed ¼ of crucible depth inside melt. This is done so that temperature at several points can be gathered which would further the understanding of solidification behaviour. Once the alloy is molten, melt is held for 20 minutes to achieve a complete melt with stable temperature. Next, the power is switched off and the furnace cools slowly to allow measurement of temperature as the alloy solidifies. The data is recorded with proprietary software Measurement & Automation Explorer by National Instruments (1999). Once both the liquidus temperature and the semi-solid region is passed, the experiment is halted. The experiment is repeated twice to ensure accuracy of the data. The alloy is molten for the third time to remove the thermocouples from the solidified alloy.

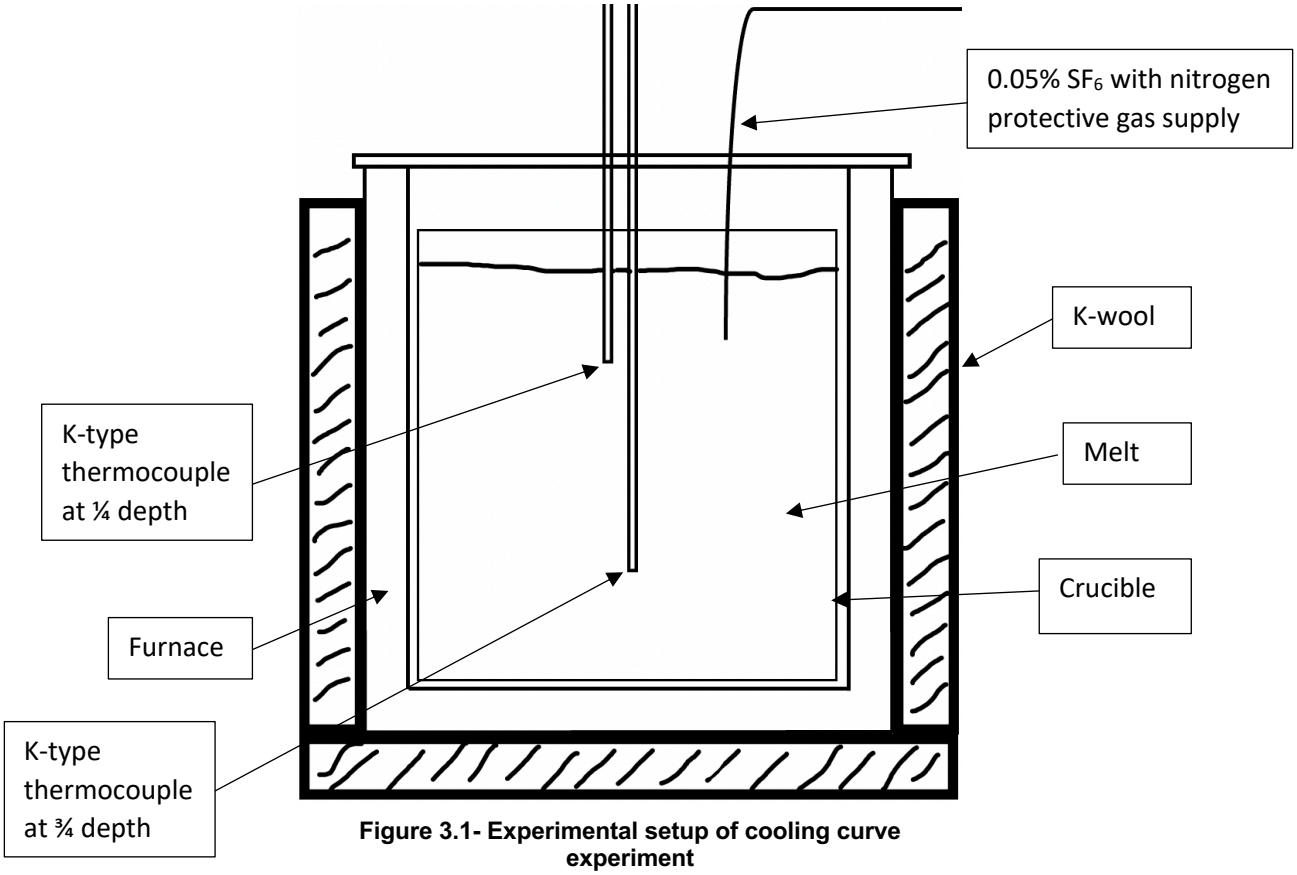


**Figure 3.1- Experimental setup of cooling curve experiment**

## 3.2 Rolling Methodology

Pre-prepared selected alloys were molten and cast into book moulds to produce cast plate that is 15cm in thickness. Casting temperature of 670°C was used which amounts to a superheat value of 25°C for Mg-1Al-1Zn-0.3Mn-(0.3Ca) and 40°C for Mg-1Al-4Zn-0.3Mn-(0.3Ca). The surface layer of the castings is removed to ensure parallel surfaces and to remove surface contaminations and to ensure a uniform thickness of 13mm. Book mould cast plates are homogenised as described in the heat treatment section. Samples are heated for 30 minutes at 300°C to allow large reductions to be done at warm rolling temperatures. Samples are rolled using number of passes to a 30% reduction, in between the passes, samples are placed in the oven at 300°C to allow recrystallisation of the alloy and to prevent cracking due to large reductions. The speed of rollers is set at 2m/min, each pass the reduction is set to 1mm. Thereafter, the hot rolled sample is heat treated and then deformed by 5% via cold rolling. A reduction of 5% from the warm rolled plate thickness is achieved by rolling at room temperature. Some samples are aged at 175°C for 15 minutes before 5% deformation while others were 5% deformed without any ageing heat treatment. The 5% deformed, pre-aged and 5% deformed samples are aged to observe the precipitation behaviour.

## 3.3 Heat Treatments

As-cast alloys are homogenised to remove or reduce the intermetallic phases in the microstructure. In order to maximise the dissolution of intermetallic phases a temperature range from 350°C to 500°C is used with up to 2 hours of homogenisation time. Samples of 30x30mm in size are heat treated in a Carbolite furnace (type: LHT6/120) and following heat treatment, they are immediately quenched in room temperature water. After homogenisation, samples are aged in an Elite furnace at 175°C for 30 minutes, 1 hour, 2 hours, 4 hours, 8 hours, 16 hours, 24 hours, 48 hours, 72 hours, 96 hours, 120 hours and finally 240 hours to observe the precipitation hardening kinetics. Following age hardening heat treatment, samples are cold water quenched and the age hardening response is measured with hardness measurements.

## 3.4 Microstructure Characterisation

### 3.4.1 Sample Preparation

The samples are cold mounted using acrylic powder and liquid combination called Quick-Set 2, provided by MetPrep using 30mm diameter moulds with resin and hardening at a ratio of 2:1 in volume. Once the cold mounting sets the samples are ground using progressively finer SiC papers. Following this, samples are polished using a chemicloth M magnetic polishing pad using oxide polishing suspension (OPS) with a speed of 110rpm through automatic polishing. Samples are cleaned with water and ethanol to remove any OPS and dried immediately. Samples are etched with an etchant comprising of 4.2g of picric acid, 100ml of ethanol, 10ml acetic acid and 10ml of distilled water. Samples are immersed into the etchant for 1-3 seconds and then immediately rinsed with ethanol.

### 3.4.2 Optical Microscopy

Optical microscopy is conducted with Carl Zeiss Axioscope 1 which is equipped with a digital camera. Both, bright-field imaging and polarised imaging modes are used to obtain micrographs. Volume fraction of intermetallic particles are analysed with Zeiss AxioVision 4.9 and the grain size was measured with ImageJ software which has measurement accuracy of 98.4%.

In AxioVision software, interactive measurement mode is selected to obtain volume fraction of intermetallic particles. Average area fraction of intermetallics is measured by analysing 5-10 different images for a given condition. For grain size measurement, the intercept method is used, this method consists of drawing straight lines along the casting direction with established length at different areas. A minimum of 5 lines was used in each image with a minimum of 5 images for each condition. To establish an accurate finding, grain size measurement of wedge samples is performed at the stated distance from tip point but also 10% $\pm$, as to address software inaccuracy. The grain size is defined following the ASTM E112 – 10 standard as:

$$\frac{\text{Line length}}{\text{No. of grains}} \times 1.5$$

**Equation 3.1**

### 3.4.3 Scanning Electron Microscopy

Scanning electron microscopy is performed using LEO 1455VP (tungsten thermal emission gun) on alloys to observe the solute segregation and intermetallics. An accelerating voltage of 10kV and a working distance of 13mm ia used. EDX (EDAX octane super SDD EDX) is performed on Zeiss SUPRA 35VP (field emission gun) to quantify the elemental composition of the respective intermetallic phases. Backscattered electron mode with a working distance of 13mm and an accelerating voltage of 20kV is used. The EDX software TEAM (Texture and Elemental Analytical Microanalysis, v.4.4.1b) was used to conduct point analysis on intermetallic phases and the matrix phase.

### 3.4.4 Transmission Electron Microscopy

Samples with a thickness of 500μm are prepared by using an Accutom50 and then mechanically ground using silicon carbide paper (800P) to a thickness of 150-200μm and punched into 3mm diameter discs. The samples are electropolished with a solution comprised of 15.3g of lithium chloride, 33.48g of magnesium perchlorate, 300ml of 2 butoxy ethanol and 1500ml of methanol using a Struers' TenuPol-5 at a voltage of 90-110V and current 0.15A with flow rate set at 28 and temperature at -45°C. JEOL2100 field emission gun transmission electron microscope operating at 200kV was used to observe samples in the TEM using bright field imaging and select area electron diffraction (SAED).

## 3.5 Mechanical Testing

### 3.5.1 Hardness Testing

Hardness testing is performed on the solution treated and precipitation hardened samples through the Vickers Hardness Tester (model no: 432SVD). Samples are prepared by mechanical grinding, up to silicon carbide paper 2500P. To begin with, the hardness tester is programmed to indent with a force of 9.8N (HV1) with a dwell time of 10 seconds. The sample is placed onto a sample holder which is positioned directly under a microscope lens. In continuation of first part, a suitable position for indentation is chosen and the lens is focused for accuracy when measuring. Then the next stage is to calibrate the measurement lines that are seen through the lens, performing this once is enough for each sample. Once measurement is complete, the digital reader shows the Vickers hardness value on its screen. This procedure is followed for up to ten more indentations for the first sample and then the other samples go through the same procedure.

### 3.5.2 Tensile Testing

Tensile samples of TRC AZMX1100 and TRC AZMX1400 alloys in as-cast and T6 conditions are machined in direction of casting, equating to 5 samples for each condition. Machining is performed in accordance with ASTM E 8M standard as shown in Figure 3.2. The tensile testing is performed at ambient temperature and measured on an Instron 5569 Universal Electromechanical Testing System with constant cross head speed of 0.5mm/min ($2x10^{-4}$ $s^{-1}$ initial strain rate) and Bluehill software for test process control. As the samples are flat, appropriate wedge grips that are designed to grip samples ranging from 0-0.65mm in width are used. A sample is placed into position and a 25mm extensometer is used by clipping it in in

the strain region. The Bluehill software is used to input sample measurement details and then the test is ready to be conducted.

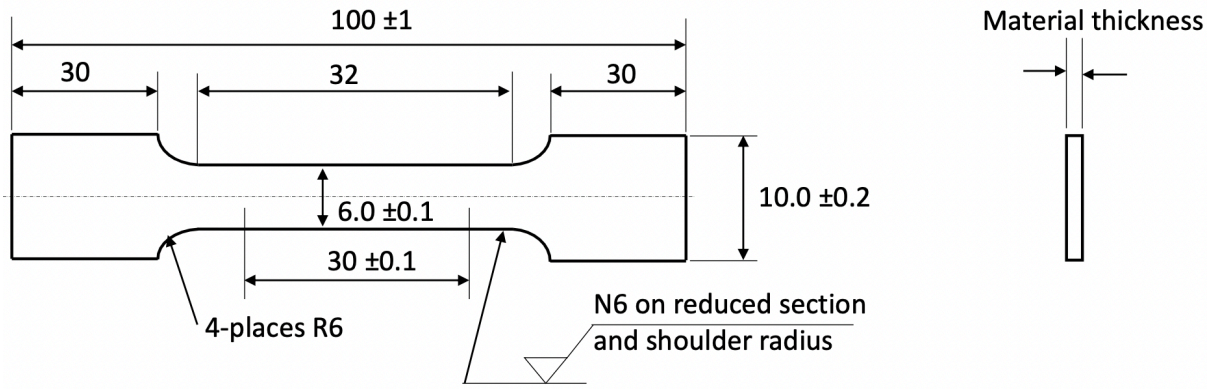


**Figure 3.2 Orthographic drawing showing dimensions of sub-size standard tensile test specimen which are in accordance with ASTM E 8M**

# Chapter 4- As-cast and Homogenised Alloys

# Contents

## 4.1 Introduction

Alloys composed of Mg-1Al-1Zn-0.3Mn (and with 0.3% Ca), Mg-4Al-1Zn-0.3Mn (and with 0.3% Ca) and Mg-1Al-4Zn-0.3Mn (and with 0.3% Ca) are permanent mould cast and then characterised in the as-cast and the homogenised conditions to understand the effect of microalloying prior to ageing heat treatment. There is an expectation that there will be significant presence of intermetallics situated at grain boundaries due to concentration of alloying elements. Understanding the behaviour of these intermetallics at this stage will play a vital role when undertaking ageing treatment to retain these phases for the purpose of enhancement in mechanical properties.

Included in this chapter is the alloy solidification behaviour i.e. cooling curve measurements and its comparison with the Scheil data calculated using thermodynamic software Pandat 2018 and the PanMg2018 database. As part of characterisation, the chapter contains volume fraction analysis of intermetallics, grain size measurement of as-cast, homogenised, as-cast wedge samples and discussion on the role calcium has on the microstructure.

### 4.1.1 Experimental Composition & Phase Diagrams

**Table 4.1 Experimental and Nominal Composition (wt%) of Novel Alloys**

| | Composition (wt%) | | | | |
|---|---|---|---|---|---|
| | Experimental | | | | |
| **Alloy** | **Al** | **Ca** | **Mn** | **Zn** | **Mg** |
| *Mg-1Al-1Zn-0.3Mn* | 0.65 | - | 0.15 | 0.8 | Bal. |
| *Mg-1Al-4Zn-0.3Mn* | 0.8 | - | 0.25 | 4.2 | Bal. |
| *Mg-4Al-1Zn-0.3Mn* | 3 | - | 0.05 | 0.8 | Bal. |
| *Mg-4Al-1Zn-0.3Mn-0.3Ca* | 3 | 0.4 | 0.12 | 0.67 | Bal. |
| *Mg-1Al-1Zn-0.3Mn-0.3Ca* | 1.6 | 0.4 | 0.04 | 1 | Bal. |
| *Mg-1Al-4Zn-0.3Mn-0.3Ca* | 0.8 | 0.13 | 0.29 | 3.7 | Bal. |

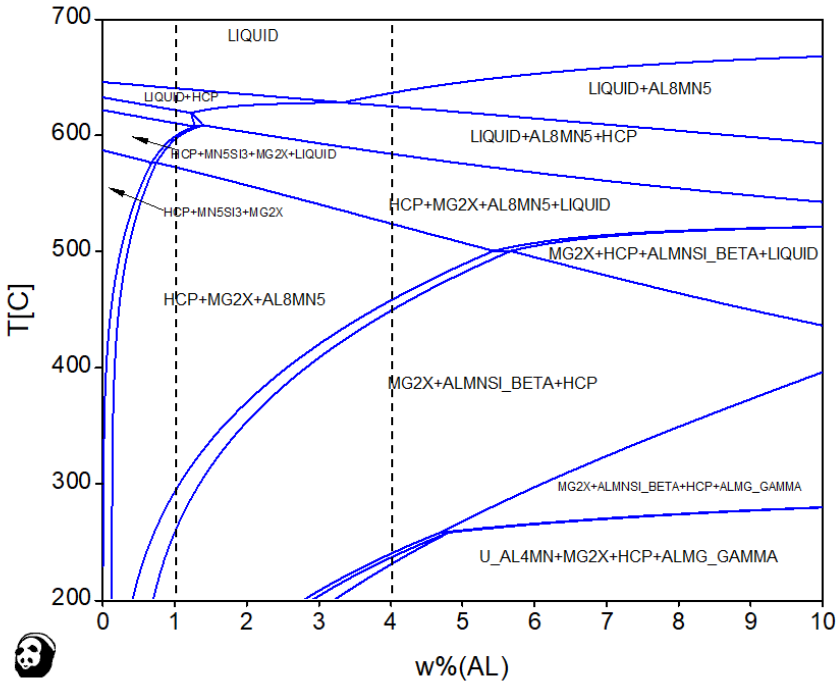


**Figure 4.1- Iso-compositional phase diagram for alloys with 1wt% Zn and 0.3wt% Mn with varying phase diagram of Mg-1Al-1Zn-0.3Mn and Mg-4Al-1Zn-0.3Mn Al concentrations. Vertical lines illustrate the Mg-1Al-1Zn-0.3Mn and Mg-4Al-1Zn-0.3Mn.**

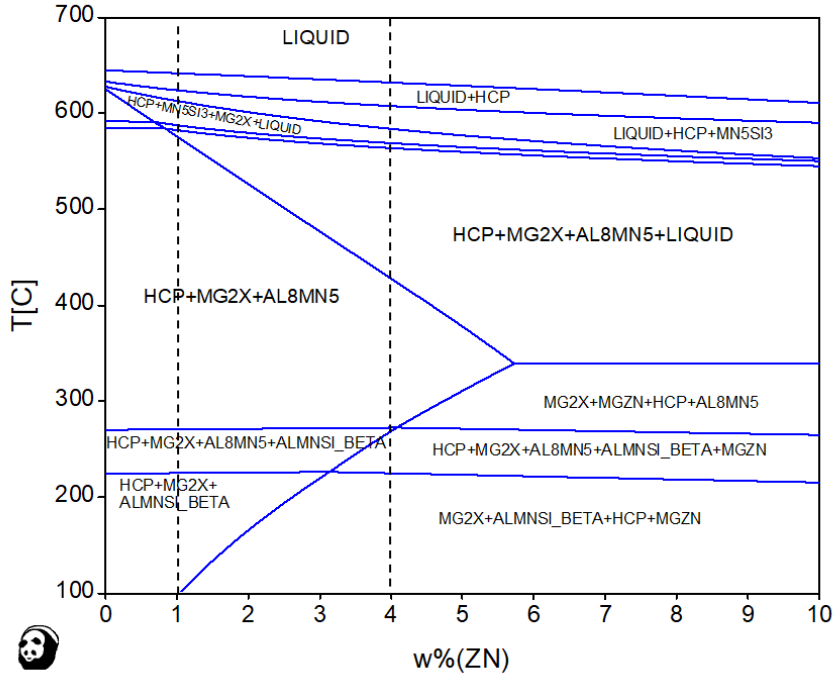


**Figure 4.2- Iso-compositional phase diagram for alloys with 1wt% Al and 0.3wt% Mn with varying phase diagram of Mg-1Al-1Zn-0.3Mn and Mg-1Al-4Zn-0.3Mn Zn concentrations. Vertical lines illustrate the Mg-1Al-1Zn-0.3Mn and Mg-1Al-4Zn-0.3Mn.**

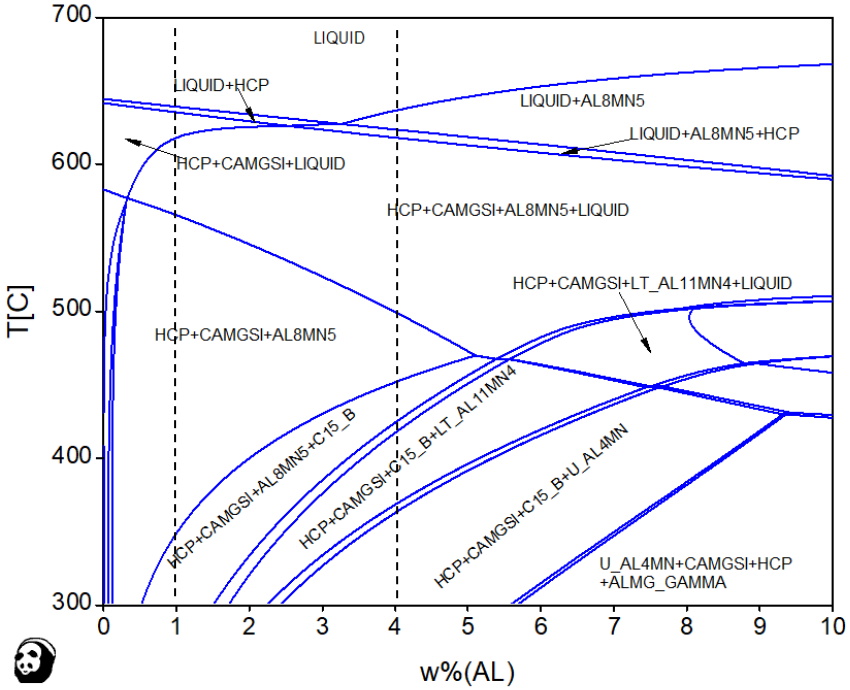


**Figure 4.3- Iso-compositional phase diagram for alloys with 1wt% Zn, 0.3wt% Mn and 0.3wt% Ca with varying phase diagram of Mg-1Al-1Zn-0.3Mn-0.3Ca and Mg-4Al-1Zn-0.3Mn-0.3Ca Al concentrations. Vertical lines illustrate the Mg-1Al-1Zn-0.3Mn-0.3Ca and Mg-4Al-1Zn-0.3Mn-0.3Ca.**

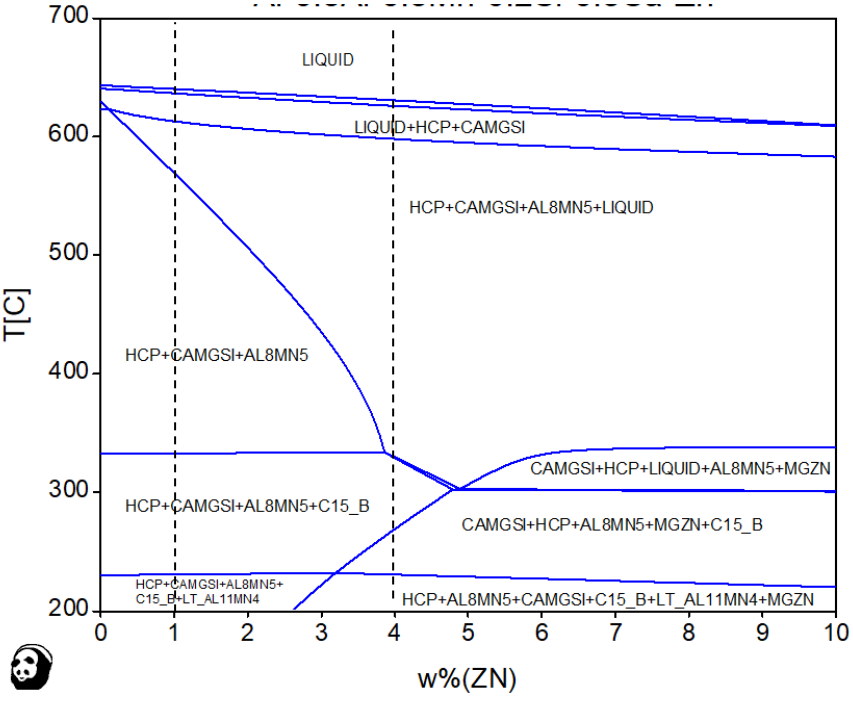


**Figure 4.4- Iso-compositional phase diagram for alloys with 1wt% Al, 0.3wt% Mn and 0.3wt% Ca with varying phase diagram of Mg-1Al-1Zn-0.3Mn-0.3Ca and Mg-1Al-4Zn-0.3Mn-0.3Ca Zn concentrations. Vertical lines illustrate the Mg-1Al-1Zn-0.3Mn-0.3Ca and Mg-1Al-4Zn-0.3Mn-0.3Ca.**

## 4.2 Solidification

The most classical way of studying a metal is by observing its behaviour when heated or cooled from one phase to another, this change or transition is regarding liquid and solid phases. Thermal analysis consisting of a cooling curve is conducted whereby a melt is left to solidify overtime. The transition from liquid to solid is identified when the occurrence of latent heat can be confirmed through a sudden increase of experimental time required over stable temperature. A pure metal solidifies at a fixed temperature, so a temperature above and beyond this point, the pure metal will remain liquid. The best term to describe this fixed temperature is the melting point. In this section, the solidification behaviour of all alloys is studied through experimental, Scheil and Lever rule methods. Shown below in Table 4.2 is the experimental liquidus ($T_L$) and chosen homogenisation temperatures ($T_H$) of all alloys considered.

**Table 4.2- Experimental liquidus and homogenisation temperatures of all alloys**

| Alloy | $T_L$ (°C) | $T_H$ (°C) |
|---|---|---|
| *Mg-1Al-1Zn-0.3Mn* | 645 ± 2.2 | 400°C/1h |
| *Mg-1Al-1Zn-0.3Mn-0.3Ca* | 642 ± 2.2 | 450°C/2h |
| *Mg-4Al-1Zn-0.3Mn* | 620 ± 2.2 | 450°C/1h |
| *Mg-4Al-1Zn-0.3Mn-0.3Ca* | 630 ± 2.2 | 500°C/1h |
| *Mg-1Al-4Zn-0.3Mn* | 635 ± 2.2 | 350°C/1h |
| *Mg-1Al-4Zn-0.3Mn-0.3Ca* | 631 ± 2.2 | 500°C/1h-350°C/1h |

### 4.2.1 AZM110-Ca

**Table 4.3- Comparison of liquidus temperature of Mg-1Al-1Zn-0.3Mn**

| | Liquidus Temperature | | |
|---|---|---|---|
| **Alloy** | **Experimental (°C)** | **Scheil (°C)** | **Lever (°C)** |
| ***AZM110*** | 645 ± 2.2 | 642 | 643 |

To understand the solidification behaviour of Mg-1Al-1Zn-0.3Mn, the liquidus temperature was sought by conducting cooling curve experiment as displayed in Table 4.3 and shown in Figure 4.5. The reduction of temperature after being left to cool from 700°C was linear until it reached approximately 644°C in reading A) and until it reached 646°C in reading B). From this stage, latent heat was given out to accommodate for the beginning of solidification which would carry on until complete solid phase is achieved from cooling. The liquidus temperature obtained for Mg-1Al-1Zn-0.3Mn is therefore 645°C after being averaged from the two readings.

According to the Scheil equation simulation the predicted liquidus temperature is 642°C and for the Lever rule method, the predicted liquidus temperature is 643°C. Figure 4.6 shows solid fraction of Mg-1Al-1Zn-0.3Mn according to the two mentioned methods. At this temperature, nucleation of α-Mg phase with HCP crystalline structure begins, this is in correlation with the solidification behaviour of experimental liquidus temperature as mentioned above.

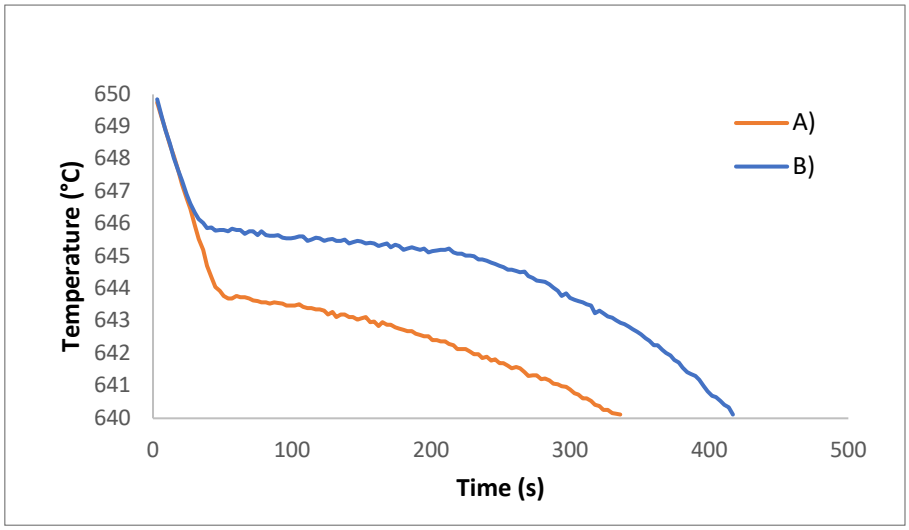


**Figure 4.5- Cooling curve measurement showing liquidus region of Mg-1Al-1Zn-0.3Mn with two experiments**

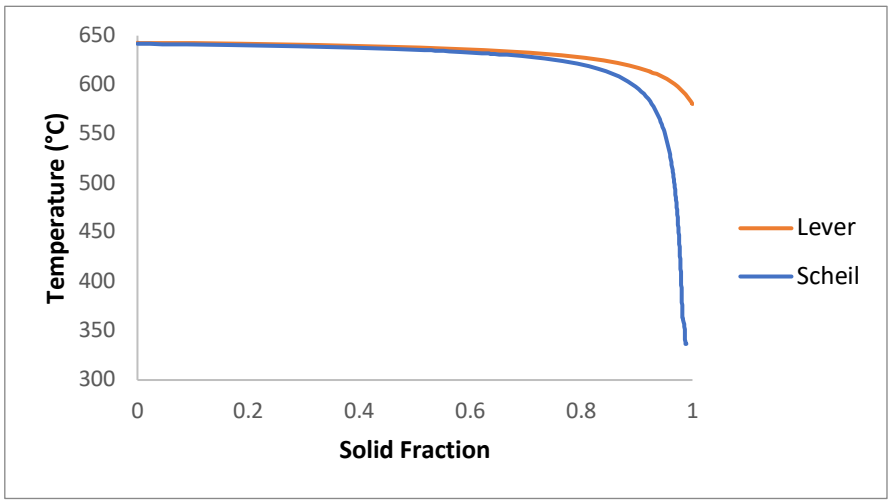


**Figure 4.6- Solid fraction of Mg-1Al-1Zn-0.3Mn according to Lever vs. Scheil**

The nucleation and growth of solid phase α-Mg with HCP crystal structure begins immediately after cooling below the liquidus temperature of 642°C. At this stage, the α-Mg phase coexists solitarily with liquid phase until an invariant reaction occurs causing formation of α-Mn phase with cubic crystal structure. The nucleation of this cubic crystal structure phase begins at 635°C, this occurs when complete solid fraction is 54%. After 3°C reduction, the nucleation and subsequent solidification of phase $Al_8Mn_5$ begins at 632°C which coincides with the disappearance of α-Mn phase. Even though, the presence of the α-Mn phase remains constant at concentration 0.012% throughout the solidification process from 632°C, this is because Scheil simulation assumes solid diffusion does not occur. The same is observed for phase $Al_8Mn_5$, in that there is a constant presence of this intermetallic compound until complete solidification. With $Al_8Mn_5$ intermetallic compound, the peak amount of solidified fraction stabilises at 441°C, with a percentage of 0.077%. At this temperature, an invariant reaction occurs with the disappearance of $Al_8Mn_5$ phase and nucleation and growth of $Al_{11}Mn_4$ phase starts. $Al_{11}Mn_4$ phase reaches a maximum phase fraction of 0.000141% before another invariant reaction occurs. At this stage of solidification in the freezing range, $Al_4Mn$ phase nucleates and grows at 408°C with phase fraction reaching 0.000047555% when the total fraction solidified is 98%. Next, $Al_4Mn$ phase disappears which leaves liquid and α-Mg phases existing together, this occurs between temperature 374°C and 364°C. With small volume of liquid remaining, two more phases consisting of Mg, Al, and Zn are formed with two distinct crystal structures. The first phase being φ-AlMgZn, which has the largest

solid fraction from the intermetallic compounds, with 0.8%. The solidification of this rich solid phase begins at 364°C. The last phase to solidify at the lowest temperature is τ-AlMgZn. The phase nucleates at 337°C and reaches maximum solid fraction of 0.05%. The nucleation and growth of all these present phases in Mg-1Al-1Zn-0.3Mn is shown sequentially in Table 4.4 and phase fraction is shown in Figure 4.7 a) and b).

**Table 4.4- Nucleation and growth sequence of phases of Mg-1Al-1Zn-0.3Mn**

| Reaction | Temp | Solid Fraction |
|---|---|---|
| $L \rightarrow \alpha\text{-Mg}$ | 641.8 to 634.8 | 0 to 0.540 |
| $L \rightarrow \alpha\text{-Mg} + \alpha\text{-Mn}$ | 634.8 to 631.7 | 0.540 to 0.636 |
| $L + \alpha\text{-Mn} \rightarrow \alpha\text{-Mg} + Al_8Mn_5$ | 631.7 | 0.636 |
| $L \rightarrow \alpha\text{-Mg} + Al_8Mn_5$ | 631.7 to 440.8 | 0.636 to 0.977 |
| $L + Al_8Mn_5 \rightarrow \alpha\text{-Mg} + Al_{11}Mn_4$ | 440.8 | 0.977 |
| $L \rightarrow \alpha\text{-Mg} + Al_{11}Mn_4$ | 440.8 to 406.7 | 0.977 to 0.980 |
| $L + Al_{11}Mn_4 \rightarrow \alpha\text{-Mg} + Al_4Mn$ | 406.7 | 0.980 |
| $L \rightarrow \alpha\text{-Mg} + Al_4Mn$ | 406.7 to 373.5 | 0.980 to 0.982 |
| $L + Al_4Mn \rightarrow \alpha\text{-Mg}$ | 373.5 | 0.982 |
| $L \rightarrow \alpha\text{-Mg}$ | 373.5 to 364.1 | 0.982 to 0.983 |
| $L \rightarrow \alpha\text{-Mg} + \varphi\text{-AlMgZn}$ | 364.1 to 337.7 | 0.983 to 0.996 |
| $L + \varphi\text{-AlMgZn} \rightarrow \alpha\text{-Mg} + \tau\text{-AlMgZn}$ | 337.7 | 0.996 |
| $L \rightarrow \alpha\text{-Mg} + \tau\text{-AlMgZn}$ | 337.7 to 336.8 | 0.996 to 1 |

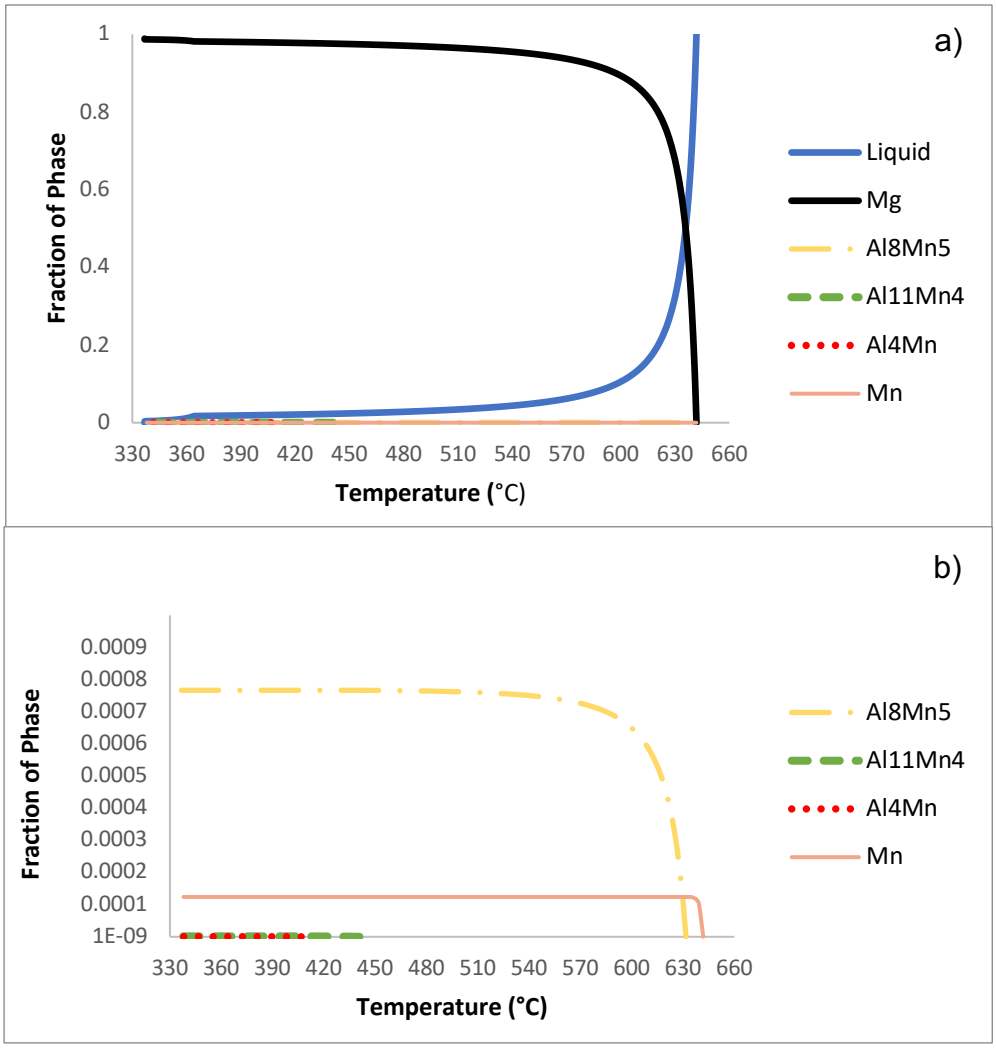


**Figure 4.7- a) and b) Scheil data showing theoretical phases present in Mg-1Al-1Zn-0.3Mn**

**Table 4.5- Comparison of liquidus temperature of Mg-1Al-1Zn-0.3Mn-0.3Ca**

| | Liquidus Temperature | | |
|---|---|---|---|
| **Alloy** | **Experimental (°C)** | **Scheil (°C)** | **Lever (°C)** |
| ***AZMX1100*** | 642 ± 2.2 | 640 | 640 |

Thermal analysis of the calcium containing Mg-1Al-1Zn-0.3Mn-0.3Ca was performed to obtain the liquidus temperature, as displayed in Table 4.5 and shown in Figures 4.8 and 4.9. At the point of solidification, two readings of 643°C and 641°C were averaged to obtain the liquidus experimental temperature of 642°C. The Scheil equation and Lever rule method simulation for this alloy revealed nucleation and growth of α-Mg phase at 640°C, showing that there is a small difference of 2°C from the experimental temperature. This is a positive indication of the reliability of predicted intermetallic phases to be studied following from here.

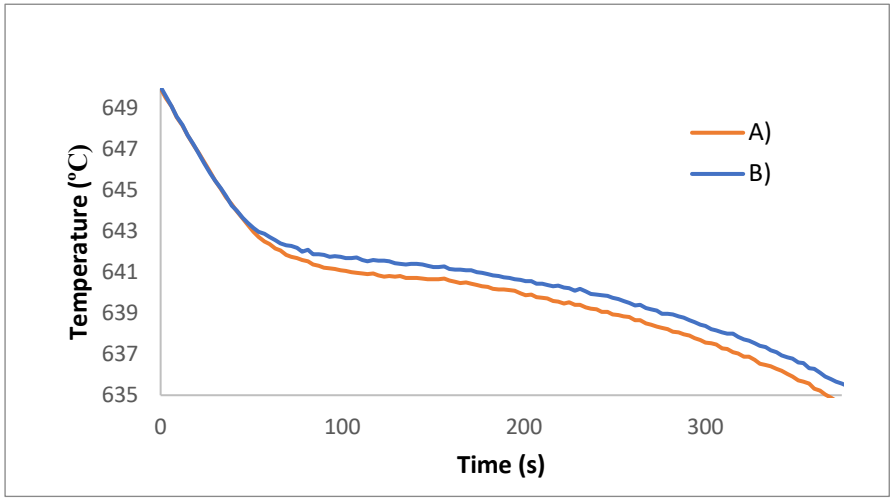


**Figure 4.8- Cooling curve measurement showing liquidus region of Mg-1Al-1Zn-0.3Mn-0.3Ca with two experiments**

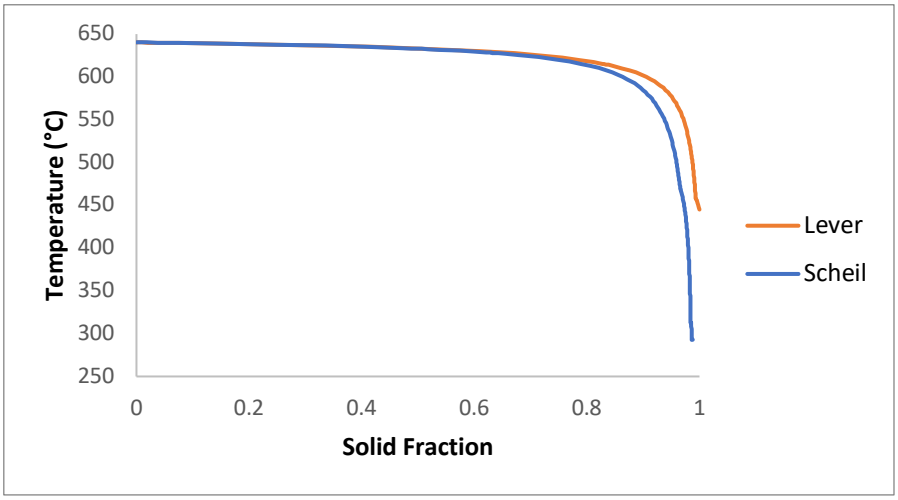


**Figure 4.9- Solid fraction of Mg-1Al-1Zn-0.3Mn-0.3Ca according to Lever vs. Scheil**

Table 4.6 sequentially shows the nucleation and growth all phases identified through Scheil simulation and Figure 4.10 a) and b) shows the phase fraction graphically. The formation of α-Mg phase at 640°C is the initial solid phase for Mg-1Al-1Zn-0.3Mn-0.3Ca. The growth of α-Mg solid phase with HCP crystal structure in relation to liquid is fractioned at 50%, whereby at this stage, a new phase begins due to an invariant reaction. As with Mg-1Al-1Zn-0.3Mn, the phase to nucleate and grow immediately after is α-Mn phase. This phase nucleates at 633°C, which means α-Mg phase and liquid phase exist simultaneously for 7°C. The α-Mn phase then grows to a maximum solid fraction of 0.017%, which then disappears due to an invariant reaction causing nucleation of $Al_8Mn_5$. The $Al_8Mn_5$ solid phase begins to grow at 628°C, the solid fraction gradually increases and stabilises at 321°C with a percentage of 0.074%.

The calcium containing Mg-1Al-1Zn-0.3Mn-0.3Ca indicates that the next phase to nucleate is $Al_2Ca$. The phase $Al_2Ca$ nucleates and grows at 470°C and the fraction solidification of $Al_2Ca$ phase continues to increase until reaching 0.44%. It coexists with α-Mg and $Al_8Mn_5$ within the transient region. A major contrast to Mg-1Al-1Zn-0.3Mn since by this stage, the phases $Al_{11}Mn_4$, $Al_4Mn$, φ-AlMgZn and τ-AlMgZn nucleate and grow. The final phase to nucleate and grow is MgZn, this phase begins at 313°C and reaches a maximum fraction of 0.49% until solidus temperature is reached which is the greatest in comparison to other intermetallic compounds for this alloy.

**Table 4.6- Nucleation and growth sequence of phases of Mg-1Al-1Zn-0.3Mn-0.3Ca**

| Reaction | Temperature (°C) | Solid Fraction |
|---|---|---|
| $L \rightarrow$ α-Mg | 640.3 to 633.1 | 0 to 0.495 |
| $L \rightarrow$ α-Mg + α-Mn | 633.1 to 628.2 | 0.495 to 0.631 |
| L + α-Mn $\rightarrow$ α-Mg + $Al_8Mn_5$ | 628.2 | 0.631 |
| $L \rightarrow$ α-Mg + $Al_8Mn_5$ | 628.1 to 469.7 | 0.631 to 0.967 |
| $L \rightarrow$ α-Mg + $Al_8Mn_5$ + $Al_2Ca$ | 469.7 to 321.2 | 0.967 to 0.989 |
| L + $Al_8Mn_5$ $\rightarrow$ α-Mg + $Al_2Ca$ | 321.2 | 0.989 |
| $L \rightarrow$ α-Mg + $Al_2Ca$ | 321.2 to 313.2 | 0.989 to 0.990 |
| $L \rightarrow$ α-Mg + $Al_2Ca$ + MgZn | 313.2 to 293.0 | 0.990 to 1 |

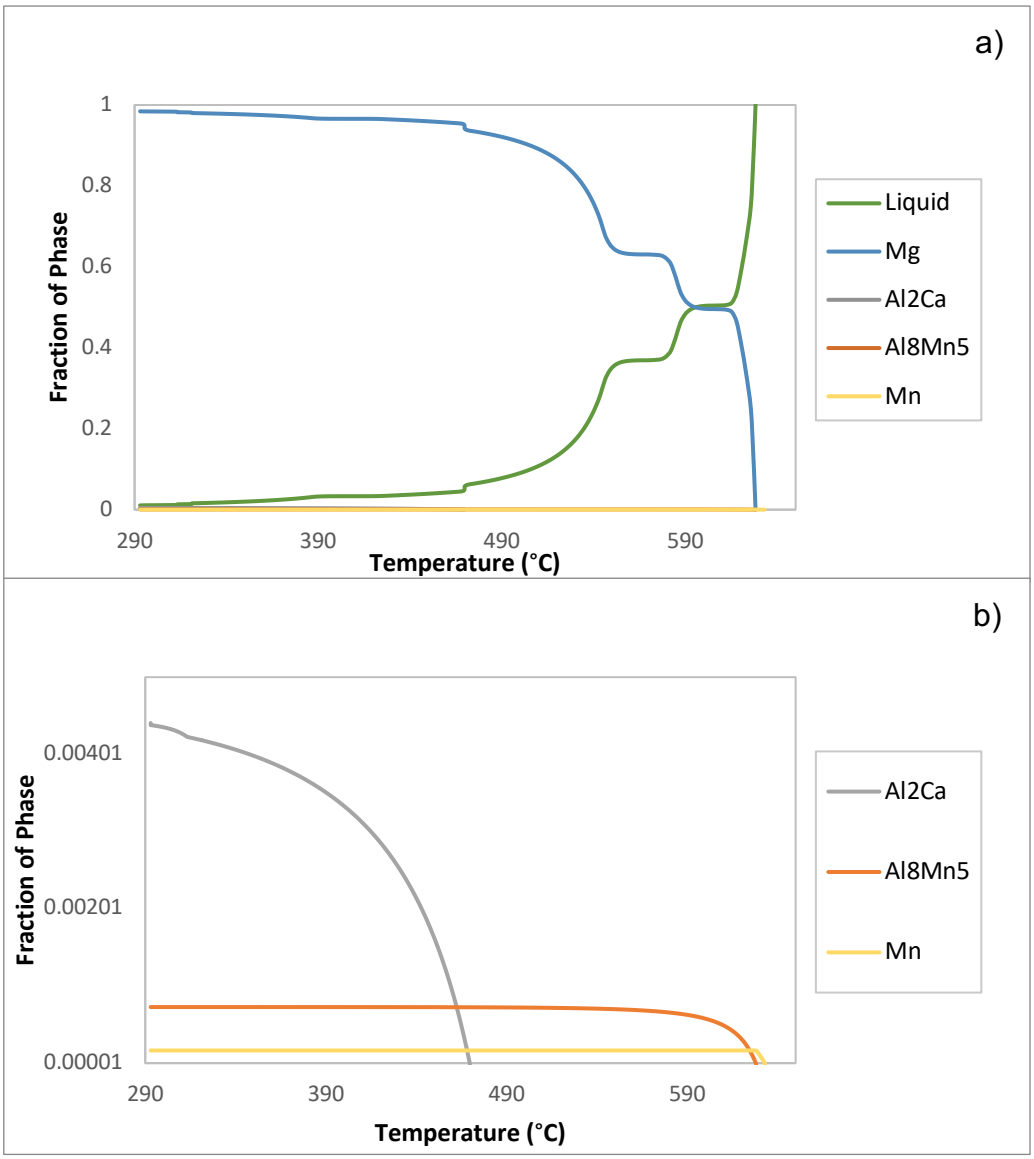


**Figure 4.10- a) and b) Scheil data showing theoretical phases present in Mg-1Al-1Zn-0.3Mn-0.3Ca**

### 4.2.2 AZM410-Ca

**Table 4.7- Comparison of liquidus temperature of Mg-4Al-1Zn-0.3Mn**

| | Liquidus Temperature | | |
|---|---|---|---|
| **Alloy** | **Experimental (°C)** | **Scheil (°C)** | **Lever (°C)** |
| ***AZM410*** | 620 ± 2.2 | 675 | 631 |

Mg-4Al-1Zn-0.3Mn consisting of increased alloying content of 4% aluminium was experimented on to establish the liquidus temperature and Table 4.7 is a comparison of acquired liquidus temperature. From the readings, latent heat was observed at approximately 620°C in the two instances as shown in Figure 4.11. In comparison to the acquired Scheil data and Lever rule method for Mg-4Al-1Zn-0.3Mn, the temperature at which solidification first begins is 675°C and 631°C respectively as shown in Figure 4.12. Interestingly, the first solid phase to form at 675°C according to Scheil data is $Al_8Mn_5$, which is in contrast to alloys Mg-1Al-1Zn-0.3Mn and Mg-1Al-1Zn-0.3Mn-0.3Ca, as for them, α-Mg solid phase nucleated and grew before $Al_8Mn_5$ phase, a phase which was preceded by α-Mn solid phase. The maximum latent heat given out by $Al_8Mn_5$ phase was 105 J, a considerably low amount compared to the next phase; α-Mg phase which gave out above 7000 J. This is the reason why there is a large disparity in experimental liquidus temperature and Scheil liquidus temperature, since observation of latent heat in cooling curve experiment coincided with the nucleation and growth of α-Mg phase.

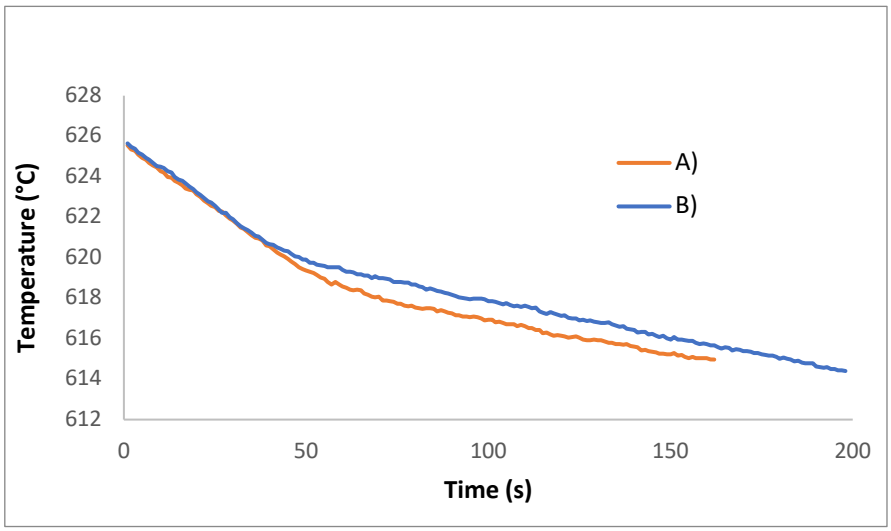


**Figure 4.11- Cooling curve measurement showing liquidus region of Mg-4Al-1Zn-0.3Mn with two experiments**

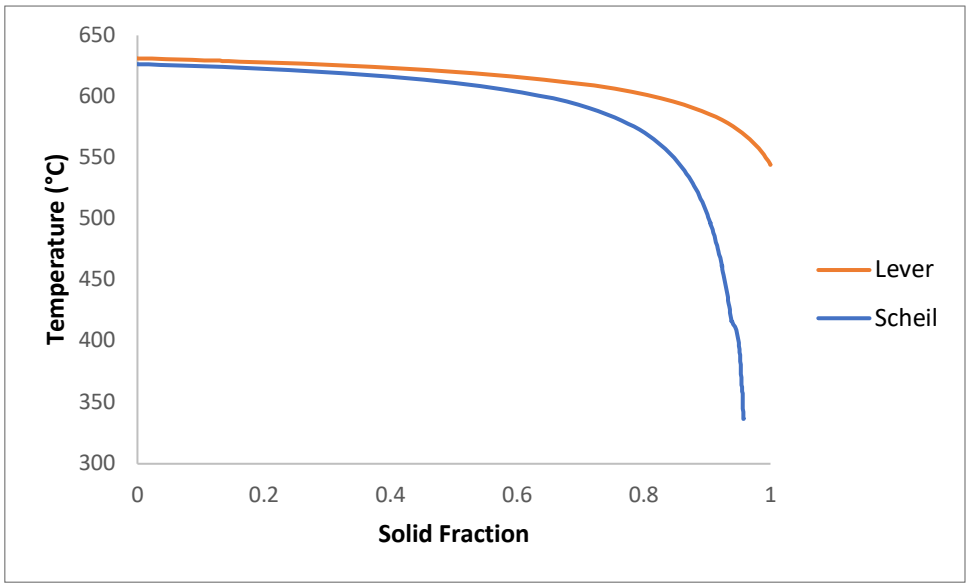


**Figure 4.12- Solid fraction of Mg-4Al-1Zn-0.3Mn according to Lever vs. Scheil**

As mentioned previously, the first solid phase to solidify is $Al_8Mn_5$, which occurs at 675°C is shown in Table 4.8 and further phases are shown in Figure 4.13 a) and b). In contrast to lower aluminium containing alloys Mg-1Al-1Zn-0.3Mn and Mg-1Al-1Zn-0.3Mn-0.3Ca, the initiation of solid through this phase is due to higher concentration of aluminium contained in Mg-4Al-1Zn-0.3Mn. Due to higher concentration of aluminium, the fraction solidified for this phase is 0.35%, which is far greater to 0.077% and 0.074% that was seen in the lower aluminium containing alloys, respectively. The presence of intermetallic compound $Al_8Mn_5$ remains alongside liquid phase for considerable amount of temperature until an invariant reaction causing the nucleation of α-Mg solid phase, a difference of 50°C. The phase α-Mg initiates at 626°C, which is a value very much comparable to the experimental liquidus temperature. With 90% of liquid solidified at 496°C, the emergence of phase $Al_{11}Mn_4$ occurs with the disappearance of $Al_8Mn_5$ with maximum solid fraction reaching 0.002004%. At 462°C, the phase $Al_{11}Mn_4$ disappears and the phase $Al_4Mn$ nucleates and reaches a maximum solid fraction of 0.001004%. This phase then disappears and is subsequently followed by $Mg_{17}Al_{12}$, which solidifies at 417°C, reaching a maximum solid fraction of 3.32%, the highest from all the intermetallic compounds. $Mg_{17}Al_{12}$ nucleates and grows when total fraction solidified is at 99%. Interestingly, this phase does not nucleate in previous alloys that contained only 1% of aluminium. The final two phases to solidify at 365°C and 338°C are φ-AlMgZn and τ-AlMgZn, with maximum solid fraction reaching 0.45% and 0.02% respectively.

**Table 4.8- Nucleation and growth sequence of phases of Mg-4Al-1Zn-0.3Mn**

| Reaction | Temperature (°C) | Solid Fraction |
|---|---|---|
| $L \rightarrow Al_8Mn_5$ | 674.5 to 626.6 | 0 to 0.002174 |
| $L \rightarrow Al_8Mn_5 + \alpha\text{-Mg}$ | 626.6 to 496.5 | 0.002174 to 0.909 |
| $L + Al_8Mn_5 \rightarrow \alpha\text{-Mg} + Al_{11}Mn_4$ | 496.5 | 0.909 |
| $L \rightarrow \alpha\text{-Mg} + Al_{11}Mn_4$ | 496.5 to 461.7 | 0.909 to 0.927 |
| $L + Al_{11}Mn_4 \rightarrow \alpha\text{-Mg} + Al_4Mn$ | 461.7 | 0.927 |
| $L \rightarrow \alpha\text{-Mg} + Al_4Mn$ | 461.7 to 416.8 | 0.927 to 0.942 |
| $L \rightarrow \alpha\text{-Mg} + Al_4Mn + Mg_{17}Al_{12}$ | 416.8 to 380.1 | 0.942 to 0.987 |
| $L + Al_4Mn \rightarrow \alpha\text{-Mg} + Mg_{17}Al_{12}$ | 378.4 | 0.988 |
| $L \rightarrow \alpha\text{-Mg} + Mg_{17}Al_{12}$ | 378.4 to 365.4 | 0.988 to 0.991 |
| $L + Mg_{17}Al_{12} \rightarrow \alpha\text{-Mg} + \varphi\text{-AlMgZn}$ | 365.3 | 0.991 |
| $L \rightarrow \alpha\text{-Mg} + \varphi\text{-AlMgZn}$ | 365.3 to 337.7 | 0.991 to 0.998 |
| $L + \varphi\text{-AlMgZn} \rightarrow \alpha\text{-Mg} + \tau\text{-AlMgZn}$ | 337.7 | 0.998 |
| $L \rightarrow \alpha\text{-Mg} + \tau\text{-AlMgZn}$ | 337.7 to 336.8 | 0.998 to 1 |

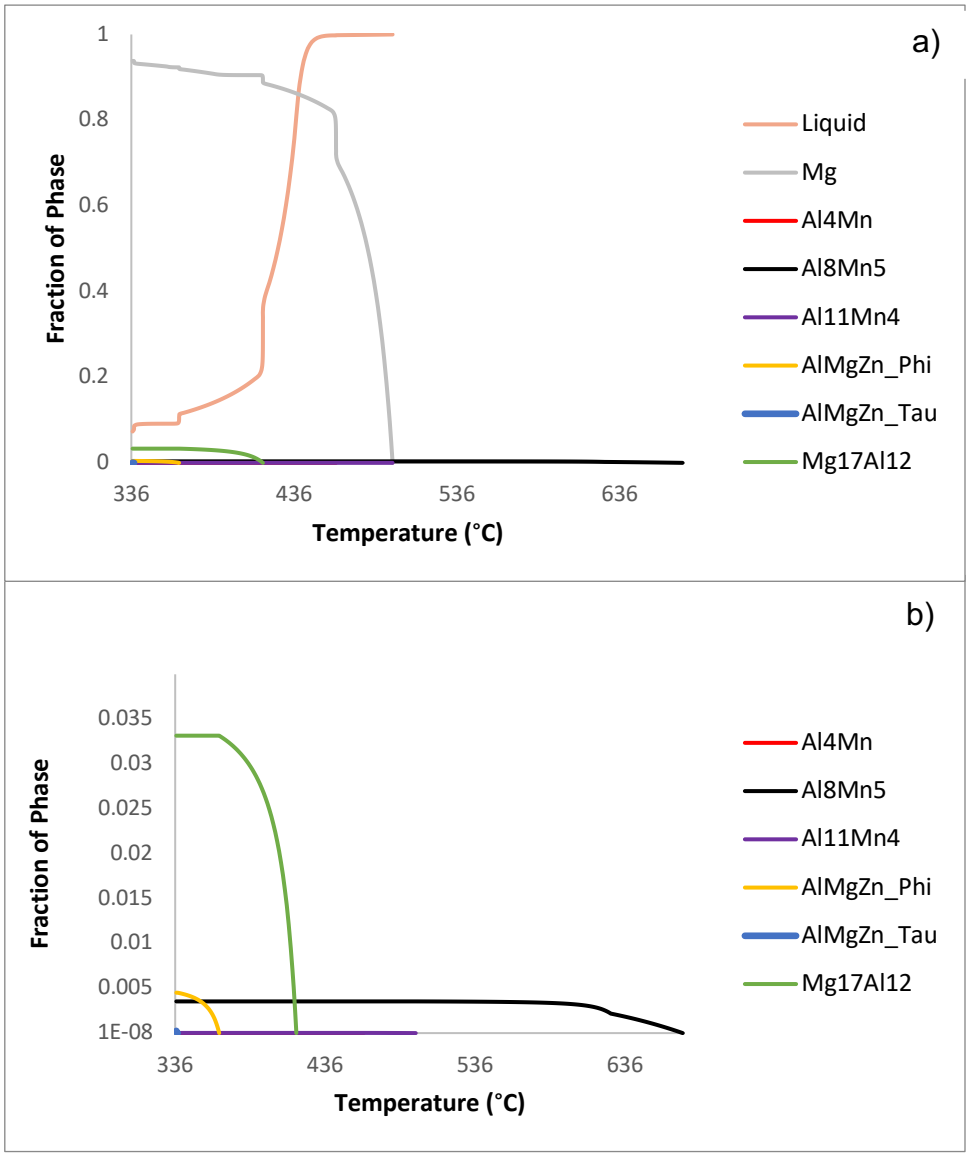


**Figure 4.13- a) and b) Scheil data showing theoretical phases present in Mg-4Al-1Zn-0.3Mn**

**Table 4.9- Comparison of liquidus temperature of Mg-4Al-1Zn-0.3Mn-0.3Ca**

| | Liquidus Temperature | | |
|---|---|---|---|
| **Alloy** | **Experimental (°C)** | **Scheil (°C)** | **Lever (°C)** |
| ***AZMX4100*** | 630 ± 2.2 | 675 | 630 |

The averaged liquidus temperature obtained for Mg-4Al-1Zn-0.3Mn-0.3Ca through cooling curve measurement is 630°C as shown in Table 4.9 and Figure 4.14. Temperature measurement taken from reading A) was 629°C and from reading B) was 631°C. The formation of a solid phase began 10°C higher in this 0.3% Ca containing alloy in comparison to Mg-4Al-1Zn-0.3Mn. As with Mg-4Al-1Zn-0.3Mn, the Scheil data for liquidus temperature shows solidification begins at 675°C and through the Lever rule method, solidification begins at 630°C as shown in Figure 4.15.

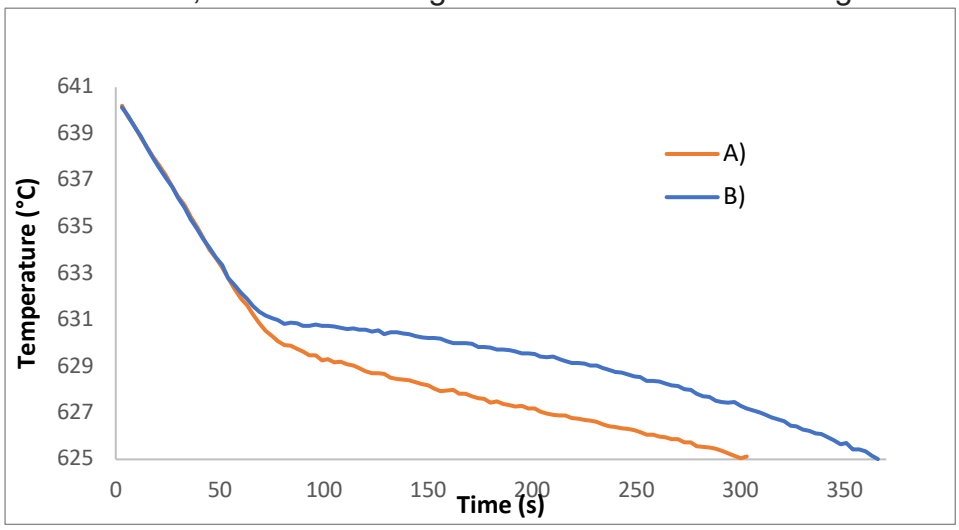


**Figure 4.14- Cooling curve measurement showing liquidus region of Mg-4Al-1Zn-0.3Mn-0.3Ca with two experiments**

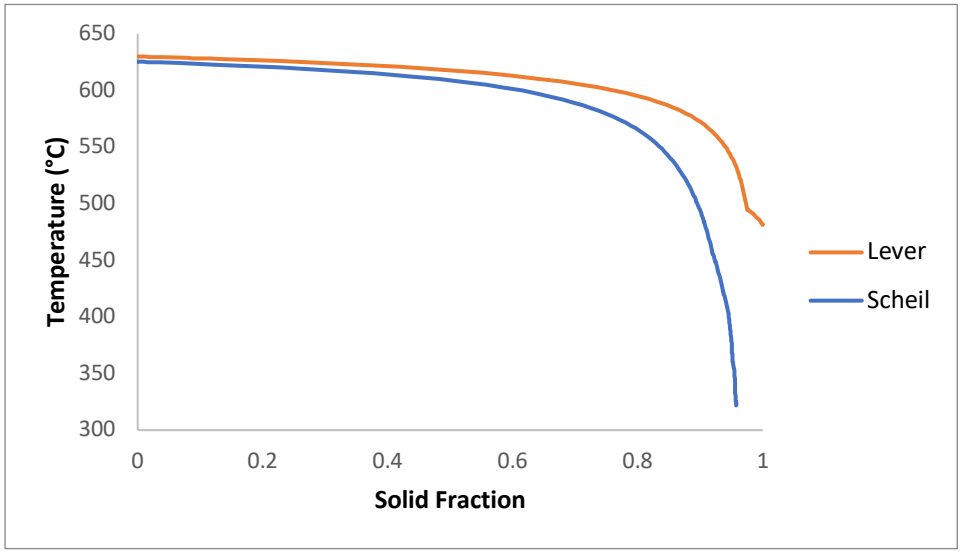


**Figure 4.15- Solid fraction of Mg-4Al-1Zn-0.3Mn-0.3Ca according to Lever vs. Scheil**

The first phase called $Al_8Mn_5$ begins to solidify at 675°C as displayed in Table 4.10, it reaches a maximum solid fraction of 0.36%. The next phase to nucleate and grow due to an invariant reaction is α-Mg phase, the occurrence of this phase at 625°C approximately coincides with the experimental liquidus temperature which was 630°C. At 484°C with 90% of solid fraction, $Al_8Mn_5$ phase disappears, giving way to $Al_{11}Mn_4$ phase to solidify which reaches a maximum solid fraction of 0.0016%. The addition of 0.3% of calcium causes this alloy to generate $Al_2Ca$ at 456°C, at this invariant point, $Al_2Ca$ phase coexists with α-Mg and $Al_{11}Mn_4$. The phase $Al_2Ca$ then reaches a maximum solid fraction of 0.32%. The following phase $Al_4Mn$ solidifies at 449°C and reaches a maximum solid fraction of 0.000741%, the occurrence of this phase happens after the disappearance of $Al_{11}Mn_4$. At 423°C, the next phase, $Mg_{17}Al_{12}$ nucleates as it also did for Mg-4Al-1Zn-0.3Mn. It grows alongside α-Mg and $Al_2Ca$ and reaches a substantially high concentration of 2.7%, the greatest in this calcium containing alloy. The next phase to solidify is φ-AlMgZn, this occurs at 360°C and the phase reaches a maximum concentration of 0.7%. The final phase to nucleate is MgZn, this occurs when φ-AlMgZn disappears and exists alongside α-Mg and $Al_2Ca$. It reaches a maximum solid fraction of 0.13%, at a period when the total solid fraction is 99.7%. All these solidified phase fractions are shown in Figure 4.16 a) and b).

**Table 4.10- Nucleation and growth sequence of phases of Mg-4Al-1Zn-0.3Mn-0.3Ca**

| Reaction | Temperature (°C) | Solid Fraction |
|---|---|---|
| $L \rightarrow Al_8Mn_5$ | 674.7 to 625.3 | 0 to 0.002222 |
| $L \rightarrow Al_8Mn_5 + α\text{-}Mg$ | 625.3 to 484.0 | 0.002222 to 0.910 |
| $L + Al_8Mn_5 \rightarrow α\text{-}Mg + Al_{11}Mn_4$ | 484.0 | 0.910 |
| $L \rightarrow α\text{-}Mg + Al_{11}Mn_4$ | 484.0 to 455.9 | 0.910 to 0.923 |
| $L \rightarrow α\text{-}Mg + Al_{11}Mn_4 + Al_2Ca$ | 455.9 to 448.9 | 0.923 to 0.929 |
| $L + Al_{11}Mn_4 \rightarrow α\text{-}Mg + Al_2Ca + Al_4Mn$ | 448.9 | 0.929 |
| $L \rightarrow α\text{-}Mg + Al_2Ca + Al_4Mn$ | 448.9 to 423.0 | 0.929 to 0.942 |
| $L + Al_2Ca \rightarrow α\text{-}Mg + Al_4Mn + Mg_{17}Al_{12}$ | 423.0 | 0.942 |
| $L \rightarrow α\text{-}Mg + Al_4Mn + Mg_{17}Al_{12}$ | 423.0 to 382.0 | 0.942 to 0.978 |
| $L + Al_4Mn \rightarrow α\text{-}Mg + Mg_{17}Al_{12}$ | 382.0 | 0.978 |
| $L \rightarrow α\text{-}Mg + Mg_{17}Al_{12}$ | 382.0 to 368.4 | 0.978 to 0.983 |
| $L \rightarrow α\text{-}Mg + Mg_{17}Al_{12} + Al_2Ca$ | 368.4 to 360.5 | 0.983 to 0.985 |
| $L + Mg_{17}Al_{12} \rightarrow α\text{-}Mg + Al_2Ca + φ\text{-}AlMgZn$ | 360.5 | 0.985 |
| $L \rightarrow α\text{-}Mg + Al_2Ca + φ\text{-}AlMgZn$ | 360.5 to 327.6 | 0.985 to 0.997 |
| $L + φ\text{-}AlMgZn \rightarrow α\text{-}Mg + Al_2Ca + MgZn$ | 327.6 | 0.997 |
| $L \rightarrow α\text{-}Mg + Al_2Ca + MgZn$ | 327.6 to 321.9 | 0.997 to 1 |

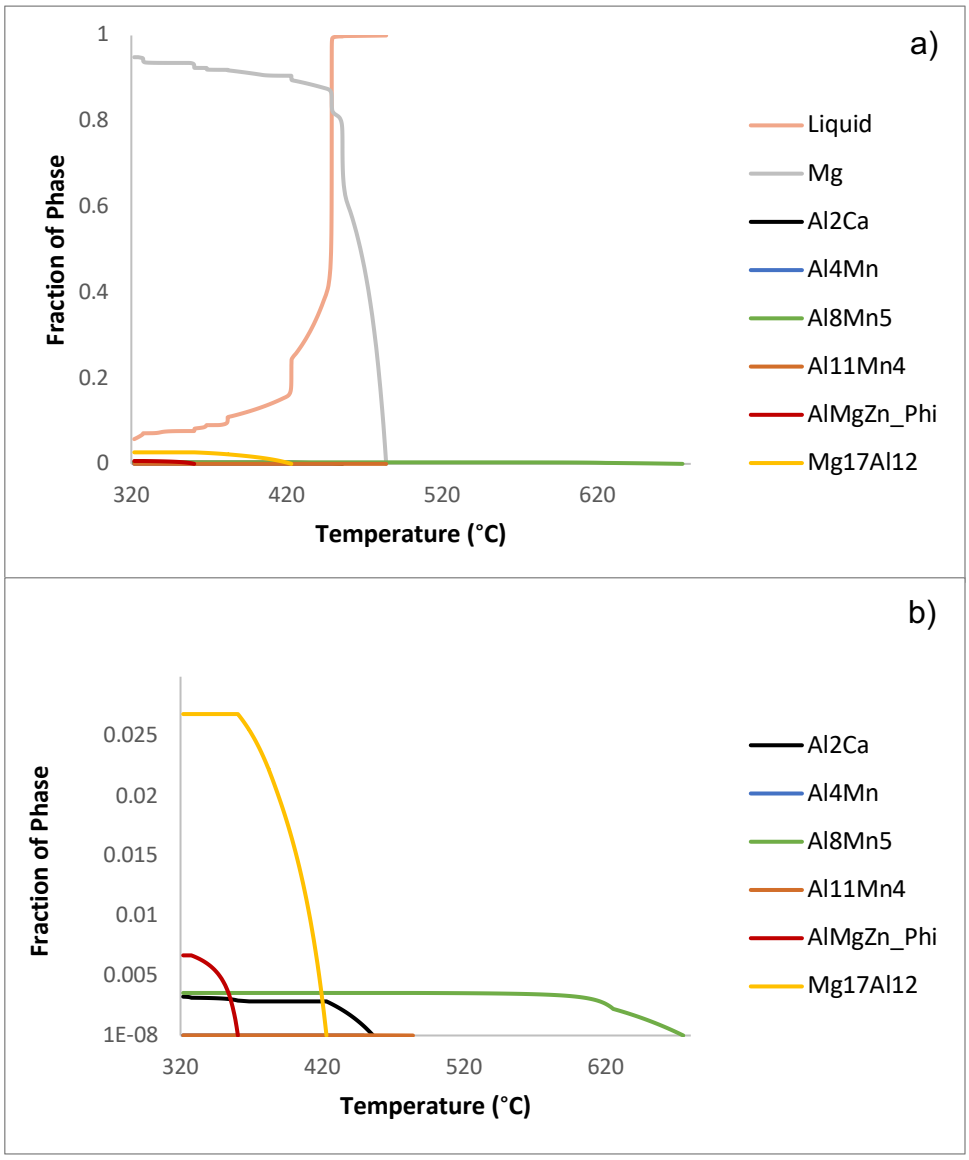


**Figure 4.16- a) and b) Scheil data showing theoretical phases present in Mg-4Al-1Zn-0.3Mn-0.3Ca**

### 4.2.3 AZM140-Ca

**Table 4.11- Comparison of liquidus temperature of Mg-1Al-4Zn-0.3Mn**

| | Liquidus Temperature | | |
|---|---|---|---|
| **Alloy** | **Experimental (°C)** | **Scheil (°C)** | **Lever (°C)** |
| ***AZM140*** | 635 ± 2.2 | 632 | 633 |

The liquidus temperature of alloy Mg-1Al-4Zn-0.3Mn displayed in Table 4.11 was obtained through cooling curve experiment with two readings being taken during cooling process. Both readings taken at the occurrence of substantial latent heat equated to 635°C. Scheil calculation of Mg-1Al-4Zn-0.3Mn shows liquidus temperature beginning at 632°C, with nucleation and growth of α-Mg solid phase. The Lever rule method displayed 633°C as the beginning temperature of solidification. Figure 4.17 and 4.18 show liquidus behaviour according to experiment, Scheil and Lever methods.

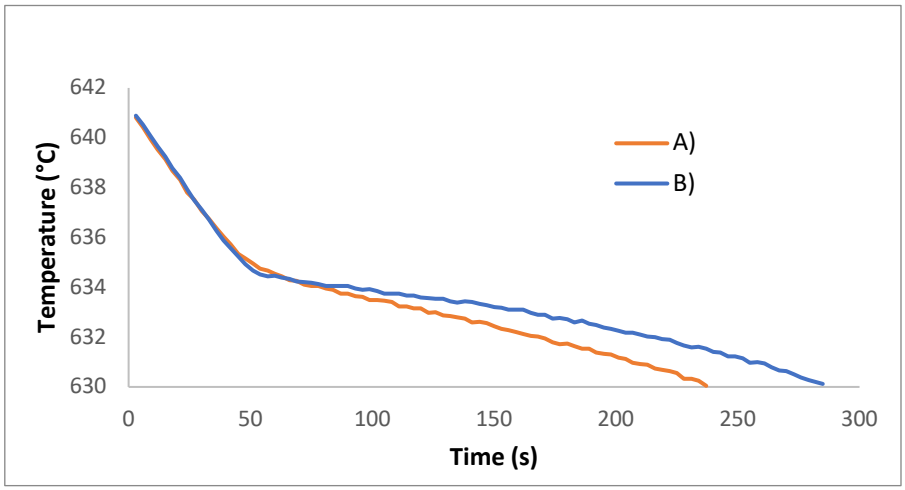


**Figure 4.17- Cooling curve measurement showing liquidus region of Mg-1Al-4Zn-0.3Mn with two experiments**

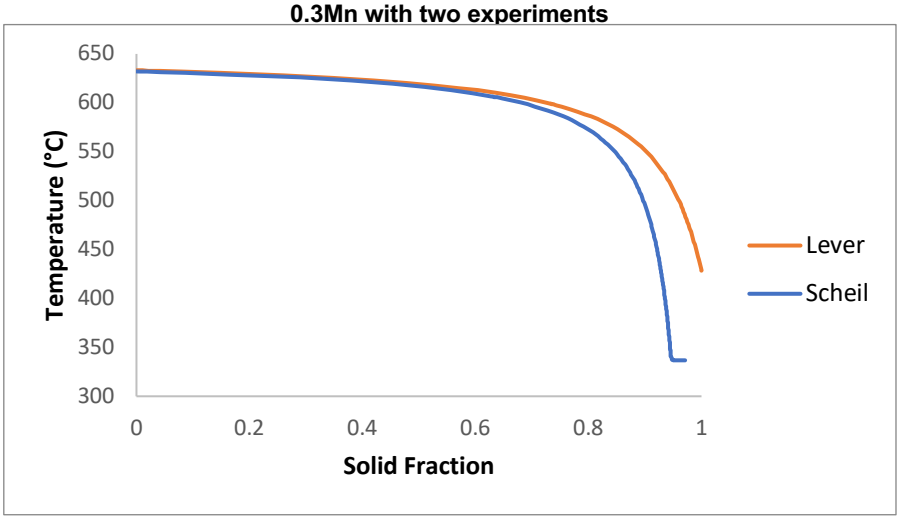


**Figure 4.18- Solid fraction of Mg-1Al-4Zn-0.3Mn according to Lever vs. Scheil**

The first phase to nucleate and grow below the liquidus range is α-Mg solid phase as displayed in Table 4.12, it remains as the sole solid phase until 625°C. At this temperature, the formation of $Al_8Mn_5$ starts with an invariant reaction, with total solid fraction till this point being 63%. The phase $Al_8Mn_5$ reaches a maximum solid fraction of 0.07%. The next phase to nucleate is $Al_{11}Mn_4$, this happens at 377°C when $Al_8Mn_5$ disappears. The nucleation and growth happens at a significantly large temperature disparity from the nucleation and growth of phase $Al_8Mn_5$. The $Al_{11}Mn_4$ phase reaches a maximum solid fraction of 0.00009%. The next phase called $Al_4Mn$ nucleates and grows at 348°C and reaches a maximum solid fraction of 0.00001%, this again occurs when $Al_{11}Mn_4$ disappears. The final phase called τ-AlMgZn, nucleates at 338°C and reaches maximum solid fraction of 0.63%. All the mentioned phases are shown in Figure 4.19 a) and b) as function of phase fraction and temperature.

**Table 4.12- Nucleation and growth sequence of phases of Mg-1Al-4Zn-0.3Mn**

| Reaction | Temperature (°C) | Solid Fraction |
|---|---|---|
| $L \rightarrow \alpha\text{-Mg}$ | 632.1 to 606.6 | 0 to 0.628 |
| $L \rightarrow \alpha\text{-Mg} + Al_8Mn_5$ | 606.6 to 377.5 | 0.628 to 0.941 |
| $L + Al_8Mn_5 \rightarrow \alpha\text{-Mg} + Al_{11}Mn_4$ | 377.5 | 0.941 |
| $L \rightarrow \alpha\text{-Mg} + Al_{11}Mn_4$ | 377.5 to 347.9 | 0.941 to 0.945 |
| $L + Al_{11}Mn_4 \rightarrow \alpha\text{-Mg} + Al_4Mn$ | 347.9 | 0.945 |
| $L \rightarrow \alpha\text{-Mg} + Al_4Mn$ | 347.9 to 340.8 | 0.945 to 0.946 |
| $L \rightarrow \alpha\text{-Mg} + Al_4Mn + \varphi$ | 340.8 to 337.7 | 0.946 to 0.951 |
| $L + \varphi \rightarrow \alpha\text{-Mg} + Al_4Mn + \tau\text{-AlMgZn}$ | 337.7 | 0.951 |
| $L + Al_4Mn \rightarrow \alpha\text{-Mg} + \tau\text{-AlMgZn}$ | 337.7 to 336.9 | 0.951 to 0.955 |
| $L \rightarrow \alpha\text{-Mg} + \tau\text{-AlMgZn} + Al_{11}Mn_4$ | 336.9 | 0.955 to 1 |

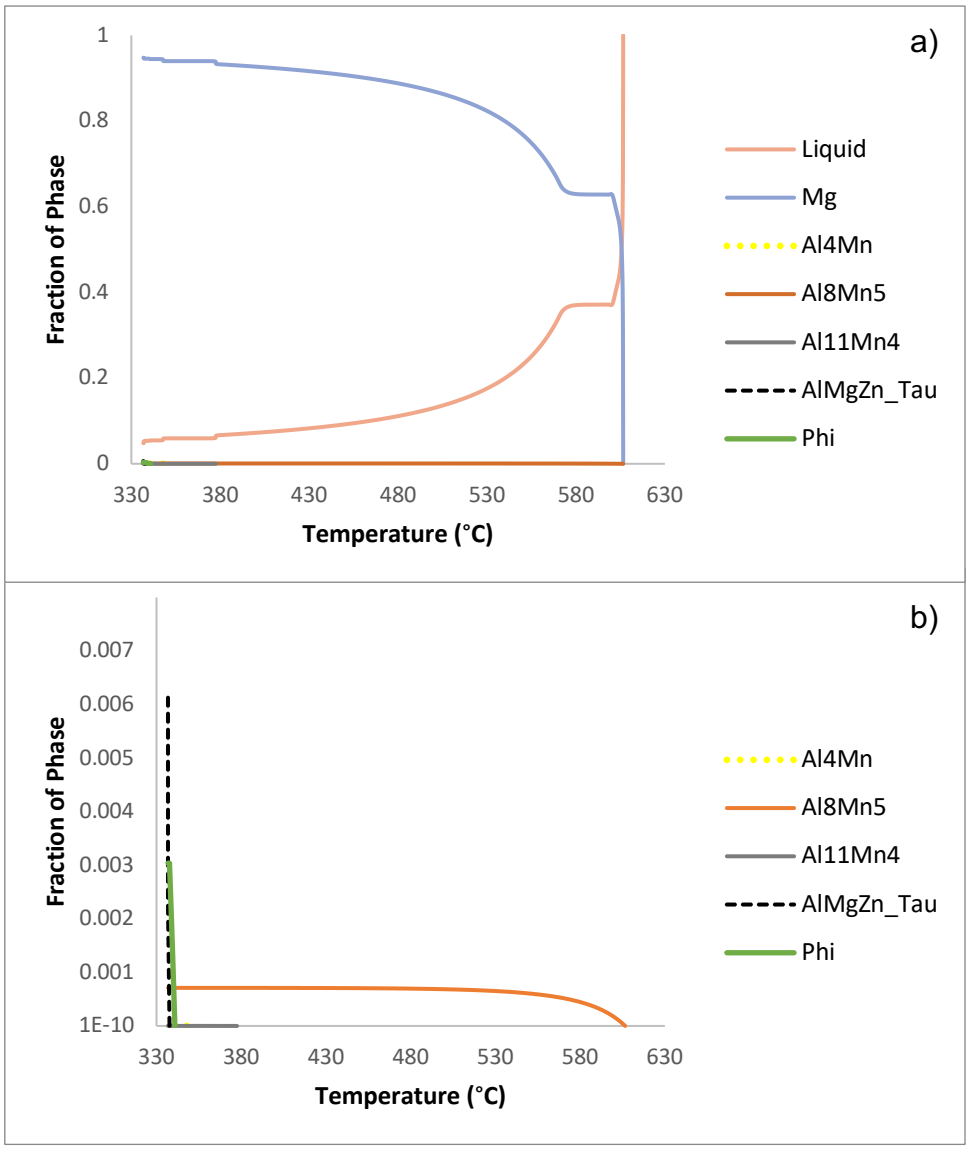


**Figure 4.19- a) and b) Scheil data showing theoretical phases present in Mg-1Al-4Zn-0.3Mn**

**Table 4.13- Comparison of liquidus temperature of Mg-1Al-4Zn-0.3Mn-0.3Ca**

| | Liquidus Temperature | | |
|---|---|---|---|
| **Alloy** | **Experimental (°C)** | **Scheil (°C)** | **Lever (°C)** |
| ***AZMX1400*** | 631 ± 2.2 | 631 | 631 |

The experimental liquidus temperature for 0.3% calcium containing Mg-1Al-4Zn-0.3Mn-0.3Ca came to 631°C after being averaged as displayed in Table 4.13 and graphically shown in Figure 4.20. As for the Scheil calculation and Lever rule method, the liquidus temperature for Mg-1Al-4Zn-0.3Mn-0.3Ca amounted to 631°C for both respectively as shown in Figure 4.21.

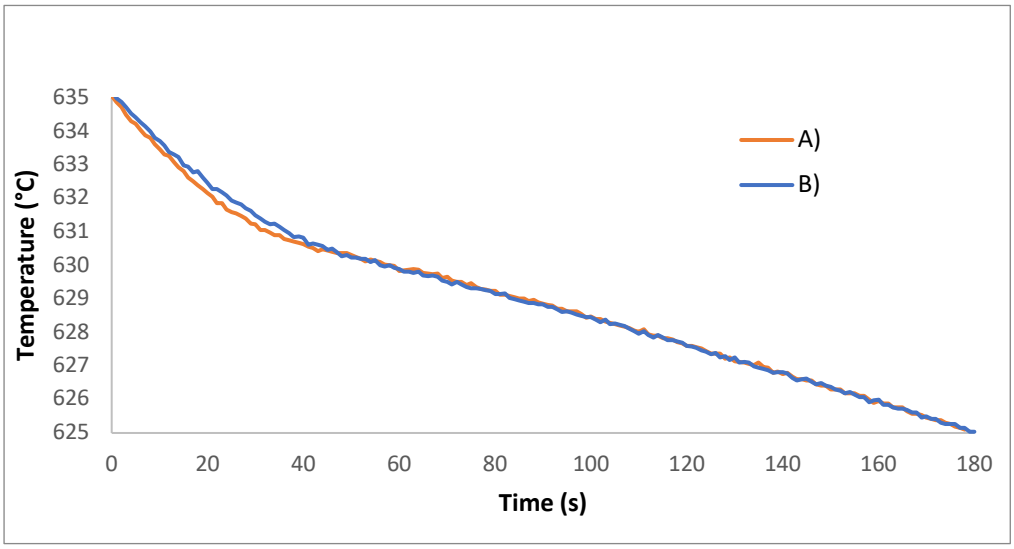


**Figure 4.20- Cooling curve measurement showing liquidus region of Mg-1Al-4Zn-0.3Mn-0.3Ca with two experiments**

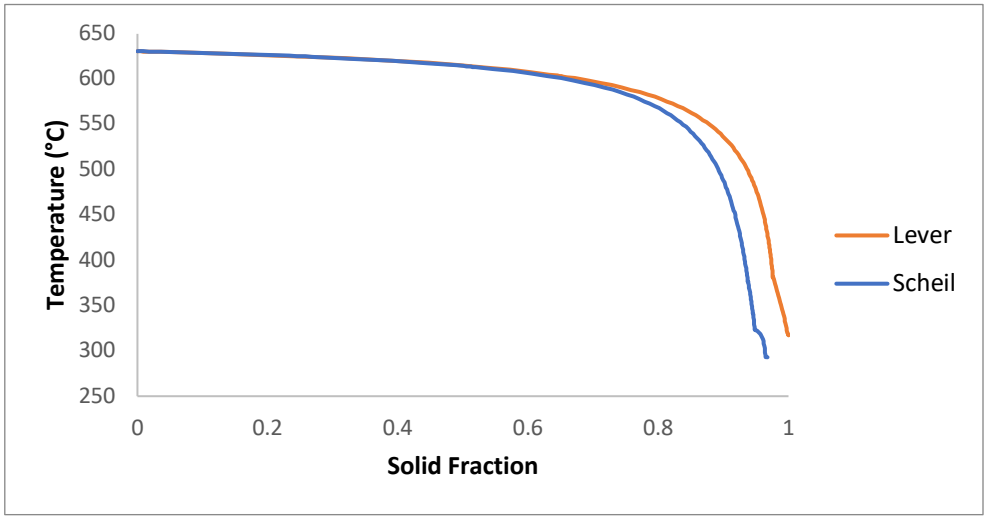


**Figure 4.21- Solid fraction of Mg-1Al-4Zn-0.3Mn-0.3Ca according to Lever vs. Scheil**

The first solid phase to nucleate and grow at liquidus temperature for Mg-1Al-4Zn-0.3Mn-0.3Ca is α-Mg as displayed in Table 4.14. At 625°C, α-Mg solid phase is followed by the formation of α-Mn phase. The nucleation and growth of α-Mn phase occurs while the total solid fraction is 25%. The maximum solid fraction of α-Mn phase reaches 0.04%. The next phase to follow the disappearance of α-Mn phase is $Al_8Mn_5$ phase which occurs at 614°C and it reaches maximum solid fraction of 0.11%. The next phase to follow is $Al_2Ca$ phase which occurs at 377°C and it reaches maximum solid fraction of 0.37%. Shortly after at 342°C, the phase $Al_{11}Mn_4$ nucleates due to disappearance of $Al_8Mn_5$ and it eventually reaches a maximum solid fraction of 0.000009%. The final solid phase to nucleate is MgZn phase which occurs at 323°C and it reaches a maximum solid fraction of 2.37%. These solidified phases are shown in Figure 4.22 a) and b).

**Table 4.14- Nucleation and growth sequence of phases of Mg-1Al-4Zn-0.3Mn-0.3Ca**

| Reaction | Temperature (°C) | Solid Fraction |
|---|---|---|
| $L \rightarrow$ α-Mg | 630.8 to 625.3 | 0 to 0.247 |
| $L \rightarrow$ α-Mg + α-Mn | 625.3 to 613.8 | 0.247 to 0.510 |
| L + α-Mn $\rightarrow$ α-Mg + $Al_8Mn_5$ | 613.8 | 0.510 |
| $L \rightarrow$ α-Mg + $Al_8Mn_5$ | 613.8 to 377.5 | 0.510 to 0.939 |
| $L \rightarrow$ α-Mg + $Al_8Mn_5$ + $Al_2Ca$ | 377.5 to 342.0 | 0.939 to 0.949 |
| L + $Al_8Mn_5$ $\rightarrow$ α-Mg + $Al_2Ca$ + $Al_{11}Mn_4$ | 342.0 | 0.949 |
| $L \rightarrow$ α-Mg + $Al_2Ca$ + $Al_{11}Mn_4$ | 342.0 to 331.7 | 0.949 to 0.951 |
| L + $Al_{11}Mn_4$ $\rightarrow$ α-Mg + $Al_2Ca$ | 331.7 | 0.951 |
| $L \rightarrow$ α-Mg + $Al_2Ca$ | 331.7 to 323.5 | 0.951 to 0.952 |
| $L \rightarrow$ α-Mg + $Al_2Ca$ + MgZn | 323.5 to 293.0 | 0.952 to 1 |

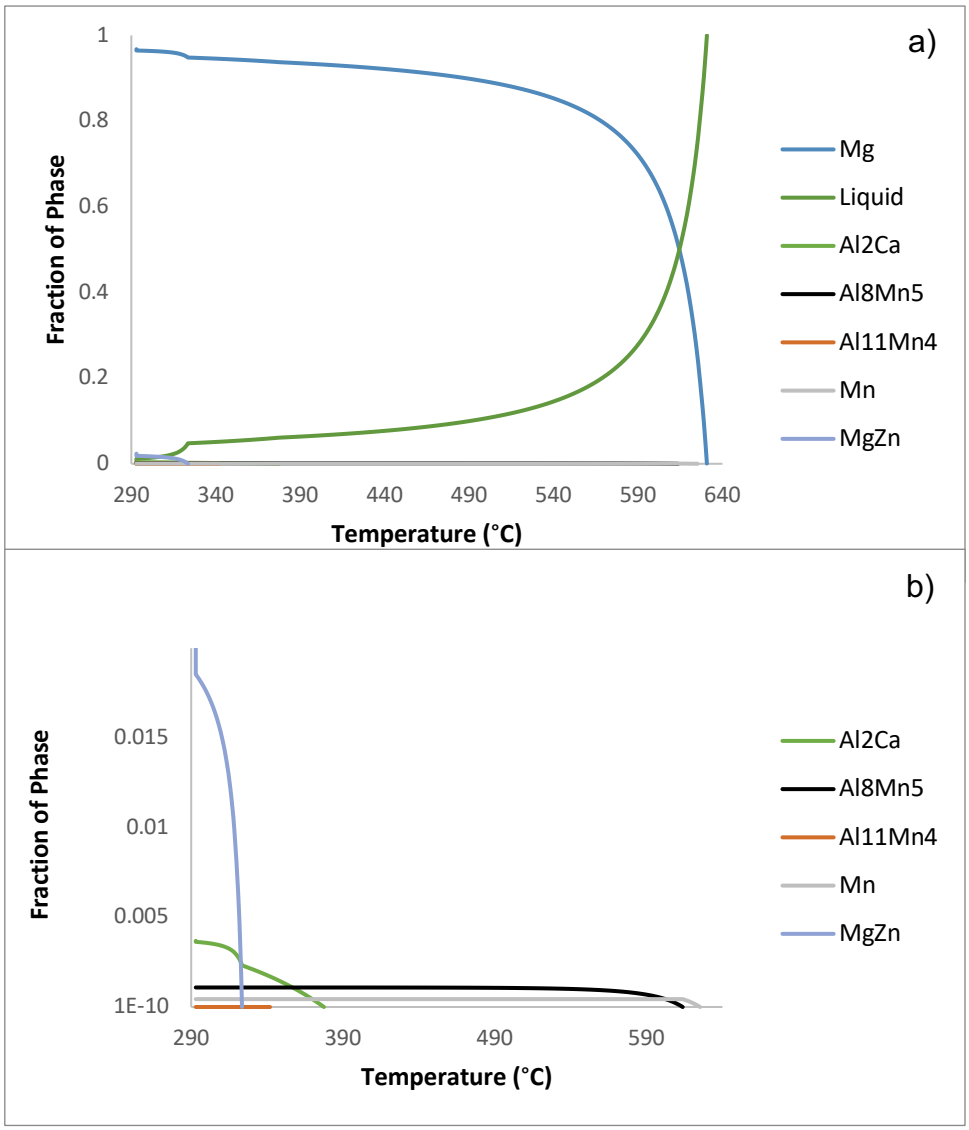


**Figure 4.22- a) and b) Scheil data showing theoretical phases present in Mg-1Al-4Zn-0.3Mn**

## 4.3 Microstructure Characterisation

### 4.3.1 AZM110-Ca

The as-cast microstructure of Mg-1Al-1Zn-0.3Mn alloy (AZM110) shown in Figure 4.23 a) contained a dendritic microstructure with an approximate grain size of 250±34μm. There was little to no observation of intermetallics in the as-cast Mg-1Al-1Zn-0.3Mn alloy (AZM110). An indication that most intermetallic compounds dissolved into the α-magnesium matrix without even requiring solid solution heat treatment. But using back-scattered electron mode on a scanning electron microscope as shown in Figure 4.23 c), there appeared a negligible amount of globular intermetallic particles measuring approximately 4.5μm in diameter.

After homogenisation heat treatment of Mg-1Al-1Zn-0.3Mn alloy (AZM110) at 400°C for 1h, the appearance of a dendritic microstructure was removed and therefore became equiaxed as shown in Figure 4.23 e). Grain size of homogenised alloy measured at 206±22μm as shown in Figure 4.24, a reduction of approximately 46μm from the dendritic state. This heat treatment completely dissolved all intermetallic particles into the α-magnesium matrix.

The as-cast microstructure of calcium added Mg-1Al-1Zn-0.3Mn-0.3Ca alloy (AZMX1100) shown in Figure 4.23 b) contained a dendritic microstructure but was not as pronounced as AZM110 alloy. The approximate grain size was 313±40μm, a grain size slightly larger than AZM110 alloy. In comparison to AZM110 alloy, segregation of solute elements within grains and along the grain boundaries was apparent, as shown in Figure 4.23 d). An indication that the intermetallic particles in the as-cast condition did not uniformly dissolve into the α-magnesium matrix. Intermetallic particles of two distinct morphology were found in the microstructure, one situated at the grain boundaries with semi-continuous distribution and the other intermetallic particles were situated inside the grains with globular morphology. The measured volume fraction of these intermetallics was approximately 1.4% as shown in Figure 4.25. The globular intermetallic particles situated within grains, measured at approximately 4.4μm in diameter. Whereas, the intermetallic particles found at the grain boundaries measured at approximately 58.5μm in length and a thickness of approximately 0.9μm. The addition of Ca showed a stark contrast in measured

volume fraction from the as-cast microstructures of Mg-1Al-1Zn-0.3Mn alloy (AZM110). An indication that elemental solid solubility decreased with the addition of calcium.

After a homogenisation heat treatment of Mg-1Al-1Zn-0.3Mn-0.3Ca alloy (AZMX1100) at 450°C for 2hrs as shown in Figure 4.23 f), the total segregation of solute elements was reduced, and a dendritic microstructure was removed. The heat treatment achieved a grain size measuring approximately 333±44µm, an indication that there was no significant activity regarding grain size change from the as-cast condition. The volume fraction of the retained intermetallic particles was now approximately 0.5%. The appearance of intermetallic particles with globular morphology situated within grains was not affected by homogenisation heat treatment. These globular particles represent $Al_8Mn_5$ phase, this phase has been confirmed to nucleate and grow early in the solidification process which indicates a significantly high melting point. It is widely reported that attempts to dissolve $Al_8Mn_5$ phase through homogenisation heat treatment does not occur.

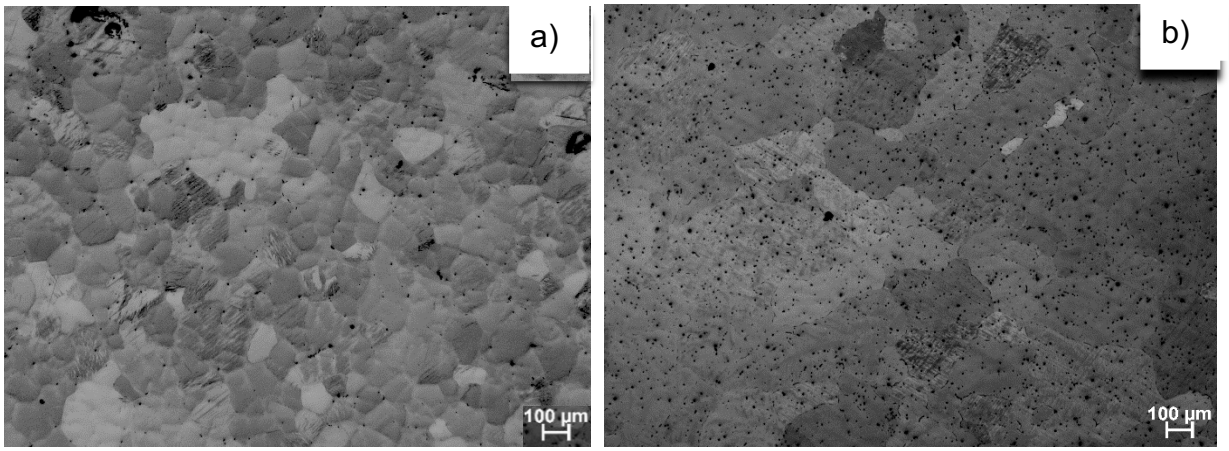

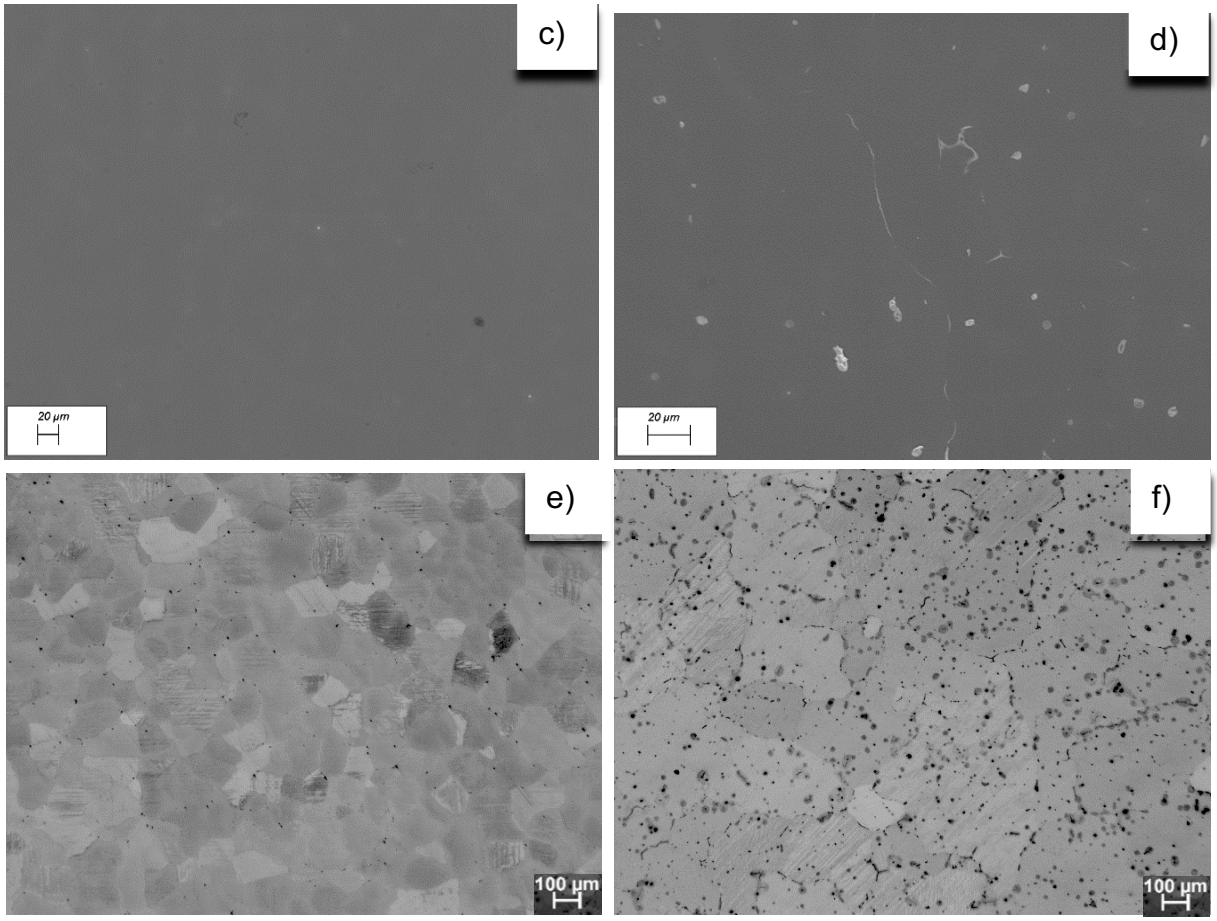


**Figure 4.23- Microstructures of AZM110-Ca, a) Bright field image of as-cast Mg-1Al-1Zn-0.3Mn, b) Bright field image of as-cast Mg-1Al-1Zn-0.3Mn-0.3Ca, c) BSD image of as-cast Mg-1Al-1Zn-0.3Mn, d) BSD image of as-cast Mg-1Al-1Zn-0.3Mn-0.3Ca, e) Bright field micrograph of homogenised Mg-1Al-1Zn-0.3Mn at 400/1hr, f) Bright field micrograph of homogenised Mg-1Al-1Zn-0.3Mn-0.3Ca at 450/2hrs**

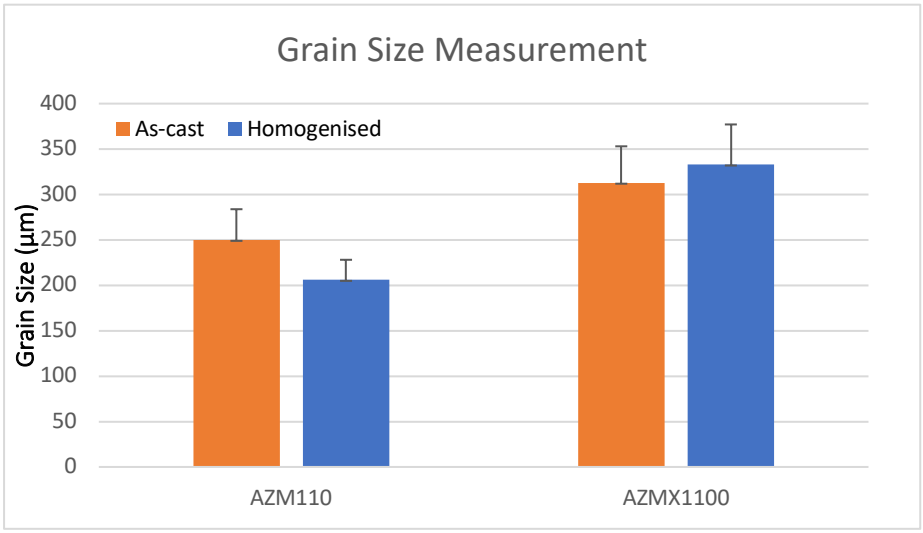


**Figure 4.24- Grain size measurement of as-cast and homogenised Mg-1Al-1Zn-0.3Mn and Mg-1Al-1Zn-0.3Mn-0.3Ca**

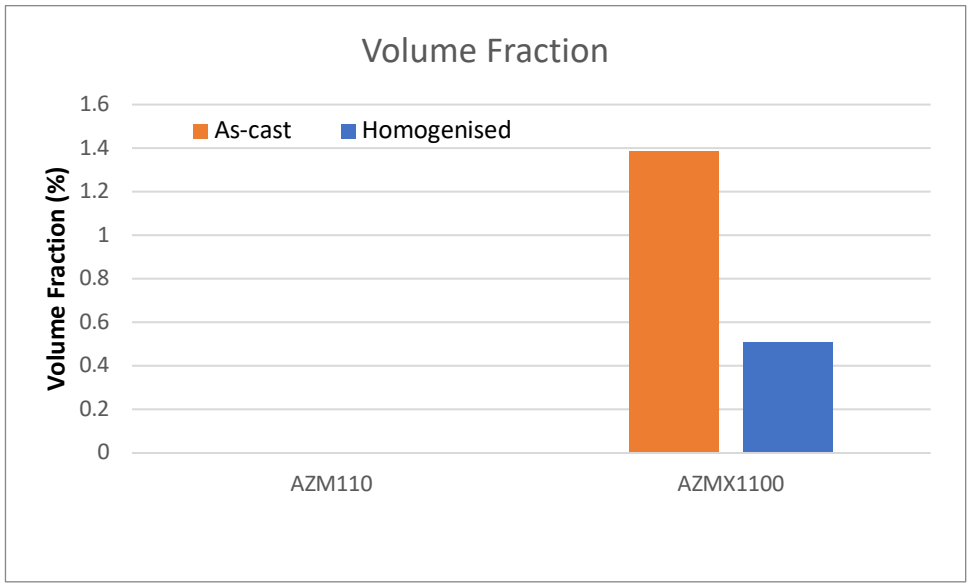


**Figure 4.25- Intermetallic volume fraction of as-cast and homogenised Mg-1Al-1Zn-0.3Mn (AZM110) and Mg-1Al-1Zn-0.3Mn-0.3Ca (AZMX1100)**

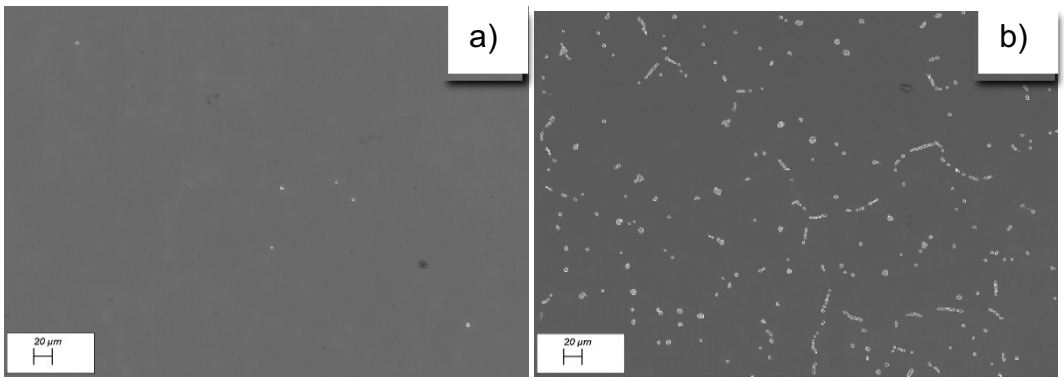


**Figure 4.26- SEM micrographs showing the distribution of intermetallic particles in as-cast alloys (a) Mg-1Al-1Zn-0.3Mn (b) Mg-1Al-1Zn-0.3Mn-0.3Ca**

EDX analysis was performed to understand the elemental composition of intermetallic compounds present in AZM110. During EDX spectra measurement, a spot was focussed upon and a phase comprising of Mg, Zn and Al appeared. The particle had a globular morphology and a composition of 85±6at% Mg, 10±2.7at% Zn and 4.6±1at% Al as shown in Table 4.15 (approximately $Mg_{17}Zn_2Al$).

**Table 4.15- EDX analysis of intermetallic particle(s) found in Mg-1Al-1Zn-0.3Mn**

| AZM110 | Mg | Zn | Al |
|---|---|---|---|
| | Atomic (%) | Atomic (%) | Atomic (%) |
| Particle 1 | 85 | 10 | 5 |

EDX analysis was performed to understand the elemental composition of intermetallic compounds present in AZMX1100. During EDX measurement, different spots and areas were focussed upon and a phase comprising of Mg, Zn, Al, Ca consistently showed up. Majority of the particles had an elongated morphology and a composition of 46.7±9at% Mg, 25.2±5at% Zn, 11.4±3.4at% Al and 14.5±2.7at% Ca as shown in Table 4.16 (approximately $Mg_8Zn_4Ca_3Al_2$).

**Table 4.16- EDX analysis of intermetallic particle(s) found in Mg-1Al-1Zn-0.3Mn-0.3Ca**

| AZMX1100 | Mg | Zn | Al | Ca |
|---|---|---|---|---|
| | Atomic (%) | Atomic (%) | Atomic (%) | Atomic (%) |
| Particle 1 | 50 | 24 | 12 | 14 |
| Particle 2 | 43 | 18 | 20 | 18 |
| Particle 3 | 30 | 9 | 33 | 28 |
| Particle 4 | 40 | 30 | 12 | 16 |
| Particle 5 | 43 | 30 | 12 | 15 |
| Particle 6 | 47 | 9 | 24 | 19 |
| Particle 7 | 48 | 32 | 10 | 10 |
| Particle 8 | 28 | 28 | 9 | 13 |
| Particle 9 | 60 | 20 | 9 | 12 |

### 4.3.2 AZM410-Ca

The as-cast microstructure of Mg-4Al-1Zn-0.3Mn alloy (AZM410) as shown in Figure 4.27 a) contained a dendritic microstructure with an approximate grain size of 139±11μm as shown in Figure 4.28. By increasing concentration of aluminium from 1% to 4%, there was observation of solute elements not dissolving completely into the α-magnesium matrix as shown in Figure 4.27 c). Distribution of globular shaped intermetallic particles was observed within grains and discrete distribution of intermetallic particles along grain boundaries. The total volume fraction of intermetallics amounted to 0.2% as shown in Figure 4.29. The measured and averaged diameter of globular intermetallic particles came to 4.32μm.

After homogenisation heat treatment of Mg-4Al-1Zn-0.3Mn alloy (AZM410) at 450°C for 1h as shown in Figure 4.27 e), the appearance of a dendritic microstructure disappeared alongside reduction in solute segregation. The volume fraction of measured intermetallic particles after homogenisation amounted to 0.03%, which indicates that majority of observed solute segregation dissolved into the α-magnesium matrix. The measurement of grain size after heat treatment approximately came to 177±23μm, which indicates grain growth occurred from the as-cast condition.

The as-cast microstructure of calcium added Mg-4Al-1Zn-0.3Mn-0.3Ca alloy (AZMX4100) as shown in Figure 4.27 b) showed a dendritic microstructure with an approximate grain size of 211±30μm. The addition of calcium in as-cast condition caused a substantial increase in grain size, approximately 72μm and an increased amount of solute element segregation at grain boundaries was also observed. There were two distinct morphologies of intermetallic particles observed: one globular, identical to the one in non-calcium containing alloy and semi-continuous distribution at grain boundaries as shown in Figure 4.27 d). Volume fraction of intermetallic particles was large as 1.3%, whereas for Mg-4Al-1Zn-0.3Mn alloy (AZM410) it was 0.2%. This is an indication that by adding calcium, this reduces solid solubility of alloying elements. The size of globular intermetallic particles was no different to the globular intermetallic particles found in AZM410 alloy. The length and thickness of semi-continuously distributed intermetallic particles at grain boundaries was averaged to be 47.0μm and 1.73μm, respectively.

After homogenisation heat treatment of Mg-4Al-1Zn-0.3Mn-0.3Ca alloy (AZMX4100) at 500°C for 1h as shown in Figure 4.27 f), the appearance of a dendritic microstructure was removed. The presence of solute segregation saw a significant reduction after homogenisation heat treatment. The grain size of AZMX4100 alloy was approximately 299±50μm, suggesting grain growth from the as-cast condition. The volume fraction of solute presence after heat treating went from 1.3% to 0.7%.

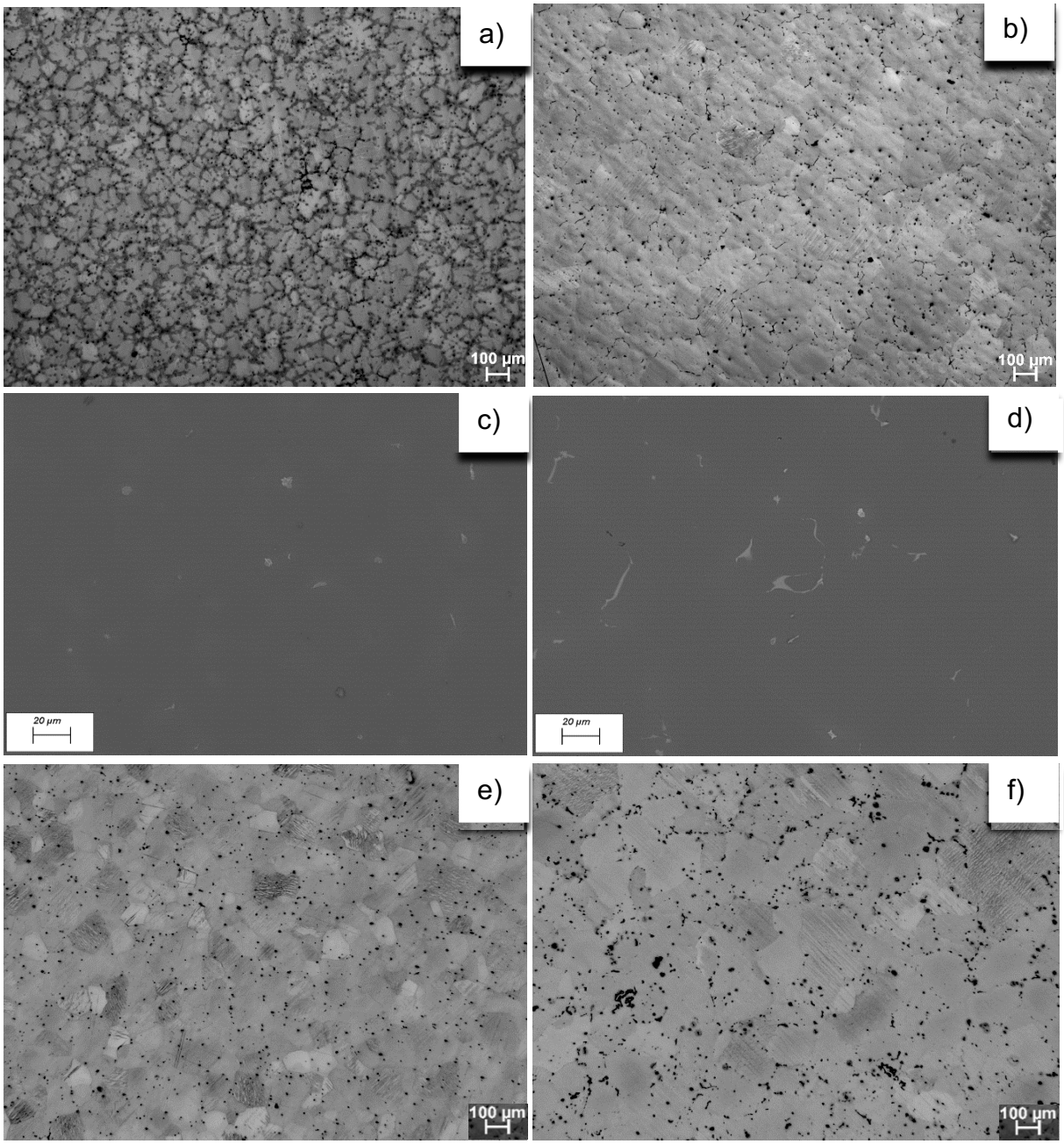


**Figure 4.27- Microstructures of AZM410-Ca, a) Bright field image of as-cast Mg-4Al-1Zn-0.3Mn, b) Bright field image of as-cast Mg-4Al-1Zn-0.3Mn-0.3Ca, c) BSD image of as-cast Mg-4Al-1Zn-0.3Mn, d) BSD image of as-cast Mg-4Al-1Zn-0.3Mn-0.3Ca, e) Bright field micrograph of homogenised Mg-4Al-1Zn-0.3Mn at 450/1hr, f) Bright field micrograph of homogenised Mg-4Al-1Zn-0.3Mn-0.3Ca at 500/1hr**

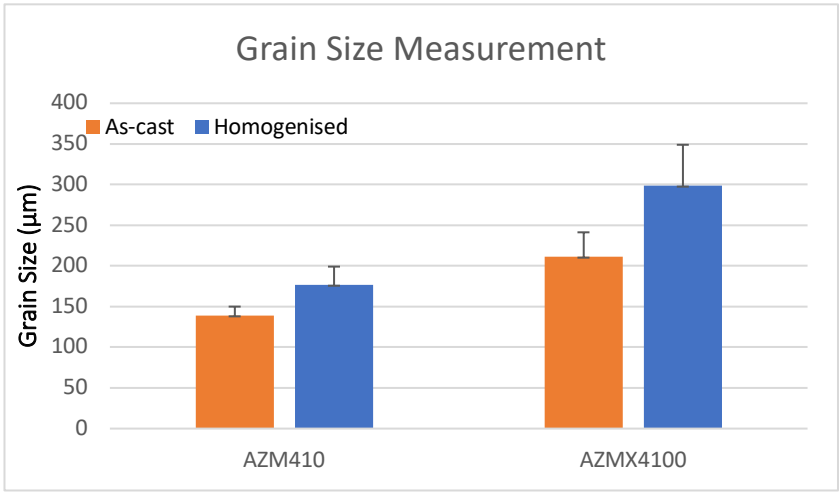


**Figure 4.28- Grain size measurement of as-cast and homogenised Mg-4Al-1Zn-0.3Mn and Mg-4Al-1Zn-0.3Mn-0.3Ca**

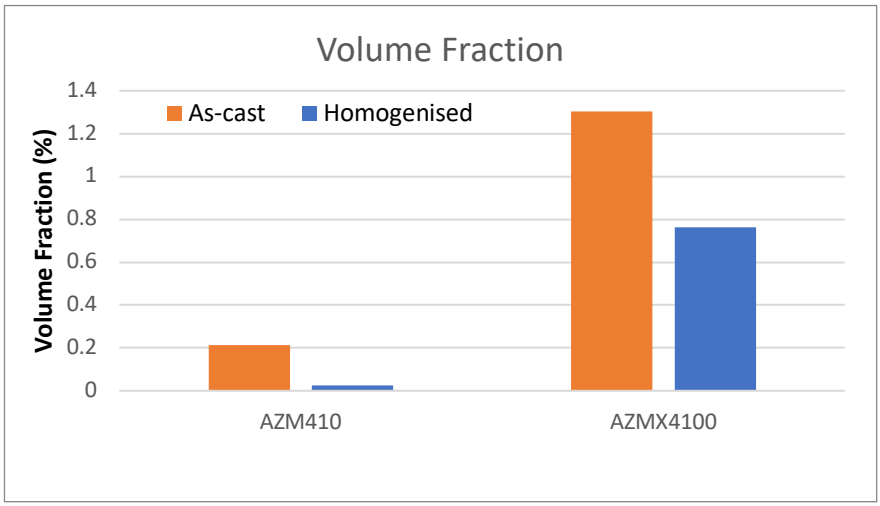


**Figure 4.29- Intermetallic volume fraction of as-cast and homogenised Mg-4Al-1Zn-0.3Mn (AZM410) and Mg-4Al-1Zn-0.3Mn-0.3Ca (AZMX4100)**

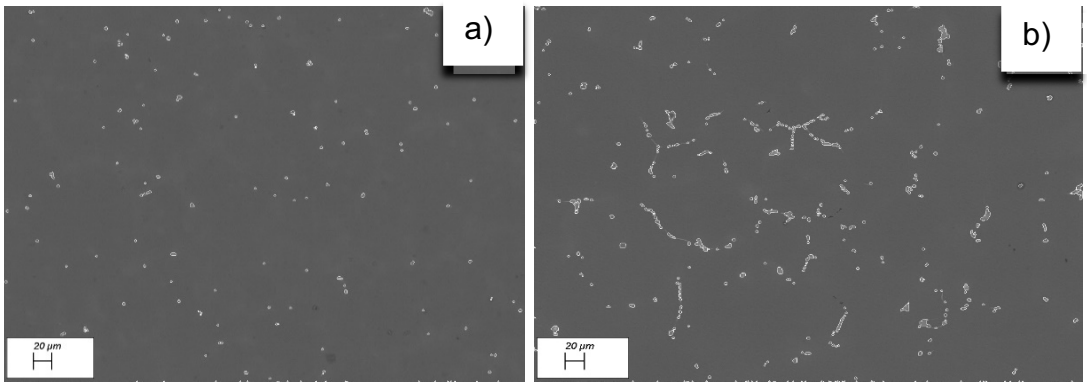


**Figure 4.30- SEM micrographs showing the distribution of intermetallic particles in as-cast alloys (a) Mg-4Al-1Zn-0.3Mn (b) Mg-4Al-1Zn-0.3Mn-0.3Ca**

Through EDX analysis, elemental composition of intermetallic compounds was sought for the purpose of characterisation of AZM410 alloy. During EDX measurement, different spots and areas were focussed upon and a phase comprising of magnesium, zinc and aluminium was present according to data. Majority of particles had a globular morphology and there was also presence of a phase at grain boundaries. The composition was 53.6±5.1at% Mg, 27.1±3.8at% Zn and 18.6±6.8at% Al as shown in Table 4.17 (approximately $Mg_6Zn_3Al_2$).

**Table 4.17- EDX analysis of intermetallic particle(s) found in Mg-4Al-1Zn-0.3Mn**

| AZM410 | Mg | Zn | Al |
|---|---|---|---|
| | Atomic (%) | Atomic (%) | Atomic (%) |
| Particle 1 | 56 | 28 | 16 |
| Particle 2 | 58 | 27 | 16 |
| Particle 3 | 58 | 28 | 14 |
| Particle 4 | 62 | 16 | 23 |
| Particle 5 | 52 | 34 | 14 |
| Particle 6 | 46 | 46 | 8 |
| Particle 7 | 56 | 30 | 14 |
| Particle 8 | 50 | 23 | 27 |
| Particle 9 | 48 | 24 | 27 |
| Particle 10 | 50 | 23 | 27 |

Through EDX analysis, elemental composition of intermetallic compounds was sought for the purpose of characterising AZMX4100 alloy. During EDX measurement, different spots and areas were focussed upon and a phase comprising of magnesium, zinc and calcium was present according to data. Majority of particles had an elongated morphology and composition of 25.8±11.9at% Mg, 49.2±7.5at% Al and 23.6±3.9at% Ca as shown in Figure 4.18 (approximately $MgAl_2Ca$).

**Table 4.18- EDX analysis of intermetallic particle(s) found in Mg-4Al-1Zn-0.3Mn-0.3Ca**

| AZMX4100 | Mg | Al | Ca |
|---|---|---|---|
| | Atomic (%) | Atomic (%) | Atomic (%) |
| Particle 1 | 30 | 46 | 22 |
| Particle 2 | 12 | 57 | 29 |
| Particle 3 | 40 | 40 | 19 |
| Particle 4 | 32 | 46 | 22 |
| Particle 5 | 15 | 57 | 26 |

### 4.3.3 AZM140-Ca

The as-cast microstructure of Mg-1Al-4Zn-0.3Mn alloy (AZM140) shown in Figure 4.31 a) contained a dendritic microstructure with an approximate grain size of 194±23μm as shown in Figure 4.32. Presence of intermetallic particles was observed throughout the microstructure in the inter-dendritic regions as shown in Figure 4.31 c). The measured volume fraction of intermetallic particles amounted to 1.8% as shown in Figure 4.33, an indication that increasing concentration of zinc to 4% enriches solute content substantially. The morphology of observed intermetallic particles in the inter-dendritic region was that of a globular shape and they approximately measured at 4.87μm.

After homogenisation heat treatment of Mg-1Al-4Zn-0.3Mn alloy (AZM140) at 350°C for 1h as shown in Figure 4.31 e), the appearance of a dendritic microstructure diminished. The volume fraction of measured intermetallic particles after homogenisation amounted to 1.45%, which indicates that the effect of heat treatment to dissolve solute presence was minimal. The measurement of grain size after heat treatment approximately came to 293±18μm, which indicates grain growth occurred from the as-cast condition.

The as-cast microstructure of Mg-1Al-4Zn-0.3Mn-0.3Ca alloy (AZMX1400) shown in Figure 4.31 b) contained a dendritic microstructure with an approximate grain size of 226±43μm. Microstructure appearance was like the non-calcium containing AZM140 alloy except there was a persistent appearance of semi-continuous distribution of intermetallic particles at the grain boundaries as shown in Figure 4.31 d). The measured volume fraction of intermetallic particles in the as-cast condition amounted to approximately 3%. From amongst all the alloys, the volume fraction of intermetallic particles is the largest in this calcium added 4% zinc containing alloy. The globular intermetallic particles situated within grains, measured at approximately 5.2μm in diameter. Whereas, the intermetallic particles found at the grain boundaries measured at approximately 73.1μm in length and a thickness of approximately 2.1μm.

After homogenisation heat treatment of Mg-1Al-4Zn-0.3Mn-0.3Ca alloy (AZMX1400) at 500°C-1h/350°C-1h as shown in Figure 4.31 f), the appearance of dendritic microstructure completely transformed to become an equiaxed microstructure. In the

homogenised condition, the grain size was measured, and it came to approximately 258±24μm. The solute elements segregated at inter-dendritic regions and at grain boundaries were not removed after the appropriate heat treatment. The volume fraction of intermetallic particles was measured to be 3.3%, an indication that the intermetallic particles did not dissolve into the a-magnesium matrix.

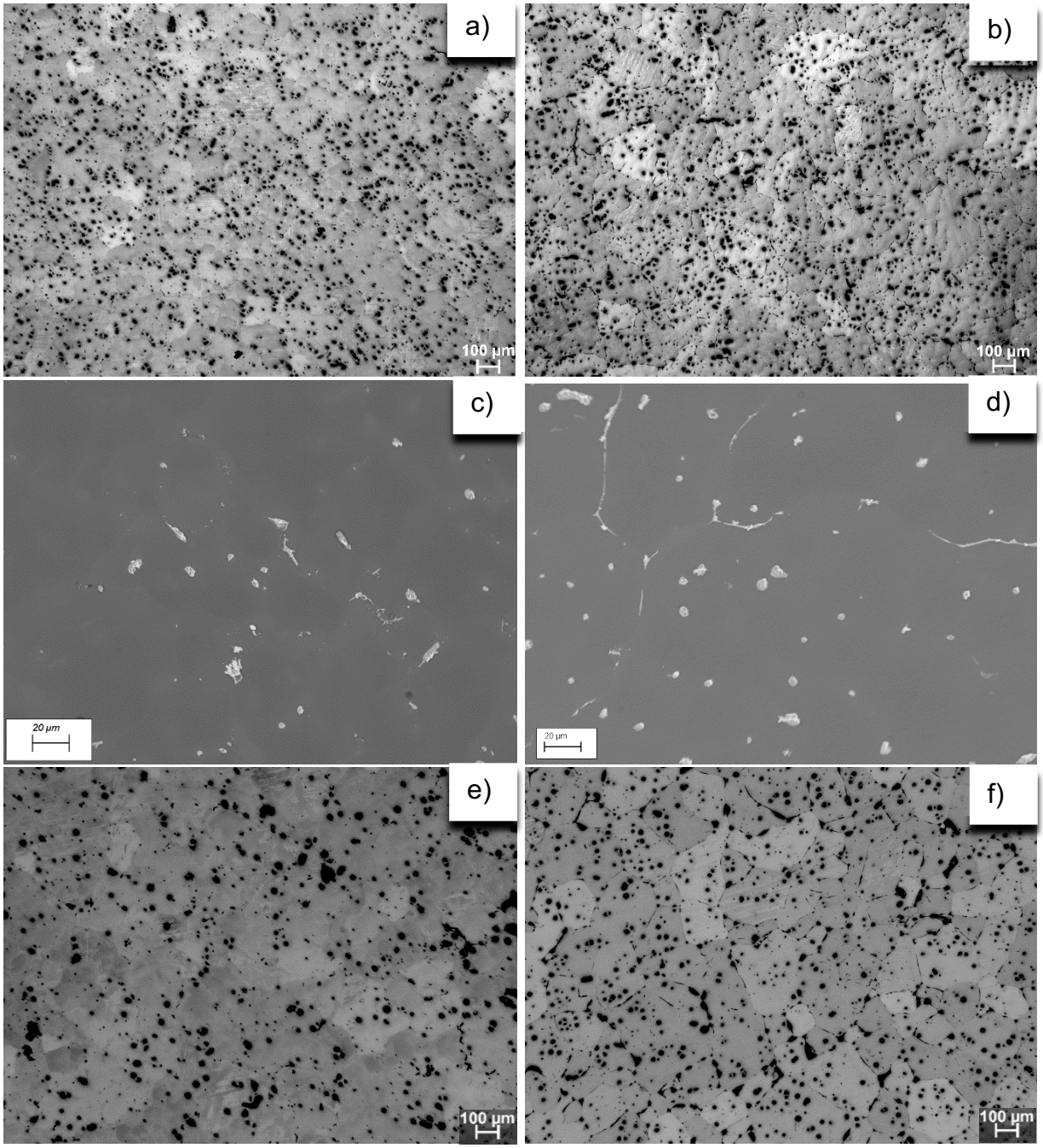


**Figure 4.31- Microstructures of AZM140-Ca, a) Bright field image of as-cast Mg-1Al-4Zn-0.3Mn, b) Bright field image of as-cast Mg-1Al-4Zn-0.3Mn-0.3Ca, c) BSD image of as-cast Mg-1Al-4Zn-0.3Mn, d) BSD image of as-cast Mg-1Al-4Zn-0.3Mn-0.3Ca, e) Bright field micrograph of homogenised Mg-1Al-4Zn-0.3Mn at 350/1hr, f) Bright field micrograph of homogenised Mg-1Al-4Zn-0.3Mn-0.3Ca at 350/1hr-500/1hr**

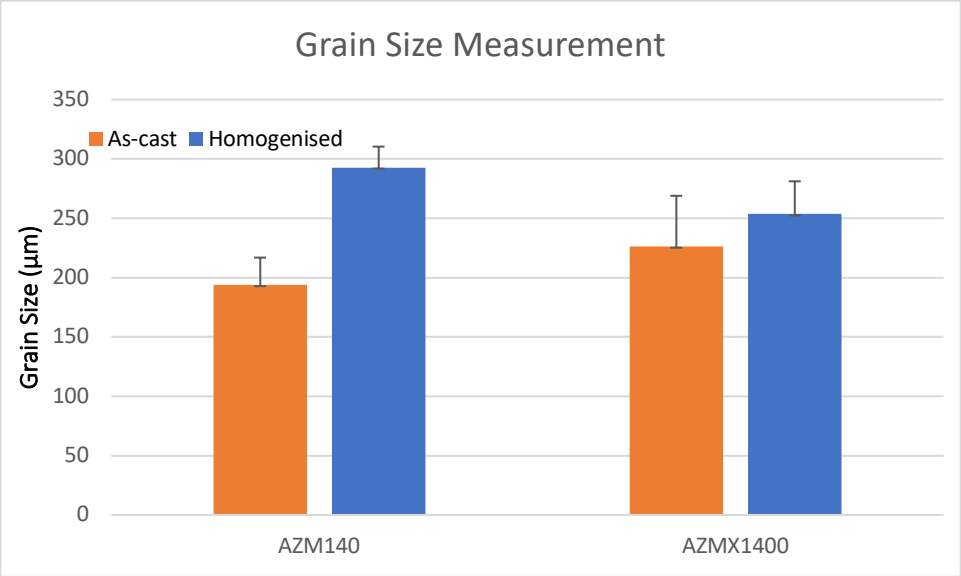


**Figure 4.32- Grain size measurement of as-cast and homogenised Mg-1Al-4Zn-0.3Mn and Mg-1Al-4Zn-0.3Mn-0.3Ca**

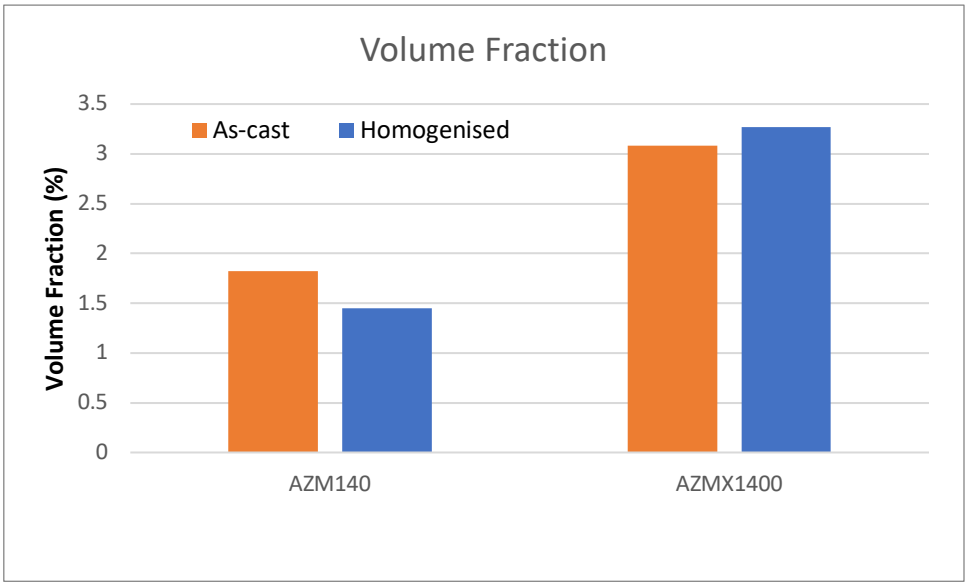


**Figure 4.33- Intermetallic volume fraction of as-cast and homogenised Mg-1Al-4Zn-0.3Mn (AZM140) and Mg-1Al-4Zn-0.3Mn-0.3Ca (AZMX1400)**

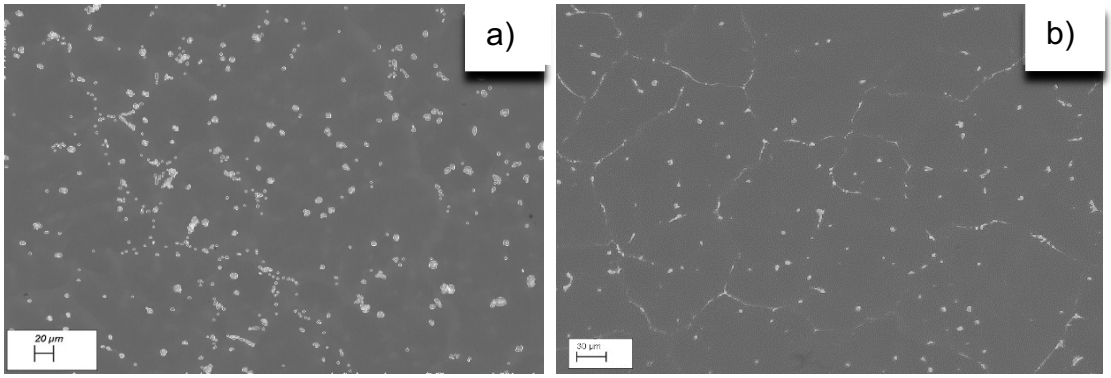


**Figure 4.34- SEM micrographs showing the distribution of intermetallic particles in as-cast alloys (a) Mg-1Al-4Zn-0.3Mn (b) Mg-1Al-4Zn-0.3Mn-0.3Ca**

EDX analysis was performed to understand the elemental composition of intermetallic compounds present in AZM140. During EDX measurement, different spots and areas were focussed upon and a phase comprising of Mg and Zn consistently showed up. Composition of particles was 54.2±18.3at% Mg and 45±17.9at% Zn as shown in Table 4.19 (approximately MgZn).

**Table 4.19- EDX analysis of intermetallic particle(s) found in Mg-1Al-4Zn-0.3Mn**

| AZM140 | Mg | Zn |
|---|---|---|
| | Atomic (%) | Atomic (%) |
| Particle 1 | 80 | 20 |
| Particle 2 | 34 | 66 |
| Particle 3 | 50 | 50 |
| Particle 4 | 38 | 60 |
| Particle 5 | 51 | 46 |
| Particle 6 | 72 | 28 |

EDX analysis was performed to understand the elemental composition of intermetallic compounds present in AZMX1400. During EDX measurement, different spots and areas were focussed upon and a phase comprising of Mg, Zn, Al and Ca consistently showed up. Composition of particles was 48±10at% Mg, 40.7±9.2at% Zn, 2.5±1.1at% Al and 9±3at% Ca as shown in Table 4.20 (approximately $Mg_5Zn_4Ca$).

**Table 4.20- EDX analysis of intermetallic particle(s) found in Mg-1Al-4Zn-0.3Mn-0.3Ca**

| AZMX1400 | Mg | Zn | Al | Ca |
|---|---|---|---|---|
| | Atomic (%) | Atomic (%) | Atomic (%) | Atomic (%) |
| Particle 1 | 51 | 37 | 3 | 9 |
| Particle 2 | 31 | 59 | 2 | 8 |
| Particle 3 | 49 | 39 | 3 | 10 |
| Particle 4 | 49 | 39 | 2 | 10 |
| Particle 5 | 59 | 29 | 4 | 8 |
| Particle 6 | 58 | 38 | 0.6 | 4 |
| Particle 7 | 39 | 44 | 3 | 14 |

## 4.4 Wedge Samples

Wedge casting is a permanent mould casting technique that is utilised to study the solidification behaviour of an alloy in non-equilibrium conditions. A typical permanent mould cast alloy is thought to have a solidification rate of approximately 50 K/s. Whereas, depending on the surface area that is of concern, a wedge cast alloy's cooling rate differs significantly. A cast alloy's tip point where the surface area is the most minimal, the rate of cooling is understood to be fastest at approximately $10^3$ K/s (He, et al., 2008). This significantly high rate of solidification at the tip is comparable to the solidification rate of a twin roll cast alloy which is known to have a solidification rate between $10^2$ K/s to $10^3$ K/s (Hadadzadeh & Wells, 2013). This makes studying the microstructure of a wedge sample interesting because of its similarity to that of a TRC alloy. What follows from here is the study of wedge cast microstructures of all alloys. Alloys were produced and microstructure characterisation was conducted from 1mm at the tip to 60mm horizontally across to understand the effect of cooling rate on grain size.

### 4.4.1 AZM110-Ca

The wedge as-cast microstructure of Mg-1Al-1Zn-0.3Mn alloy (AZM110) shown in Figure 4.34 a) contained a dendritic microstructure at tip point where rate of solidification is comparable to a TRC alloy. At 1mm horizontally into microstructure, the approximate grain size amounted to 238±9μm as shown in Figure 4.35. Going further away from the tip at regions 5mm-10mm, the microstructure appearance did not change, and the averaged grain size was 215±9μm. At 20mm horizontally along the wedge sample, the dendritic microstructure substantially coarsens with approximate grain size at 497±27μm, an increase of nearly 50% from previous measurements taken at 1mm, 5mm and 10mm. At regions 30mm-40mm, the microstructure appeared deformed due to elongated grains, the average grain size in these regions measured at 532±42μm. The appearance of large globular intermetallic compounds began at this stage of microstructure. At regions 50mm-60mm, the microstructure contained dendrites and there was no observation of deformed grains that were seen in previous regions. Volume fraction of globular

intermetallic compounds increased, and the grain size measurement amounted to 387±16μm.

At 1mm horizontally across, the wedge as-cast microstructure of Mg-1Al-1Zn-0.3Mn-0.3Ca alloy (AZMX1100) shown in Figure 4.34 b) contained a significantly refined dendritic microstructure with approximate grain size of 114±7μm. At the 1mm stage, the alloy without calcium had an enlarged grain size average of 238±9μm. The addition of calcium caused 48% in grain refinement which is a significant reduction. At 5mm point, the microstructure remains identical but with marginal grain size increase of 128±9μm. With reduction in cooling rate, there is steady grain size growth for the dendritic microstructure between 10mm-20mm, averaging approximately 206±25μm. At 30mm point, the dendritic microstructure considerably coarsens with approximate grain size of 358±14μm. Following from this point, the microstructure remains dendritic and coarse but with increased size of globular intermetallic compounds found in the inter-dendritic regions. From 40mm-60mm stage, the average grain size reaches a maximum value of 417±19μm.

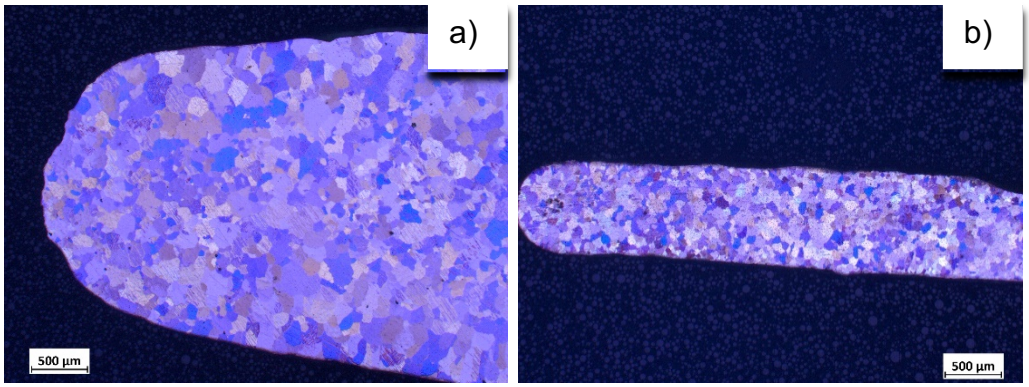


**Figure 4.34- Wedge sample start points of a) Mg-1Al-1Zn-0.3Mn and b) Mg-1Al-1Zn-0.3Mn-0.3Ca**

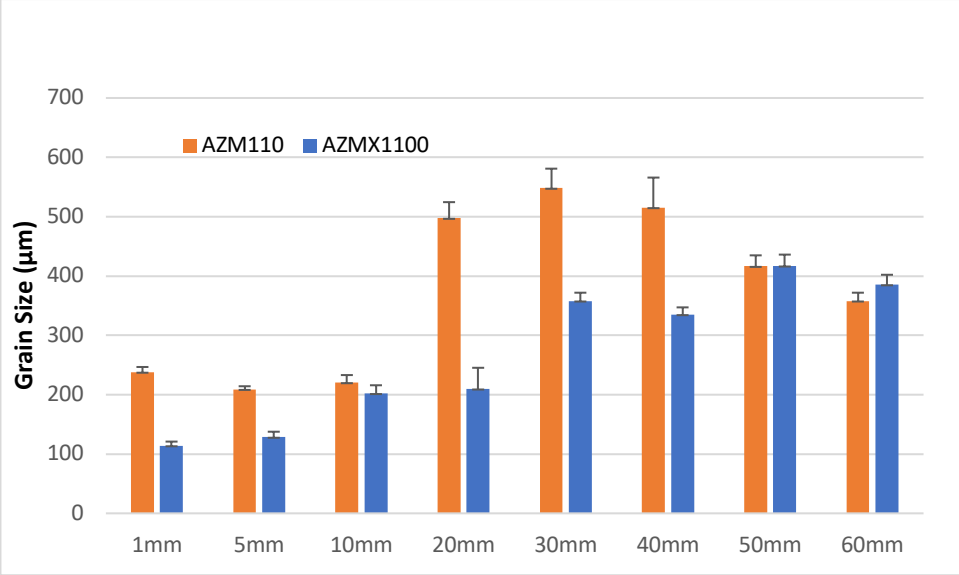


**Figure 4.35- Grain size measurement of wedge samples Mg-1Al-1Zn-0.3Mn and Mg-1Al-1Zn-0.3Mn-0.3Ca**

### 4.4.2 AZM410-Ca

At 1mm horizontally across, the wedge as-cast microstructure of Mg-4Al-1Zn-0.3Mn alloy (AZM410) shown in Figure 4.36 a) contained a dendritic microstructure with approximate grain size of 219±27μm as shown in Figure 4.37. Thereafter at 5mm stage, the dendritic microstructure remained with approximate grain size being 204±25μm, an indication that the intended effect of cooling rate did not occur. Between 10mm-30mm, the dendritic microstructure remained similar throughout without major change to grain size. The averaged grain size between these regions amounted to 260±27μm. Interestingly, at 40mm point, the dendritic microstructure appeared far more refined with approximate grain size being 166±11μm. Thereafter, the microstructure between regions 50mm-60mm had an average grain size of 250±25μm.

At 1mm horizontally across, the wedge as-cast microstructure of Mg-4Al-1Zn-0.3Mn-0.3Ca alloy (AZMX4100) shown in Figure 4.36 b) contained a dendritic microstructure with approximate grain size of 255±66μm. At the point of fastest solidification, the addition of calcium to the high aluminium containing alloy does not indicate any substantial reduction or enlargement to grain size. This contrasts with the 1% aluminium containing alloy where the effect of calcium addition is evident with substantial reduction in grain size. In the regions 5mm-10mm, the dendritic microstructure's grain size did not change from the 1mm point, with average grain size measuring at 253±31μm. Thereafter at the region 20mm, the microstructure showed an increase in grain size with the average grain measuring at 304±36μm. As expected, from the regions 30mm-60mm the microstructure coarsened due to rate of solidification decreasing. At these points, the grain size measured from 401±61μm all the up to 527±61μm. Alongside coarsening of grains, there was clear sign that intermetallic compounds coarsened with slowing of cooling rate.

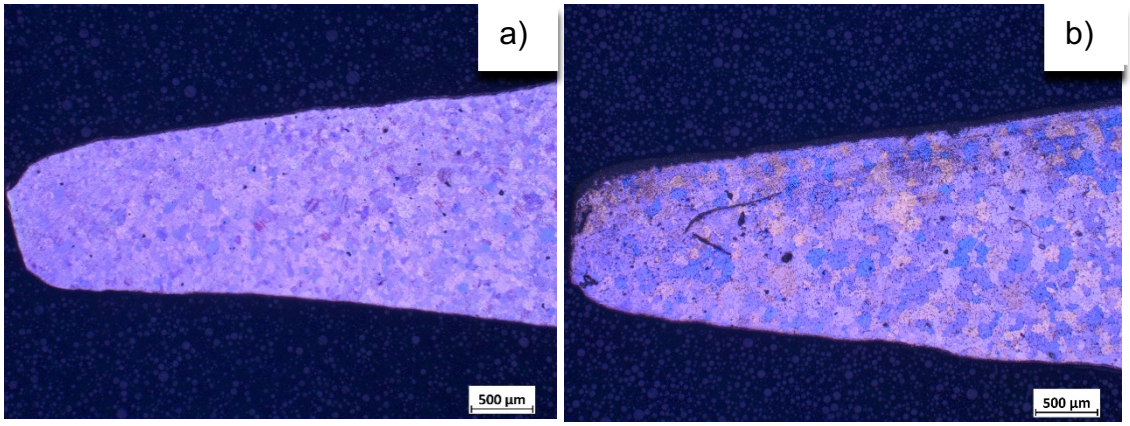


**Figure 4.36- Wedge sample start points of a) Mg-4Al-1Zn-0.3Mn and b) Mg-4Al-1Zn-0.3Mn-0.3Ca**

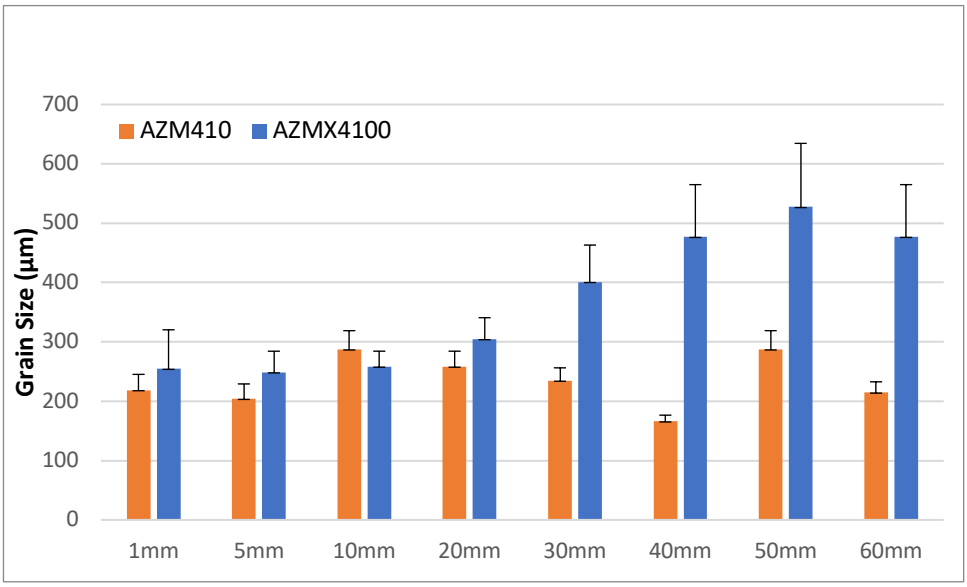


**Figure 4.37- Grain size measurement of wedge samples Mg-4Al-1Zn-0.3Mn and Mg-4Al-1Zn-0.3Mn-0.3Ca**

### 4.4.3 AZM140-Ca

At 1mm horizontally across, the wedge as-cast microstructure of Mg-1Al-4Zn-0.3Mn alloy (AZM140) shown in Figure 4.38 a) contained a dendritic microstructure with approximate grain size of 304±16μm as shown in Figure 4.39. Further along at 5mm, a dendritic microstructure was observed with coarsening of grains amounting to 353±27μm. The observation of microstructure coarsening continued at 10mm point with grain size measuring at 416±18μm. At 20mm point, the dendrites became significantly enlarged in which they approximately measured at 617±41μm. This behaviour was again seen at 30mm point, with grains measuring at 641±0μm, an indication that reduction in cooling rate had a considerably observable effect by increasing the amount of zinc. From the region 40mm to 60mm, the coarse microstructure contained enlarged globular intermetallic compounds and had a grain size beginning from 671±53μm to 713±0μm at the end.

At 1mm horizontally across, the wedge as-cast microstructure of Mg-1Al-4Zn-0.3Mn-0.3Ca alloy (AZMX1400) shown in Figure 4.38 b) contained a dendritic microstructure with approximate grain size of 231±16μm. The addition of calcium to 4% containing zinc alloy reduced substantially the grain size which was above 300μm. Further along at 5mm, a dendritic microstructure was observed with coarsening of grains amounting to 297±14μm. The observation of microstructure coarsening continued at 10mm point with grain size measuring at 312±0μm. At 20mm point, the dendrites became enlarged in which they approximately measured at 376±17μm. This behaviour was again seen at 30mm point, with grains measuring at 453±23μm, an indication that reduction in cooling rate continued to the perceived effect microstructure coarsening. From the region 40mm to 60mm, the coarse microstructure contained enlarged globular intermetallic compounds and had a grain size between 513±0μm and 551±33μm.

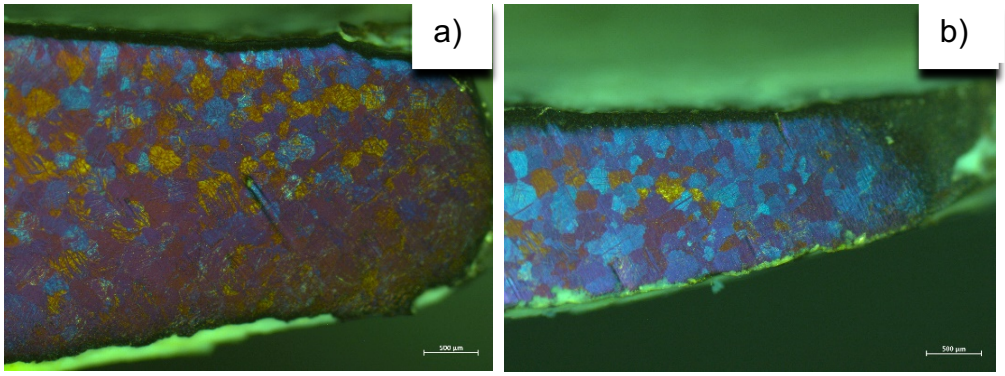


**Figure 4.38- Wedge sample start points of a) Mg-1Al-4Zn-0.3Mn and b) Mg-1Al-4Zn-0.3Mn-0.3Ca**

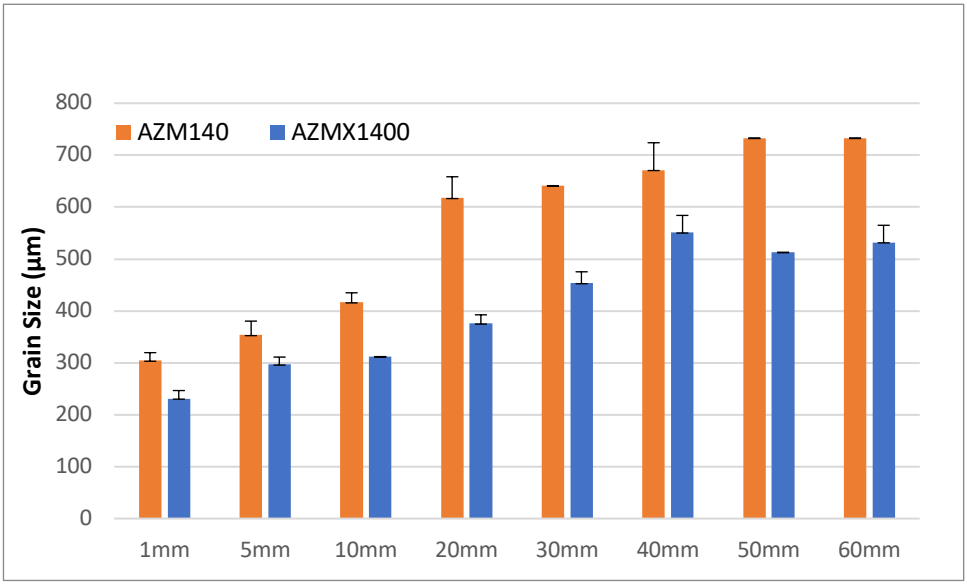


**Figure 4.39- Grain size measurement of wedge samples Mg-1Al-4Zn-0.3Mn and Mg-1Al-4Zn-0.3Mn-0.3Ca**

## 4.5 Discussion

The process of solidification occurs through the mechanism of nucleation and growth. This process involves crystal growth at the expense of liquid until complete solid is formed. To understand solidification behaviour, cooling curve measurements and theoretical modelling was performed to ascertain liquidus temperature and potential phases present in the alloys. Since it is well established that non-equilibrium solidification occurs, for this reason, Scheil data was considered as an important factor and the more traditional understanding of solidification through the Lever rule method was also adopted.

Alloys Mg-1Al-1Zn-0.3Mn (AZM110) and Mg-1Al-1Zn-0.3Mn-0.3Ca (AZMX1100) indicated nucleation and growth of α-Mg after initial solidification from liquid state. The nucleation and growth of α-Mg phase during first instance of solidification was also observed for alloys Mg-1Al-4Zn-0.3Mn (AZM140) and Mg-1Al-4Zn-0.3Mn-0.3Ca (AZMX1400), this observance positively correlates with the established wrought alloy AZ31. The thermodynamic calculations through the Scheil model for AZ31 alloy indicate primary magnesium phase to be the first phase to nucleate and grow (Hadadzadeh & Wells, 2015). Based on the Scheil model, the alloys showed considerable number of phases that solidify into the magnesium matrix. The preliminary sequence of phase formation for Mg-1Al-1Zn-0.3Mn (AZM110) and Mg-1Al-1Zn-0.3Mn-0.3Ca (AZMX1100) was as follows, primary α-Mg, then a eutectic reaction including α-Mn, this phase was then transformed which paved way to the solidification of $Al_8Mn_5$. The formation of α-Mn occurred when there was insufficient amount of aluminium. Low amount of aluminium containing alloys begin to get this phase according to the phase diagram, once aluminium content in the liquid becomes high, AlMn phases then nucleates and grows. Manganese is commonly added to magnesium alloys because it has shown to prevent corrosion by removing the detrimental effect of iron (Polmear, 2005). According to Wang et al, manganese is readily seen in aluminium containing magnesium alloys in the form of equilibrium $Al_8Mn_5$ intermetallic phase and sometimes $Al_8(Mn, Fe)_5$. In the latter intermetallic phase, some iron atoms replace manganese atoms (Wang, et al., 2010).

Recently, an in-depth study was performed on $Al_8Mn_5$ particles and it was concluded that the crystal structure of this phase is the rhombohedral crystal structure (Zeng, et

al., 2018). The phase $Al_8Mn_5$ also has a prolonged presence in Mg-1Al-4Zn-0.3Mn (AZM140) and Mg-1Al-4Zn-0.3Mn-0.3Ca (AZMX1400), it nucleates when solid fraction is as low as approximately 50% and remains in its original form until 96% and 97% of solid fraction is achieved, respectively. It can be understood that aluminium interacts favourably with manganese, forming a compound at a very early stage of solidification. Interestingly, the alloys Mg-4Al-1Zn-0.3Mn (AZM410) and Mg-4Al-1Zn-0.3Mn-0.3Ca (AZMX4100) which have an increased concentration of aluminium by 4%, show that the solidification path begins with $Al_8Mn_5$, a stark contrast to previous alloys which begin with α-Mg. It has been proven that $Al_8Mn_5$ phase is the first to solidify in alloys with high concentration of aluminium, such as AZ91. Byun et al studied whether $Al_8(Mn, Fe)_5$ act as heterogenous nucleation sites for primary magnesium phase, the study observed $Al_8(Mn, Fe)_5$ particles at the centre of α-Mg grains (Byun, et al., 2003). Tamura et al reported that Al-Mn-(Fe) particles were frequently observed when AZ91E alloy melt was rapidly cooled from a superheating temperature to the pouring temperature of 700°C (Tamura, et al., 2003).

The addition of calcium to Mg-1Al-1Zn-0.3Mn-0.3Ca (AZMX1100), Mg-4Al-1Zn-0.3Mn-0.3Ca (AZMX4100) and Mg-1Al-4Zn-0.3Mn-0.3Ca (AZMX1400) paved way for nucleation and growth of $Al_2Ca$ phase which occurred in a ternary eutectic reaction according to thermodynamic calculations. In contrast to $Al_8Mn_5$, this intermetallic phase nucleates at a late stage when solid fraction is achieved at above 93% in all instances and the temperature between 378-470°C. Just like manganese, calcium has a strong attraction to aluminium, both elements come together to form a compound. As previously mentioned, $Al_2Ca$ phase has readily been observed at grain boundaries with the phase having high thermal stability and ultimately increasing the strength of magnesium alloys, as shown by (Bae, et al., 2009) in their study of AZ31-0.7Ca that was twin roll cast processed.

Another interesting phase that the Scheil model predicted was $Mg_{17}Al_{12}$, this phase was predicted to nucleate and grow for the 4% aluminium containing alloys Mg-4Al-1Zn-0.3Mn (AZM410) and Mg-4Al-1Zn-0.3Mn-0.3Ca (AZMX4100). In both alloys, the phase is formed by ternary eutectic reaction at low solidification temperatures ranging between 423-416°C. Just like $Al_2Ca$ phase, the late occurrence of solidification of eutectic $Mg_{17}Al_{12}$ phase means it is readily observed situated at grain

boundaries. Dargusch et al's study on increasing $Mg_{17}Al_{12}$ concentration in Mg-Al alloys showed a substantial strengthening increase with increase of volume fraction of this eutectic phase (Dargusch, et al., 2006).

The average grain size in the permanent mould as-cast microstructure of Mg-1Al-1Zn-0.3Mn (AZM110) was 250±34μm while the average grain size in the permanent mould as-cast microstructure of Mg-1Al-1Zn-0.3Mn-0.3Ca (AZMX1100) was 313±40μm. The understanding taken from this revelation is that the quinary addition of calcium did not seem to refine grain size under this present condition. In previous work, the addition of 0.4%wt calcium to pure magnesium was done to understand the effect of grain refinement, the work suggested significant reduction in grain size from approximately 2100μm to 270μm at the centre of casting (Lee, et al., 2000). Also, tertiary addition of 0.5%wt calcium to as-cast Mg-Zn (1%wt zinc) alloy showed reduction in grain size from 150-200μm to 120-150μm (Zhang, et al., 2012). Having said this, the quinary addition and the subsequent presence of aluminium, zinc and manganese as alloying elements certainly impacted the grain refining ability of calcium. The average grain size in the permanent mould as-cast microstructure of Mg-4Al-1Zn-0.3Mn (AZM410) was 139±11μm and the average grain size in the permanent mould as-cast Mg-4Al-1Zn-0.3Mn-0.3Ca (AZMX4100) was 211±30μm. The increased 4%wt addition of aluminium significantly reduced the average grain size, a difference of approximately 111μm in the without calcium added alloy and approximately 136μm in the calcium added alloy. In previous work on the effect of binary addition of aluminium to magnesium, it was reported that increasing aluminium concentration reduces average grain size from 50-100μm to 10-50μm (Dargusch, et al., 2006). Again, calcium addition did not reduce average grain size but rather there was an increase of approximately 72μm in the permanent mould as-cast Mg-4Al-1Zn-0.3Mn-0.3Ca (AZMX4100). In the alloys with increased concentration of 4%wt zinc, there was a reduction in average grain size, as seen similarly in increasing concentration of aluminium. The average grain size of permanent mould as-cast Mg-1Al-4Zn-0.3Mn (AZM140) was 194±23μm and the average grain size of permanent mould as-cast Mg-1Al-4Zn-0.3Mn-0.3Ca (AZMX1400) was 226±43μm. It has been reported that zinc has a grain refining effect that correlates with increasing Hall–Petch effect on the strength as the concentration of Zn increases (Caceres & Blake, 2002).

After homogenisation of all alloys except Mg-1Al-1Zn-0.3Mn (AZM110), there was noticeable observance of grain growth from the original as-cast average grain size. This ranged from as low as approximately 20μm in AZMX1100 alloy to as great as approximately 99μm in AZM140 alloy. During microstructure recrystallization, it is common for grains to grow, this has been observed previously in magnesium alloys such as in Bao et al's study of the effect of homogenisation on various quaternary and quinary magnesium alloys (Bao, et al., 2013).

Overall, the addition of calcium resulted in increased volume fraction of primary intermetallic particles at grain boundary sites. Addition of 0.3wt% of calcium to Mg-1Al-1Zn-0.3Mn (AZM110) led to 1.4% of intermetallic particles from a negligible amount. Adding the same amount of calcium to Mg-4Al-1Zn-0.3Mn (AZM410) meant that intermetallic particles increased from 0.2% to 1.3%. Adding calcium to 4% zinc concentrated alloy allowed the number of intermetallic particles to increase from 1.8% to 3%. In previous works, alloying of calcium has led to increase of intermetallic particles in magnesium alloys also containing aluminium and zinc. Mendis et al reported 1.4% and 2.3% increased volume fraction of primary intermetallics in Mg-Zn-Al alloy with 0.5wt% and 1wt% additions of calcium (Mendis, 2005). Calcium has been observed to react favourably with aluminium in magnesium alloys, leading to formation of $Al_2Ca$ at grain boundaries (Yim, et al., 2004), in a shape and form very similar to what has been observed in these alloys.

Prior to choosing the most optimal homogenisation treatments with the assistance of CALPHAD software generated phase diagrams, several homogenisation treatments were performed in order to maximise the dissolution of intermetallic phases. The temperatures ranged from 350°C to 500°C with time durations 30 minutes, 1 hour ad 2 hours. After homogenisation treatment of calcium containing AZMX1100 alloy, the volume fraction of primary intermetallic particles was reduced by 75%. In the case of AZM410, there was a significant reduction of primary intermetallic particles from 0.2% to 0.03%, a near complete dissolving of solid solution into the matrix. Through homogenisation treatment of calcium added AZMX4100, there was a reduction of 50% in the amount of primary intermetallic particles. After homogenisation treatment of alloys AZM140 and AZMX1400, there was an insignificant change in the amount of primary intermetallic particles present. The most probable reason to explain existence of intermetallic particles after homogenisation is the nucleation and growth

of $Al_8Mn_5$ phase early in the solidification path. This phase has a high melting point, leading to difficulty in dissolving. A study was conducted on as-cast and rolled AT63 alloys, the author mentioned $Al_8Mn_5$ phase formed as a eutectic reaction and was not dissolved after attempting homogenisation treatment (Kim, et al., 2017). An investigation on AM50A, AM60B and AZ91D through rheo-high pressure die casting technology was performed, the author concluded that the presence of $Al_8Mn_5$ phase significant due it be dispersed throughout the microstructure. Even after homogenisation treatment for 16hrs at 415°C, there was no effect on this phase, while $Mg_{17}Al_{12}$ did dissolve (Curle, et al., 2013). Due to slow solidification rate of permanent mould casting, the high temperature formation of $Al_8Mn_5$ intermetallic particles allows particles to become coarse as seen in this study and understood by others such as Trang et al in their work to develop a similar alloy AZMX3100 (Trang, et al., 2018). Due to this issue, the rapid solidification rate associated with TRC processing is potentially a good solution which undoubtedly means the size of this phase being minimised.

Energy dispersive x-ray analysis was performed on AZM110 alloy even though it had minimal number of intermetallic particles present in both as-cast and homogenisation conditions. The intermetallic particle investigated comprised highly of magnesium with 85at% with aluminium and zinc elements included in the phase. Due to preferable atomic radii of aluminium/zinc to magnesium and the dilute addition of 1% each, these two elements dissolved into the matrix with relative ease (Yasi, et al., 2010). By increasing concentration of aluminium to 4wt% in AZM410, appearance of globular intermetallic particles became visible with composition measuring to be $Mg_6Zn_3Al_2$. While introduction of 4wt% zinc meant most intermetallic particles' composition became approximately MgZn, therefore the effect of aluminium diminished and dissolved into the matrix. By adding 0.3wt% calcium to AZM110, AZM410 and AZM140 alloys, the EDX detector consistently traced presence of this element in all intermetallic particles. These intermetallic particles were mostly elongated and situated at grain boundaries. This type of morphology at grain boundaries has previously been observed in calcium containing magnesium alloys such as AZ31-0.7Ca (Yim, et al., 2004), AZMX3100 (Trang, et al., 2018), Mg-3.7Al-1.8Ca-0.4Mn (Wang, et al., 2019) and many more. All these studies identified $Al_2Ca$ as the intermetallic phase. In AZMX1100 alloy, the $Al_2Ca$ intermetallic phase situated

at grain boundaries had a semi-continuous distribution but also featured globular in morphology, this finding positively correlates with Jiang at al's work on dilute Mg-0.57-0.42Ca alloy. Interestingly, their study mentioned when Ca/Al ratio is lower than 0.8 in Mg-Al-Ca alloys, the primary intermetallic phase to nucleate and grow is always $Al_2Ca$ (Jiang, et al., 2015). By increasing the concentration of aluminium to 4wt% in AZMX4100, the presence of $Al_2Ca$ became more prominent at grain boundaries, this was confirmed by increased overall volume fraction. In AZMX1400 alloy, the increased concentration of zinc allowed zinc to play a greater role in forming intermetallic particles with calcium. On average, majority of intermetallic particles consisted of 40.7±9.2at% of zinc with negligible amount of aluminium but with 9±3at% of calcium.

This present study looked at the grain size evolution during solidification of wedge mould cast specimens. The reason for this is due to similarity in solidification behaviour between a twin roll cast alloy and a wedge mould cast alloy. The solidification rate of twin roll cast alloy has been established to range between $10^2$ K/s to $10^3$ K/s (Hadadzadeh & Wells, 2013). Elsewhere, an investigation on AZ31 wedge mould cast specimen was performed to understand the effect of cooling rate on the microstructure. It was calculated that at tip, the rate of cooling amounted to 1053 K/s and at the opposite end, the rate of cooling amounted to 32 K/s (He, et al., 2008). This finding correlates with another study which concluded that the solidification rate of a wedge mould cast alloy can have a high solidification rate of up to $10^3$ K/s (Perepezko & Hildal, 2005). He et al predicted a significant drop in the cooling rate at 10mm point from the tip, a value of approximately 350 K/s from 1053 K/s at the tip. Then from 20mm to 140mm, cooling rate relatively stabilises between 100 K/s to 50 K/s. In the present study, at tip point where cooling rate was highest, the grain sizes were found to be smallest in size. Interestingly, the addition of calcium to AZM110 led to grain refinement of 48% near tip point, the grain size went from 238±9μm to 114±7μm. Similarly, there was clear observance of grain refinement through addition of calcium to AZM140 alloy, the grain size reduced from 304±16μm to 231±16μm. It has previously been postulated that calcium has growth restriction effect on pure magnesium (Lee, et al., 2000), this effect has certainly played a role in this study. As for AZM110, there was a sudden increase of average grain size between 20mm to 40mm. The average grain size went from approximately

200µm at 10mm point to approximately 500µm and then between 50-60mm, the grain decreased and stabilised of 350-400µm. This could be due to the processing stage of preparing this sample as the grains were elongated and had the appearance of being deformed.

## 4.6 Conclusions

1. According to Scheil non-equilibrium solidification model, the phase $Al_8Mn_5$ nucleates and grows early on in all alloys under consideration. The alloys Mg-4Al-1Zn-0.3Mn (AZM410) and Mg-4Al-1Zn-0.3Mn-0.3Ca (AZMX4100) which have an increased concentration of aluminium by 4wt%, show that the solidification path begins with $Al_8Mn_5$. So, it is important to note that dissolving this phase through homogenisation treatment has proven to be impossible due to extremely high melting point of 675°C according to Scheil data. This was reflected during volume fraction analysis which showed partial reduction of intermetallic particles.

2. Addition of calcium to permanent mould cast alloys did not appear to refine microstructure but rather there was increase in average grain size. Average grain size of Mg-1Al-1Zn-0.3Mn (AZM110) was 250±34µm while the average grain size in of Mg-1Al-1Zn-0.3Mn-0.3Ca (AZMX1100) was 313±40µm. The average grain size of as-cast Mg-4Al-1Zn-0.3Mn (AZM410) was 139±11µm and the average grain size of as-cast Mg-4Al-1Zn-0.3Mn-0.3Ca (AZMX4100) was 211±30µm. The average grain size of as-cast Mg-1Al-4Zn-0.3Mn (AZM140) was 194±23µm and the average grain size of as-cast Mg-1Al-4Zn-0.3Mn-0.3Ca (AZMX1400) was 226±43µm. After homogenisation treatment, there was noticeable observance of grain growth from the original as-cast average grain size.

3. Overall, the addition of calcium resulted in increased volume fraction of primary intermetallic particles at grain boundary sites. Addition of 0.3wt% of calcium to Mg-1Al-1Zn-0.3Mn (AZM110) led to 1.4% of intermetallic particles from a negligible amount. Adding the same amount of calcium to Mg-4Al-1Zn-0.3Mn (AZM410) meant that intermetallic particles increased from 0.2% to

1.3%. Adding calcium to 4% zinc concentrated alloy allowed the number of intermetallic particles to increase from 1.8% to 3%.

4. After homogenisation treatment of calcium containing AZMX1100 alloy, the volume fraction of primary intermetallic particles was reduced by 75%. In the case of AZM410, there was a significant reduction of primary intermetallic particles from 0.2% to 0.03%, a near complete dissolving of solid solution into the matrix. Through homogenisation treatment of calcium added AZMX4100, there was a reduction of 50% in the amount of primary intermetallic particles. After homogenisation treatment of alloys AZM140 and AZMX1400, there was an insignificant change in the amount of primary intermetallic particles present. The most probable reason to explain existence of intermetallic particles after homogenisation is the nucleation and growth of $Al_8Mn_5$ phase early in the solidification path. This phase has a high melting point of 675°C according to Scheil data, leading to difficulty in dissolving.

5. In the case of AZM110 alloy, due to preferable atomic radii of aluminium/zinc in comparison to magnesium and the dilute addition of 1% each, these two elements dissolved into the matrix with relative ease. By increasing concentration of aluminium to 4wt% in AZM410, appearance of globular intermetallic particles became visible with composition measuring to be $Mg_6Zn_3Al_2$. While introduction of 4wt% zinc meant most intermetallic particles' composition became approximately MgZn, therefore the effect of aluminium diminished and dissolved into the matrix. By adding 0.3wt% calcium to AZM110, AZM410 and AZM140 alloys, the EDX detector consistently traced presence of this element in all intermetallic particles. These intermetallic particles were mostly elongated and situated at grain boundaries. There is a strong correlation $Al_2Ca$ is the intermetallic phase in question due to thermodynamic calculations, morphology, and empirical data.

6. At tip point of wedge samples where cooling rate was highest, the grain sizes were found to be smallest in size. Interestingly, the addition of calcium to AZM110 led to grain refinement of 48% near tip point, the grain size went from 238±9μm to 114±7μm. Similarly, there was clear observance of grain

refinement through addition of calcium to AZM140 alloy, the grain size reduced from 304±16μm to 231±16μm. It has previously been postulated that calcium has growth restriction effect on pure magnesium. As for AZM410, the solidification rate did not impact grain size evolution throughout different stages. The addition of calcium to this alloy did show an obvious trend of grain enlargement as the solidification rate slowed down.

# Chapter 5- Age-Hardening and Transmission Electron Microscopy

# Contents

## 5.1 Introduction

The homogenisation treatment highlighted in Chapter 4 of Mg-1Al-1Zn-0.3Mn-(0.3)Ca, Mg-4Al-1Zn-0.3Mn-(0.3)Ca and Mg-1Al-4Zn-0.3Mn-(0.3)Ca alloys resulted in reduction of intermetallic particles in the as-cast microstructures. The varying homogenisation treatments were followed by water quenching at room temperature. The dissolving of solute particles in the magnesium matrix is therefore likely to be supersaturated in the quenched samples. Supersaturation of solute elements provides an opportunity for generating a relatively high-volume fraction of precipitates. Therefore, it is important to understand whether the quenched samples react to age hardening when they are aged isothermally at low temperatures.

In this chapter the age hardening response of as-cast Mg-1Al-1Zn-0.3Mn-(0.3)Ca, Mg-4Al-1Zn-0.3Mn-(0.3)Ca and Mg-1Al-4Zn-0.3Mn-(0.3)Ca alloys in the temperature range 150-200°C will be reported. In addition to this, the alloys are age hardened in hot rolled, 5% deformed and pre-aged conditions to examine whether there is an increase in hardness values. Characterisation of the structure, composition, size and distribution of major precipitate phase(s) formed in samples aged in various mentioned conditions were conducted with the use of transmission electron microscopy.

## 5.2 Isothermal Ageing of As-cast Alloys

### 5.2.1 AZM110-Ca

#### *5.2.1.1 Isothermal Ageing at 150°C*

The age hardening curves of Mg-1Al-1Zn-0.3Mn and Mg-1Al-1Zn-0.3Mn-0.3Ca isothermally aged at 150°C are presented in Figure 5.1. The as-quenched hardness was approximately 42VHN for the Mg-1Al-1Zn-0.3Mn alloy and the alloy containing an addition of 0.3% Ca, the as-quenched hardness was approximately 46VHN. Thereafter, Mg-1Al-1Zn-0.3Mn was age hardened from 30mins to 240hrs, within this period of time there was minimal increase in ageing. Peak response in hardness at isothermal ageing temperature of 150°C occurred at 240hrs with 44VHN. As for the 0.3% Ca containing Mg-1Al-1Zn-0.3Mn-0.3Ca alloy, maximum hardness was achieved at 1hr time with 55VHN which is an increase of 9VHN from the as-quenched condition. Further isothermal ageing at 150°C resulted in gradual decrease in hardness value from the maximum achieved at 1hr.

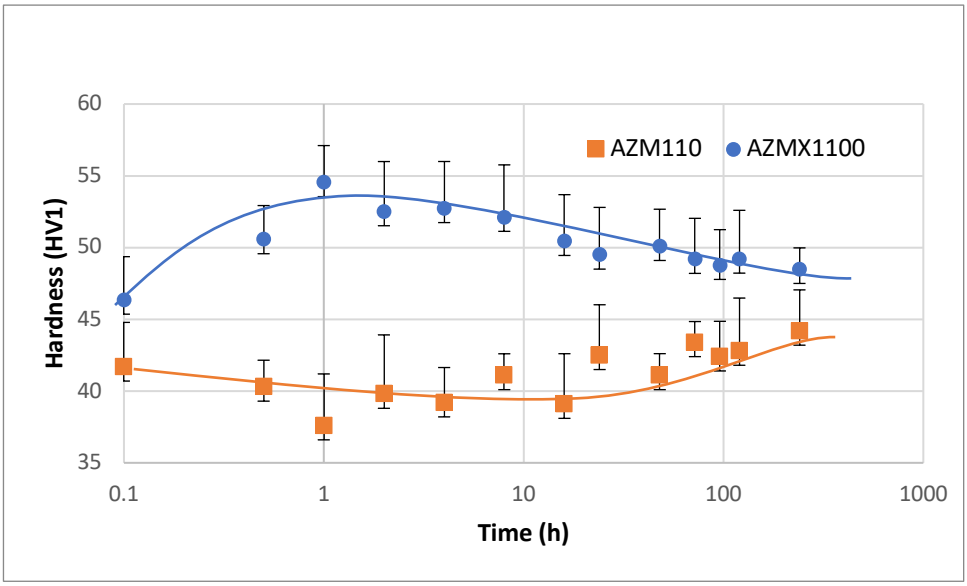


**Figure 5.1- Isothermal ageing of Mg-1Al-1Zn-0.3Mn and Mg-1Al-1Zn-0.3Mn-0.3Ca at 150°C**

### *5.2.1.2 Isothermal Ageing at 175°C*

The age hardening curves of Mg-1Al-1Zn-0.3Mn and Mg-1Al-1Zn-0.3Mn-0.3Ca isothermally aged at 175°C are presented in Figure 5.2. The as-quenched hardness was approximately 42VHN for the Mg-1Al-1Zn-0.3Mn alloy and the alloy containing an addition of 0.3% Ca, the as-quenched hardness was approximately 46VHN. Thereafter, Mg-1Al-1Zn-0.3Mn was age hardened from 30mins to 240hrs, within this period of time there was no response to ageing treatment. As for the 0.3% Ca containing Mg-1Al-1Zn-0.3Mn-0.3Ca alloy, there was a gradual increase of hardness until reaching a maximum value, thereafter the ageing response decreased. The maximum hardness achieved in the Mg-1Al-1Zn-0.3Mn-0.3Ca alloy was approximately 56VHN, that is an increase of 10VHN from the as-quenched condition. This maximum hardness was reached after isothermal ageing for 1hr at 175°C. Further isothermal ageing at 175°C, after achieving maximum hardness, resulted in a slight decrease in the hardness. Values close to peak hardness remained throughout the ageing process until 240hrs.

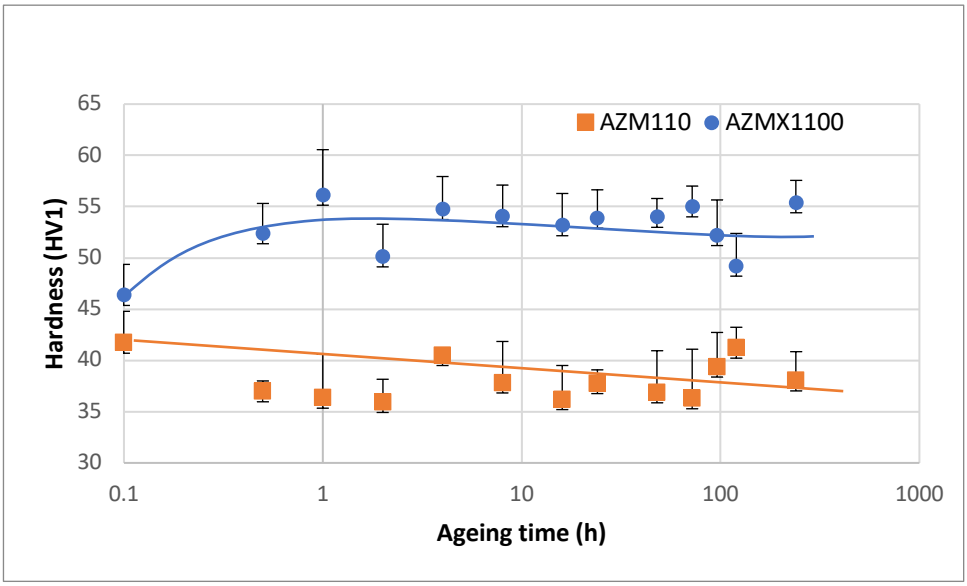


**Figure 5.2- Isothermal ageing of Mg-1Al-1Zn-0.3Mn and Mg-1Al-1Zn-0.3Mn-0.3Ca at 175°C**

### *5.2.1.3 Isothermal Ageing at 200°C*

The age hardening curves of Mg-1Al-1Zn-0.3Mn and Mg-1Al-1Zn-0.3Mn-0.3Ca isothermally aged at 200°C are presented in Figure 5.3. The as-quenched hardness was approximately 42VHN for the Mg-1Al-1Zn-0.3Mn alloy and the alloy containing an addition of 0.3% Ca, the as-quenched hardness was approximately 46VHN. From this point, Mg-1Al-1Zn-0.3Mn alloy was isothermally aged at 200°C up until 240hrs. During this period, there was no hardness response throughout, an indication that ageing did not have the desired impact. As for the 0.3% Ca containing Mg-1Al-1Zn-0.3Mn-0.3Ca alloy, there was a gradual increase of hardness until reaching a maximum value, thereafter the ageing response decreased. The maximum hardness achieved in the Mg-1Al-1Zn-0.3Mn-0.3Ca alloy was approximately 55VHN, that is an increase of 9VHN from the as-quenched condition. This maximum hardness was reached after isothermal ageing for 1hr at 200°C. Further isothermal ageing at 200°C, after achieving maximum hardness, resulted in continuous decrease in the hardness.

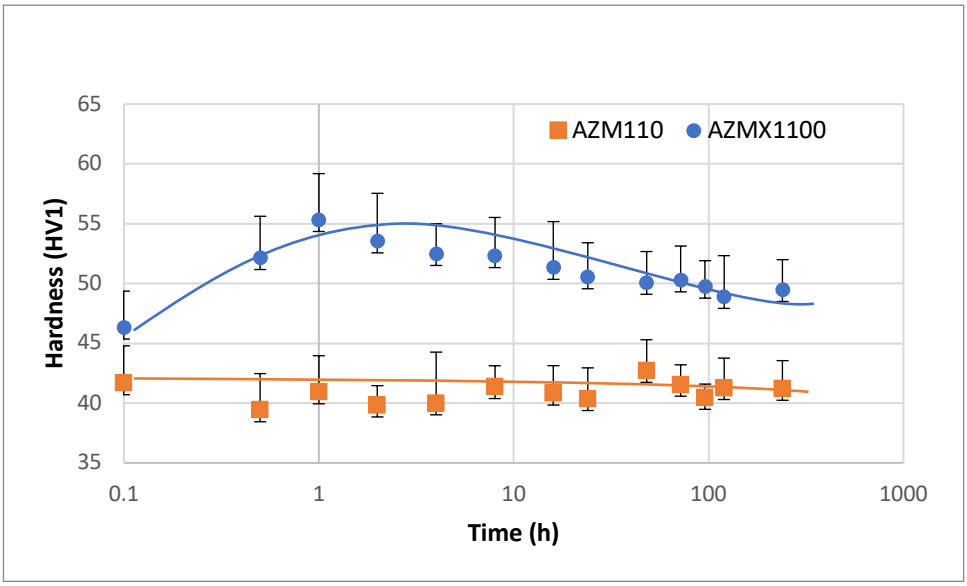


**Figure 5.3- Isothermal ageing of Mg-1Al-1Zn-0.3Mn and Mg-1Al-1Zn-0.3Mn-0.3Ca at 200°C**

## 5.2.2 AZM410-Ca

### *5.2.2.1 Isothermal Ageing at 150°C*

The age hardening curves of Mg-4Al-1Zn-0.3Mn and Mg-4Al-1Zn-0.3Mn-0.3Ca isothermally aged at 150°C are presented in Figure 5.4. The as-quenched hardness was approximately 37VHN for the Mg-4Al-1Zn-0.3Mn alloy and the alloy containing an addition of 0.3% Ca, the as-quenched hardness was approximately 46 VHN. In the as-quenched condition, there was an increase of 9VHN by adding 0.3% Ca. Thereafter, an isothermal ageing treatment was applied to Mg-4Al-1Zn-0.3Mn alloy, there was a considerable rise of 12VHN hardness value to 49VHN after 30mins of ageing. Except for a slight decrease in hardness values during 8hrs to 48hrs, the isothermal ageing response at 150°C throughout the time duration remained considerably stable. As for isothermal ageing at 150°C for Mg-4Al-1Zn-0.3Mn-0.3Ca alloy, there was a gradual increase of hardness value throughout, reaching maximum at 96hrs. The maximum hardness value at 96hrs was therefore 56VHN, an increase of 10VHN from the as-quenched condition. After 96hrs, there was an observable decline in hardness values.

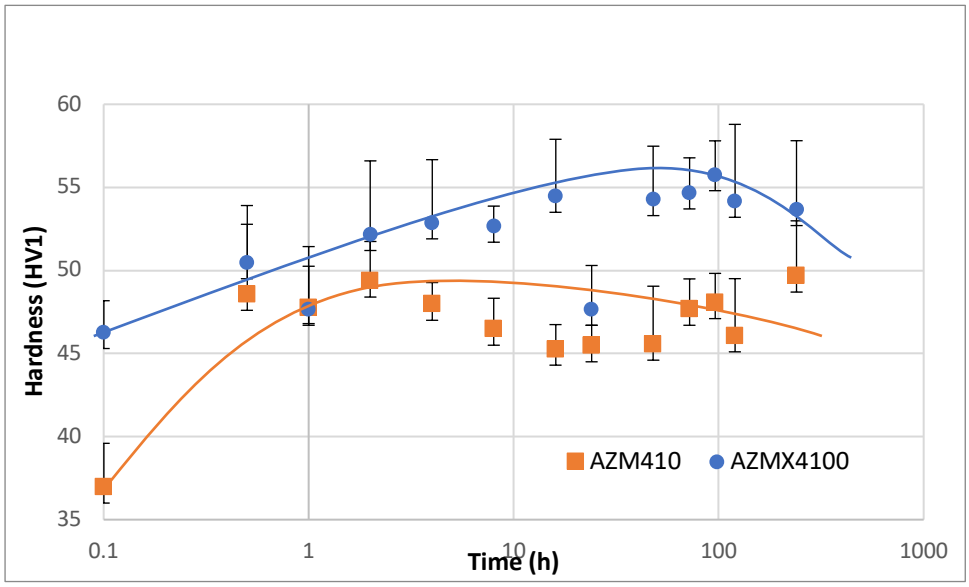


**Figure 5.4- Isothermal ageing of Mg-4Al-1Zn-0.3Mn and Mg-4Al-1Zn-0.3Mn-0.3Ca at 150°C**

### *5.2.2.2 Isothermal Ageing at 175°C*

The age hardening curves of Mg-4Al-1Zn-0.3Mn and Mg-4Al-1Zn-0.3Mn-0.3Ca isothermally aged at 175°C are presented in Figure 5.5. The as-quenched hardness was approximately 37VHN for the Mg-4Al-1Zn-0.3Mn alloy and the alloy containing an addition of 0.3% Ca, the as-quenched hardness was approximately 46 VHN. In the as-quenched condition, there was an increase of 9VHN by adding 0.3% Ca. Thereafter, the ageing response of Mg-4Al-1Zn-0.3Mn alloy remained relatively stable without substantial increase or decrease in hardness. The Mg-4Al-1Zn-0.3Mn alloy achieved maximum hardness through isothermal ageing at 120hrs with a hardness value of 48VHN, this is a hardness increase of 11VHN from the as-quenched condition. As for Mg-4Al-1Zn-0.3Mn-0.3Ca alloy, there was a gradual increase of hardness until reaching a maximum value. The maximum hardness achieved in the Mg-4Al-1Zn-0.3Mn-0.3Ca alloy was approximately 56VHN, that is an increase of 10VHN from the as-quenched condition. This hardness value was achieved during isothermal ageing to 120hrs at 175°C.

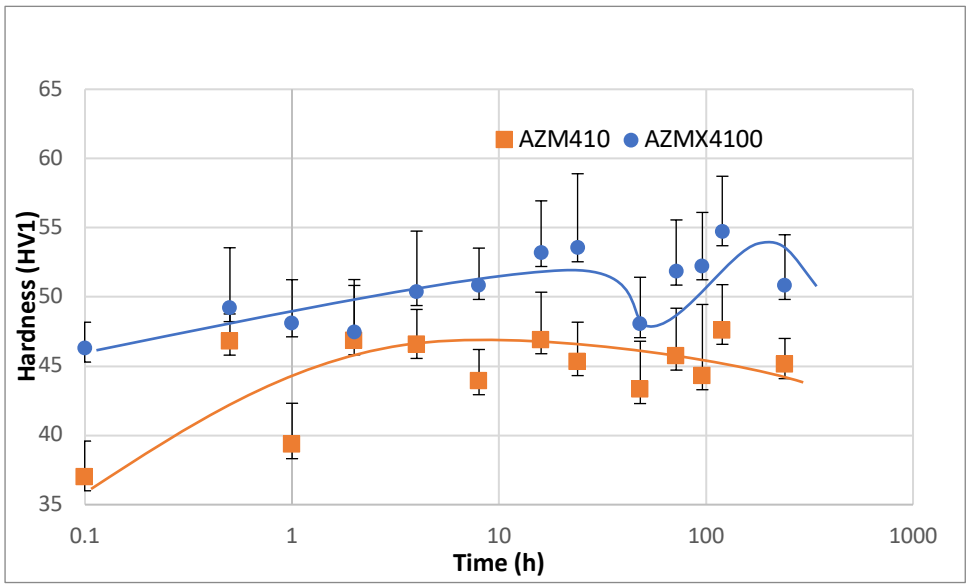


**Figure 5.5- Isothermal ageing of Mg-4Al-1Zn-0.3Mn and Mg-4Al-1Zn-0.3Mn-0.3Ca at 175°C**

### *5.2.2.3 Isothermal Ageing at 200°C*

The age hardening curves of Mg-4Al-1Zn-0.3Mn and Mg-4Al-1Zn-0.3Mn-0.3Ca isothermally aged at 200°C are presented in Figure 5.6. The as-quenched hardness was approximately 37VHN for the Mg-4Al-1Zn-0.3Mn alloy and the alloy containing an addition of 0.3% Ca, the as-quenched hardness was approximately 46 VHN. In the as-quenched condition, there was an increase of 9VHN by adding 0.3% Ca. Thereafter, an isothermal ageing treatment was applied to Mg-4Al-1Zn-0.3Mn alloy, there was a considerable rise of 10VHN hardness value to 49VHN after 30mins of ageing. The isothermal ageing response at 200°C throughout the time duration remained considerably stable. Maximum hardness was achieved after isothermal ageing for 4hrs at 50VHN. As for isothermal ageing at 200°C for Mg-4Al-1Zn-0.3Mn-0.3Ca alloy, again there was significant instance of increase in hardness. The maximum hardness was achieved at 2hrs with 55VHN, half the time of Mg-4Al-1Zn-0.3Mn alloy.

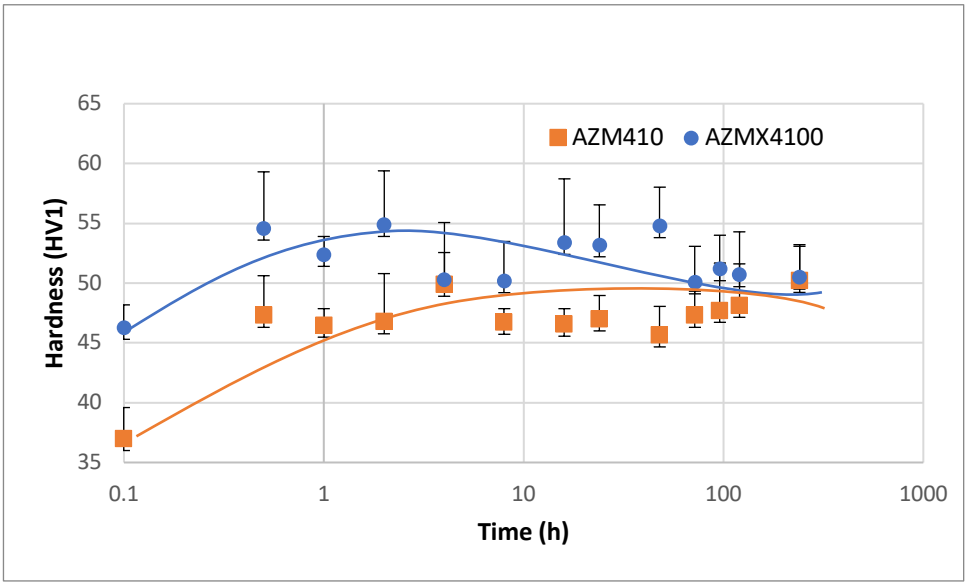


**Figure 5.6- Isothermal ageing of Mg-4Al-1Zn-0.3Mn and Mg-4Al-1Zn-0.3Mn-0.3Ca at 200°C**

## 5.2.3 AZM140-Ca

### *5.2.3.1 Isothermal Ageing at 150°C*

The age hardening curves of Mg-1Al-4Zn-0.3Mn and Mg-1Al-4Zn-0.3Mn-0.3Ca isothermally aged at 150°C are presented in Figure 5.7. The as-quenched hardness was approximately 46VHN for the Mg-1Al-4Zn-0.3Mn alloy and the alloy containing an addition of 0.3% Ca, the as-quenched hardness was approximately 51VHN. Thereafter, Mg-1Al-4Zn-0.3Mn alloy saw a gradual increase in hardness overtime and reached maximum hardness at 120hrs. The maximum hardness value during isothermal ageing at 150°C for Mg-1Al-4Zn-0.3Mn alloy was 68VHN. This is a substantial hardness increment of 22VHN from the as-quenched condition. As for Mg-1Al-4Zn-0.3Mn-0.3Ca alloy, there was a gradual increase of hardness value until reaching maximum at 72hrs. The maximum hardness value during isothermal ageing at 150°C came to 68VHN which is a substantial increase of 17VHN from the as-quenched condition.

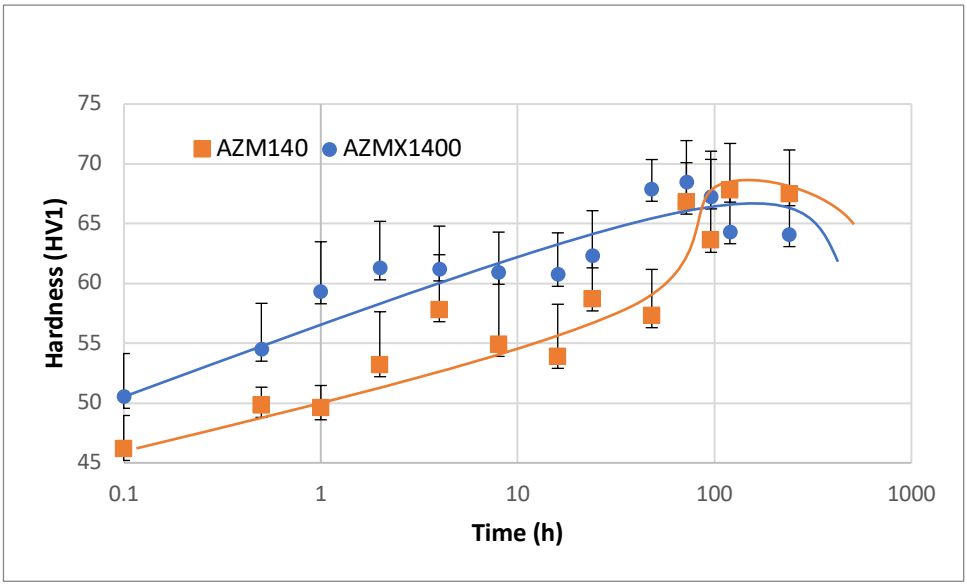


**Figure 5.7- Isothermal ageing of Mg-1Al-4Zn-0.3Mn and Mg-1Al-4Zn-0.3Mn-0.3Ca at 150°C**

### *5.2.3.2 Isothermal Ageing at 175°C*

The age hardening curves of Mg-1Al-4Zn-0.3Mn and Mg-1Al-4Zn-0.3Mn-0.3Ca isothermally aged at 175°C are presented in Figure 5.8. The as-quenched hardness was approximately 46VHN for the Mg-1Al-4Zn-0.3Mn alloy and the alloy containing an addition of 0.3% Ca, the as-quenched hardness was approximately 51VHN. Thereafter, Mg-1Al-4Zn-0.3Mn alloy saw a gradual increase in hardness overtime until 96hrs whereby the hardness began to decrease. The maximum hardness value during isothermal ageing at 175°C for Mg-1Al-4Zn-0.3Mn alloy was 64VHN, achieved at 96hrs. Interestingly, this is a substantial hardness increment of 18VHN from the as-quenched condition. As for Mg-1Al-4Zn-0.3Mn-0.3Ca alloy, again there was a gradual increase of hardness value until a time where there was a sudden decrease in hardness values. To reach maximum hardness value, it took 0.3% Ca containing alloy 48hrs which equates to half the time it took the alloy without calcium to reach maximum hardness value. The maximum hardness value during isothermal ageing at 175°C came to 71VHN which is a substantial increase of 20VHN from the as-quenched condition. Thereafter, the hardness continued to decrease until reaching the final ageing treatment time of 240hrs.

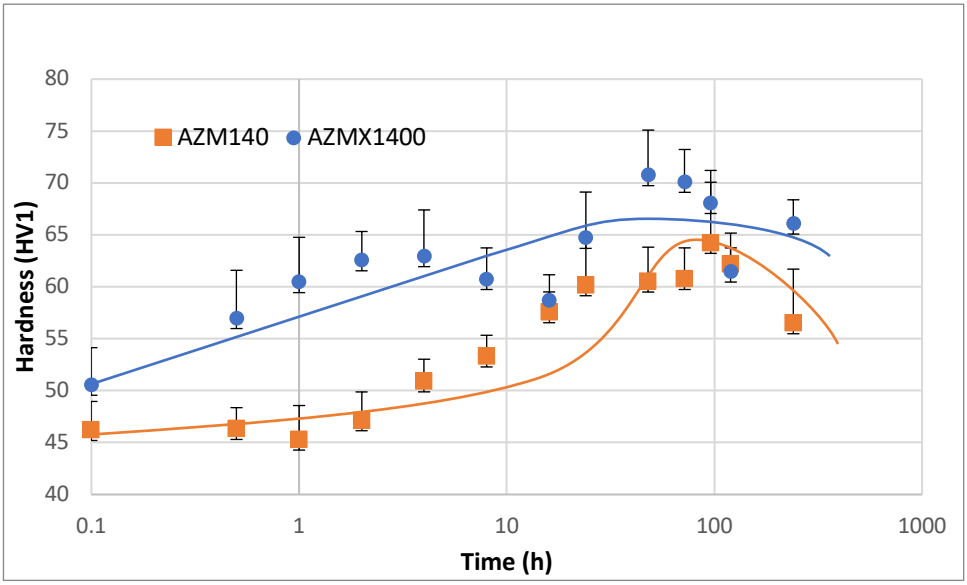


**Figure 5.8- Isothermal ageing of Mg-1Al-4Zn-0.3Mn and Mg-1Al-4Zn-0.3Mn-0.3Ca at 175°C**

### *5.2.3.3 Isothermal Ageing at 200°C*

The age hardening curves of Mg-1Al-4Zn-0.3Mn and Mg-1Al-4Zn-0.3Mn-0.3Ca isothermally aged at 200°C are presented in Figure 5.9. The as-quenched hardness was approximately 46VHN for the Mg-1Al-4Zn-0.3Mn alloy and the alloy containing an addition of 0.3% Ca, the as-quenched hardness was approximately 51VHN. Thereafter, Mg-1Al-4Zn-0.3Mn alloy saw a gradual increase in hardness overtime until 72hrs whereby the hardness began to decrease. The maximum hardness value during isothermal ageing at 200°C for Mg-1Al-4Zn-0.3Mn alloy was 66VHN, achieved at 72hrs. Interestingly, this is a substantial hardness increment of 20VHN from the as-quenched condition. As for Mg-1Al-4Zn-0.3Mn-0.3Ca alloy, again there was a gradual increase of hardness value until a time where there was a sudden decrease in hardness value. The maximum hardness value during isothermal ageing at 200°C came to 70VHN at 72hrs which is a substantial increase of 19VHN from the as-quenched condition. Thereafter, the hardness continued to decrease until reaching the final ageing treatment time of 240hrs.

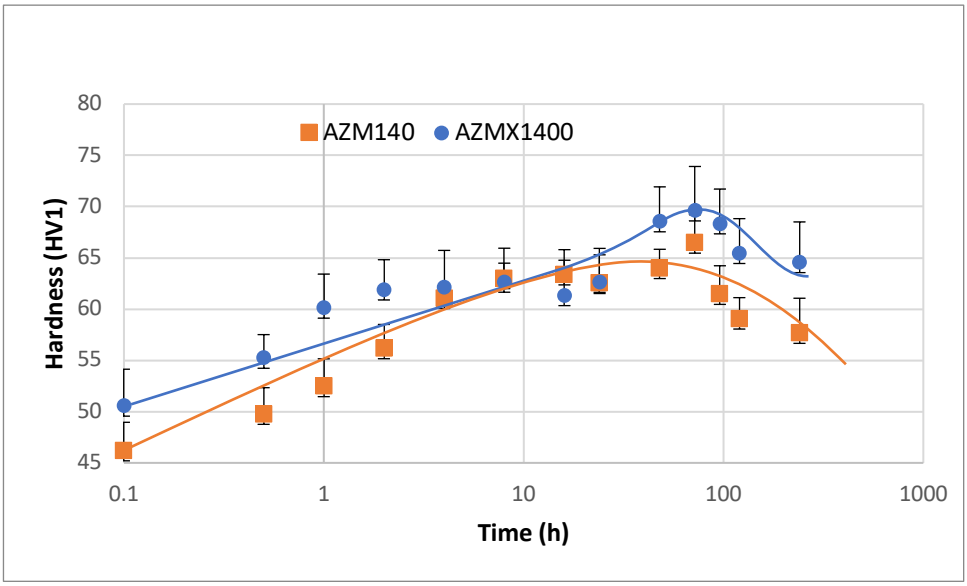


**Figure 5.9- Isothermal ageing of Mg-1Al-4Zn-0.3Mn and Mg-1Al-4Zn-0.3Mn-0.3Ca at 200°C**

## 5.3 Microstructure Characterisation & Ageing of Rolled Alloys

### 5.3.1 AZM110-Ca

#### *5.3.1.1 Microstructure Characterisation of AZM110 Rolled Alloys*

A polarised light micrograph of hot rolled Mg-1Al-1Zn-0.3Mn alloy is shown in Figure 5.11 a). The microstructure has typical features of a deformed alloy with considerably elongated grains. The process of recrystallisation through the chosen heat treatment path has taken little effect with vast majority of microstructure indicating significant deformity. The grain size of hot rolled Mg-1Al-1Zn-0.3Mn alloy measured to be at 33±4.5μm as shown in Figure 5.10, this is a considerable reduction from the grain size measured in the as-cast condition which equated to 250±34μm.

A polarised light micrograph of 5% deformed Mg-1Al-1Zn-0.3Mn alloy is shown in Figure 5.11 b). The microstructure has typical features of a deformed alloy with elongated grains but the occurrence of recrystallisation can be observed at a greater scale in comparison to the hot rolled Mg-1Al-1Zn-0.3Mn alloy. The grain size of 5% deformed Mg-1Al-1Zn-0.3Mn alloy measured to be at 37±6μm.

A polarised light micrograph of pre-aged Mg-1Al-1Zn-0.3Mn alloy is shown in Figure 5.11 c). As seen previously in the hot rolled and 5% deformed conditions of Mg-1Al-1Zn-0.3Mn alloy, there are elongated grains present in the microstructure, an indication that complete recrystallisation did not occur. The grain size was measured of pre-aged Mg-1Al-1Zn-0.3Mn alloy and it amounted to 26±1.5μm, a decrease of 7μm and 11μm from the previous respective conditions.

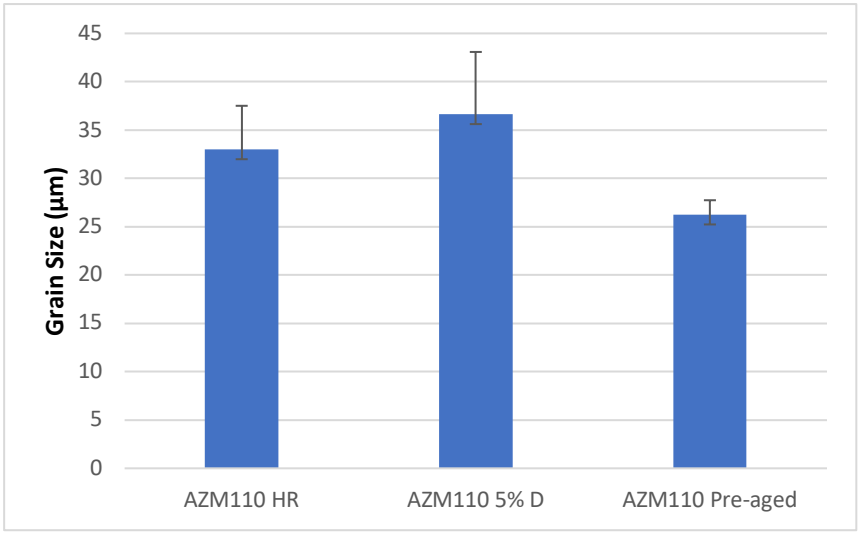


**Figure 5.10- Grain size measurement of Mg-1Al-1Zn-0.3Mn in three conditions, hot rolled, deformed and pre-aged**

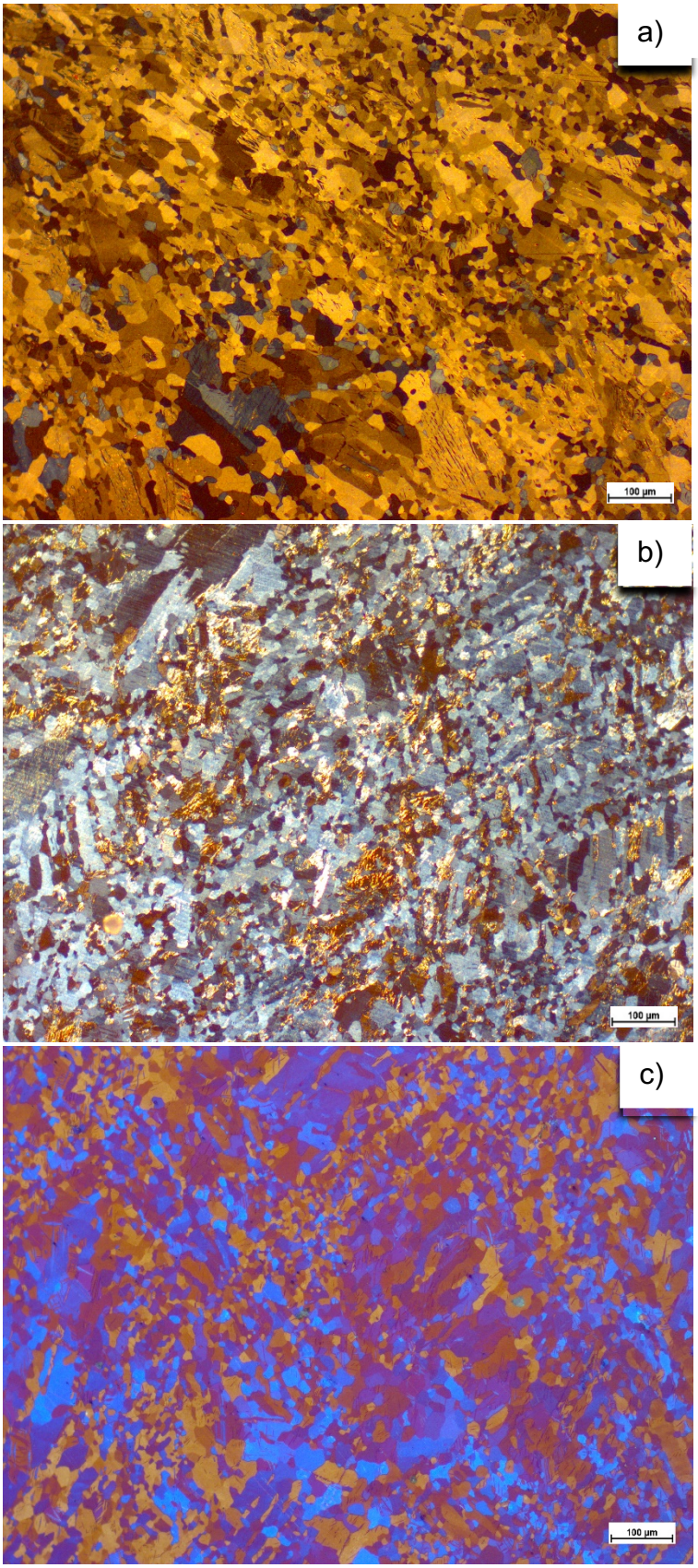


**Figure 5.11- Polarised light micrographs of Mg-1Al-1Zn-0.3Mn in a) hot rolled condition, b) 5% deformed condition, c) pre-aged condition**

#### ***5.3.1.2 Ageing of AZM110 Rolled Alloys***

The age hardening curves of Mg-1Al-1Zn-0.3Mn were isothermally aged at 175°C in several deformed conditions and are presented in Figure 5.12. Before being aged hardened, the hot rolled Mg-1Al-1Zn-0.3Mn conditioned alloy displayed a hardness value of 51VHN, this is a significant increase of 9VHN from the as-quenched condition. Thereafter, ageing treatment was applied from 5mins to 10 days to ascertain hardness response. During ageing of hot rolled Mg-1Al-1Zn-0.3Mn alloy, hardness response remained stable throughout without an obvious peak. The hardness value at 1hr was 53VHN, the most significant increase throughout the ageing process.

Before isothermal ageing at 175°C, the 5% deformed Mg-1Al-1Zn-0.3Mn alloy had hardness measurement of 59VHN, an increase of 17VHN from as-quenched condition and an increase of 8VHN from the hot rolled condition. During ageing of 5% deformed Mg-1Al-1Zn-0.3Mn alloy, hardness response remained stable throughout without an obvious peak. During ageing process, a peak hardness of 58VHN was achieved at 1hr period. Further highlighting how stable and non-responsive Mg-1Al-1Zn-0.3Mn alloy is to age hardening.

The pre-aged Mg-1Al-1Zn-0.3Mn alloy displayed similar characteristics to as-cast, hot rolled and 5% deformed alloys. Before ageing, the alloy in this condition had a hardness measurement of 55VHN, an increase of 13VHN from the as-quenched condition. In line with other conditions, the hardness response of pre-aged Mg-1Al-1Zn-0.3Mn alloy remained stable without showing a peak response. The maximum hardness was achieved at 240hrs with 55VHN.

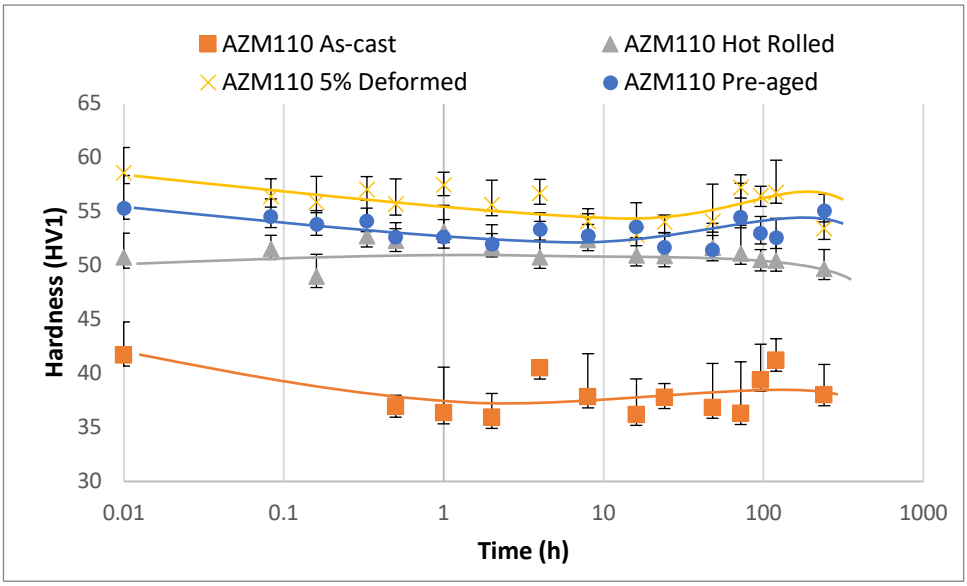


**Figure 5.12- Age hardening response of Mg-1Al-1Zn-0.3Mn in various conditions**

### *5.3.1.3 Microstructure Characterisation of AZMX1100 Rolled Alloys*

A polarised light micrograph of hot rolled Mg-1Al-1Zn-0.3Mn-0.3Ca alloy is shown in Figure 5.14 a). The microstructure indicates crystallisation has taken place with equiaxed grains throughout the micrograph. The grain size of hot rolled Mg-1Al-1Zn-0.3Mn-0.3Ca alloy measured to be at 37±2.5μm as shown in Figure 5.13, this is a considerable reduction from the grain size measured in the as-cast condition which equated to 313±40μm.

A polarised light micrograph of 5% deformed Mg-1Al-1Zn-0.3Mn-0.3Ca alloy is shown in Figure 5.14 b). The microstructure of Ca containing deformed alloy displays equiaxed grains indicating recovery through recrystallisation. The grain size of 5% deformed Mg-1Al-1Zn-0.3Mn-0.3Ca alloy measured to be at 35±1.5μm.

A polarised light micrograph of pre-aged Mg-1Al-1Zn-0.3Mn-0.3Ca alloy is shown in Figure 5.14 c). As seen previously in the hot rolled and 5% deformed conditions of Mg-1Al-1Zn-0.3Mn-0.3 alloy, there are equiaxed grains present in the microstructure, an indication that complete recrystallisation did occur. The grain size was measured of pre-aged Mg-1Al-1Zn-0.3Mn-0.3Ca alloy and it amounted to 33±1.2μm.

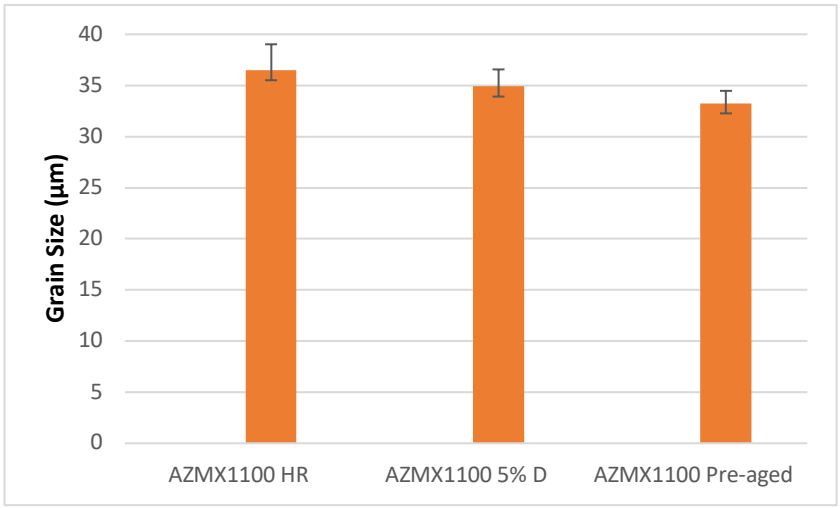


**Figure 5.13 - Grain size measurement of Mg-1Al-1Zn-0.3Mn-03Ca in three conditions, hot rolled, deformed and pre-aged**

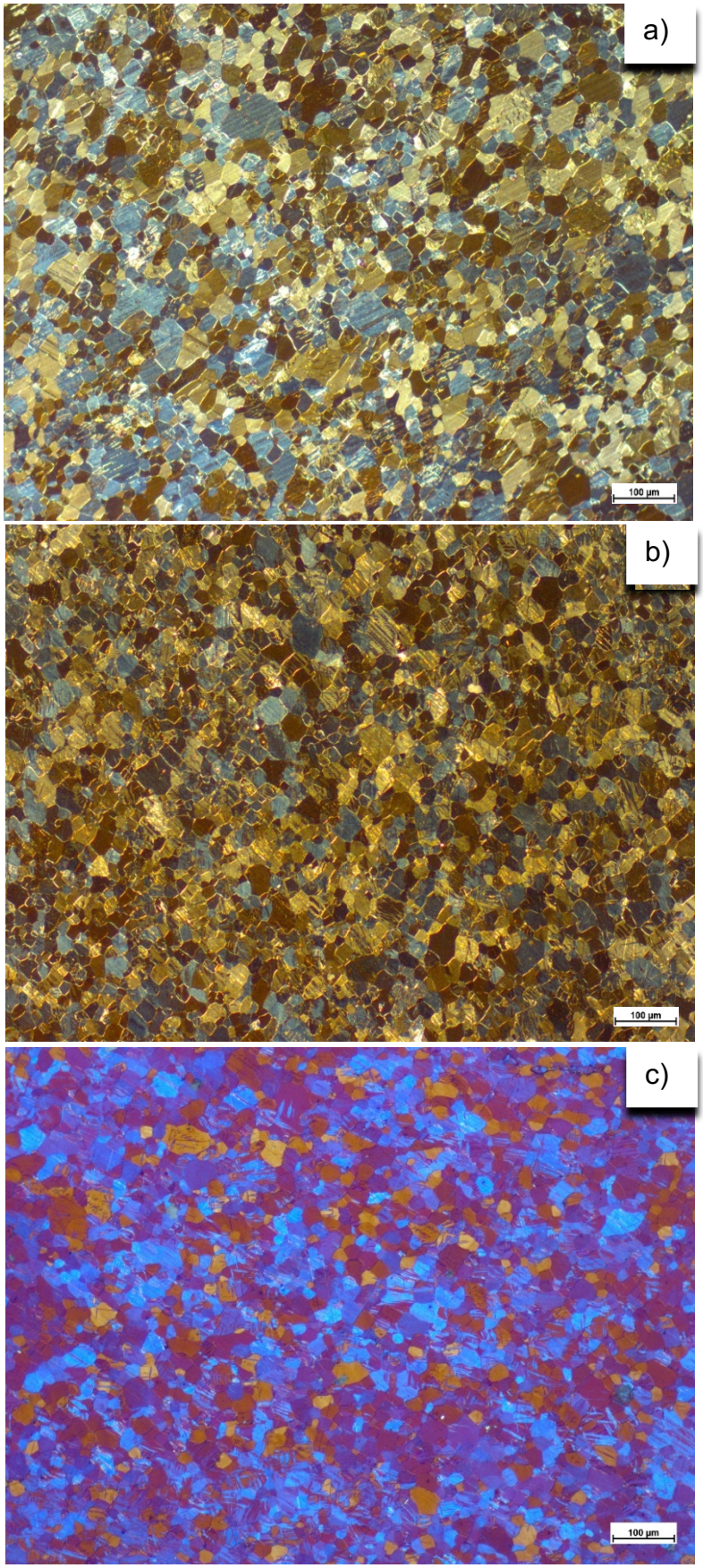


**Figure 5.14- Polarised light micrographs of Mg-1Al-1Zn-0.3Mn-0.3Ca in a) hot rolled condition, b) 5% deformed condition, c) pre-aged condition**

#### ***5.3.1.4 Ageing of AZMX1100 Rolled Alloys***

The age hardening response of Mg-1Al-1Zn-0.3Mn-0.3Ca was sought through isothermal ageing at 175°C in several deformed conditions, they are presented in Figure 5.15. Before being aged hardened, the hot rolled Mg-1Al-1Zn-0.3Mn-0.3Ca conditioned alloy displayed a hardness value of 52VHN, this is an increase of 6VHN from the as-quenched condition. From here, an ageing treatment is applied from 5 mins to 10 days. During ageing, there was gradual increase in hardness until reaching peak hardness, after this stage, a steady decline in hardness is observed. The maximum hardness achieved in the hot rolled Mg-1Al-1Zn-0.3Mn-0.3Ca alloy was approximately 68VHN, that is an increase of 14VHN from the before ageing condition. It took 8hrs to reach maximum hardness in this condition, whereas peak hardness is achieved far quicker in the as-cast condition in 1hr. There is a substantial increase in hardness in this condition with 12VHN.

Before isothermal ageing at 175°C, the 5% deformed Mg-1Al-1Zn-0.3Mn-0.3Ca alloy had hardness measurement of 67VHN, an increase of 21VHN from as-quenched condition and an increase of 15VHN from the hot rolled condition. During ageing, there was gradual increase in hardness until reaching maximum hardness, after this stage, a steady decline in hardness is observed. The peak hardness achieved in the 5% deformed Mg-1Al-1Zn-0.3Mn-0.3Ca alloy was approximately 79VHN, that is an increase of 12VHN from the before ageing condition. In this deformed condition, peak hardness is achieved within 2hrs, which is 75% the time it reached peak in hot rolled condition. Comparing the peak hardness of rolled condition and 5% deformed condition, there is a substantial increase in hardness in the latter with 11VHN.

As for the pre-aged Mg-1Al-1Zn-0.3Mn-0.3Ca alloy, the ageing curve profile followed a similar trend to those observed for as-cast, hot rolled and 5% deformed condition. Before ageing, the alloy in this condition had a hardness measurement of 68VHN, a substantial increase of 22VHN from the as-quenched condition. In comparison to hot rolled and 5% deformed conditions, it is an increased value of 16VHN and 2VHN, respectively. Maximum hardness of pre-aged Mg-1Al-1Zn-0.3Mn-0.3Ca alloy was achieved at 8hrs with a value of 74VHN.

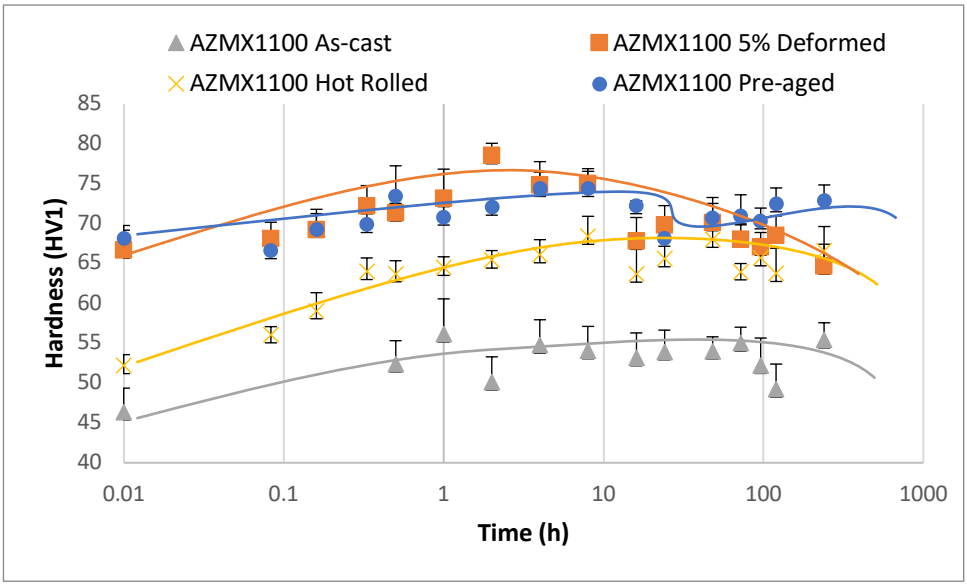


**Figure 5.15- Age hardening response of Mg-1Al-1Zn-0.3Mn-0.3Ca in various conditions**

## 5.3.2 AZM140-Ca

### *5.3.2.1 Microstructure Characterisation of AZM140 Rolled Alloys*

A polarised light micrograph of hot rolled Mg-1Al-4Zn-0.3Mn alloy is shown in Figure 5.17 a). The microstructure indicates crystallisation has taken place with presence of equiaxed grains seen in the micrograph. The grain size of hot rolled Mg-1Al-4Zn-0.3Mn alloy measured to be at 31±3μm as shown in Figure 5.16, this is a considerable reduction from the grain size measured in the as-cast condition which equated to 194±23μm.

A polarised light micrograph of 5% deformed Mg-1Al-4Zn-0.3Mn alloy is shown in Figure 5.17 b). The microstructure of 5% deformed alloy displays equiaxed grains indicating recovery through recrystallisation. The grain size of 5% deformed Mg-1Al-4Zn-0.3Mn alloy measured to be at 41±6μm, in comparison to the hot rolled conditioned alloy, it is an increase of 10μm from 31±3μm.

A polarised light micrograph of pre-aged Mg-1Al-4Zn-0.3Mn alloy is shown in Figure 5.17 c). As seen previously in the hot rolled and 5% deformed conditions of Mg-1Al-1Zn-0.3Mn alloy, there are equiaxed grains present in the microstructure, an indication that recrystallisation did occur. The grain size was measured of pre-aged Mg-1Al-4Zn-0.3Mn alloy and it amounted to 34±1.5μm.

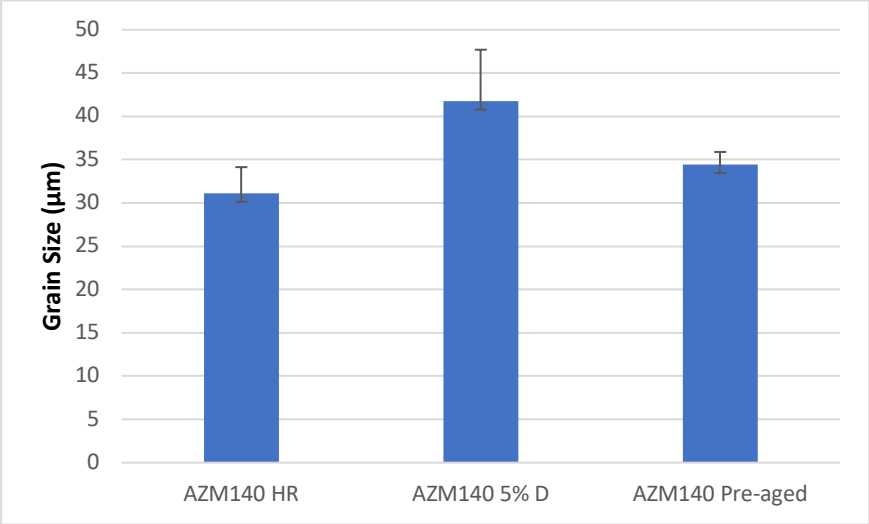


**Figure 5.16- Grain size measurement of Mg-1Al-4Zn-0.3Mn in three conditions, hot rolled, deformed and pre-aged**

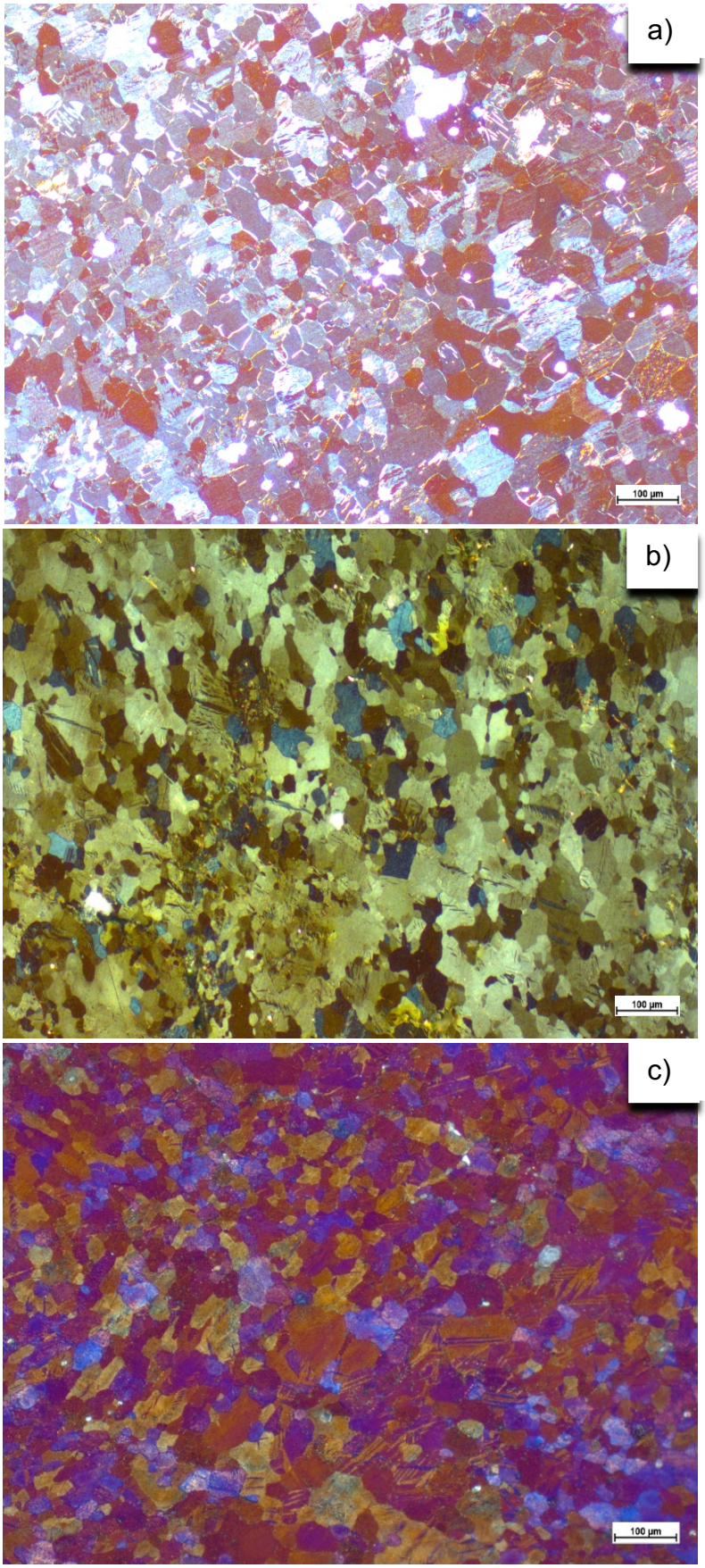


**Figure 5.17- Polarised light micrographs of Mg-1Al-4Zn-0.3Mn in a) hot rolled condition, b) 5% deformed condition, c) pre-aged condition**

#### ***5.3.2.2 Ageing of AZM140 Rolled Alloys***

The age hardening response of Mg-1Al-4Zn-0.3Mn was sought through isothermal ageing at 175°C in several deformed conditions, they are presented in Figure 5.18. Before being aged hardened, the hot rolled Mg-1Al-4Zn-0.3Mn conditioned alloy displayed a hardness value of 55VHN, this is an increase of 9VHN from the as-quenched condition. From here, an ageing treatment is applied from 5 mins to 10 days. During ageing, there was gradual increase in hardness until reaching peak hardness, after this stage, a decline in hardness is observed. The maximum hardness achieved in the hot rolled Mg-1Al-4Zn-0.3Mn alloy was approximately 72VHN, that is an increase of 17VHN from the before ageing condition. It took 120hrs to reach maximum hardness in this condition, whereas peak hardness is achieved earlier in the as-cast condition in 96hrs. Both alloys in respective conditions peak at different hardness values too with a difference of 6VHN.

Before isothermal ageing at 175°C, the 5% deformed Mg-1Al-4Zn-0.3Mn alloy had hardness measurement of 53VHN, an increase of 7VHN from as-quenched condition and a decrease of 2VHN from the hot rolled condition. During ageing, there was gradual increase in hardness until reaching maximum hardness, after this stage, a decline in hardness is observed. The peak hardness achieved in the 5% deformed Mg-1Al-4Zn-0.3Mn alloy was approximately 72VHN, that is an increase of 19VHN from the before ageing condition. In this deformed condition, peak hardness is achieved within 48hrs, which is considerably faster than the alloy in hot rolled condition which reached peak hardness in 120hrs. Comparing the peak hardness of rolled condition and 5% deformed condition, there is no difference in hardness values.

As for the pre-aged Mg-1Al-4Zn-0.3Mn alloy, the ageing curve profile followed a similar trend to those observed for as-cast, hot rolled and 5% deformed condition. Before ageing, the alloy in this condition had a hardness measurement of 54VHN,

significant increase of 8VHN from the as-quenched condition. Maximum hardness of pre-aged Mg-1Al-4Zn-0.3Mn alloy was achieved at 48hrs with a value of 71VHN.

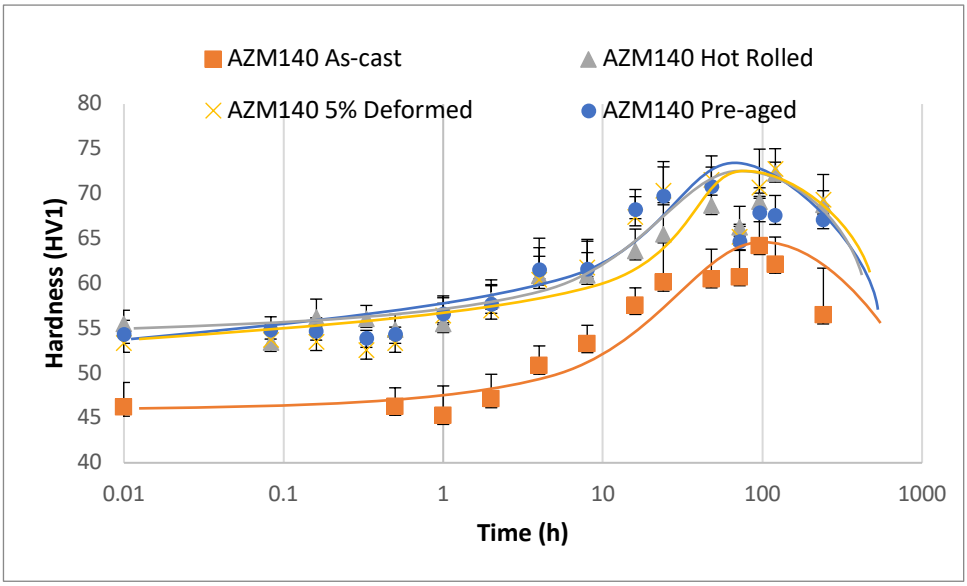


**Figure 5.18- Age hardening response of Mg-1Al-4Zn-0.3Mn in various conditions**

### *5.3.2.3 Microstructure Characterisation of AZMX1400 Rolled Alloys*

A polarised light micrograph of hot rolled Mg-1Al-4Zn-0.3Mn-0.3Ca alloy is shown in Figure 5.20 a). The microstructure indicates crystallisation has taken place with presence of equiaxed grains seen in the micrograph but with considerable twinning. The grain size of hot rolled Mg-1Al-4Zn-0.3Mn-0.3Ca alloy measured to be at 279±11µm as shown in Figure 5.19, this is a considerable increase from the grain size measured in the as-cast condition which equated to 226±43µm, an indication that deformation did not have an impact on the microstructure in comparison to all the previous alloys.

A polarised light micrograph of 5% deformed Mg-1Al-4Zn-0.3Mn-0.3Ca alloy is shown in Figure 5.20 b). The microstructure indicates crystallisation has taken place with presence of equiaxed grains seen in the micrograph but with considerable twinning. The grain size of 5% deformed Mg-1Al-4Zn-0.3Mn-0.3Ca alloy measured to be at 265±9µm. In comparison to the hot rolled conditioned alloy, it is a decrease of 14µm from 279±11µm.

A polarised light micrograph of pre-aged Mg-1Al-4Zn-0.3Mn-0.3Ca alloy is shown in Figure 5.20 c). As seen previously in the hot rolled and 5% deformed conditions of Mg-1Al-1Zn-0.3Mn-0.3Ca alloy, there are equiaxed grains present in the microstructure, an indication that recrystallisation did occur. The grain size was measured of pre-aged Mg-1Al-4Zn-0.3Mn-0.3Ca alloy and it amounted to 248±18µm, a decrease of 30µm and 16µm from the previous respective conditions.

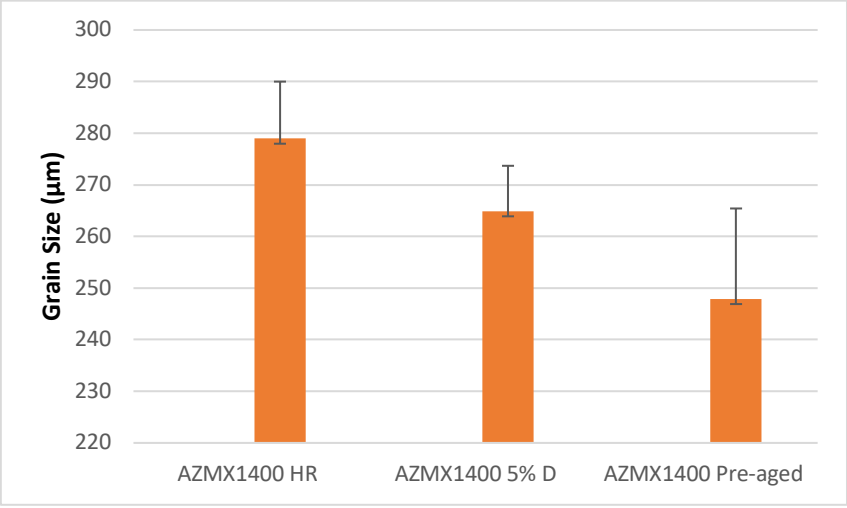


**Figure 5.19- Grain size measurement of Mg-1Al-4Zn-0.3Mn-03Ca in three conditions, hot rolled, deformed and pre-aged**

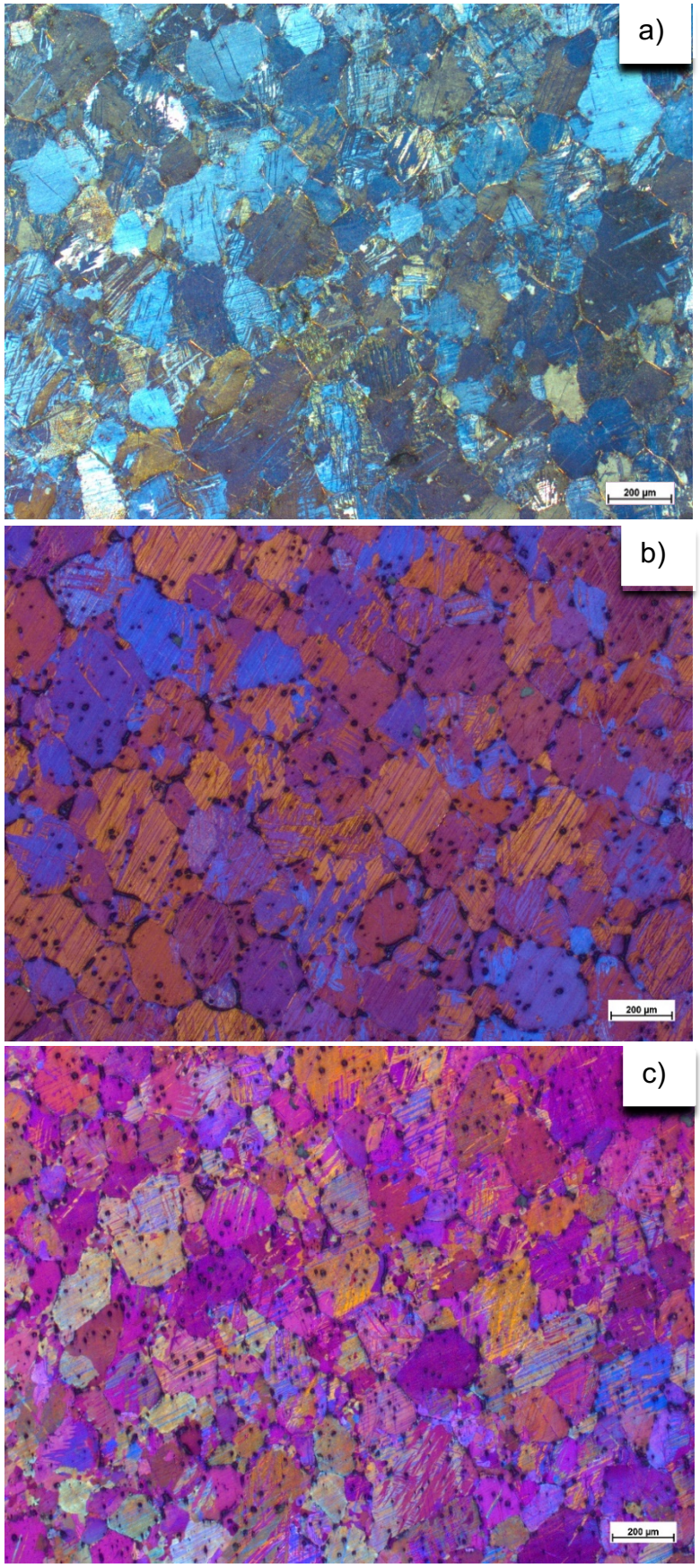


**Figure 5.20- Polarised light micrographs of Mg-1Al-4Zn-0.3Mn-0.3Ca in a) hot rolled condition, b) 5% deformed condition, c) pre-aged condition**

#### ***5.3.2.4 Ageing of AZMX1400 Rolled Alloys***

The age hardening response of Mg-1Al-4Zn-0.3Mn-0.3Ca alloy was sought through isothermal ageing at 175°C in several deformed conditions, they are presented in Figure 5.21. Before being aged hardened, the hot rolled Mg-1Al-4Zn-0.3Mn-0.3Ca conditioned alloy displayed a hardness value of 61VHN, this is an increase of 10VHN from the as-quenched condition. From here, an ageing treatment is applied from 5 mins to 10 days. During ageing, there was gradual increase in hardness until reaching peak hardness, after this stage, a decline in hardness is observed. The maximum hardness achieved in the hot rolled Mg-1Al-4Zn-0.3Mn-0.3Ca alloy was approximately 70VHN, that is an increase of 9VHN from the before ageing condition. It took 240hrs to reach maximum hardness in this condition, whereas peak hardness is achieved earlier in the as-cast condition in 48hrs.

Before isothermal ageing at 175°C, the 5% deformed Mg-1Al-4Zn-0.3Mn-0.3Ca alloy had hardness measurement of 63VHN, an increase of 12VHN from as-quenched condition and an increase of 2VHN from the hot rolled condition. During ageing, there was gradual increase in hardness until reaching maximum hardness, after this stage, a decline in hardness is observed. The peak hardness achieved in the 5% deformed Mg-1Al-4Zn-0.3Mn-0.3Ca alloy was approximately 71VHN, that is an increase of 8VHN from the before ageing condition. In this deformed condition, peak hardness is achieved within 24hrs, which is considerably faster than the alloy in hot rolled condition which reached peak hardness in 240hrs.

As for the pre-aged Mg-1Al-4Zn-0.3Mn-0.3Ca alloy, the ageing curve profile followed a similar trend to those observed for as-cast, hot rolled and 5% deformed condition. Before ageing, the alloy in this condition had a hardness measurement of 64VHN, a significant increase of 13VHN from the as-quenched condition. In comparison to hot rolled and 5% deformed conditions, it is an increased value of 3VHN and decreased value of 1VHN, respectively. Maximum hardness of pre-aged Mg-1Al-4Zn-0.3Mn-0.3Ca alloy was achieved at 96hrs with a value of 72VHN.

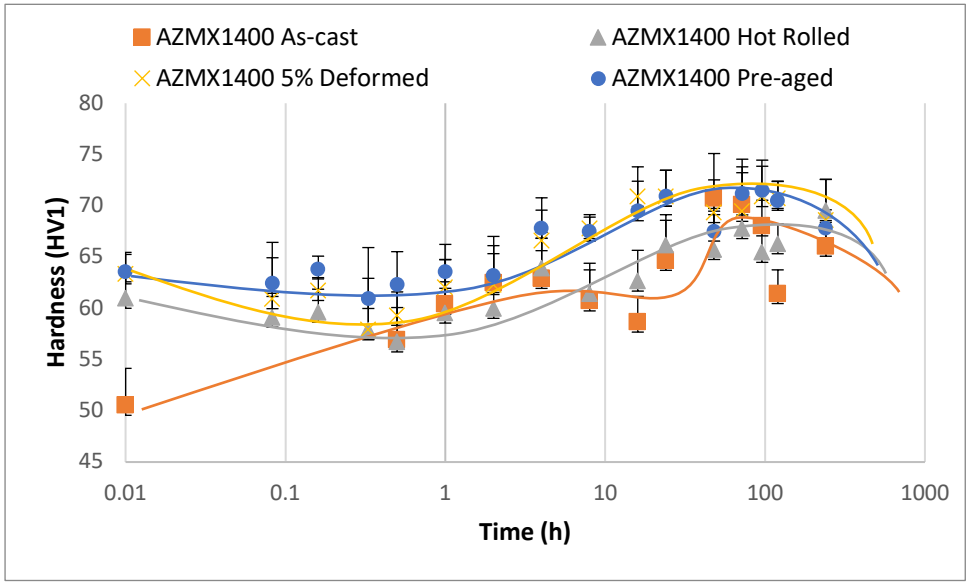


**Figure 5.21- Age hardening response of Mg-1Al-4Zn-0.3Mn-0.3Ca in various conditions**

## 5.4 Transmission Electron Microscopy of As-cast and Deformed Alloys

### 5.4.1 AZM110-Ca

#### *5.4.1.1 As-cast*

Transmission electron microscopy (TEM) micrograph of as-cast and peak-aged Mg-1Al-1Zn-0.3Mn is shown in Figure 5.22 a). Mg-1Al-1Zn-0.3Mn was thermo-mechanically processed by homogenising at 400°C for 1 hour and then peak-aged at an isothermal temperature of 175°C for 1 hour. As evidenced, negligible amount of plate shaped particles are observed and therefore their number density is too low for precipitate strengthening to be achieved as confirmed by ageing hardening curves. Particles were observed with the electron beam parallel to <$11\bar{2}0$> direction.

TEM micrograph of as-cast and peak-aged Mg-1Al-1Zn-0.3Mn-0.3Ca showing distribution of precipitates is shown in Figure 5.22 b). The calcium containing Mg-1Al-1Zn-0.3Mn-0.3Ca was thermo-mechanically processed by homogenising at 450°C for 2 hours and then peak-aged at an isothermal temperature of 175°C for 1 hour. It was observed that addition of 0.3wt% calcium increased very fine plate-like precipitates in the microstructure. These precipitates show up as streak parallel to the $11\bar{2}0$ reflections at 1/3 and 2/3 distances from the $11\bar{2}0$ reflections. Precipitates are observed along <$10\bar{1}0$> direction parallel to electron beam.

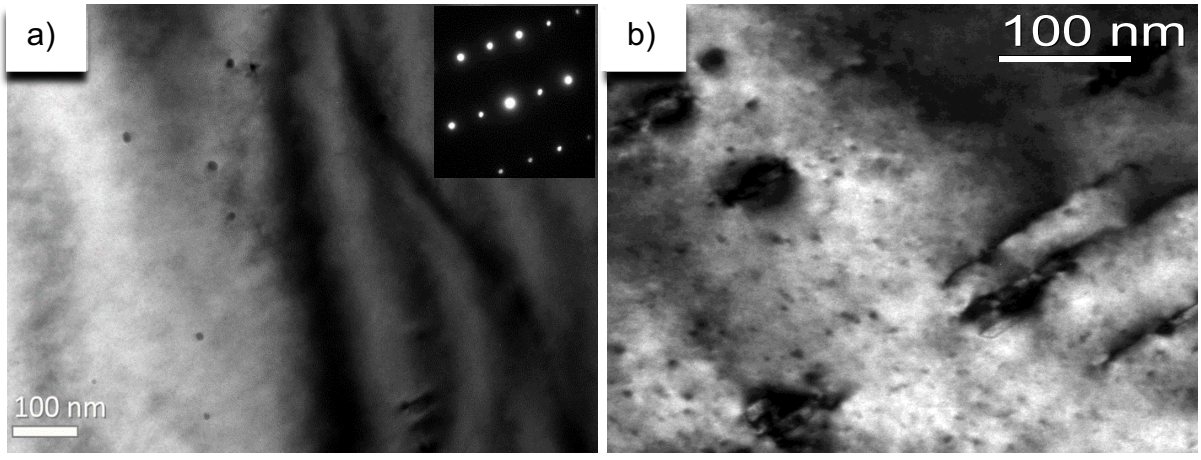


**Figure 5.22- TEM micrograph of as-cast and peak-aged, a) Mg-1Al-1Zn-0.3Mn and b) Mg-1Al-1Zn-0.3Mn-0.3Ca**

### *5.4.1.2 Rolled and Pre-aged*

TEM micrograph of deformed and peak-aged Mg-1Al-1Zn-0.3Mn-0.3Ca showing distribution of precipitates is shown in Figure 5.23 a) and b). Mg-1Al-1Zn-0.3Mn-0.3Ca was thermo-mechanically processed by homogenising at 450°C for 2 hours and then peak-aged at an isothermal temperature of 175°C for 1 hour. Hot rolling considerably increased the number density of the very fine precipitates as observed in this microstructure. These precipitates showed up as streak parallel to the $11\bar{2}0$ reflections at 1/3 and 2/3 distances from the $11\bar{2}0$ reflections. Precipitates are observed along <$10\bar{1}0$> direction parallel to electron beam. As seen in Figure 5.23 c), there is significant twinning and dislocation structures present in the microstructure.

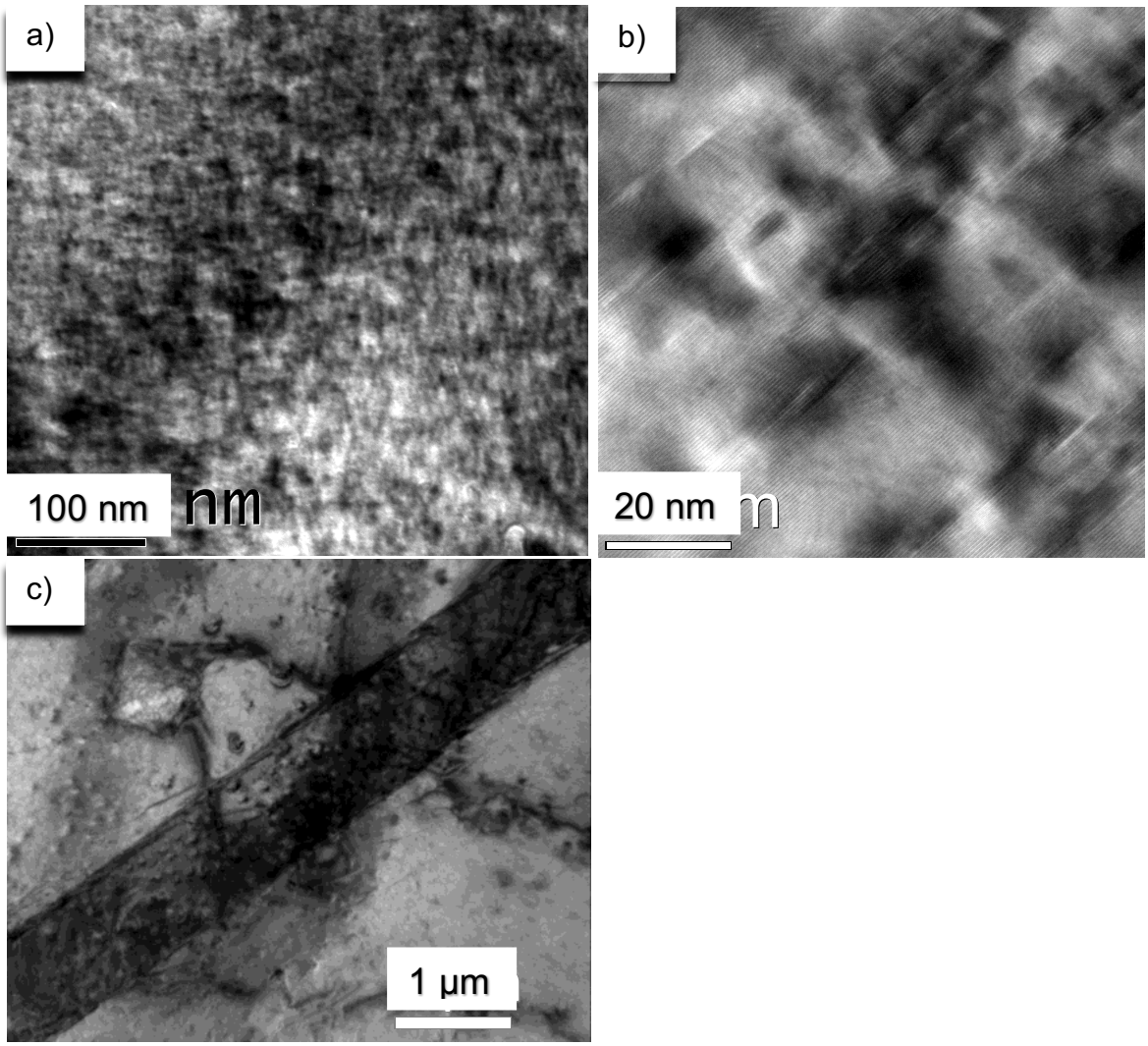


**Figure 5.23- TEM micrograph of deformed and peak-aged Mg-1Al-1Zn-0.3Mn-0.3Ca, a) In low magnification, b) In high magnification and c) Observation of twinning in microstructure**

TEM micrograph of pre-aged Mg-1Al-1Zn-0.3Mn-0.3Ca showing distribution of precipitates is shown in Figure 5.24 a) and b). Mg-1Al-1Zn-0.3Mn-0.3Ca was thermo-mechanically processed by homogenising at 450°C for 2 hours, pre-aged for 15 minutes at 175°C, 5% deformed through cold rolling and finally peak-aged at an isothermal temperature of 175°C for 1 hour. Precipitates are mainly very fine plate like particles forming on (0001) planes. In comparison to permanent mould cast Mg-1Al-1Zn-0.3Mn-0.3Ca, the precipitates are longer. However, there are more precipitates in a given area and as result, the increase in strength seen through ageing hardening curves is due to the number density increase. Particles were observed with the electron beam parallel to $<10\bar{1}0>$ direction.

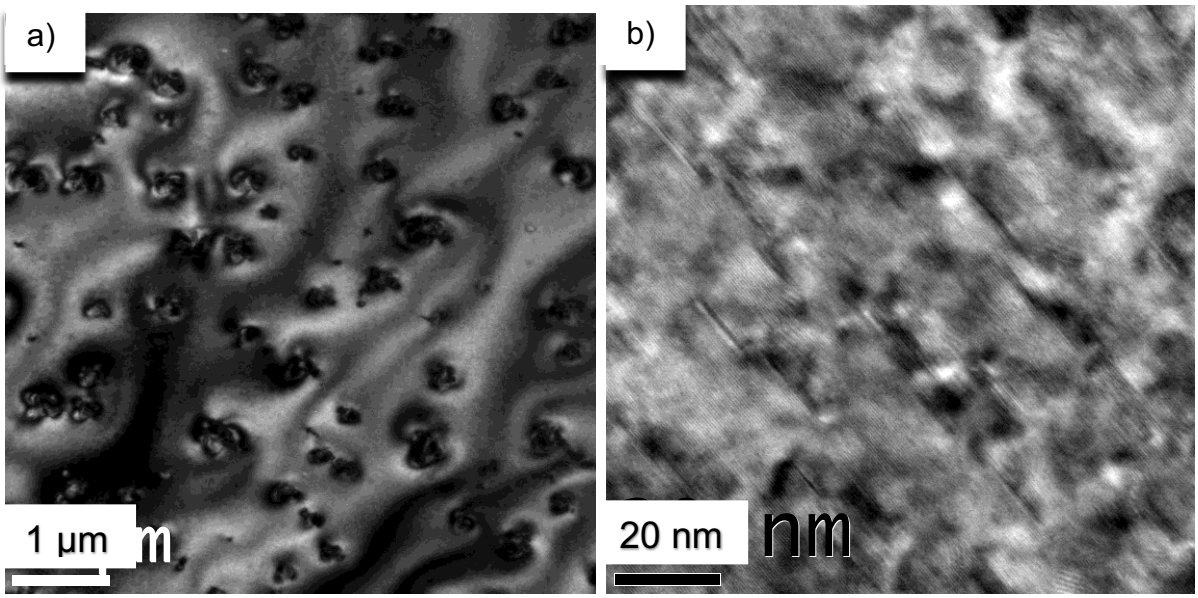


**Figure 5.24- TEM micrograph of pre-aged Mg-1Al-1Zn-0.3Mn-0.3Ca, a) In low magnification, b) In high magnification**

## 5.4.2 AZM140-Ca

### *5.4.2.1 As-cast*

TEM micrograph of as-cast and peak-aged Mg-1Al-4Zn-0.3Mn showing distribution of precipitates is shown in Figure 5.25 a). Mg-1Al-4Zn-0.3Mn was thermo-mechanically processed by homogenising at 350°C for 1 hour and then peak-aged at an isothermal temperature of 175°C for 48 hours. As can be seen, precipitates are mainly rod like precipitates with rods forming parallel to the (0001) directions. Alongside the mentioned precipitates, there are a small number of plate or cube looking precipitates forming parallel to the (0001) planes. Particles were observed with the electron beam parallel to <11$\bar{2}$0> direction.

TEM micrograph of as-cast and peak-aged Mg-1Al-4Zn-0.3Mn-0.3Ca showing distribution of precipitates is shown in Figure 5.25 b). Mg-1Al-4Zn-0.3Mn-0.3Ca was thermo-mechanically processed by homogenising at 350°C-1h/500°C-1h and then peak-aged at an isothermal temperature of 175°C for 48 hours. The addition of calcium did not alter the microstructure with appearance of mainly rod like precipitates that formed parallel to the (0001) directions. There were a small number of plate or cube looking particles forming parallel to the (0001) planes. Particles were observed with the electron beam parallel to <11$\bar{2}$0> direction.

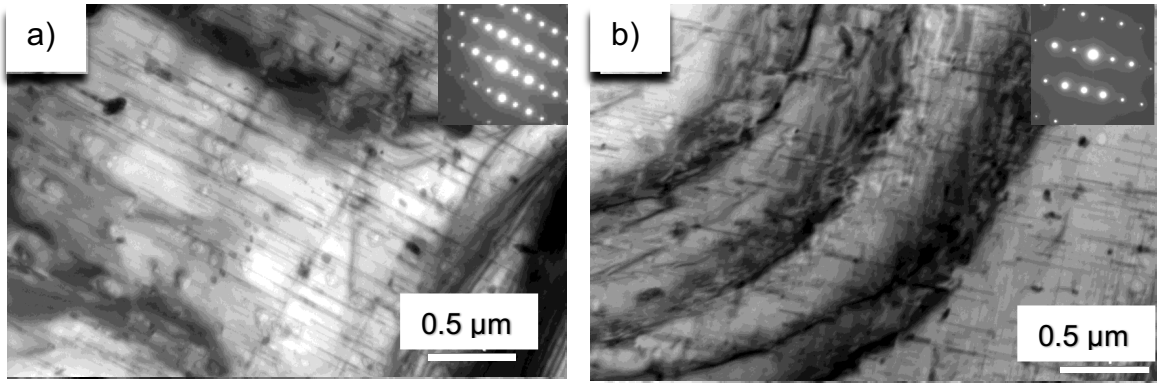


**Figure 5.25- TEM micrograph of as-cast and peak-aged, a) Mg-1Al-4Zn-0.3Mn and b) Mg-1Al-4Zn-0.3Mn-0.3Ca**

***5.4.2.2 Rolled and Pre-aged***

TEM micrograph of deformed and peak-aged Mg-1Al-4Zn-0.3Mn showing distribution of precipitates is shown in Figure 5.26 a). Mg-1Al-4Zn-0.3Mn was thermo-mechanically processed by homogenising at 350°C for 1 hour and then peak-aged at an isothermal temperature of 175°C for 48 hours. Precipitates were mainly rod like precipitates with these rods forming parallel to the (0001) direction. There are a small number of plate or cube looking particles forming parallel to the (0001) planes, there was a reduction in the basal plate like precipitates. The precipitates have a shorter length than the permanent mould cast Mg-1Al-4Zn-0.3Mn. Having said this, the quantity of precipitates is greater, a strong indication of increase in number density which ultimately means strengthening. Particles were observed with the electron beam parallel to <$11\bar{2}0$> direction.

TEM micrograph of deformed and peak-aged Mg-1Al-4Zn-0.3Mn-0.3Ca showing distribution of precipitates is shown in Figure 5.26 b). Mg-1Al-1Zn-0.3Mn-0.3Ca was thermo-mechanically processed by homogenising at 350°C-1h/500°C-1h and then peak-aged at an isothermal temperature of 175°C for 48 hours. Precipitates were mainly rod like precipitates with these rods forming parallel to the (0001) direction. There was an increase in the basal plate or cube like precipitates which formed parallel to the (0001) planes. The rod-like precipitates have a shorter length than the permanent mould cast Mg-1Al-4Zn-0.3Mn-0.3Ca. Having said this, there are more precipitates in general, a strong indication of increase in number density which ultimately means strengthening. Particles were observed with the electron beam parallel to <$11\bar{2}0$> direction.

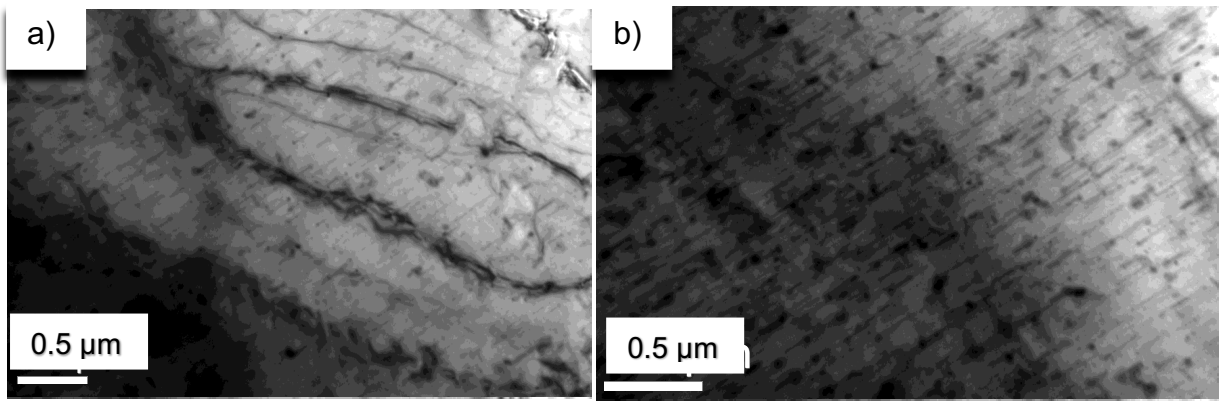


**Figure 5.26- TEM micrograph of deformed and peak-aged, a) Mg-1Al-4Zn-0.3Mn and b) Mg-1Al-4Zn-0.3Mn-0.3Ca**

TEM micrograph of pre-aged Mg-1Al-4Zn-0.3Mn showing distribution of precipitates is shown in Figure 5.27 a). Mg-1Al-4Zn-0.3Mn was thermo-mechanically processed by homogenising at 350°C for 1 hour, pre-aged for 12 hours at 175°C, 5% deformed through cold rolling and finally peak-aged at an isothermal temperature of 175°C for 48 hours. The quantity of plate or cube looking particles forming parallel to the (0001) planes has increased in comparison to hot rolled condition. The rod-like precipitates have a longer length than the permanent mould cast Mg-1Al-4Zn-0.3Mn. Also, their concentration has increased which indicates high number density which ultimately means strengthening. Particles were observed with the electron beam parallel to $<11\bar{2}0>$ direction.

TEM micrograph of pre-aged Mg-1Al-4Zn-0.3Mn-0.3Ca showing distribution of precipitates is shown in Figure 5.27 b). Mg-1Al-4Zn-0.3Mn-0.3Ca was thermo-mechanically processed by homogenising at 350°C-1h/500°C-1h, pre-aged for 12 hours at 175°C, 5% deformed through cold rolling and finally peak-aged at an isothermal temperature of 175°C for 48 hours. There was a reduction in the basal plate like precipitates as there are a small number of plate or cube looking particles forming parallel to the (0001) planes. The rod-like precipitates have a longer length than the permanent mould cast Mg-1Al-4Zn-0.3Mn-0.3Ca. Having said this, there are more precipitates, a strong indication of increase in number density which ultimately means strengthening. Particles were observed with the electron beam parallel to $<11\bar{2}0>$ direction.

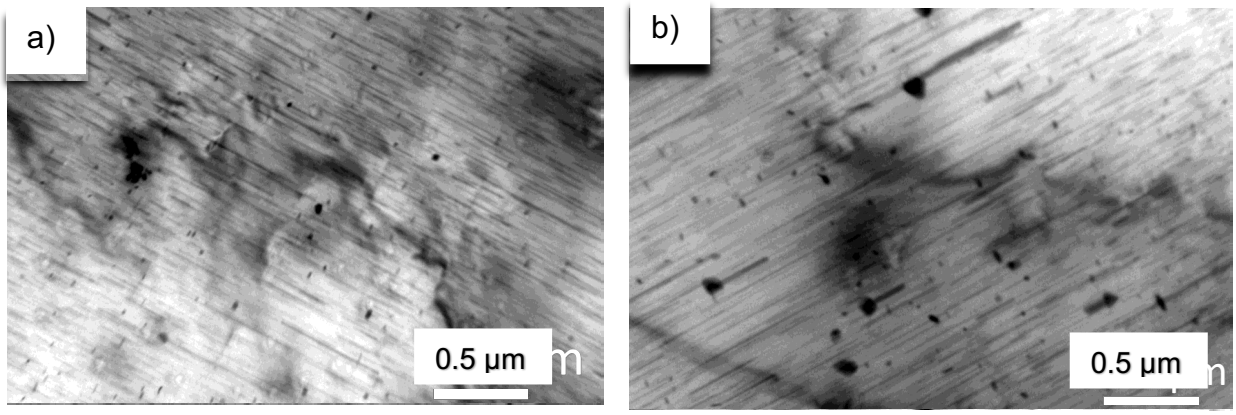


**Figure 5.27- TEM micrograph of pre-aged, a) Mg-1Al-4Zn-0.3Mn and b) Mg-1Al-4Zn-0.3Mn-0.3Ca**

## 5.5 Discussion

Isothermal ageing of Mg-1Al-1Zn-0.3Mn (AZM110) at 150°C, 175°C and 200°C resulted in no noticeable response to precipitation hardening. Isothermal ageing at 150°C led to +2HV increase in hardness after 10 days of ageing, while isothermal ageing at 175°C and 200°C, the hardness did not improve from the as-quenched condition. TEM micrographs of as-cast and peak-aged Mg-1Al-1Zn-0.3Mn confirmed no precipitation activity. It is well established that wrought alloy AZ31 with increased concentration of aluminium does not respond to ageing (Huang, et al., 2008) even though aluminium is primarily added to magnesium alloys to enhance strength which arises from the formation of $Mg_{17}Al_{12}$ intermetallic compound. It is therefore clear to understand that 1%wt of aluminium in combination with 1%wt zinc and 0.3%wt manganese is not sufficient amount to enhance precipitation kinetics. The established wrought magnesium alloys including AZ31 have historically shown poor age-hardening characteristics (Kim, 2014).

In contrast to Mg-1Al-1Zn-0.3Mn, the addition of 0.3%wt calcium in Mg-1Al-1Zn-0.3Mn-0.3Ca (AZMX1100) led to rapid ageing response in all isothermal ageing conditions. It took 1 hour to reach maximum hardness of 55HV, 56HV and 55HV through isothermal ageing of 150°C, 175°C and 200°C respectively. The as-quenched hardness was 46HV, so a maximum increase of 10HV occurred during 175°C isothermal ageing. TEM analysis of peak-aged AZMX1100 at 175°C for 1 hour showed appearance of very fine plate-like precipitates, an indication that microalloying of calcium enhanced precipitation kinetics. This finding of rapid ageing response is corroborated through the work of Bian et al on their alloy development work on Mg-1.2Al-0.8Zn-0.4Mn-0.5Ca (wt%) which strengthened by ageing at 200°C for 1 hour (Bian, et al., 2017). The as-quenched hardness amounted to 53HV and it increased to 61HV during mentioned ageing treatment. Introduction of zinc alloying element hastened age hardening kinetics from 2 hours to 1 hour, but the overall strengthening is attributed to G.P. zones enriched with aluminium and calcium. Bian et al's alloy contained greater amount of aluminium, manganese, and calcium but interestingly, the developed Mg-1Al-1Zn-0.3Mn-0.3Ca displayed better precipitation kinetics in comparison. Low concentration of calcium to similar alloy systems has shown to not aid precipitation kinetics as the study of Chino et al was able to show

with addition of 0.1%wt (Chino, et al., 2011). Having said this, high concentration of calcium leads to embrittlement and subsequently weakens elongation to failure behaviour as seen during addition of 1%wt calcium to AZ31 (Yim, et al., 2004).

Alloys Mg-4Al-1Zn-0.3Mn (AZM410) and Mg-4Al-1Zn-0.3Mn-0.3Ca (AZMX4100) with increased concentration of aluminium from 1%wt to 4%wt were isothermally aged at 150°C, 175°C and 200°C. In all isothermal ageing conditions, alloy Mg-4Al-1Zn-0.3Mn remained stable throughout duration of ageing treatment, indicating it is not an age-hardenable alloy which is in similarity to the established AZ31 wrought alloy that has the same composition except a decrease in aluminium concentration. The addition of calcium to Mg-4Al-1Zn-0.3Mn-0.3Ca did indicate a response to ageing treatment especially during isothermal ageing at 150°C. A maximum hardness was achieved after 96hrs with increase of 10HV from as-quenched condition. Increasing concentration of aluminium to 4%wt has shown no response to ageing in the case of AZM410 but has shown a sluggish response in ageing with calcium as an alloying addition.

By increasing concentration of zinc from 1%wt to 4%wt in alloys Mg-1Al-4Zn-0.3Mn (AZM140) and Mg-1Al-4Zn-0.3Mn-0.3Ca (AZMX1400), there was observation of greater strengthening in all isothermal ageing conditions. During isothermal ageing at 150°C, both alloys achieved a maximum hardness of 68HV which equates to increase of 22HV and 17HV from as-quenched condition, respectively. The addition of calcium enhanced precipitation kinetics by 48 hours as peak hardness was achieved at 72 hours in comparison to 120 hours which was achieved in the alloy without calcium. By isothermal ageing Mg-1Al-4Zn-0.3Mn at 175°C, the maximum hardness came to 64HV which was achieved within 96 hours, an improvement in precipitation kinetics but hardness was reduced by 4HV. The calcium containing Mg-1Al-4Zn-0.3Mn-0.3Ca had a remarkable response to ageing. Maximum hardness amounted to 71HV which was achieved within 48 hours. In comparison to isothermal ageing at 150°C, it took 24 hours less time to achieve a greater hardness value. As for isothermal ageing at 200°C for both alloys, hardness values did not improve in comparison to isothermal ageing at 175°C and in the case of calcium containing alloy, it took 72 hours to achieve maximum hardness. TEM micrographs of as-cast and peak-aged Mg-1Al-4Zn-0.3Mn and Mg-1Al-4Zn-0.3Mn-0.3Ca showed precipitates are mainly rod like precipitates that form parallel to the 0001 direction. In

an age-hardened Mg-Zn binary alloy, rod-shaped precipitates identified as $MgZn_2$ are readily observed to be distributed coarsely but by adding alloying elements such as calcium, number density increase has been achieved. A combined addition of calcium and silver led to enhancement of the age-hardening response due to the reduction in inter-particle spacing making it difficult for the dislocations to bypass the precipitates (Mendis, et al., 2009). Increasing concentration of zinc improves overall maximum hardness by two-fold but it takes considerably longer, going from a timeframe of 1 hour to 48 hours, as is evidenced by isothermal ageing at 175°C. Previous study by Mendis et al on Mg-8Zn-4Al-0.5Ca showed that there is no effect of calcium on strengthening or enhancement in peak ageing time due to high concentration of zinc and aluminium (Mendis, 2005). Therefore, the effect of rapid ageing due to calcium addition reduces with increased zinc concentration as seen in previous studies and with Mg-1Al-4Zn-0.3Mn-0.3Ca.

From the acquired isothermal ageing results, ageing at 175°C was selected for further processing due to observed better strengthening and enhanced precipitation kinetics in Mg-1Al-1Zn-0.3Mn-0.3Ca (AZMX1100), Mg-1Al-4Zn-0.3Mn (AZM140) and Mg-1Al-4Zn-0.3Mn-0.3Ca (AZMX1400).

Novel thermo-mechanical treatment was performed by incorporating a deformation stage in between two-step ageing to obtain increased mechanical properties. This novel thermo-mechanical treatment been named pre-ageing which consists of solution heat treatment, pre-ageing, 5% deformation through cold rolling and then peak ageing. Such a thermo-mechanical treatment has previously been used for aluminium alloy Al-Mg-Si-Cu sheet, as a result, the strength of the thermo-mechanically treated sheet has shown to be much higher than those of the conventionally peak-aged 6061 aluminium alloy (Wang, et al., 2014). Previously for magnesium alloys, two-step ageing termed as double ageing has shown to improve mechanical properties of Mg-6Zn-3Al-1Mn (wt%) which does not incorporate a deformation stage in between two-step ageing. The mentioned alloy was twin-roll cast and hot rolled, followed by double ageing with an initial pre-ageing treatment of 70°C for 24hrs and then subsequent ageing treatment at 150°C for 24hrs (Park, et al., 2007). The same alloy was processed through extrusion in a separate study, it contained pre-ageing treatment of 70°C for 48hrs and then subsequent ageing treatment at 150°C for 48hrs (Oh-ishi, et al., 2008).

Mg-1Al-1Zn-0.3Mn and Mg-1Al-1Zn-0.3Mn-0.3Ca alloys were experimented on in three conditions. Firstly, they were hot rolled which consisted of 30% reduction in plate thickness, solution heat treatment and then aged. In the second condition, they were 5% deformed through cold rolling and aged and thirdly pre-aged for 15 minutes then 5% deformed through cold rolling and aged. The microstructures of Mg-1Al-1Zn-0.3Mn had a deformed structure with consistent evidence of elongated grains. The grain size in hot rolled condition was 33±4.5μm, while in the 5% deformed condition, the grain size measured to be 37±6μm and in the peak-aged condition, the grain size was further reduced to 26±1.5μm. The rolling and subsequent deformation led to considerable reduction in overall grain size which amounted to 250±34μm in permanent mould cast condition. The addition of calcium had a substantial effect on the microstructures of hot rolled, 5% deformed and pre-aged conditioned Mg-1Al-1Zn-0.3Mn-0.3Ca. The grains were equiaxed in all conditions with no sign of deformation as was readily evidenced in the alloy without calcium. The grain size in hot rolled condition was 37±2.5μm, while in the 5% deformed condition, the grain size measured to be 35±1.5μm and in the peak-aged condition, the grain size was further reduced to 33±1.2μm. Again, there was a substantial reduction in grain size after rolling procedures in comparison to permanent mould cast condition which amounted to 313±40μm.

From the permanent mould cast condition, the age-hardening response of Mg-1Al-1Zn-0.3Mn and Mg-1Al-1Zn-0.3Mn-0.3Ca alloys in rolled conditions improved drastically which corresponds with the considerable reduction in grain sizes. Deformation led to increase in dislocation density which increased precipitation activity at these defect sites. The hardness value of hot rolled Mg-1Al-1Zn-0.3Mn before being aged was 9HV greater than the as-cast condition. After 5% deformation through cold rolling, the hardness value increased by a further 8HV from the hot rolled hardness value. In the case of the pre-aged condition rolled Mg-1Al-1Zn-0.3Mn alloy, the hardness value decreased by 4HV in comparison to the cold rolled condition. Nonetheless, the ageing response of Mg-1Al-1Zn-0.3Mn alloy remained stable without peaking during the whole duration. The hardness value of hot rolled Mg-1Al-1Zn-0.3Mn-0.3Ca before being aged was 6HV greater than the as-cast condition. The alloy in this condition peak-aged at 8 hours with a maximum hardness value of 68HV, which in comparison to as-cast condition, it is an increase of 12HV. It

therefore took longer to peak age, but the hardness increase is significant. The most remarkable increase in hardness was witnessed after 5% deformation through cold rolling. Before being aged, there was an increase of 15HV from hot rolled condition with a hardness value of 67HV. Also, maximum hardness during ageing was achieved at 2 hours with a value of 79HV. The precipitation kinetics dramatically hastened with a 11HV increase from the peak aged hot rolled condition. The pre-aged condition Mg-1Al-1Zn-0.3Mn-0.3Ca alloy displayed a similar trend of ageing to cold rolled condition but peak-ageing occurred later at 8 hours. As evidenced in TEM analysis, the number density of precipitates present in deformed and pre-aged Mg-1Al-1Zn-0.3Mn-0.3Ca increased drastically. This shows that heterogenous nucleation readily occurred due to deformation of structure.

Alloys containing an increased concentration of zinc were also rolled and their grain sizes and hardness behaviour were examined. The processing of hot rolled and 5% deformed conditioned Mg-1Al-4Zn-0.3Mn and Mg-1Al-4Zn-0.3Mn-0.3Ca alloys was the same as 1%wt zinc containing alloys. The third condition consisted of pre-ageing for 12 hours, 5% deforming through cold rolling and peak ageing. The microstructures of rolled Mg-1Al-4Zn-0.3Mn alloys resembled that of an equiaxed structure with grain sizes considerably reduced. The approximate grain size of permanent mould cast condition Mg-1Al-4Zn-0.3Mn alloy was 194±23μm, whereas the hot rolled grain size measured to be 31±3μm while 5% deformed measured to be 41±6μm and pre-aged grain size was 34±1.5μm. The microstructures of calcium containing Mg-1Al-4Zn-0.3Mn-0.3Ca alloy had an equiaxed structure but considerable presence of twinning. Calcium addition seemed to hamper grain size reduction which has clearly been seen in previously rolled alloys. To demonstrate this, the permanent mould cast conditioned alloy had a grain size measurement of 226±43μm, while the hot rolled conditioned alloy saw an increase in grain size to 279±11μm. The grain size of 5% deformed alloy measured to be approximately 265±9μm and the pre-aged rolled alloy had a grain size measurement of approximately 248±18μm.

Age-hardening of rolled Mg-1Al-4Zn-0.3Mn and Mg-1Al-4Zn-0.3Mn-0.3Ca alloys indicated improvement in mechanical properties in comparison to permanent mould cast alloys. Before being age-hardened, Mg-1Al-4Zn-0.3Mn alloy had hardness value of 55HV in hot rolled condition, 53HV in 5% deformed condition and 54HV in

pre-aged condition. This is an increase of 9HV, 7HV and 8HV respectively from the as-quenched permanent mould cast alloy. Thereafter, peak-ageing occurred at 48 hours with 72HV maximum hardness value for hot rolled and 5% deformed alloys and 71HV for pre-aged alloy. The calcium containing rolled Mg-1Al-4Zn-0.3Mn-0.3Ca alloys with grain sizes similar to permanent mould cast saw a similar trend in ageing response. The three rolled conditions displayed an increase of 10HV, 12HV and 13HV from as-quenched alloy. Thereafter, ageing treatment did slightly improve hardness values but not to the same extent as rolled Mg-1Al-4Zn-0.3Mn alloys, rolled Mg-1Al-1Zn-0.3Mn alloys and rolled Mg-1Al-1Zn-0.3Mn-0.3Ca alloys. Maximum hardness of hot rolled alloy amounted to 70HV, in 5% deformed condition maximum hardness is 71HV and in pre-aged condition the value is 72HV. In comparison, the permanent mould cast alloy displayed a maximum hardness value of 71HV at 48 hours. In comparison to permanently mould cast Mg-1Al-4Zn-0.3Mn and Mg-1Al-4Zn-0.3Mn-0.3Ca, the rod-like precipitates found in deformed and pre-aged conditions were observed in greater quantity and their length shortened. As a result, the interparticle spacing between the precipitates reduced leading to increase in number density.

## 5.6 Conclusions

1. Isothermal ageing of Mg-1Al-1Zn-0.3Mn (AZM110) at 150°C, 175°C and 200°C resulted in no noticeable response to precipitation hardening. TEM micrographs of peak-aged permanent mould cast Mg-1Al-1Zn-0.3Mn confirmed no precipitation activity. The addition of 0.3%wt calcium in permanent mould cast Mg-1Al-1Zn-0.3Mn-0.3Ca (AZMX1100) led to rapid ageing response in all isothermal ageing conditions. It took 1 hour to reach maximum hardness of 55HV, 56HV and 55HV through isothermal ageing of 150°C, 175°C and 200°C respectively. TEM analysis of peak-aged AZMX1100 at 175°C for 1 hour showed appearance of very fine plate-like precipitates on the basal plane, an indication that microalloying of calcium enhanced precipitation kinetics.

2. In all isothermal ageing conditions, alloy Mg-4Al-1Zn-0.3Mn (AZM410) remained stable throughout duration of ageing treatment, indicating it is not an age-hardenable alloy. The addition of calcium to Mg-4Al-1Zn-0.3Mn-0.3Ca (AZMX4100) did indicate a response to ageing treatment especially during isothermal ageing at 150°C. A maximum hardness was achieved after 96hrs with increase of 10HV from as-quenched condition. Overall, increasing concentration of aluminium and adding calcium showed a sluggish response in ageing.

3. By increasing concentration of zinc from 1%wt to 4%wt in alloys Mg-1Al-4Zn-0.3Mn (AZM140) and Mg-1Al-4Zn-0.3Mn-0.3Ca (AZMX1400), there was observation of greater strengthening in all isothermal ageing conditions. During isothermal ageing at 150°C, both alloys achieved a maximum hardness of 68HV which equates to increase of 22HV and 17HV from as-quenched condition, respectively. The calcium containing Mg-1Al-4Zn-0.3Mn-0.3Ca had a remarkable response to ageing at 175°C. Maximum hardness amounted to 71HV which was achieved within 48 hours. TEM micrographs of peak-aged permanent mould cast Mg-1Al-4Zn-0.3Mn and Mg-1Al-4Zn-0.3Mn-0.3Ca showed precipitates are mainly rod like precipitates that form parallel to the <0001> direction.

4. From the acquired isothermal ageing results, ageing at 175°C was selected for further processing due to observed better strengthening and enhanced precipitation kinetics in Mg-1Al-1Zn-0.3Mn-0.3Ca (AZMX1100), Mg-1Al-4Zn-0.3Mn (AZM140) and Mg-1Al-4Zn-0.3Mn-0.3Ca (AZMX1400). Following on, novel thermo-mechanical treatment was performed by incorporating a deformation stage in between two-step ageing to obtain increased mechanical properties. This novel thermo-mechanical treatment been named pre-ageing which consists of solution heat treatment, pre-ageing, 5% deformation through cold rolling and then peak ageing.

5. The microstructures of rolled Mg-1Al-1Zn-0.3Mn had deformed structures with consistent evidence of elongated grains. The addition of calcium had a substantial effect on the microstructures of hot rolled, 5% deformed and pre-aged conditioned Mg-1Al-1Zn-0.3Mn-0.3Ca. The grains were equiaxed in all conditions with no sign of deformation as was readily evidenced in the alloy without calcium. For both alloys, the rolling and subsequent deformation led to considerable reduction in overall grain size from the permanent mould cast condition.

6. The age-hardening response of Mg-1Al-1Zn-0.3Mn and Mg-1Al-1Zn-0.3Mn-0.3Ca alloys in rolled conditions improved considerably which corresponds with the considerable reduction in grain sizes. Nonetheless, the ageing response of Mg-1Al-1Zn-0.3Mn alloy remained stable without peaking during the whole duration. The most remarkable increase in hardness was witnessed after 5% deformation through cold rolling of AZMX1100. Maximum hardness during ageing was achieved at 2 hours with a value of 79HV. As evidenced in TEM analysis, the number density precipitates present in deformed and pre-aged Mg-1Al-1Zn-0.3Mn-0.3Ca increased considerably. This shows that heterogenous nucleation readily occurred due to deformation of structure.

7. The microstructures of rolled Mg-1Al-4Zn-0.3Mn alloys resembled that of an equiaxed structure with grain sizes considerably reduced. The microstructures of calcium containing Mg-1Al-4Zn-0.3Mn-0.3Ca alloy had an equiaxed structure but considerable presence of twinning. Calcium addition seemed to

hamper grain size reduction. Age-hardening of rolled Mg-1Al-4Zn-0.3Mn and Mg-1Al-4Zn-0.3Mn-0.3Ca alloys indicated improvement in mechanical properties in comparison to permanent mould cast alloys. Deformation led to increase in dislocation density which increased precipitation activity at these defect sites. Peak-ageing occurred at 48 hours with 72HV maximum hardness value for hot rolled and 5% deformed alloys and 71HV for pre-aged alloy. The rod-like precipitates found in deformed and pre-aged conditions were observed in greater quantity and their length shortened. As a result, the interparticle spacing between the precipitates reduced leading to increase in number density.

# Chapter 6- Validation of Mg Alloys Developed for Low-Pressure Twin Roll Casting

## Contents

## 6.1 Introduction

The low-pressure TRC processing used to produce alloys was developed within BCAST. It has been established in previous chapters that the most dilute alloy consisting of 1wt% each of aluminium and zinc with 0.3wt% calcium shows rapid age hardening kinetics when aged at 175$^{o}$C and this was further enhanced when the alloy was aged for 15 minutes and then deformed by 5% cold rolling and further aged. The peak hardness during isothermal ageing at 175°C was achieved in 1hr, with an increase of 10VHN from as-quenched condition in the permanent mould cast alloy. In the samples that were hot rolled to mimic conventional TRC or rolled sheet microstructures, a maximum hardness of 68VHN was achieved within 8hrs, an increment of 12VHN from isothermal ageing peak condition. The samples subjected to deformation through cold rolling led to further enhancement in precipitation kinetics as peak hardness was 79VHN, achieved in 2hrs. From hot rolled condition, 5% cold rolling deformation showed an increase of 11VHN during peak ageing which was also achieved 6hrs faster. Pre-aged for 15 minutes was the finally condition, a maximum hardness of 74VHN was achieved in 8hrs. Due to these positive findings, alloy AZMX1100 was TRC processed and the findings are included in this final chapter. Increasing the concentration of zinc to 4wt% showed enhancement in ageing in the alloy Mg-1Al-4Zn-0.3Mn-0.3Ca (AZMX1400) as shown in Chapter 5. The maximum hardness value during isothermal ageing at 175°C came to 71VHN and it was achieved within 48hrs. This is a substantial increase of 20VHN from the as-quenched condition. Further, enhanced kinetics were observed during cold rolling deformation with halving the time required to achieve peak hardness. The alloy chosen for further investigation into be developed into TRC alloy through trial of the alloy AZMX1400 to test its suitability for the low-pressure TRC. The 4 alloys namely, AZM110, AZM410, AZMX4100 and AZM140 were eliminated in the process as they did not provide scope to further strengthening through precipitation hardening or provided low hardening response. Alloy AZM110 did not respond to ageing treatment in the various conditions, whereas alloys AZM410 and AZMX4100 showed sluggish response to ageing. Alloy AZM140 did show appreciable age hardening but the enhancement was not as pronounced as for the AZMX1400 alloy. For this reason, it was not further investigated. In this chapter, the microstructure and tensile behaviour

of as-cast and T6 conditions of TRC alloys Mg-1Al-1Zn-0.3Mn-0.3Ca and Mg-1Al-4Zn-0.3Mn-0.3Ca are investigated.

## 6.2 Process Parameters of TRC Alloys

### 6.2.1 Optimisation for Stable Strip

To obtain a stable strip, optimal operating parameters has to be established which meant conducting experiments to find the most appropriate casting conditions for novel alloy composition of the alloys used in the low-pressure TRC processing. To ascertain a stable strip, focus was put on examining macroscopic strip quality, morphology of microstructure and performance of low-pressure TRC in regards to temperature behaviour during casting. Following on, it can be understood that there is a strong correlation between stability of low-pressure TRC apparatus temperature and the ability to produce a quality thin strip. To understand the influence of melt feeding system on the outcome of strip production, nozzle tip temperature profiles were taken. Below, figure 6.1 a) and b) show temperature during onset of melt pouring into the tundish which is then transferred into nozzle simultaneously. Figure 6.1 a) represents pouring temperature 5°C below optimal and figure 6.1 b) represents the optimal pouring conditions. As can be seen in figure 6.1 a), once the melt comes into contact with the tundish, there is a sudden drop in temperature of approximately 8°C in a timeframe of 60 seconds. As a result of this, the molten metal froze inside the tundish and experiment did not yield a strip. Figure 6.1 b) is an instance of a successful casting of a thin strip, the nozzle temperature firstly has an increase but then remains stable through miniature fluctuations for approximately 200 seconds. Even though the nozzle is thermally controlled, the resultant molten metal's propensity to freeze due to low pouring temperature has a significant correlation with nozzle temperature behaviour.

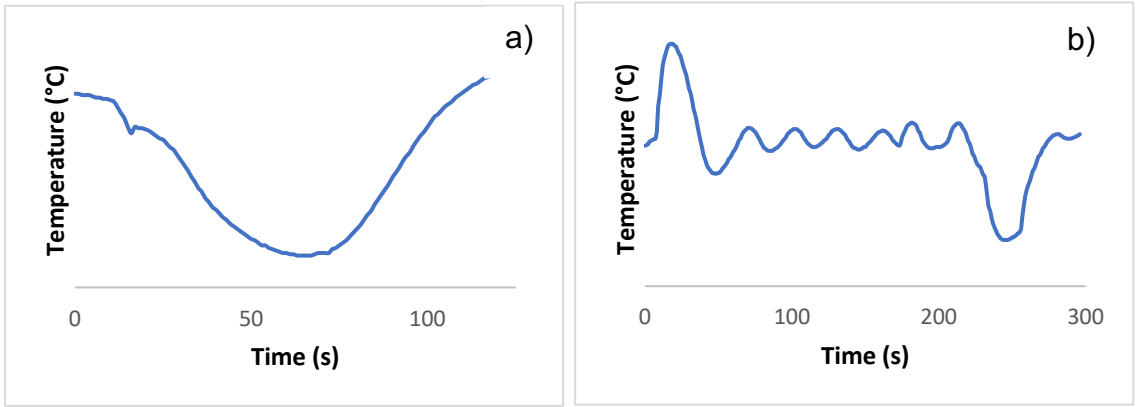


**Figure 6.1- TRC nozzle temperature behaviour, a) sudden drop and subsequent melt freezing, b) stable strip production due to constant nozzle temperature**

Below are light micrographs showing evolution of low-pressure TRC strip microstructure at the beginning shown in Figure 6.2 a), at 1m stage shown in Figure 6.2 b) and finally at 2m stage shown in Figure 6.2 c). The 2m stage strip shows formation of distinct grains has been achieved with clear signs of intermetallic particles having a completed morphology within respective grains. The morphology of globular intermetallic particles situated within grains becomes further concentrated at 2m stage of strip. These particles have been identified as Al-Mn phase which are known to not completely dissolve as discussed in Chapter 4. As for the beginning microstructure and 1m stage, the microstructures do not show stability with individual grains having overlapping morphology with clear boundaries yet to be obvious and visible. A microstructure which is not fully formed leads to undesirable mechanical properties such as low yield strength and therefore the propensity to fracture in a brittle manner.

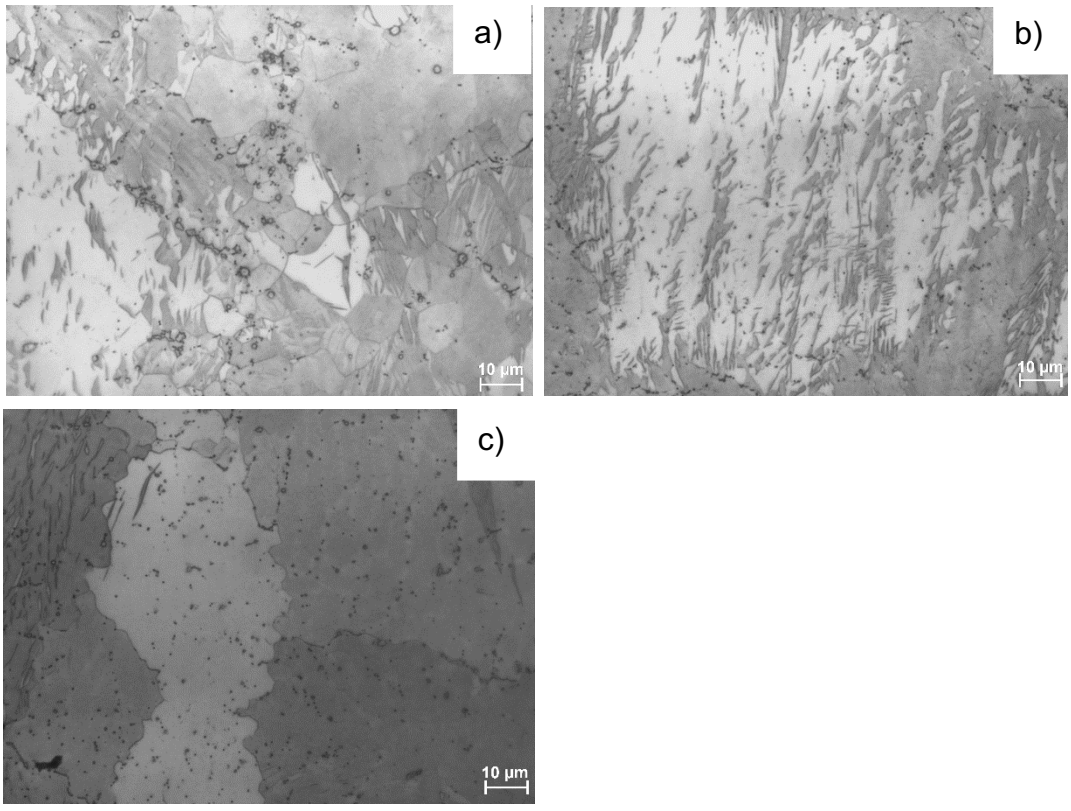


**Figure 6.2- Microstructure of low-pressure TRC strip of Mg-1Al-1Zn-0.3Mn-0.3Ca, (a) at the start of the strip b) at 1m from the start, c) at 2m from the start**

Below are light micrographs of low-pressure TRC thin strip with various pouring temperatures, these are 650°C shown in Figure 6.3 a), 660°C shown in Figure 6.3 b), 665°C shown in Figure 6.3 c) and 670°C shown in Figure 6.3 d) respectively. All the mentioned pouring temperatures were not sufficient to produce stable strip due to sudden freezing which led to melt solidifying at the nozzle. Macroscopically, these alloys appeared deformed with strip quality showing ripple effects, a sign of melt becoming prematurely cold. Therefore, superheat values of 19°C, 29°C, 34°C and 39°C were not suitable and was increased to allow a more stable low-pressure TRC thin strip alloy to be produced.

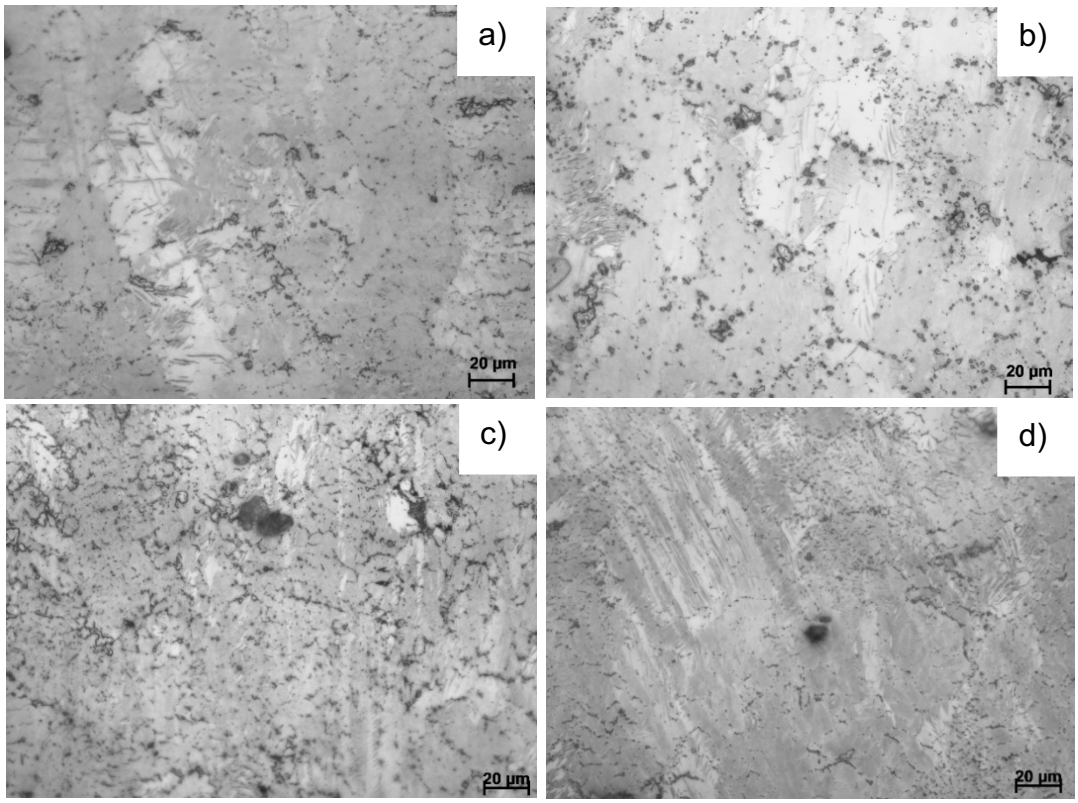


**Figure 6.3- a) Low-pressure TRC Mg-1Al-4Zn-0.3Mn-0.3Ca strip produced with pour temperature of (a) 650℃ and a temperature difference of 19°C between pouring temperature and the liquidus, b) 660°C and a temperature difference of 29°C between pouring temperature and the liquidus, c) 665°C and a temperature difference of 34°C between pouring temperature and the liquidus, d) 670°C and a temperature difference of 39°C between pouring temperature and the liquidus**

### 6.2.2 TRC Variables

**Table 6.1- TRC experiment variables for both produced alloys**

| Alloy | Pouring Temp (°C) | Tundish Temp (°C) | Nozzle Temp (°C) | Inlet Temp (°C) | Flow Rate (L/min) | Roll Gap (mm) | Roll Speed (m/min) |
|---|---|---|---|---|---|---|---|
| AZMX1100 | 678 | 680 | 680 | 30 | 12 | 1 | 8 |
| AZMX1400 | 700 | 690 | 670 | 30 | 12 | 1.5 | 8 |

The pouring temperature of the melt for TRC alloy Mg-1Al-1Zn-0.3Mn-0.3Ca (AZMX1100) was 678℃ as shown in Table 6.1, this equates to 36℃ superheat from the experimental liquidus temperature. The tundish and nozzle which constitute the melt feeding system were heated to 680℃ each. To produce a relatively thin strip for minimised post-processing as this is one of the main objectives, the roll gap was kept to 1mm which is the absolute minimum that can be achieved with the low-pressure twin-roll caster. The measured strip thickness amounted to an average of 1.27mm, it is a greater amount due to melt flowing through the rolls at a certain speed in semi-solid stage. The understanding obtained is that the roll gap is the most important parameter that controls strip thickness. The pouring temperature of the melt for TRC alloy Mg-1Al-4Zn-0.3Mn-0.3Ca was 700°C, this equates to 69℃ superheat from the experimental liquidus temperature. The tundish and nozzle which constitute the melt feeding system were heated to 690℃ and 670℃, respectively. The roll gap was set to 1.5mm which led to strip thickness having an average of 1.83mm. This contrasted with TRC AZMX1100 alloy due to constant freezing at nozzle.

The roll speed was set to 8m/min, this was done so that strip production could be time efficient. Another reason was to minimise roll surface contact which leads to significant reduction in strip deformation. The water flow rate is set to 12 L/min, it has been established that 8 L/min and above is the optimal amount and that 30℃ is within the range of acceptable water temperature (Yang, 2016). The thermal state of the rolls is influenced by the flow rate of cooling water and subsequent inlet water temperature. As melt meets roll surface, the temperature of the rolls exponentially increases, therefore water flowing through the rolls creates a much important balance to keep the rolls cool.

## 6.3 Microstructure and Tensile Properties

### 6.3.1 Microstructure of AZMX1100 and AZMX1400

Polarised light micrographs of as-cast TRC Mg-1Al-1Zn-0.3Mn-0.3Ca (AZMX1100) alloy is shown in Figure 6.4 a) and b). Throughout the microstructure, there is strong observance of α-magnesium columnar grains that are positioned parallel to the casting direction. These columnar grains are measured from three separate sections and their size amounts to approximately 153±13μm as shown in Figure 6.5. The approximate grain size was 114±7μm for wedge as-cast AZMX1100 which is known to have comparable solidification rate. In contrast to permanent mould cast Mg-1Al-1Zn-0.3Mn-0.3Ca (AZMX1100), there was no appearance of globular shaped intermetallic particles situated within grains as shown in Figure 6.4 c), albeit their presence was dominant in permanent mould cast AZMX1100. Due to significant difference in solidification rate, such contrasting observance was expected. Whereas the semi-continuous distributed intermetallic particles at grain boundaries were present as they were in the permanent mould cast alloy.

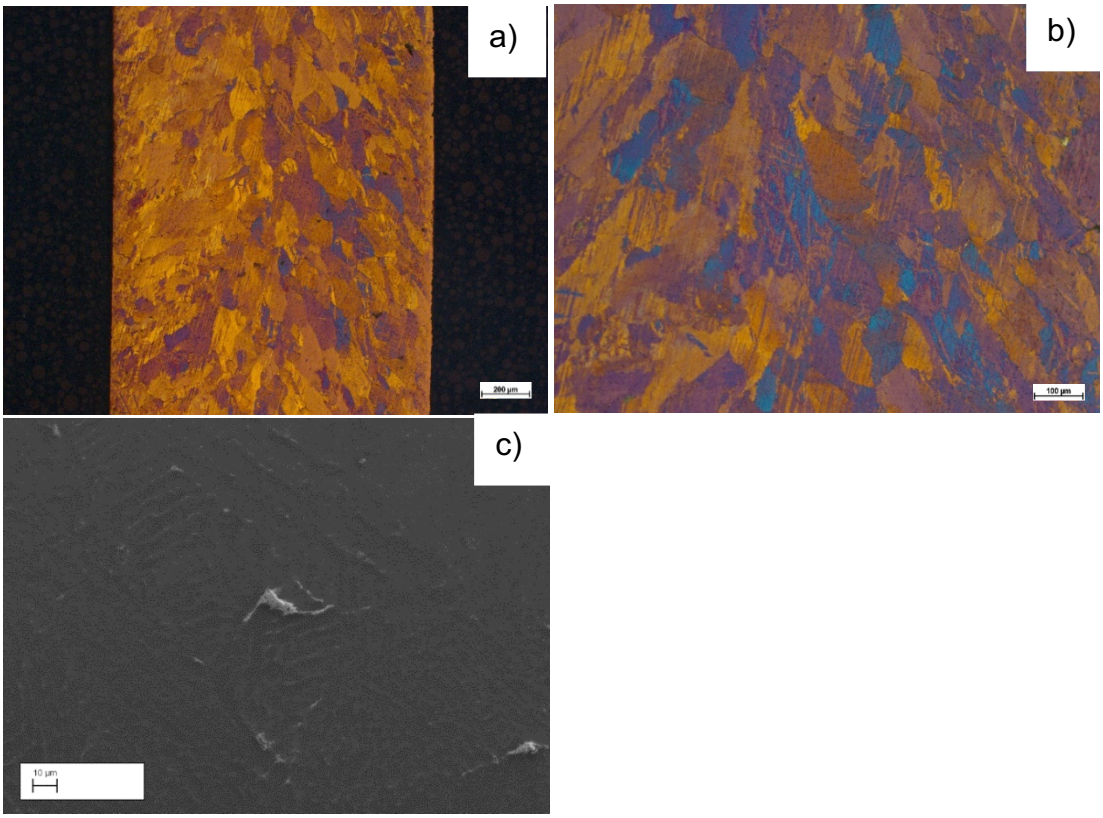


**Figure 6.4- a) Low magnification polarised light, b) High magnification polarised light micrograph from the centre and c) Secondary electron SEM micrograph of low-pressure TRC Mg-1Al-1Zn-0.3Mn-0.3Ca**

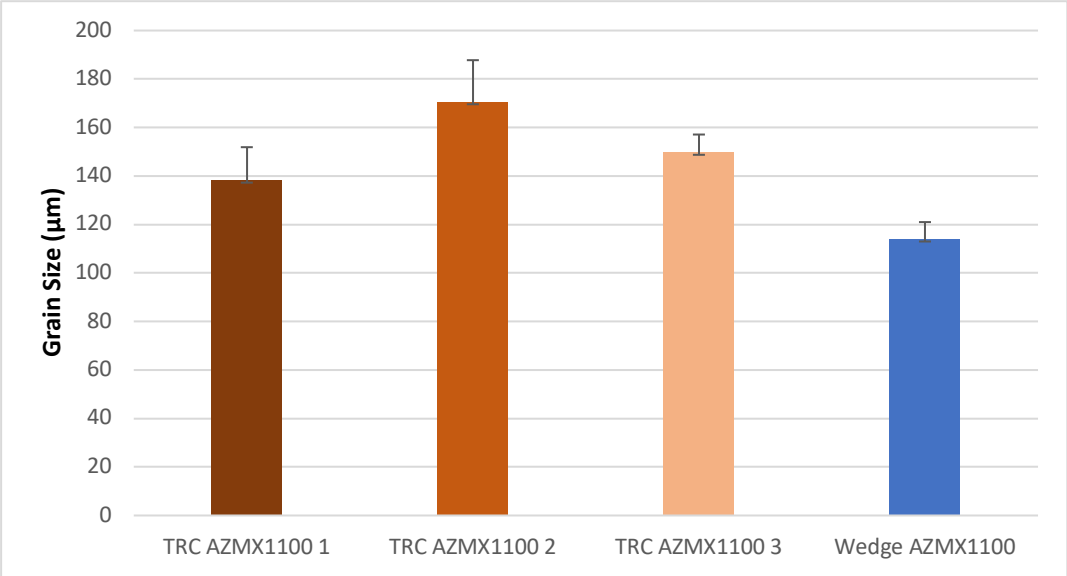


**Figure 6.5- Measured grain sizes of low-pressure TRC Mg-1Al-1Zn-0.3Mn-0.3Ca in three separate positions and permanent mould wedge cast Mg-1Al-1Zn-0.3Mn-0.3Ca**

Polarised light micrographs of as-cast TRC Mg-1Al-4Zn-0.3Mn-0.3Ca (AZMX1400) alloy are shown in Figure 6.6 a) and b). Throughout the microstructure, there is observance of refined α-magnesium dendritic structure that is positioned parallel to the casting direction. These refined dendrites are measured from three separate sections their size amounts to approximately 43±3μm. The approximate grain size was 231±16μm for wedge as-cast AZMX1400 which is known to have comparable solidification rate. From among the permanent mould cast alloys, this alloy which contains 4%wt zinc and calcium had the greatest volume of intermetallic particles. As for presence of intermetallic particles, their volume and subsequent size was significantly reduced due to rapid solidification rate as shown in Figure 6.6 c). To reiterate, an appearance of semi-continuous intermetallic particles was observed at grain boundaries which measured at approximately 10-15μm while presence of globular intermetallic particles was observed within grains and they approximately measured to be 1-2μm diameter.

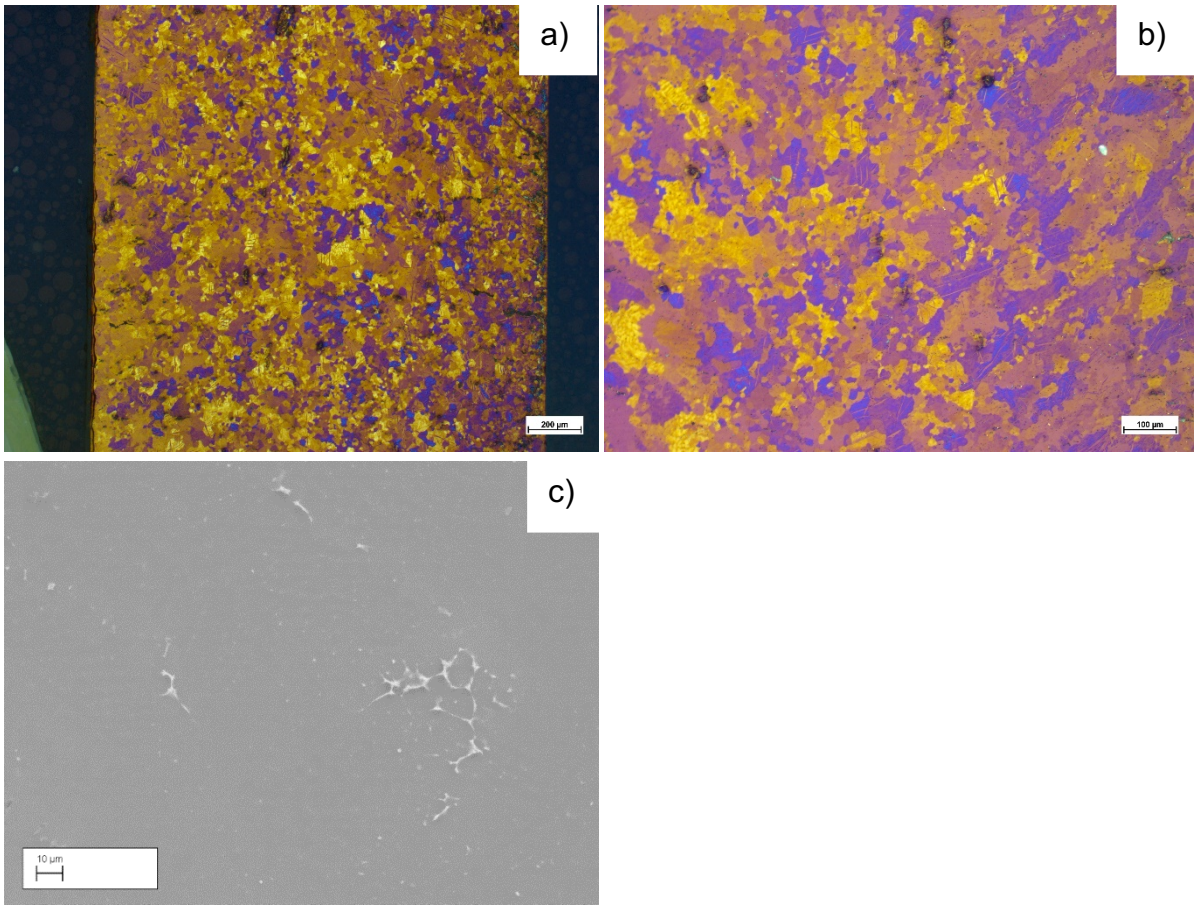


**Figure 6.6- a) Low magnification polarised light, b) High magnification polarised light micrograph from the centre and c) Secondary electron SEM micrograph of low-pressure TRC Mg-1Al-4Zn-0.3Mn-0.3Ca**

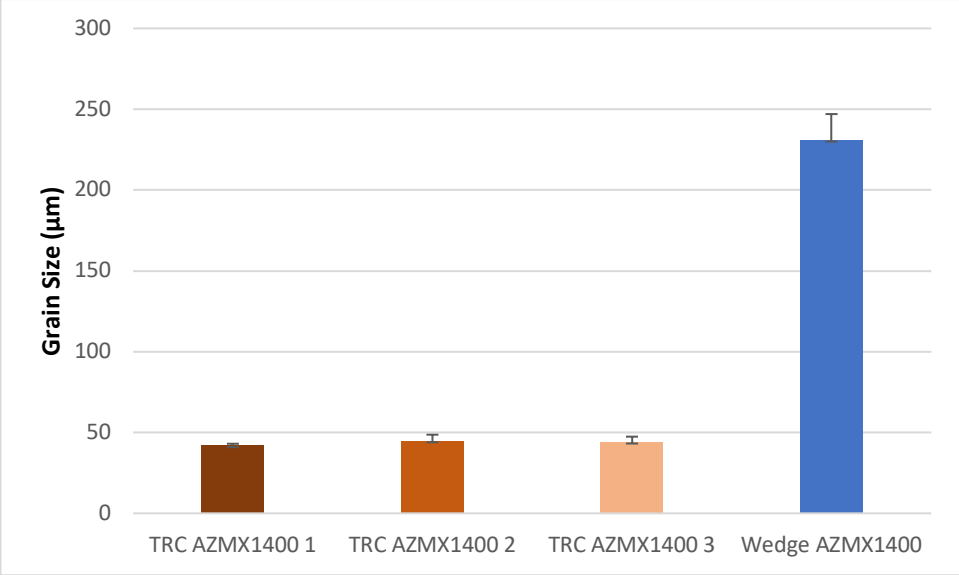


**Figure 6.7- Measured grain sizes of low-pressure TRC Mg-1Al-4Zn-0.3Mn-0.3Ca in three separate positions and permanent mould wedge cast Mg-1Al-4Zn-0.3Mn-0.3Ca**

### 6.3.2 Tensile Properties of AZMX1100 and AZMX1400

**Table 6.2- Tensile properties of low-pressure TRC Mg-1Al-1Zn-0.3Mn-0.3Ca**

| TRC AZMX1100 | Yield Strength (MPa) | Ultimate Tensile Strength (MPa) | Elongation to Failure (%) |
|---|---|---|---|
| **As-cast** | 93.5 | 211.6 | 15.2 |
| **T6** | 140.3 | 220.7 | 14.2 |

Tensile properties of low-pressure TRC Mg-1Al-1Zn-0.3Mn-0.3Ca in casting direction were sought in two separate conditions as shown in Table 6.2, these were, as-cast and T6. As for the as-cast condition, low-pressure TRC Mg-1Al-1Zn-0.3Mn-0.3Ca displayed a maximum yield strength of 93.5MPa, an ultimate tensile strength of 211.6MPa and elongation of 15.2%. After T6 treatment, which included homogenisation treatment of 400°*C* for 1hr and subsequent peak ageing at 175℃ for 1hr, the maximum yield strength amounted to 140.3MPa, ultimate tensile strength was 220.7MPa and elongation was 14.2%. A considerable improvement in yield properties from as-cast to T6 is a positive indication that low-pressure TRC Mg-1Al-1Zn-0.3Mn-0.3Ca is heat treatable. Figure 6.8 shows graphically the tensile behaviour of low-pressure TRC Mg-1Al-1Zn-0.3Mn-0.3Ca.

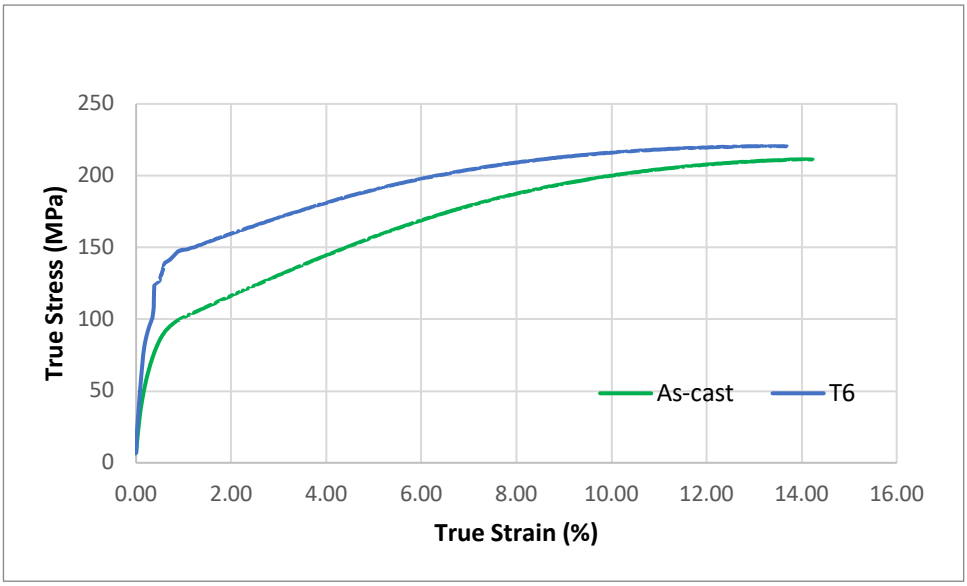


**Figure 6.8- Tensile properties of low-pressure TRC Mg-1Al-1Zn-0.3Mn-0.3Ca in as-cast and T6 conditions**

**Table 6.3- Tensile properties of low-pressure TRC Mg-1Al-4Zn-0.3Mn-0.3Ca**

| TRC AZMX1400 | Yield Strength (MPa) | Ultimate Tensile Strength (MPa) | Elongation to Failure (%) |
|---|---|---|---|
| **As-cast** | 85.1 | 122.9 | 2.1 |
| **T6** | 171.4 | 225.7 | 3.3 |

Tensile properties of low-pressure TRC Mg-1Al-4Zn-0.3Mn-0.3Ca in casting direction were sought in two separate conditions as shown in Table 6.3, these were, as-cast and T6. As for the as-cast condition, low-pressure TRC Mg-1Al-4Zn-0.3Mn-0.3Ca displayed a maximum yield strength of 85.1MPa, an ultimate tensile strength of 122.9MPa and elongation of 2.1%. After T6 treatment, which included homogenisation treatment of 500°C-1hr/350°*C*-1hr and subsequent peak ageing at 175°*C* for 48hrs, the maximum yield strength amounted to 171.4MPa, ultimate tensile strength was 225.7MPa and elongation was 3.3%. A considerable improvement in yield properties from as-cast to T6 is a positive indication that low-pressure TRC Mg-1Al-4Zn-0.3Mn-0.3Ca is heat treatable. Figure 6.9 shows graphically the tensile behaviour of low-pressure TRC Mg-1Al-4Zn-0.3Mn-0.3Ca.

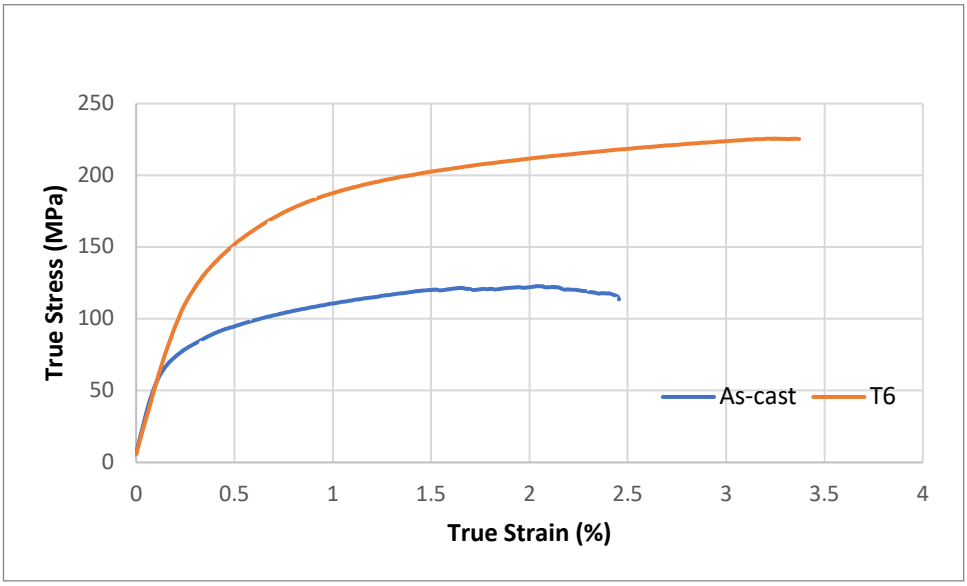


**Figure 6.9- Tensile properties of low-pressure TRC Mg-1Al-4Zn-0.3Mn-0.3Ca in as-cast and T6 conditions**

## 6.4 Discussion

The in-house built low-pressure twin-roll caster was utilised to produce two alloys, Mg-1Al-1Zn-0.3Mn-0.3Ca (AZMX1100) and Mg-1Al-4Zn-0.3Mn-0.3Ca (AZMX1400). A commonality between the two alloys was the addition of 0.3wt% calcium. The presence of calcium had a noticeable effect, it allowed casting conditions to be met without uncontrollable combustion due to emergence of calcium oxide. Attempts were made to cast non-calcium containing AZM140 alloy through TRC processing, but magnesium oxide interaction with ambient air caused significant combustion. It has been empirically evidenced that the flammability of magnesium alloys is considerably reduced with calcium additions. The formation of calcium oxide layer on the molten alloy surface meant it covered the reactive magnesium oxide layer. By doing so, flow of magnesium vapour towards atmosphere is limited. Interestingly, this positive effect of inhibiting combustion has been shown to occur over a considerable time period with magnesium and calcium layer thicknesses remaining constant (Kawabata, et al., 2018).

Due to their novelty, TRC alloys were cast by establishing the optimal pouring temperatures through trial and error experiments. Cold pouring temperature resulted in melt freezing at tundish nozzle whereas a higher than required superheat temperature resulted in melt not solidifying during contact with rolls. As a consequence, this led to melt dripping and subsequent combustion.

It was found that a stable TRC AZMX1100 strip can be produced with a superheat value of 36℃, whereas for TRC AZMX1400 strip, the superheat temperature came to a considerably higher value of 69℃. Previously, low-pressure TRC AZ31 was produced with below, medium and high superheat temperatures. TRC AZ31 with a pouring temperature of 4℃ below liquidus solidified prematurely. The melt froze at the tip of nozzle, such early solidification was observed for alloys AZMX1100 and AZMX1400 due to low superheat temperatures. The microstructure showed significant signs of deformation as the α-magnesium phase grains were severely elongated along the casting direction and there was evidence of rosette structure of α-magnesium grains. A high superheat temperature of 50℃ produced TRC AZ31 strip, there were signs of severe surface defects due to oxidation and combustion on onset of strip production. The microstructure had large columnar grains with extra

fine equiaxed grains on the edge of the chilled zone. Whereas a superheat temperature of 20℃ produced a TRC AZ31 alloy with optimal surface quality. The microstructure had more equiaxed coarse grains along casting direction (Yang, 2016).

Alloys produced through the smaller roll diameter of low-pressure twin-roll caster showed reduction in strip deformation. Conventionally produced TRC AZ31 with a thickness of 6mm had significant solute centreline segregation and large columnar grains measuring 687±290μm. With such an undesirable microstructure, further processing through rolling and thermal processing is a necessity. As for low-pressure TRC AZMX1100, the columnar grains measured to approximately 153±13μm with minimal sign of centreline segregation. By producing a sheet to the desired thickness with acceptable mechanical properties, the need to perform rolling is eliminated which empirically leads to anisotropic properties due to prevalence of basal texture. In another study, melt conditioning of low-pressure TRC AZ31 had finer grains measuring below 100μm (Yang, et al., 2018).

Low-pressure TRC AZMX1400 had a distinct grain morphology in that it was significantly refined and dendritic in nature, the grain size measured to approximately 43±3μm. Grain size of 43±3μm is in stark contrast to AZMX1400 wedge grain size of 231±16μm. The TRC alloy had a pouring temperature of 700℃ with a processing method known for little deformation while wedge casting had a pouring temperature of 680℃ and was a permanent mould casting. Previously, it has been proven that superheating has a positive effect on grain size reduction. In highly concentrated AZ91 alloy, formation of intermetallic compound $Al_4C_3$ was found at superheating values above 800°C, this compound heterogeneously nucleated allowing α-magnesium grains to grow finer (Motegi, 2005). It is also established that addition of aluminium above 1wt% and small concentration of manganese has a grain refining effect as seen in previous study of AZ31 (Cao, et al., 2005). Primary solidification of aluminium and manganese therefore suggests these phases potentially acted as heterogeneous nucleation sites for higher volume growth of α-magnesium grains. In contrast to AZMX1100, the increased addition of 4%wt zinc alongside higher superheat temperature led to no centreline segregation in AZMX1400. Complete elimination of centreline segregation was previously reported through the use of melt conditioning technology. This technology promoted heterogeneous nucleation of α-

magnesium grains in AZ31 by dispersing magnesium oxide with rotor-stator high shear device.

As expected, low-pressure TRC AZMX1100 which contained the least amount of alloying additions proved to be far more ductile in comparison to low-pressure TRC AZMX1400 that contained higher zinc concentration. In the as-cast condition, elongation to failure was valued at 15.2% with yield strength of 93.5MPa and ultimate tensile strength of 211.6MPa. In comparison to as-cast low-pressure TRC AZ31 produced through melt conditioning, it had a significantly lower elongation to failure value of 6% but reported ductility was greater than conventional TRC AZ31 which was approximately 4% (Neh, et al., 2015). It can be ascertained that low-pressure TRC AZMX1100 in as-cast condition has a more randomised basal texture due to far superiority ductility.

T6 treatment of low-pressure TRC AZMX1100 drastically improved yield strength from 93.5MPa to 140.3MPa. While there was noticeable increase in strength, there was minimal change to ductility as it remained at a high value of 14.2%. Observations through TEM micrographs of peak aged AZMX1100 has shown there is volume increase in precipitate density. Low-pressure TRC AZMX1400 with increased concentration of zinc displayed a meagre elongation to failure value of 2.1%. Elongation to failure value slightly increased to 3.3% after T6 treatment but increase of yield strength from 85.1MPa to 171.4MPa and ultimate tensile strength from 122.9MPa to 225.7MPa was more revealing. Similar composition alloy ZMA611 was previously twin-roll cast with roll speed 4m/min and sheet thickness approximately 2mm. It displayed far superior tensile properties with yield strength at 307MPa, ultimate tensile strength at 330MPa and elongation to failure value at 16.2%. Finely distributed Al8Mn5 was observed in ZMA611 which resulted in a finer grain size after T6 treatment. This therefore improved the microstructure and as a result the tensile properties (Park, et al., 2007). The poorer mechanical properties of AZMX1400 alloy through low-pressure TRC production is not as a result of addition of calcium but because of combination of increased roll speed and microstructural defects.

## 6.5 Conclusions

1. Addition of 0.3%wt calcium to AZM110 and AZM140 successfully allowed low-pressure TRC to be performed without combustion occurring. The formation of calcium oxide layer on the molten alloy surface meant it covered the reactive magnesium oxide layer. $SF_6$ cover gas did not provide sufficient protection from occurrence of combustion for alloys AZM110 and AZM140.

2. Optimal pouring temperatures had to be trialled and errored and it was found that a stable TRC AZMX1100 strip can be produced with a superheat value of 36℃, whereas for TRC AZMX1400 strip, the superheat temperature came to a considerably higher value of 69℃.

3. Alloys produced through the smaller roll diameter of low-pressure twin-roll caster showed reduction in strip deformation. In low-pressure TRC AZMX1100, the columnar grains measured to approximately 153±13μm with minimal sign of centreline segregation. Low-pressure TRC AZMX1400 had a distinct grain morphology in that it was significantly refined and dendritic in nature, the grain size measured to approximately 43±3μm with no sign of centreline segregation.

4. Low-pressure TRC AZMX1100 which contained the least amount of alloying additions proved to be far more ductile in comparison to low-pressure TRC AZMX1400. T6 treatment of low-pressure TRC AZMX1100 drastically improved yield strength from 93.5MPa to 140.3MPa. While there was noticeable increase in strength, there was minimal change to ductility as it remained at a high value of 14.2%.

5. Low-pressure TRC AZMX1400 with increased concentration of zinc displayed a meagre elongation to failure value of 2.1%. Elongation to failure value slightly increased to 3.3% after T6 treatment but increase of yield strength from 85.1MPa to 171.4MPa and ultimate tensile strength from 122.9MPa to 225.7MPa was more revealing.

# Chapter 7- Conclusions

1. The average grain size of permanent mould cast Mg-1Al-1Zn-0.3Mn (AZM110), Mg-1Al-1Zn-0.3Mn-0.3Ca (AZMX1100), Mg-4Al-1Zn-0.3Mn (AZM410), Mg-4Al-1Zn-0.3Mn-0.3Ca (AZMX4100), Mg-1Al-4Zn-0.3Mn (AZM140) and Mg-1Al-4Zn-0.3Mn-0.3Ca (AZMX1400) was approximately 250±34μm, 313±40μm, 139±11μm, 211±30μm, 194±23μm and 226±43μm. The addition of calcium to respective alloys did not seem to refine the microstructure. The volume fraction of primary intermetallics found in AZM110 was of negligible amount. As for AZMX1100, it was 1.4% and it reduced to 0.5% after homogenisation treatment. The volume fraction of primary intermetallics found in AZM410 and AZMX4100 was 0.2% and 1.3% but after homogenisation treatment, it was reduced to 0.03% and 0.7% respectively. Finally, the volume fraction of primary intermetallics found in AZM140 and AZMX1400 amounted to 1.8% and 3%. Due to homogenisation treatment, the volume fraction to 1.45% and 3.3%, clearly the treatment did not have the desired effect of significant reduction.

2. Scheil modelling predicted the nucleation and growth of $Al_8Mn_5$ phase early in the solidification path for all alloys. This phase has a high melting point and dissolving it through homogenisation treatments proved to be difficult. By increasing concentration of aluminium to 4wt% in AZM410, appearance of globular intermetallic particles became visible with composition measuring to be $Mg_6Zn_3Al_2$. While introduction of 4wt% zinc in AZM140 meant most intermetallic particles' composition became approximately MgZn, therefore the effect of aluminium diminished and dissolved into the matrix. By adding 0.3wt% calcium to AZM110, AZM410 and AZM140 alloys, the intermetallic particles mostly appeared as elongated and situated at grain boundaries. There is a strong correlation $Al_2Ca$ is the intermetallic phase in question due to thermodynamic calculations, morphology, and empirical data.

3. The wedge samples which have comparable solidification rate as TRC alloys saw grain refinement with calcium. The addition of calcium in AZMX1100 led

to grain refinement of 48% near tip point, the grain size went from 238±9μm to 114±7μm. Similarly, there was clear observance of grain refinement through addition of calcium in AZMX1400 alloy, the grain size reduced from 304±16μm to 231±16μm. As for AZMX4100, the solidification rate did not impact grain size evolution throughout different stages. The addition of calcium to this alloy did show an obvious trend of grain enlargement as the solidification rate slowed down.

4. The addition of 0.3%wt calcium to permanent mould cast AZMX1100 led to rapid ageing response in all isothermal ageing conditions. It took 1 hour to reach maximum hardness of 55HV, 56HV and 55HV through isothermal ageing of 150°C, 175°C and 200°C respectively. The microstructures of hot rolled, 5% deformed and pre-aged conditioned were equiaxed in all conditions with no sign of deformation. The rolling and subsequent deformation led to considerable reduction in overall grain size from the permanent mould cast condition. The most remarkable increase in hardness was witnessed after 5% deformation through cold rolling, maximum hardness during ageing was achieved at 2 hours with a value of 79HV. As evidenced in TEM analysis, the number density of precipitates present in hot rolled, 5% deformed and pre-aged AZMX1100 increased drastically. This shows that heterogenous nucleation readily occurred due to deformation of structure.

5. In AZMX1400, deformation due to rolling led to increase in dislocation density which increased precipitation activity at these defect sites. Peak-ageing occurred at 48 hours with 72HV maximum hardness value for hot rolled and 5% deformed alloys and 71HV for pre-aged alloy. The rod-like precipitates found in hot rolled, 5% deformed and pre-aged conditions were observed in greater quantity and their length shortened. As a result, the interparticle spacing between the precipitates reduced leading to increase in number density.

6. Low-pressure TRC AZMX1100 strip was produced with a superheat value of 36℃, whereas TRC AZMX1400 strip, the superheat temperature came to a considerably higher value of 69℃. In low-pressure TRC AZMX1100, the columnar grains measured to approximately 153±13μm with minimal sign of centreline segregation. Low-pressure TRC AZMX1400 had a distinct grain morphology in that it was significantly refined and dendritic in nature, the grain size measured to approximately 43±3μm with no sign of centreline segregation. Low-pressure TRC AZMX1100 which contained the least amount of alloying additions proved to be far more ductile in comparison to low-pressure TRC AZMX1400. T6 treatment of low-pressure TRC AZMX1100 drastically improved yield strength from 93.5MPa to 140.3MPa with elongation to failure value of 14.2%.

# Chapter 8- Future Work

The present investigation provided an understanding as to the microstructures formed during permanent mould castings, rolling deformation, low-pressure TRC of AZM110, AZM410 and AZM140 with and without calcium additions. Alongside this, mechanical behaviour was sought primarily through hardness testing of age-hardened permanent mould castings and deformed alloys. Low-pressure TRC alloys AZMX1100 and AZMX1400 were put through tensile testing to establish their yielding characteristics. However, further characterisation is required to gain a deeper understanding of developed alloys.

Measurement of crystallographic orientation through EBSD of developed low-pressure TRC alloys would have given an insight into the effect of calcium addition on texture distribution. Previous investigations on calcium addition to magnesium alloys have shown to weaken basal texture, such a texture negatively impacts formability especially at room temperature.

In depth characterisation of precipitation activity of peak-aged permanent mould cast alloys and deformed alloys through high resolution TEM would have been beneficial. This would have meant characterising the structure, composition, size, and distribution of rod-like precipitates found in AZM140 and AZMX1400 and plate-like precipitates found in AZM110 and AZMX1100.

Mechanical properties of low-pressure TRC AZMX1100 and AZMX1400 at perpendicular to and 45° to casting direction would have given an insight into the isotropy of mechanical behaviour. Alongside this, it would have been beneficial to gain an understanding of yielding characteristics of rolled low-pressure TRC alloys.

# References

Aghion, E., Bronfin, B. & Von, B. F., 2003. Newly developed magnesium alloys for powertrain applications. *Journal of Metals,* 55(11), pp. 30-33.

Allen, R. V., Johnson, T. J., Borbidge, W. E. & Liang, D., 2001. Magnesium Alloy Sheet Produced by Twin Roll Casting. In: J. N. Hryn, ed. *Magnesium Technology 2001.* s.l.:Wiley.

Bae, G. et al., 2009. Effect of Ca Addition on Microstructure of Twin-Roll Cast AZ31 Mg Alloy. *Metals and Materials International,* 15(1), pp. 1-5.

Bao, L. et al., 2013. Effect of homogenization treatment on microstructure evolution and the distributions of RE and Zr elements in various Mg-Li-RE-Zr alloys. *Journal of Magnesium and Alloys,* I(1), pp. 139-144.

Barekar, N. S. & Dhindaw, B. K., 2014. Twin-Roll Casting of Aluminum Alloys – An Overview. *Materials and Manufacturing Processes,* 29(6), pp. 651-661.

Barnett, M., Keshavarz, Z., Beer, A. & Atwell, D., 2004. Influence of grain size on the compressive deformation of wrought Mg-3Al-1Zn. *Acta Materialia,* 52(17), pp. 5093-5103.

Barrilao, J. K. L., 2017. *Microstructure Evolution of Laves Phase Strengthened Ferritic Steels for High Temperature Applications,* Jülich: Forschungszentrum Jülich GmbH.

Bettles, C., Humble, P. & Nie, J., 1997. *Proceedings of 3rd International Magnesium Conference.* London, The Institute of Materials.

Bhattacharjee, T., 2014. *(PhD Thesis) Effect of microalloying elements on Mg-Zn alloys,* Tsukuba: University of Tsukuba.

Bian, M. et al., 2017. A heat-treatable Mg-Al-Ca-Mn-Zn sheet alloy with good room temperature formability. *Scripta Materialia.*

Bian, M. et al., 2016. Improving Formability of Mg-Ca-Zr Sheet Alloy by Microalloying of Zn. *Advanced Engineering Materials,* 18(10), pp. 1763-1769.

Bian, Z., Bayandorian, I. & Fan, Z., 2008. Extremely fine and uniform microstructure of magnesium AZ91D alloy sheets produced by melt conditioned twin roll casting. *Materials Science and Technology,* Volume 0, pp. 1-8.

Byun, J. Y., Kwon, S. I., Ha, H. P. & Yoon, J. K., 2003. A Manufacturing Technology of AZ91-Alloy Slurry for Semi Solid Forming. In: K. U. Kainer, ed. *Magnesium: Proceedings of the 6th International Conference Magnesium Alloys and Their Applications.* Weinham: Wiley V-CH, pp. 713-718.

Caceres, C. H. & Blake, A., 2002. The Strength of Concentrated Mg–Zn Solid Solutions. *physica status solidi (a),* 194(1), pp. 147-158.

Callister, W., 2007. *Materials Science and Engineering An Introduction.* 7th ed. USA: Wiley.

Cao, P., John, D. H. & Qian, M., 2005. The Effect of Manganese on the Grain Size of Commercial AZ31 Alloy. *Materials Science Forum,* Issue 488-489, p. 139.

Celotto, S., 2000. TEM study of continuous precipitation in Mg–9 wt%Al–1 wt%Zn alloy. *Acta Materialia,* 48(8), pp. 1775-1787.

Chen, H. et al., 2009. Effect of heat treatment on microstructure and mechanical properties of twin roll cast and sequential warm rolled ZK60 alloy sheets. *Journal of Alloys and Compounds,* 476(1-2), pp. 324-328.

Chino, Y., Huang, X., Suzuki, K. & Mabuchi, M., 2010. Enhancement of Stretch Formability at Room Temperature by Addition of Ca in Mg-Zn Alloy. *Materials Transactions ,* 51(4), pp. 818-821.

Chino, Y. et al., 2011. Effects of Ca on tensile properties and stretch formability at room temperature in Mg-Zn and Mg-Al alloys. *Materials Transactions,* 52(7), pp. 1477-1482.

Crawley, A. F. & Miliken, K. S., 1974. Precipitate morphology and orientation relationships in an aged Mg-9% Al-1% Zn-0.3% Mn alloy. *Acta Materialia,* 22(5), pp. 557-562.

Curle, U. A., Wilkins, J. D. & Govender, G., 2013. R-HPDC of Magnesium Alloys. *Solid State Phenomena,* Volume 192-193, pp. 225-230.

Dargusch, M. S. et al., 2006. The Effect of Aluminium Content on the Mechanical Properties and Microstructure of Die Cast Binary Magnesium-Aluminium Alloys. *Materials Transactions,* 47(4), pp. 977-982.

Das, S. et al., 2013. Melt Conditioned Twin Roll Casting (MC-TRC) of Thin Mg-Alloy Strips for Direct Stamping of Mg Components. *Materials Science Forum,* Volume 765, pp. 170-174.

Ding, H. L., Zhang, P., Cheng, G. P. & Kamado, S., 2015. Effect of calcium addition on microstructure and texture modification of Mg rolled sheets. *Transactions of Nonferrous Metals Society of China,* 25(9), pp. 2875-2883.

DoD, 2011. *Statement by Commandant of the Marine Corps Gen. James Amos on Efficiencies.* [Online]
Available at:
https://web.archive.org/web/20110301004919/http://www.defense.gov/releases/release.aspx?releaseid=14179
[Accessed 12 October 2017].

Ferry, M., 2006. *Direct strip casting of metals and alloys.* 1st ed. Cambridge: Woodhead Publishing.

Fleischer, R. L., 1963. Solidification in substitution mixed crystals. *Acta Metallurgica,* 11(3), pp. 203-209.

Gao, X. & Nie, J. F., 2007. Structure and thermal stability of primary intermetallic particles in an Mg–Zn casting alloy. *Scripta Materialia,* 57(7), pp. 655-658.

Gottstein, G., 2007. *Physical basics of materials science.* 3rd ed. s.l.:Springer.

Gradwell, K., 1972. *PhD Thesis,* Manchester: University of Manchester.

Hadadzadeh, A. & Wells, M. A., 2013. Mathematical modeling of thermo-mechanical behavior of strip during twin roll casting of an AZ31 magnesium alloy. *Journal of Magnesium and Alloys,* 1(2), pp. 101-114.

Hadadzadeh, A. & Wells, M. A., 2015. Inverse and centreline segregation formation in twin roll cast AZ31 magnesium alloy. *Materials Science and Technology,* 31(14), pp. 1715-1726.

He, J., Javaid, A., Essadiqi, E. & Shehata, M., 2008. Numerical simulation and experimental study of the solidification of a wedge shaped AZ31 Mg alloy casting. *Canadian Metallurgical Quarterly,* 48(2), pp. 1-12.

Hilditch, T., Nie, J. & Muddle, B., 1998. *The Effect of Cold Work on Precipitation In Alloy WE54.* Frankfurt, Werkstoff-Informationsgesellschaft.

Hono, K., Mendis, C., Sasaki, T. & Oh-ishi, K., 2010. Towards the development of heat-treatable high-strength wrought Mg alloys. *Scripta Materialia,* Volume 63, pp. 710-715.

Hoppe, R., Kurz, G. & Letzig, D., 2016. Substitution of Rare Earths in Magnesium Alloys. *Materials Science Forum,* Volume 854, pp. 51-56.

Huang, G. et al., 2008. Microstructure and Texture Evolution of AZ31 Magnesium Alloy During Rolling. *Transaction of Non-ferrous Metals Society of China,* 18(1), pp. 170-174.

Jain, A. et al., 2008. Grain size effects on the tensile properties and deformation mechanisms of a magnesium alloy, AZ31B, sheet. *Materials Science and Engineering A,* 486(1-2), pp. 545-555.

Jayaraj, J. et al., 2010. Enhanced Precipitation Hardening of Mg-Ca alloy by Al addition. *Scripta Materialia,* 63(8), pp. 831-834.

Jeal, N., 2005. High-Performance Magnesium. *Advanced Materials and Processes ,* pp. 65-67.

Jiang, Z. et al., 2015. Influence of the Al2Ca phase on microstructure and mechanical properties of Mg-Al-Ca alloys. *Journal of Alloys and Compounds,* Volume 647, pp. 357-363.

Kabirian, F. & Mahmudi, R., 2010. Effects of Zr Additions on the Microstructure and Impression Creep Behavior of AZ91 Magnesium Alloy. *Metallurgical and Materials Transactions A,* 41(13), p. 3488–3498.

Kadambi, S. B., Divya, V. D. & Ramamurty, U., 2017. Evaluation of Solid-Solution Hardening in Several Binary Alloy Systems Using Diffusion Couples Combined with Nanoindentation. *Metallurgical and Materials Transaction A,* Volume 48, p. 4574–4582.

Kainer, K., 2003. *Magnesium - Alloys and Technologies.* Weinheim: WILEY-VCH.

Kawabata, H. et al., 2018. Effect of Calcium on the Combustion Behavior of Molten AZ91 Magnesium Alloy. *Materials Transactions,* 59(2), pp. 272-279.

Kelly, A. & Nicholson, R., 1971. *Strengthening Methods in Crystals.* s.l.:Elsevier Science Ltd.

Kim, N., 2014. Critical Assessment 6: Magnesium sheet alloys: viable alternatives to steels?. *Materials Science and Technology,* 30(15), pp. 1925-1928.

Kim, S. H. et al., 2017. Effect of Al and Sn on Discharge Behavior of Mg Alloy as Anode for Mg-Air Battery. In: K. N. Solanki, D. Orlov, A. Singh & N. R. Neelameggham, eds. *Magnesium Technology 2017.* s.l.:Springer, pp. 413-419.

Koike, J., 2005. Enhanced Deformation Mechanisms by Anisotropic Plasticity in Polycrystalline Mg Alloys at Room Temperature. *METALLURGICAL AND MATERIALS TRANSACTIONS A,* Volume 36A, pp. 1689-1696.

Krbetschek, C. et al., 2016. MICROSTRUCTURE INVESTIGATIONS OF INVERSE SEGREGATIONS IN TWIN-ROLL CAST AZ31 STRIPS. *Magnesium Technology 2016,* pp. 369-374.

Kulekci, M. K., 2008. Magnesium and its alloys applications in automotive industry. *International Journal of Advanced Manufacturing Technology,* Volume 39, pp. 851-865.

Labusch, R., 1972. Statistical theories of solid solution hardening. *Acta Metallurgica,* 20(7), pp. 917-927.

Lee, Y. C., Dahle, A. K. & StJohn, D. H., 2000. The Role of Solute in Grain Refinement of Magnesium. *Metallurgical and Materials Transactions A,* I(31), p. 2895–2906.

Liang, D. & Cowley, C. B., 2004. The twin-roll strip casting of magnesium. *The Journal of The Minerals, Metals & Materials Society,* Volume 56, pp. 26-28.

Mendis, C., 2005. *Effects of Calcium Additions on Microstructure and Creep Behaviour of Mg-8Zn-4Al Casting Alloy,* Victoria: Monash University.

Mendis, C., Bae, J., Kim, N. & Hono, K., 2010. Microstructures and tensile properties of a twin roll cast and heat treated Mg-2.4Zn-0.1Ag-0.1Ca-0.1Zr alloy. *Scripta Materialia,* Volume 64, pp. 335-338.

Mendis, C., Kainer, K. & Hort, N., 2015. High Strength Magnesium Alloys Through Precipitation Hardening and Micro Alloying: Considerations for Alloy Design. *JOM,* 67(10), pp. 2427-2432.

Mendis, C. L., 2005. *Effects of Calcium Additions on Microstructure and Creep Behaviour of Mg-8Zn-4Al Casting Alloy,* Melbourne: Monash University.

Mendis, C. et al., 2009. Precipitation-hardenable Mg–2.4Zn–0.1Ag–0.1Ca–0.16Zr (at.%) wrought magnesium alloy. *Acta Materialia,* Volume 57, pp. 749-760.

Mendis, C., Oh-ishi, K., Ohkubo, T. & Hono, K., 2011. Precipitation of prismatic plates in Mg–0.3Ca alloys with In additions. *Scripta Materialia,* 64(2), pp. 137-140.

Mino, T. et al., 2006. Twin-roll strip casting of AZ61 magnesium alloy and improvement offormability by structure-control rolling. *Journal of Materials Processing Technology,* Volume 177, pp. 534-538.

Motegi, T., 2005. Grain-refining mechanisms of superheat-treatment of and carbon addition to Mg–Al–Zn alloys. *Materials Science and Engineering A,* Issue 413-414, pp. 408-411.

Murray, J. L., 1982. The Al-Mg (Aluminum-Magnesium) system. *Bulletin of Alloy Phase Diagrams,* 3(1), pp. 60-74.

Neh, K. et al., 2015. *Twin Roll Casting and Strip Rolling of Several Magnesium Alloys.* s.l., MaterialsToday: Proceedings.

Nie, J., 2002. *Precipitation And Strengthening In Selected Magnesium Alloys.* Warrendale, Magnesium Technology, pp. 103-110.

Nie, J., 2012. Precipitation and Hardening in Magnesium Alloys. *Metallurgical and Materials Transactions A,* Volume 43A, pp. 3891-3939.

Noda, M. et al., 2014. *Texture, Microstructure, and Mechanical Properties of Calcium- Containing Flame-Resistant Magnesium Alloy Sheets Produced by Twin-*

*Roll Casting and Sequential Warm Rolling, Magnesium Alloys - Properties in Liquids and Solid States.* s.l.:InTech.

Oh-ishi, K., Hono, K. & Shin, K., 2008. Effect of pre-aging and Al addition on age-hardening and microstructure in Mg-6 wt% Zn alloys. *Materials Science and Engineering: A,* 496(1-2), pp. 425-433.

Oh, J., Ohkubo, T., Mukai, T. & Hono, K., 2005. TEM and 3DAP characterization of an age-hardened Mg–Ca–Zn alloy. *Scripta Materialia,* 53(6), pp. 675-679.

Okamoto, H., 1994. *Journal of Phase Equilibria,* Volume 15, p. 129.

Okamoto, H., 1998. *Journal of Phase Equilibria,* 19(6), p. 598.

Pan, H. et al., 2016. Recent developments in rare-earth free wrought magnesium alloys having high strength: A review. *Journal of Alloys and Compounds,* pp. 321-331.

Park, S. et al., 2007. Microstructure and tensile properties of twin-roll cast Mg–Zn–Mn–Al alloys. *Scripta Materilia,* 57(9), pp. 793-796.

Park, S. et al., 2007. Microstructure and tensile properties of twin-roll cast Mg–Zn–Mn–Al alloys. *Scripta Materialia,* Issue 57, pp. 793-796.

Patel, J. B., Yang, X. L., Mendis, C. L. & Fan, Z., 2017. Melt Conditioning of Light Metals by Application of High Shear for Improved Microstructure and Defect Control. *The Journal of The Minerals, Metals & Materials Society,* 69(6), pp. 1071-1076.

Perepezko, J. H. & Hildal, K., 2005. Analysis of solidification microstructures during wedge-casting. *Philosophical Magazine,* 86(24), p. 3681–3701.

Pérez-Prado, M., del Valle, J., Contreras, J. & Ruano, O., 2004. Microstructural evolution during large strain hot rolling of an AM60 Mg alloy. *Scripta Materialia,* 50(5), pp. 661-665.

Pettersen, K., Bakke, P. & D., A., 2002. *Magnesium Die Casting Alloy Design.* Seattle, Magnesium Technology (TMS).

Polmear, I., 2005. *Light Alloys, From Traditional Alloys to Nanocrystals.* 4th ed. s.l.:Butterworth-Heinemann.

Polmear, I. J., 1994. Materials Science and Technology. In: *Magnesium Alloys and Applications.* s.l.:s.n., p. 250.

Riehle, M. & Simmchen, E., 2000. *Basics of Materials Technology.* Stuttgart: Wiley-VCH.

Smallman, R., 1985. *Modern Physical Metallurgy.* 4th ed. Oxford: Butterworth-Heinemann.

Smith, W., 1993. *Foundations of Material Science and Engineering.* 2nd ed. New York: McGraw-Hill.

Suh, B., Shim, M., Shin, K. & Kim, N., 2014. Current issues in magnesium sheet alloys: where do we go from here?. *Scripta Materialia,* Volume 84-85, pp. 1-6.

Sun, M., Wu, G., Wang, W. & Ding, W., 2009. Effect of Zr on the microstructure, mechanical properties and corrosion resistance of Mg–10Gd–3Y magnesium alloy. *Materials Science and Engineering: A,* 523(1-2), pp. 145-151.

Tamura, Y. et al., 2003. Observation of Manganese-Bearing Particles in Molten AZ91 Magnesium Alloy by Rapid Solidification. *Materials Transactions ,* 44(4), pp. 552-557.

Trang, T. T. T. et al., 2018. Designing a magnesium alloy with high strength and high formability. *Nature Communications,* 2522(9), pp. 1-6.

Uchida, S. H. et al., 2007. Mechanical Properties of Twin Roll Cast AZ91 Magnesium Alloy at Room Temperature. *Advanced Materials Research,* Volume 26-28, pp. 145-148.

Wang, C. et al., 2019. Improving Strength and Ductility of a Mg-3.7Al-1.8Ca-0.4Mn Alloy with Refined and Dispersed Al2Ca Particles by Industrial-Scale ECAP Processing. *Metals,* pp. 1-15.

Wang, Y. et al., 2010. The effect of Al8Mn5 intermetallic particles on grain size of as-cast Mg-Al-Zn AZ91D alloy. *Intermetallics,* Issue 18, pp. 1683-1689.

Wang, Z. et al., 2014. Improving the strength and ductility of Al-Mg-Si-Cu alloys by a novel thermo-mechanical treatment. *Materials Science & Engineering A,* Volume 607, pp. 313-317.

Wei, L. Y., Dunlop, G. L. & Westengen, H., 1995. Precipitation Hardening of Mg-Zn and Mg-Zn-RE Alloys. *Metallurgical and Materials Transactions A,* 26A(7), pp. 1705-1716.

Wells, M. & Hadadzadeh, A., 2014. Twin Roll Casting (TRC) of Magnesium Alloys – Opportunities and Challenges. *Materials Science Forum,* Volume 783-786, pp. 527-533.

Xu, C. et al., 2012. Ultra high-strength Mg–Gd–Y–Zn–Zr alloy sheets processed by large-strain hot rolling and ageing. *Materials Science and Engineering: A,* Volume 547, pp. 93-98.

Yang, X. L., 2016. *Particle dispersion in aluminium and magnesium alloys,* London: Brunel University.

Yang, X. L., 2016. *Particle Dispersion in Aluminium and Magnesium Alloys,* London: Brunel University London.

Yang, X. L. et al., 2019. Towards directly formable thin gauge AZ31 Mg alloy sheet production by melt conditioned twin roll casting. *Materials & Design,* Volume 179, pp. 1-10.

Yang, X. M. C. L., Patel, J. B., Huang, Y. & Fan, Z., 2018. *Devolopment of Melt-Conditioned Twin-Roll Casting (MC-TRC) Process for Thin Gauge Mg Alloy Strip Production.* Uxbridge, Brunel University Press.

Yang, X. M. C., Patel, J. & Fan, Z., 2018. Microstructure evolution and mechanical properties of thin strip twin roll cast (TRC) Mg sheet. *Magnesium Technology 2018,* pp. 429-432.

Yang, X. et al., 2018. *Development of Melt-Conditioned Twin-Roll Casting (MC-TRC) Process for Thin Gauge Mg Alloy Strip Production.* Old Windsor, BCAST.

Yasi, J. A., Hector Jr, L. G. & Trinkle, D. R., 2010. First-Principles Data for Solid-Solution Strengthening of Magnesium: From Geometry and Chemistry to Properties. *Acta Materialia,* 58(17), pp. 5704-5713.

Yim, C., You, B., Lee, J. & Kim, W., 2004. *Materials Transactions,* 45(10), pp. 3018-3022.

Yim, C., You, B., Lee, J. & Kim, W., 2004. Optimization of Hot Rolling Process of Gravity Cast AZ31-Ca Alloys. *Materials Transactions,* 45(10), pp. 3018-3022.

Zeng, G., Xian, J. W. & Gourlay, C. M., 2018. Nucleation and growth crystallography of Al8Mn5 on B2-Al(Mn,Fe) in AZ91 magnesium alloys. *Acta Materialia,* Volume 153, pp. 364-376.

Zhang, B., Wang, Y., Geng, L. & Lu, C., 2012. Effects of calcium on texture and mechanical properties of hot-extruded Mg–Zn–Ca alloys. *Materials Science and Engineering: A,* Volume 539, pp. 56-60.

Zhang, D., Qi, F., Shi, G. & Dai, Q., 2010. Effects of Mn content on microstructure and mechanical properties of Mg-Zn-Mn wrought alloys. *Rare Metal Materials and Engineering,* 39(12), pp. 2205-2210.

Zhang, D., Shi, G., X.B., Z. & Qi, F., 2011. Microstructure evolution and mechanical properties of Mg-x%Zn-1%Mn (x=4, 5, 6, 7, 8, 9) wrought magnesium alloys. *Transactions of Nonferrous Metals Society of China,* 21(1), pp. 15-25.

Zheng, W., Li, S., Tang, B. & Zeng, D., 2006. Microstructure and properties of Mg-Al binary alloys. *China Foundry,* pp. 270-274.

Zheng, Z. et al., 2015. Annealing strengthening in a dilute Mg-Zn-Ca sheet alloy. *Scripta Materialia,* pp. 127-130.